U.S. DEPARTMENT OF THE INTERIOR
U.S. GEOLOGICAL SURVEY

Hydrogeology of the Regional Aquifer near Flagstaff, Arizona, 1994–97

Water-Resources Investigations Report—4122

Prepared in cooperation with the CITY OF FLAGSTAFF

USGS
science for a changing world

U.S. DEPARTMENT OF THE INTERIOR
U.S. GEOLOGICAL SURVEY

Hydrogeology of the Regional Aquifer near Flagstaff, Arizona, 1994–97

By Donald J. Bills, Margot Truini, Marilyn E. Flynn, Herbert A. Pierce, Rufus D. Catchings, *and* Michael J. Rymer

Water-Resources Investigations Report 00—4122

Prepared in cooperation with the
CITY OF FLAGSTAFF

Tucson, Arizona
2000

U.S. DEPARTMENT OF THE INTERIOR
GALE A. NORTON, Secretary

U.S. GEOLOGICAL SURVEY
Charles G. Groat, Director

The use of firm, trade, and brand names in this report is for identification purposes only and does not constitute endorsement by the U.S. Geological Survey.

For additional information write to:

District Chief
U.S. Geological Survey
Water Resources Division
520 N. Park Avenue, Suite 221
Tucson, AZ 85719–5035

Copies of this report can be purchased from:

U.S. Geological Survey
Information Services
Box 25286
Federal Center
Denver, CO 80225–0046

Information regarding research and data-collection programs of the U.S. Geological Survey is available on the Internet via the World Wide Web. You may connect to the home page for the Arizona District Office using the URL *http://az.water.usgs.gov*.

CONTENTS

PLATES

FIGURES

FIGURES—Contined Page

FIGURES—Continued Page

FIGURES—Continued Page

TABLES

CONVERSION FACTORS AND VERTICAL DATUM

Multiply	By	To obtain
inch (in)	25.4	millimeter
foot (ft)	0.3048	meter
mile (mi)	1.609	kilometer
square mile (mi^2)	2.590	square kilometer
gallon (gal)	3.785	liter
million gallons (Mgal)	3,785	cubic meter
acre-foot (acre-ft)	0.001233	cubic hectometer
cubic foot per second (ft^3/s)	0.02832	cubic meter per second
cubic foot per day (ft^3/d)	0.02832	cubic meter per day
gallon per minute (gal/min)	0.06309	liter per second
gallon per day (gal/d)	0.003785	cubic meter per day
gallons per minute per foot[1] [(gal/min)/ft)]	0.2070	liters per second per meter
gallons per day per foot squared[1] [(gal/d)/ft^2]	0.041	liter per day per meter squared
foot per mile (ft/mi)	0.1894	meter per kilometer
gallons per day per foot [(gal/d)/ft]	0.0124	meters squared per day

[1]The standard unit for transmissivity is cubic foot per day per square foot per foot of aquifer thickness [($(ft^3/d)/ft^2$]ft and generally the mathematically reduced form, foot squared per day (ft^2/d), is used for convenience. The standard unit for hydraulic conductivity is foot per day (ft/d). In this report, however, transmissivity is reported in gallons per day per foot, and hydraulic conductivity is reported in gallons per day per foot squared. If the reader wishes to use the standard units, the hydraulic conductivity factor of gallons per day per foot squared would be multiplied by 0.134 to obtain the standard factor of foot per day. For transmissivity, the factor of gallons per day per foot would be multiplied by 0.134 to obtain the standard factor of foot squared per day.

Temperature in degrees Celsius (°C) may be converted to degrees Fahrenheit (°F) as follows:

$$°F=1.8(°C)+32$$

ABBREVIATED WATER-QUALITY UNITS

Chemical concentration and water temperature are given only in metric units. Chemical concentration in water is given in milligrams per liter (mg/L) or micrograms per liter (μg/L). Milligrams per liter is a unit expressing the solute mass (milligrams)

per unit volume (liter) of water. One thousand micrograms per liter is equivalent to 1 milligram per liter. For concentrations less than 7,000 milligrams per liter, the numerical value is about the same as for concentrations in parts per million. Specific conductance is given in microsiemens per centimeter at 25 degrees Celsius (μS/cm at 25°C). Radioactivity is expressed in picocuries per liter (pCi/L) or picocuries per gram (pCi/g), which is the amount of radio-active decay producing 2.2 disintegrations per minute in a unit volume (liter) of water or mass (gram) of sediment.

VERTICAL DATUM

Sea level: In this report, "sea level" refers to the National Geodetic Vertical Datum of 1929 (NGVD of 1929)—A geodetic datum derived from a general adjustment of the first-order level nets of both the United States and Canada, formerly called "Sea Level Datum of 1929".

Hydrogeology of the Regional Aquifer near Flagstaff, Arizona, 1994–97

By Donald J. Bills, Margot Truini, Marilyn E. Flynn, Herbert A. Pierce, Rufus D. Catchings, *and* Michael J. Rymer

Abstract

Sandstones, siltstones, and limestones that are Pennsylvanian to Permian in age underlie the southern part of the Colorado Plateau near Flagstaff, Arizona, and contain a complex regional aquifer that has become increasingly important as a source of water for domestic, municipal, and recreational uses. Ground-water flow in the regional aquifer is poorly understood in this area because (1) depth of the aquifer limits exploratory drilling and testing and (2) the geologic structure increases the complexity of the aquifer characteristics and the ground-water flow system.

Four methods were used to improve the understanding of the hydrogeology of the regional aquifer near Flagstaff.

- Remote-sensing techniques and geologic mapping provided data to identify many structural features that indicate a more complex structural environment and history than previously realized.
- Data from surface-geophysical techniques that included ground-penetrating radar, seismic reflection and seismic refraction, and square-array resistivity, verified that some of the geologic structures expressed at land surface propagate deep into the subsurface and through the principal water-bearing zones of the regional aquifer at near-vertical angles.
- A well and spring inventory, borehole-geophysical methods, and well and aquifer tests provided additional information relating aquifer and ground-water flow characteristics to geologic structure.
- Water-chemistry data, which included major ion, nutrient, trace-element, and radioactive and stable-isotope analyses, provided an independent means of verifying the hydrogeologic characteristics of the aquifer and were used to determine recharge and discharge areas, ground-water movement, and ground-water age.

Ground-water recharge occurs throughout the area but is greatest at higher altitudes where precipitation is greater and in areas where heavily fractured rock units of the aquifer are exposed. The estimated annual average recharge to the regional aquifer in the study area is about 290,000 acre-feet. Ground water flows laterally and vertically through pore spaces in the rock and along faults and other fractures from high-altitude areas in the southern part of the study area to regional drains north of the study area along the Little Colorado and Colorado Rivers, and to drains south of the study area along Oak Creek and the Verde Valley. Ground-water discharge in these areas—about 400,000 acre-feet per year—exceeds the annual recharge to the aquifer in the Flagstaff area, but ground water from areas outside the study area contributes to this discharge as well. The saturated thickness of the regional aquifer

averages about 1,200 feet, and the amount of water in storage could be as much as 4,800,000 acre-feet, or about 10 percent of the total volume of the aquifer.

The quality of water in the regional aquifer in terms of dissolved-solids concentrations is good for most uses throughout the area. Dissolved-solids concentrations generally are less than 500 milligrams per liter. Water in the regional aquifer is primarily a calcium magnesium bicarbonate type. In some areas near the Rio de Flag, the water has significant nitrate and chloride components, which indicate direct recharge in these areas from the Rio de Flag. Oxygen and deuterium data indicate a common recharge source for water in the aquifer and that some sites receive recharge from surface waters where evaporation has occurred. Estimated carbon-14 ages and tritium activities indicate ground-water ages from less than 200 years in the Lake Mary area to more than 5,000 years in the Wupatki area.

The regional aquifer is heterogeneous and anisotrophic and has a complex ground-water flow system. The most productive water-bearing material tends to be fine- to medium-grained sandstones, and ground-water flow and potential well yields are related to geologic structure. Fracturing associated with structural deformation increases recharge locally and also increases the potential for high well yields. Surface-geophysical techniques provided information on the orientation of high-angle, deep-seated structure in the saturated zone. Borehole-geophysical data identified horizontal to near-horizontal fractures as significant components of the fracture-flow system not apparent in the surface-geophysical data. Structural features that strike northwest appear to be areas that have the greatest potential for high well yields. A north-northeastward-striking structure may be just as promising, but additional data are needed to verify this relation.

INTRODUCTION

Ground water is a major source of public and domestic water supply on the Colorado Plateau in northern Arizona (**fig. 1**). Water resources near Flagstaff are obtained from surface runoff, shallow perched water-bearing zones, and a deep regional aquifer. Surface-water resources are limited because runoff in the area is small, and surface-water rights either are fully appropriated or under adjudication. Ground water, therefore, is one of the few remaining alternatives for communities in the area. Because the depth to ground water in the regional aquifer significantly affects the cost of drilling and developing wells, high-yield wells are desired for public and municipal supply; however, the hydrogeology and flow characteristics of the regional aquifer are poorly understood.

Until the 1950s, the water needs of Flagstaff and the surrounding area were met by developed springs, surface-water impoundments, and a few shallow wells developed in perched water-bearing zones. By the early 1960s, Flagstaff had grown to a community of about 18,000, and the need to increase development of the water resources was apparent. In the late 1950s to the early 1960s, a cooperative investigation between the U.S. Geological Survey (USGS) and the City of Flagstaff resulted in the drilling and development of high-yield wells; this investigation recognized a relation between geologic faults and the occurrence of ground water in the Flagstaff area. As the community continued to grow, the City of Flagstaff and water companies in the surrounding area drilled deep wells that met with varied results. Some wells yielded hundreds of gallons per minute; however, most wells yielded less than 50 gal/min. By the mid-1990s, development of high-yield wells completed in fault zones had reached the point where the water table was being drawn down, which reduced the yield of other wells in the surrounding areas (Ron Doba, Utilities Director, City of Flagstaff, written commun., 1995).

In recent years, the City of Flagstaff has become more dependent on ground water from the regional aquifer. Water use in the study area increased about 30 percent from the mid-1980s to the mid-1990s, and the use of ground water has surpassed the use of surface water (U.S. Geological Survey, 1985; Anning and Duet, 1994; **fig. 2**A). In 1995, the population of Flagstaff was 58,500. Recent studies of community growth and development project a population of about 100,000 by the year 2020 (City of Flagstaff, 1996).

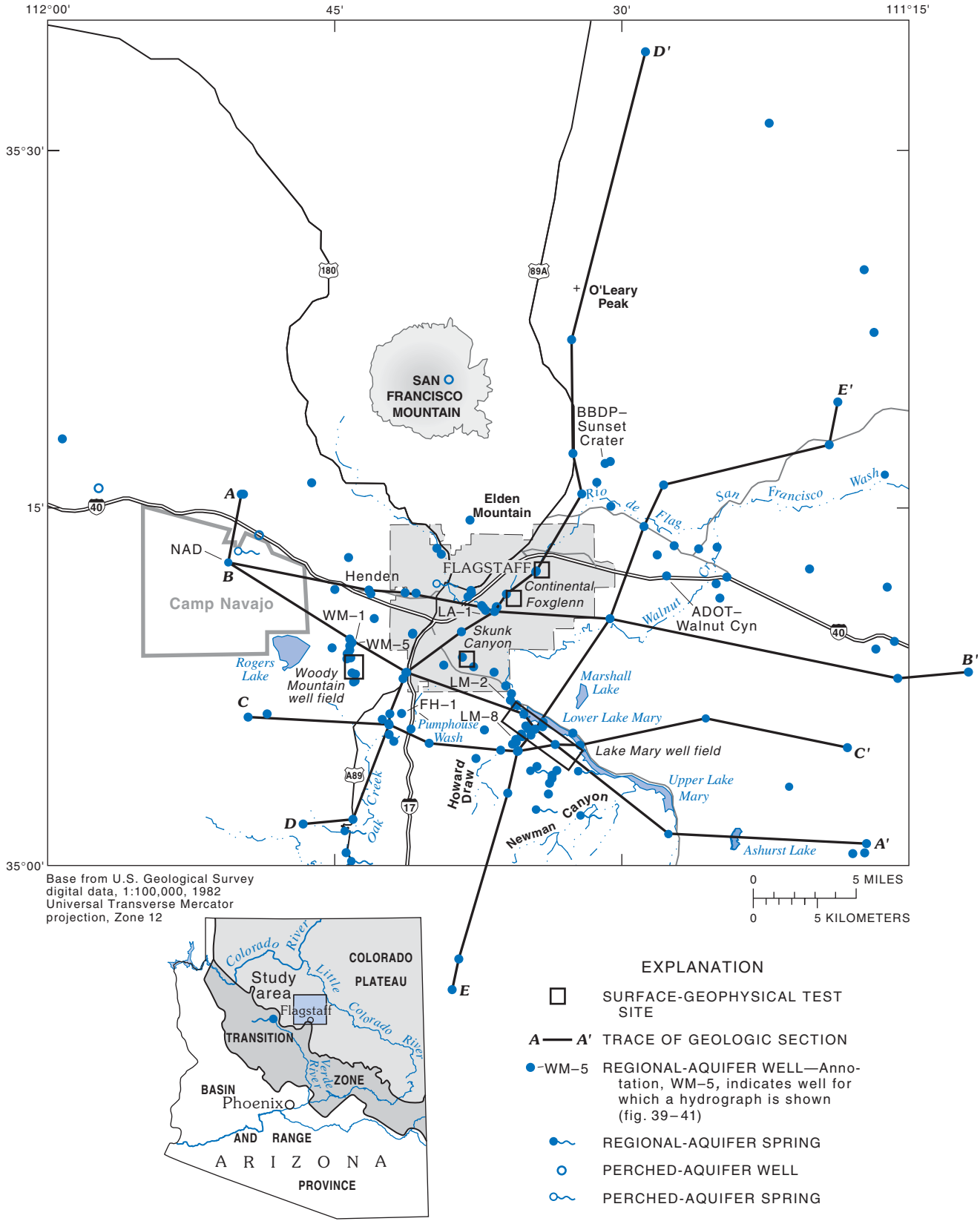

Figure 1. Study area, and locations of wells and springs that discharge water from the regional aquifer, selected wells and springs that discharge water from perched water-bearing zones, traces of geologic sections, and surface-geophysical test sites, Flagstaff, Arizona.

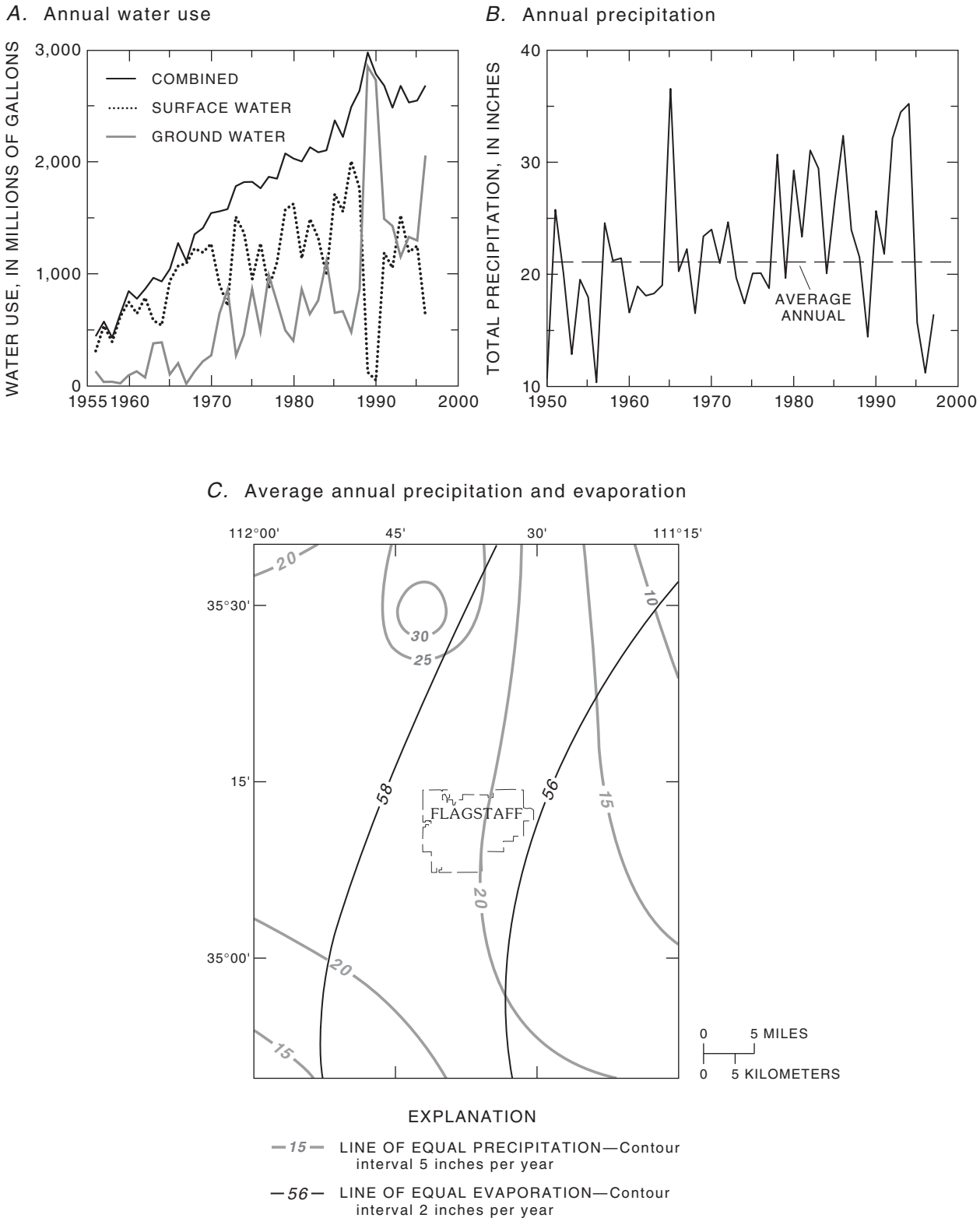

Figure 2. Water use, annual precipitation, and evaporation, Flagstaff, Arizona. *A*, Annual water use for the City of Flagstaff, 1956–96. *B*, Annual precipitation at Pulliam Field near Flagstaff, Arizona, 1950–97, and average annual precipitation (National Oceanic and Atmospheric Administration, 1998). *C*, Average annual precipitation and evaporation (Arizona Water Commission, 1975).

Long-range resource-management plans foresee the need to secure additional dependable water supplies to meet the future demands of an increasing population and a developing commercial environment. In September 1995, the USGS, in cooperation with the City of Flagstaff, began a study to improve the understanding of the occurrence and movement of water and the relation between hydrogeologic characteristics and well productivity in the regional aquifer.

Flagstaff and the surrounding area overlie a complex series of volcanic and sedimentary rocks. These rock formations are deformed locally and regionally by a series of folds and fractures that collectively are the geologic structure of the area. This structure partly controls the occurrence and movement of ground water. Ground water in some areas is perched close to the land surface by dense and unfractured volcanic rocks or by fine-grained sediments or sedimentary rocks. The results of previous studies indicate that ground water is recharged by precipitation and surface flows throughout the area and along the Mogollon Rim. Water that filters down to the regional water table moves laterally and vertically until it discharges as springs along the Little Colorado and Colorado Rivers to the north, Oak and Sycamore Creeks to the south, or is pumped out of the ground by wells. None of the previous studies, however, discuss the effects of highly fractured rocks on the general flow of ground water.

To provide an improved understanding of the ground-water flow system, the USGS used geophysical and geological techniques in addition to traditional hydrologic approaches to delineate the regional aquifer and ground-water flow paths, and to locate zones of greatest permeability in the regional aquifer. Ground-water chemistry was characterized to delineate the sources and areas of ground-water recharge, ground-water flow directions, and the hydraulic connection among different rock units. This information was used to evaluate relations between certain types of geologic structure and high-yield wells.

Purpose and Scope

This report presents hydrogeologic, geophysical, and water-chemistry data of the regional aquifer near Flagstaff, Arizona. The data are used to define the availability and flow of ground water in the area and evaluate areas where geologic structure, hydraulic properties, and water chemistry provide the most favorable conditions for ground-water development.

The scope of the report includes the following.

1. Background material on the physical setting of the study area and description of the methods used to collect hydrogeologic, geophysical, and water-chemistry data.
2. Description of the application of these methods and collection of data to describe ground-water flow directions, recharge and discharge areas, and hydraulic properties that affect regional ground-water flow.
3. Comparison of historic water-level data with data collected during this study to evaluate temporal trends.
4. Evaluation of the hydrogeology of the regional aquifer and the hydraulic connection among water-bearing zones.
5. Chemical analysis of ground water to refine and corroborate the conceptual flow model developed using the hydrogeologic, geologic, and geophysical methods.
6. A summary of the principal findings of the study focusing on the investigative methods that best establish relations among known geologic and structural characteristics, hydrologic properties, water chemistry, and high well yields.

Primary data were collected in 1995 and 1996. Supplemental data that verify and refine spatial and temporal trends were collected in 1997 and are presented in the section entitled "**Supplemental Data**" at the end of this report.

Overview of Study Methods

Field programs were established to collect the data needed to define the hydrogeologic, geophysical, and water-chemistry characteristics in the study area. All accessible wells and springs that discharge water from the regional aquifer in and adjacent to the study area were inventoried. Data were collected from depth-to-water measurements, well-yield calculations, pumping tests, borehole-geophysical logs, and water-chemistry analyses. Where appropriate, an attempt was made to fill in data gaps by the collection of additional borehole-geophysical logs or the collection of new well-test data. These data were used to determine hydrogeologic patterns that relate to potential high-

yield well development. Surface-geophysical surveys that included ground-penetrating radar, seismic reflection and seismic refraction, and square-array resistivity techniques were made in selected areas where remote-sensing data and surface structure indicated potential fracturing in the subsurface. These techniques were evaluated to determine if they were capable of delineating areas of significant fracturing in the aquifer units. Existing regional gravity data also were evaluated. Where geophysical data were used by the City of Flagstaff to locate and develop wells, borehole-geophysical logs and well-test data were used to verify the location and extent of structural deformation in the subsurface that was indicated by surface-geophysical techniques.

Water samples from selected wells and springs were analyzed for major ions, nutrients, trace elements, and radioactive and stable isotopes. These data were used to help determine recharge areas, ground-water flow directions, and hydraulic connectivity of different rock units, and possibly to indicate hydraulic conductivity and recharge rates.

Description of the Study Area

The study area is on the southern edge of the Colorado Plateau in north-central Arizona (Fenneman and Johnson, 1946; **fig. 1**, this report). The study area includes about 1,600 mi^2 of the Little Colorado River and Upper Verde River Basins that extend about 40 mi north of latitude 35°00 ' N. and about 40 mi east of longitude 112°00 ' W. The eastern part of the San Francisco volcanic field covers most of the area and provides much of the topographic relief. Cinder cones and hills, basalt flows, and San Francisco Mountain of the San Francisco volcanic field are the principal features superimposed onto the consolidated sedimentary rocks of the Colorado Plateau. Erosion of the consolidated sediments exposed at land surface has created a complex series of low-relief hills and mesas in the southern and southeastern parts of the study area. A few deeply incised streams drain the area to the north and south. Altitude of the study area ranges from 12,633 ft at the top of San Francisco Mountain to about 5,450 ft in Oak Creek Canyon. The average altitude of the study area is about 7,200 ft.

The climate of the study area is semiarid with extremes of precipitation and temperature during the year (**fig. 2**B). The average precipitation for Flagstaff is 21.1 in./yr, and amounts vary from year to year (Sellers and others, 1985). Generally, precipitation is greater at the higher altitudes in the study area. Precipitation ranges from about 15 in. at the eastern end of the study area where the altitude is about 5,500 ft to more than 30 in. on the flanks of San Francisco Mountain (fig. 2C). The amounts of summer and winter precipitation are about equal (Sellers and others, 1985). Winter storms moving into the area from the northern Pacific Ocean produce moderate to large amounts of snow and rain. Because of low evapotranspiration in the winter months, much of this moisture can infiltrate the land surface. In middle to late summer, large amounts of moisture move into Arizona from the southern Pacific Ocean and the Gulf of California. The orographic effect of the high altitude of the study area results in frequent, intense short-duration thunderstorms. The high summer temperatures also result in evapotranspiration rates far in excess of precipitation. Intense but sporadic rains that last for one to several days occasionally can result in significant runoff. Vegetation consists mainly of dense to thin stands of ponderosa pine, gambles oak, and aspen that are interspersed with many flat meadows populated with drought-tolerant grasses and brush.

A few deeply incised streams drain the area to the north and south. The Rio de Flag, which is the principal drainage in the study area, heads on the west flanks of San Francisco Mountain and flows into the Little Colorado River Basin to the north. Perennial springs typically flow for short distances before the water either infiltrates the surficial sediments or evaporates. Perennial springs in the southwestern corner of the study area in Oak Creek Canyon discharge from the regional aquifer and sustain the base flow of Oak Creek. Although base flow varies seasonally in response to evapotranspiration, the long-term base flow of Oak Creek appears to be stable (Levings, 1980). Blee (1988) indicated that evaporation losses of 27 percent of the average annual precipitation are possible in the Lake Mary area. The few shallow natural lakes in the area dry up during extended periods without precipitation.

Previous Investigations

Evaluation of the local geology and hydrogeology began with Darton (1910) who made a reconnaissance of parts of northwestern New Mexico and northern

Arizona to assess ground-water supplies. Darton focused on the geology and structure of the region, defined the character, thickness, and boundaries of geologic formations, and commented on the occurrence of open fractures and sinks. Robinson (1913) made the first detailed study of the San Francisco volcanic field and provided a general summary of surface and underground drainage, and the occurrence and nature of springs and the "bottomless" pits and fissures common to the area.

The first detailed investigations of ground water in the Flagstaff area were made by the USGS in cooperation with the City of Flagstaff. Akers (1962) reported the general relation of faulting to the occurrence of ground water. Cooley (1963) and Akers and others (1964) provided summaries and a synopsis of ground-water conditions. In both cases, the authors recognized a general relation between ground-water flow and major faults. Detailed investigations in these two studies were restricted to a triangle-shaped area between Lake Mary, Woody Mountain, and San Francisco Mountain. A general reconnaissance of ground-water resources was made of the surrounding areas. Feth (1953) studied the ground-water resources of the Doney and Black Bill Parks northeast of Flagstaff, and Cosner (1962) assessed ground water in the Wupatki and Sunset Crater National Monuments. J.H. Feth (hydrologist, USGS, written communs., 1950, 1951, 1952) evaluated ground-water resources to the west of Flagstaff at the Navajo Army Depot near Bellmont. Yost and Gardner (1961) studied water requirements for the City of Flagstaff.

Cooley (1963) evaluated the ground-water resources near Flagstaff in relation to regional ground-water flow on the Colorado Plateau and the adjacent transition zone. Feth and Hem (1963) discussed ground-water flow and the occurrence of springs along the Mogollon Rim. As more data became available, these regional evaluations of the ground-water flow system were updated by McGavock (1968), Appel and Bills (1981), and McGavock and others (1986).

As Flagstaff continued to grow, several consultants were contracted to study and evaluate the potential for expanding well fields in the Woody Mountain and Lake Mary areas (**fig. 1**). The more comprehensive of these reports were Harshbarger and Associates and John Carollo Engineers, Inc. (1972, 1973), and Harshbarger and Associates (1976, 1977). Duren Engineering (1983) analyzed yield for the well fields at Lake Mary and Woody Mountain and indicated that no long-term declines of the water table had occurred in either well field. Duren Engineering (1983) also estimated the average annual flow through the Lake Mary and Woody Mountain well fields as 1 to 1.5 Mgal/d and 4.9 to 6.9 Mgal/d, respectively. These studies culminated in the early 1990s with drilling and testing of exploratory and observation wells in the Lake Mary area (Errol L. Montgomery and Associates, 1992). A 90-day aquifer test and ground-water flow model resulted in projections for long-term yield of the regional aquifer in the Lake Mary well field (Errol L. Montgomery and Associates, 1993). Errol L. Montgomery and Associates (1993) indicated that large ground-water withdrawals from 1985 through 1991 resulted in a 90-foot water-level decline in the Lake Mary well field. Using pumping scenarios then in use by the city, Errol L. Montgomery and Associates (1993) estimated aquifer yields of 4.5 Mgal/d in the Lake Mary area.

The general geology of the area was updated by Moore and others (1960) and by Cooley (1960a, b; 1963). These works were revised and updated for inclusion into a geologic map of Arizona by Reynolds (1988). Beginning in the 1970s, the geology and structure of the San Francisco volcanic field was revisited in detail as part of a national mineral and energy evaluation. This study resulted in detailed geologic maps of parts of the San Francisco volcanic field by Wolf and others (1987) and Moore and Wolf (1987). Ulrich and others (1984) compiled the work by Wolf and others (1987) and Moore and Wolf (1987) into a geology and structure map of the area. Weir and others (1989) completed geologic mapping of the adjacent Sedona area. Although these reports contain great detail on the surface geology of the area surrounding Flagstaff, the treatment of only the major structural features of the area and only general treatment of the subsurface geology was insufficient for the needs of this study. In spite of all of the previous work, little detailed information was available on the structural evolution of rocks in the study area. Most of what is known about geologic structure is inferred from surrounding areas (Karlstrom and others, 1974; Elston, 1989) and broader regional studies (Davis, 1978; Shoemaker and others, 1978). A few local geophysical investigations have been done principally by consultants for local water companies and suppliers.

Chavez and others (1997) used remote sensing and aerial photography to evaluate in detail the surface geologic structure of the area. This information was the

basis for detailed field investigation and mapping of surface structure (G.M. Mann and Dr. A.E. Springer, geologists, Northern Arizona University (NAU), written commun., 1997). Both studies provided the basis for the investigation of subsurface structure for this study.

Acknowledgments

The City of Flagstaff, the National Park Service, and many private water companies contributed well data and hydrologic information. In addition, Ron Doba, Randy Pellatz, Don Perry, Jack Rathgen, and Paul Peters, City of Flagstaff and the Flagstaff Water Commission provided logistical support to all aspects of the study. George Billingsley, USGS, provided much needed insight into the geologic structural environment and subsurface geology of the Flagstaff area. International students from the USGS Volunteers for Science Program assisted in the seismic-data collection and analysis. Dr. A.E. Springer, NAU, also organized volunteers from NAU to assist in the seismic-data collection. A. Wesley Ward, Bob Hart, Sue Beard, Sue Priest, and Don Thorstenson, USGS, provided equipment and logistical support and collected data. Gary Mann, USGS, provided instruction in the collection and analysis of ground-penetrating radar data. Jeff Phillips, Ray Davis, Dawn McDoniel, Christie O'Day, Brad Baum, Curt Crouch, and Anita Rowlands, USGS, provided additional data-collection and data-processing support. Fred Paillet and Richard Hodges, USGS, provided help in collection and interpretation of borehole-geophysical logs. Dr. A.E. Springer and Dr. Ron Parnell, NAU, directed graduate students who provided size analysis and X-ray defraction of selected well cuttings.

METHODS OF INVESTIGATION

The principal hypothesis of this study is that geologic structure has a significant influence on the hydraulic properties of the regional aquifer, and consequently, the most favorable areas for ground-water development would be concentrated along structural trends. Hydrogeologic, remote sensing, surface-geologic mapping, geophysical, and water-chemistry methods were used to evaluate the relation of geologic structure to ground-water flow. This hypothesis was tested by compiling hydrologic data from wells developed in the regional aquifer throughout the study area to relate data spatially and geostatistically with structural trends and alignments. Several surface-geophysical techniques were evaluated for their ability to identify geologic structure in the shallow and deep subsurface. Those techniques that proved most promising were applied to selected areas where surface-structural trends suggest a high likelihood of these features in the deeper subsurface. At sites where wells were later completed, borehole-video logs and selected borehole-geophysical techniques were used to verify zones of subsurface fracturing that resulted in substantial ground-water flow to the well. These data were used to corroborate the data from the surface geophysics.

Several different qualitative and quantitative analyses of aquifer characteristics and hydraulic properties were used to determine structural control of ground-water flow. These analyses included (1) evaluation of the effects of aquifer characteristics on local and regional ground-water flow, (2) evaluation of the effects of geologic structure on local and regional ground-water flow, and (3) evaluation of water chemistry to determine sources, flow directions, and hydraulic connections of different rock units. Hydraulic gradients were used to determine structural influence. Well yields and hydraulic properties were correlated and used to identify aquifer characteristics and hydrogeologic patterns that are related to high-yield wells. Selected data were evaluated spatially and temporally. Statistical and regression analysis were used to evaluate aquifer characteristics, hydraulic properties, and the relation of these attributes to structural features. Water-chemistry methods provided an independent means to determine the relations between the regional aquifer and geologic structure by determination of recharge areas, ground-water flow directions and rates, and hydraulic connections.

Fracturing is one of the most important features related to the development of ground-water resources in the study area. A fracture is defined as any opening in the formation where formation continuity is interrupted or lost. Fractures that include shear are called faults; fractures that have no offset are called joints. Fault and joint orientation was determined by measuring the strike of interpreted surface lineaments from remote-sensing data and aerial photographs. About 220 faults were mapped, and hundreds of other fractures were identified (**pl. 1**). The potentiometric surface of the regional aquifer and the general direction

of ground-water flow were determined in this study. Selected hydraulic properties of the regional aquifer were evaluated in relation to geologic structure and the potentiometric surface of the regional aquifer.

The field work for this study was done in 1995–97. Results of the remote-sensing work by Chavez and others (1996, 1997) were used with additional photogrammetry to develop the detailed surface geology and structure of the area (G.M. Mann and Dr. A.E. Springer, geologists, NAU, written commun., 1997). These data, in turn, were used as the basis for much of the hydrogeologic analysis and interpretations in this report.

Well and Spring Data

Data in the USGS Ground-Water Site Inventory (GWSI) data base for 124 wells and 12 springs near Flagstaff were used to provide information on the regional aquifer. Well and spring data also were obtained from the Arizona Department of Water Resources (ADWR). Data in the historical ground-water files of the USGS were compared with the data in the GWSI, and updates were made in the data base where appropriate. Many sites were field checked to resolve data discrepancies, measure water levels where possible, and update information on lithology, well yield, zones of well development, and specific capacity. Specific-capacity and aquifer-test data were used to estimate hydrologic properties that included transmissivity, hydraulic conductivity, storage coefficient, and (or) specific yield.

Hydraulic Properties

Data on hydraulic properties of wells in the regional aquifer were obtained from historical and recent well logs, specific-capacity, and aquifer-test data. Much of the historical field data were re-evaluated for this study, and additional well and aquifer tests were done on new wells as access allowed. No laboratory analyses of porosity from well cuttings could be found for wells in the study area. Porosity estimated from well logs in this study was compared with porosity determined for the regional aquifer in northeastern Arizona by Cooley and others (1969). Secondary porosity estimates from geophysical techniques also are compared to porosity data from Cooley and others (1969) and from well logs.

The analysis of field data consisted of the evaluation of specific-capacity and aquifer tests to determine transmissivity, hydraulic conductivity, and storage coefficients. Transmissivity is the rate at which water is transmitted through a unit width of the aquifer under a unit hydraulic gradient. Hydraulic conductivity is the volume of water that flows through a unit thickness of an aquifer under a unit hydraulic gradient. The transmissivity and hydraulic conductivity are functions of the amount of interconnection of open space in the aquifer materials. Fractures and folds increase the transmissivity and hydraulic conductivity in the aquifer by creating more interconnected openings. The specific storage, which is dimensionless, is the storage component for confined aquifers and is defined as the amount of water released from storage from a unit volume of an aquifer under a unit decline in hydraulic head. The primary storage coefficient for unconfined aquifers is specific yield and represents the ratio of the volume of water that will drain from a unit volume of an aquifer by gravity. These hydraulic properties reflect those of the aquifer surrounding a well or wells and generally integrate the primary porosity and permeability of the formation with secondary porosity and permeability that are the result of structural deformation of the rock units.

Well tests done in the Flagstaff area typically included a 12-hour drawdown period followed by a 12-hour recovery period. Pumping periods longer than 12 hours are required to determine the effects that hydrologic boundaries caused by lithologic changes or geologic structure have on the hydraulic properties of the aquifer near a well. Recovery data are desirable because well recovery is unaffected by well and pump efficiencies and delayed-yield response. Most of these tests were too short for equilibrium to be reached; therefore, nonequilibrium techniques were used to evaluate well- and aquifer-test data for this study.

Equilibrium and nonequilibrium well- and aquifer-testing methods that are used to determine hydraulic properties of aquifers are suspect when applied to fractured-rock environments for several reasons. Most of the aquifer-test methods are designed to evaluate porous media that is homogeneous and isotropic. In many cases, fractured consolidated rocks are characterized by extreme heterogeneity and anisotropy. Fracture characteristics, such as orientation, spacing,

aperture, extent, and interconnectivity, can vary considerably within the formation and from one formation to the next formation. Anisotropy is attributed to preferred flow directions along parallel to subparallel fracture sets that are either vertical or horizontal. To fully characterize the anisotropy, it is necessary to determine the magnitudes of the hydraulic conductivity in three principal directions (Kaehler and Hsieh, 1991). Often it is assumed (as in this study) that one principal direction is vertical and the other two are horizontal. Data needed to quantify the heterogeneity and anisotropy in most of the regional aquifer are undefined.

Recognizing the limitations of many of the well and aquifer tests analyzed, estimates of transmissivity were derived from the specific capacity calculated for most of these well tests conducted in the study area. A few selected wells that had drawdown and recovery data of sufficient time to use the nonequilibrium methods of either Theis (1935) and (or) Cooper and Jacob (1946) were processed using the software Aquifer Test (Waterloo Hydrogeologic, Inc., 1999). Corrections for both unconfined (Jacob, 1950) and partial-penetrating conditions (Hantush, 1962; Roscoe Moss Co., 1990) were applied where necessary. Calculations were made on both drawdown and recovery data because the respective data provide a useful and independent check on the calculated values and reflect different aspects of the well, formation, and structural characteristics. Resulting transmissivity and effective saturated-thickness estimates were used to derive hydraulic conductivity.

Storage coefficient and (or) specific yield were available from previously published or reported well and aquifer tests. Storage coefficient and (or) specific yield can be determined from either drawdown or recovery data from observation wells monitored during aquifer tests. Storage-coefficient and (or) specific-yield data derived from a pumping well generally are not considered valid. Storage-coefficient or specific-yield estimates were available on the basis of drawdown or recovery data at 11 observation wells. Storage coefficients were calculated for wells where confined conditions exist, and specific yield was calculated where unconfined conditions exist.

Remote Sensing

Remote-sensing data and methods developed by Chavez and others (1997) for this study include (1) remote-sensing satellite images, (2) digital-elevation models, and (3) digital-image processing. These data and methods have been helpful in detecting and mapping regional physiographic and structural trends that include major fracture systems (Chavez, 1984; Chavez and Bowell, 1988; and Chavez, 1992). The main focus of this work was to use digital-image processing, digital-satellite images, and a digital-elevation model (DEM) to extract spatial information related to structural and topographic patterns. Data used were from the Landsat Thematic Mapper (TM) and the French S*ysteme Probatorie d'Observation de la Terre* (SPOT) imaging system along with a DEM of the study area (figs. 3–5). Linear features on the images, such as the trace of fractures and fracture zones, ridges and valleys, deflected stream-channel segments, vegetation lines, and abrupt changes in soil color, were associated with structural elements such as joints, faults, and grabens. These structural elements were investigated in greater detail as part of the surface-geology mapping.

Surface-Geologic Mapping

Geologic structure inferred photogrammetically and from remote-sensing data provided the basis for field mapping and interpretations of geologic structural features on the surface completed by G.M. Mann and Dr. A.E. Springer (geologists, NAU, written commun., 1997; pls. 1 and 2, this report). This information was re-evaluated for use in this report, and additional structural information was obtained for adjacent areas (pls. 1 and 2).

Geophysics

Geophysical methods—ground-penetrating radar (GPR), seismic reflection, seismic refraction, square-array direct-current azimuthal resistivity (SAR), gravity, and borehole logging—were used to locate fractures in the subsurface, and, in some cases, zones of water saturation and enhanced permeability. As a fracture propagates toward the surface, its vertical and directional orientation can change and horizontal- and bedding-plane fractures may have no surface expression. Once a surface trend is identified, surface-geophysical methods can image the subsurface in a noninvasive manner to determine if there is a geologic structure relative to the surface trend. Each of the methods, however, is limited by the physical properties of the material being measured. In addition, some of these methods are labor and cost intensive, which makes them better suited for detailed site investigations rather than reconnaissance tools.

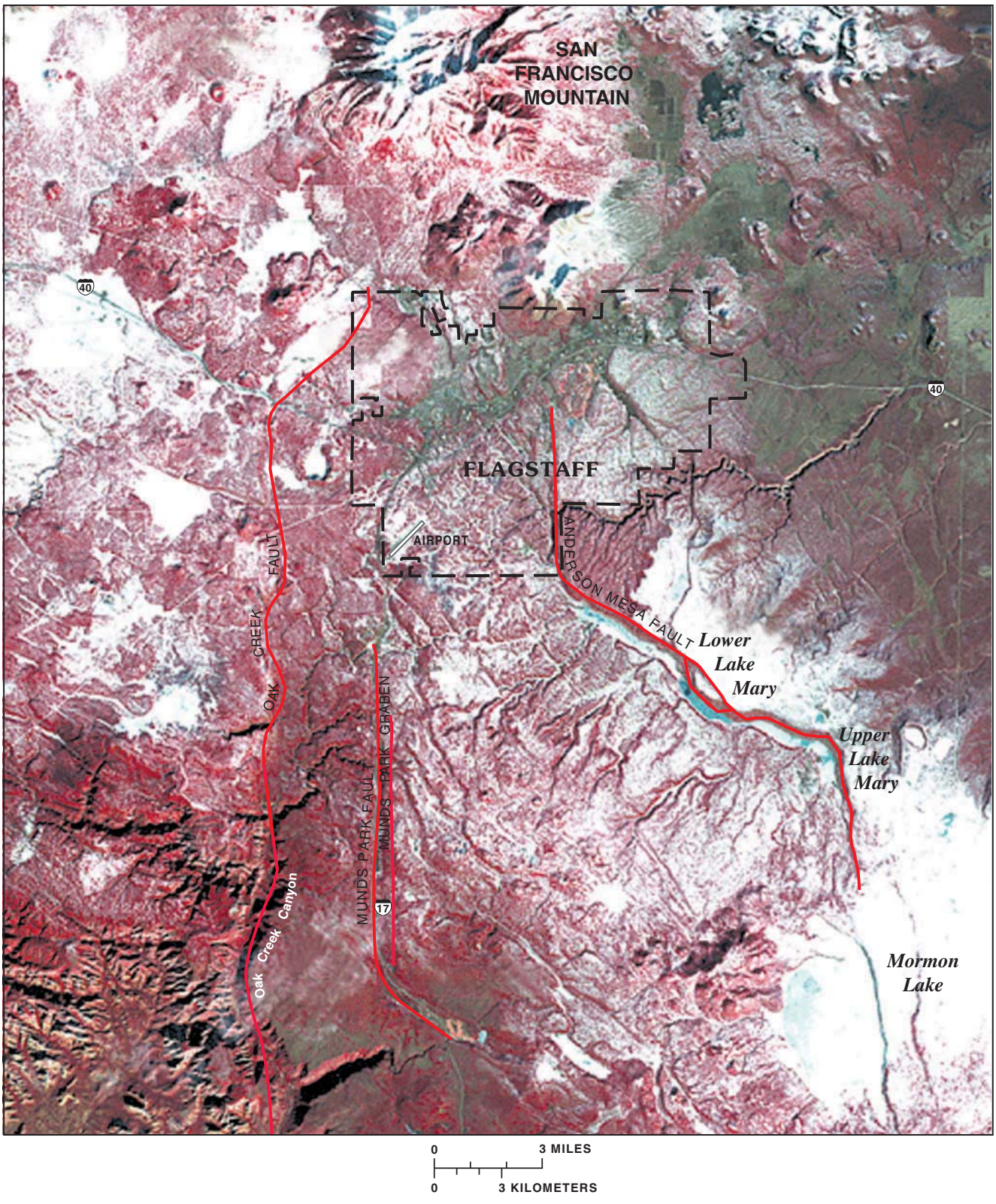

Figure 3. Landsat Thematic Mapper image, January 15, 1983, Flagstaff, Arizona (from Chavez and others, 1997).

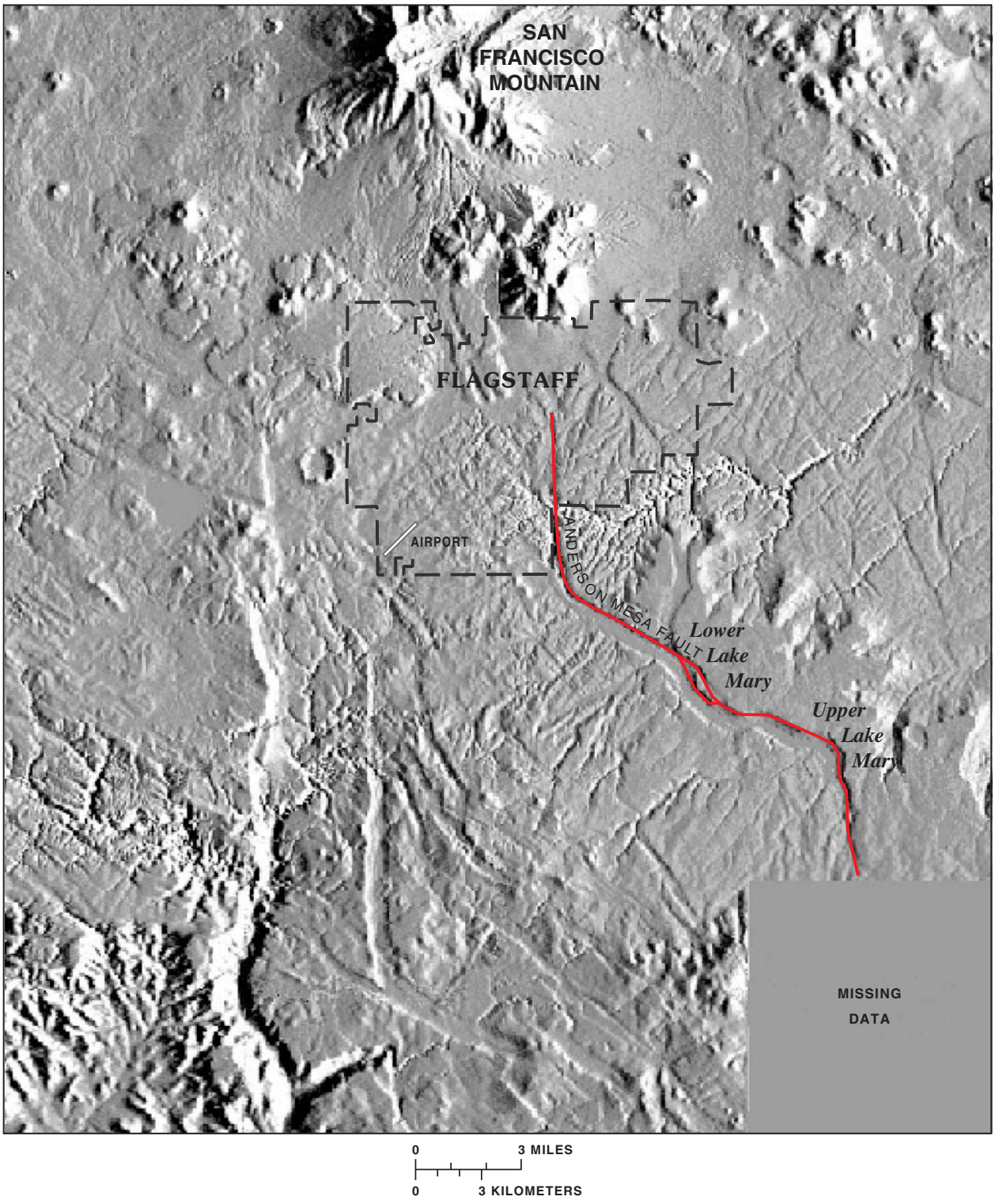

Figure 4. Shaded relief digital-elevation model of Flagstaff, Arizona (from Chavez and others, 1997).

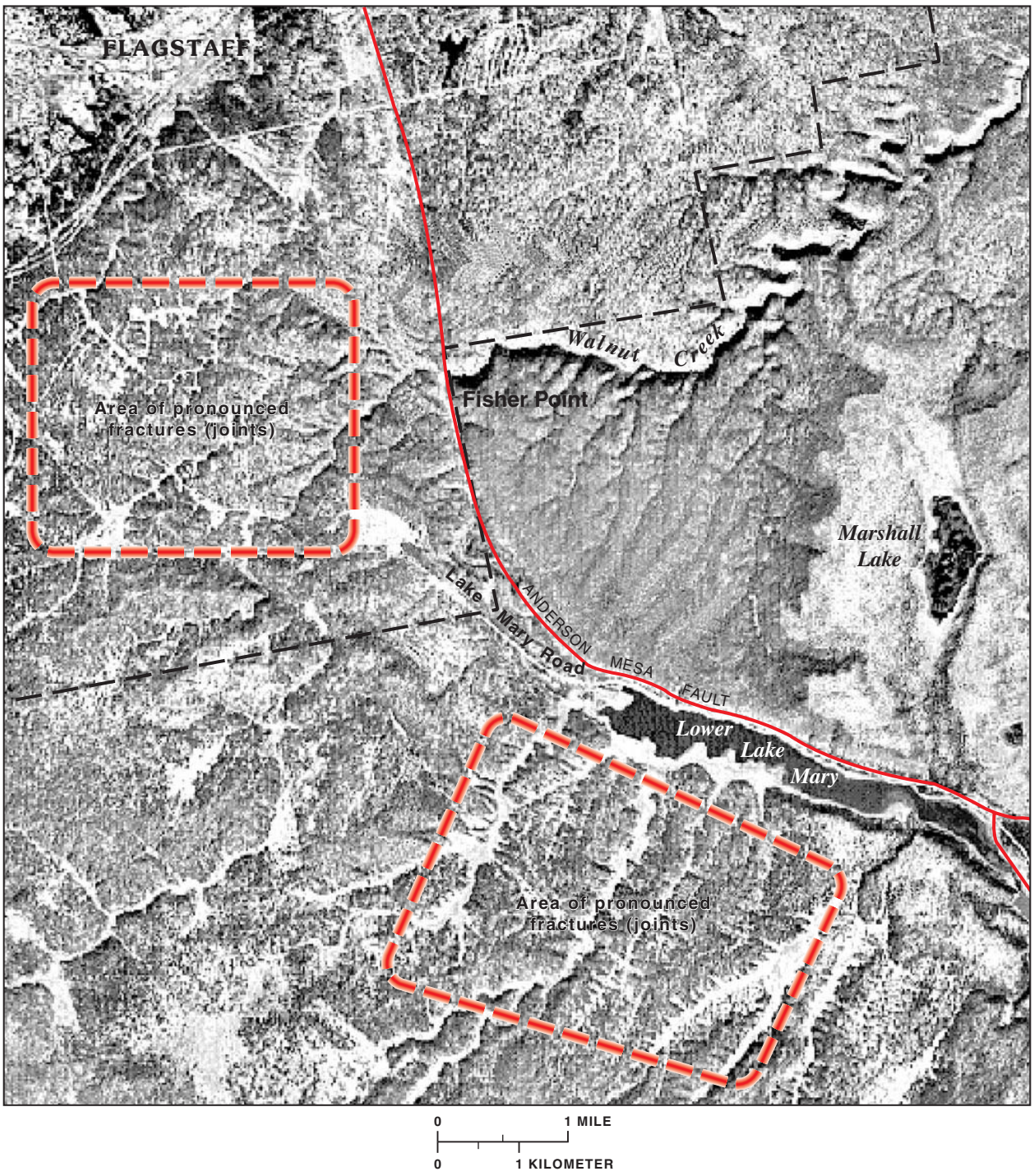

Figure 5. SPOT panchromatic image enlargement of the Fisher Point-Lower Lake Mary area, November 7–8, 1995, Flagstaff, Arizona (from Chavez and others, 1997).

The five sites chosen for application of surface-geophysical methods were the Lake Mary and Woody Mountain well fields, Skunk Canyon, Foxglenn, and Continental (**fig. 1**). The Lake Mary area was chosen as the principal test site for GPR and SAR because it is accessible and the hydrogeologic characteristics have been well documented. The Woody Mountain area was used to further test SAR because the area allowed investigations to the limit of the equipment. Seismic-reflection and seismic-refraction methods were not tested before their use because the application of these methods in similar geologic environments is well documented.

Four surface-geophysical methods—GPR, seismic reflection, seismic refraction, and SAR—were used to investigate subsurface structure of the Skunk Canyon, Foxglenn, and Continental areas (**fig. 6**). These sites were selected for geophysical investigations as a result of the analysis of remotely sensed data, photogrammetry, and mapping of surface-structural features. The GPR data are represented as cross-section profiles that show bedding and other horizontal features as reflectors of radar energy. Fractures and other subsurface features are indicated by disruptions of the main reflectors and (or) as hyperbolic events in the profile.

Seismic data also are represented as cross-sectional profiles of the subsurface; however, in this case, the horizontal features are represented as reflectors of seismic energy. Fractures and other subsurface features also are indicated by disruptions of the horizontal reflectors. The square-array data sets produce azimuthal plots of apparent resistivity and apparent-strike direction, coefficient of anisotropy, and secondary porosity percentage with depth (see the "**Supplemental Data**, Part A" at the back of the report).

Ground-Penetrating Radar

GPR is an electromagnetic technique that uses radio waves—typically in the 1 to 1,000-megahertz frequency range—to map underground structures and is similar to seismic-reflection and sonar methods. A transmitting antenna radiates a short pulse of high-frequency electromagnetic energy into the subsurface. As the radiated energy propagates through the subsurface, variations in the electrical properties of the subsurface material cause part of the radiated energy to be reflected back toward the surface and part to be transmitted deeper into the subsurface (**fig. 7**). In soils, variations in electrical properties usually correspond to changes in volumetric water content. In rock, the radar is sensitive to changes in rock type and water-filled or dry fractures (Davis and Annan, 1989). The reflected signal is detected by the receiver where it is amplified; transformed to audio-frequency range; and recorded, processed, and displayed by the receiving antenna and processing software. Depending on the frequency and the permittivity properties of the host rock, GPR can penetrate to depths of about 140 ft. Permittivity is an electrical property of matter that influences radar returns. In most cases in the Flagstaff area, 140 ft is not deep enough to image rock units in the regional aquifer. The depth, however, is enough to verify that surface expressions of fractures extend far enough into the subsurface to warrant further investigation using other geophysical methods.

GPR was selected as a reconnaissance tool to verify the extent in the shallow subsurface of surface trends that were identified by remote sensing and surface-geologic mapping. GPR is portable, easy to use, and allows for the rapid evaluation of many potential sites. Unless otherwise noted, surveying was done using the single-fold, fixed-offset, reflection-profiling method described by Sensors and Software (1994) in step mode because of the rough terrain. Survey lines were staked and surveyed to determine elevation differences so the radar profiles could be corrected.

Seismic Reflection and Seismic Refraction

Seismic reflection and seismic refraction are used to map trends of geologic structure at depth by imaging discontinuities or offsets in marker beds, which are rock layers that show significant contrast in seismic velocity, and measuring changes in compressional- and shear-wave velocities and attenuation. Seismic reflection provides an image of the subsurface and is best suited for layered stratigraphy. Seismic refraction measures the velocity at which seismic waves propagate through the subsurface and is well suited for locations where there are assumed to be vertical and lateral changes in velocity. Seismic-wave velocity is directly related to the density and saturation of formation material (R.D. Catchings and W.H.K. Lee, geophysicists, USGS, written commun., 1997); therefore, seismic- refraction measurements can enhance the seismic-reflection imaging by providing data that can be used to infer composition and physical conditions in the subsurface.

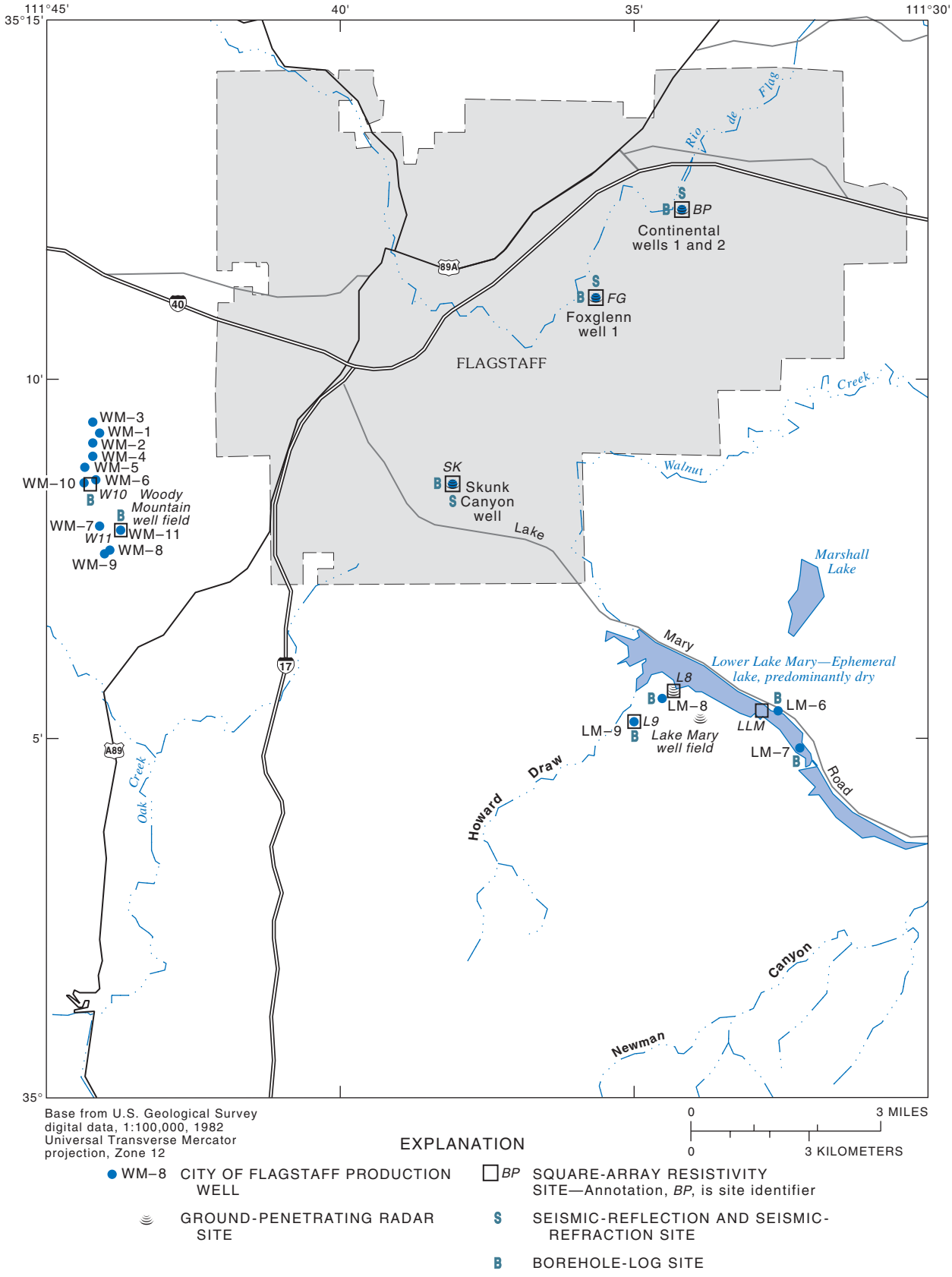

Figure 6. Locations of selected wells and geophysical test sites, Flagstaff, Arizona.

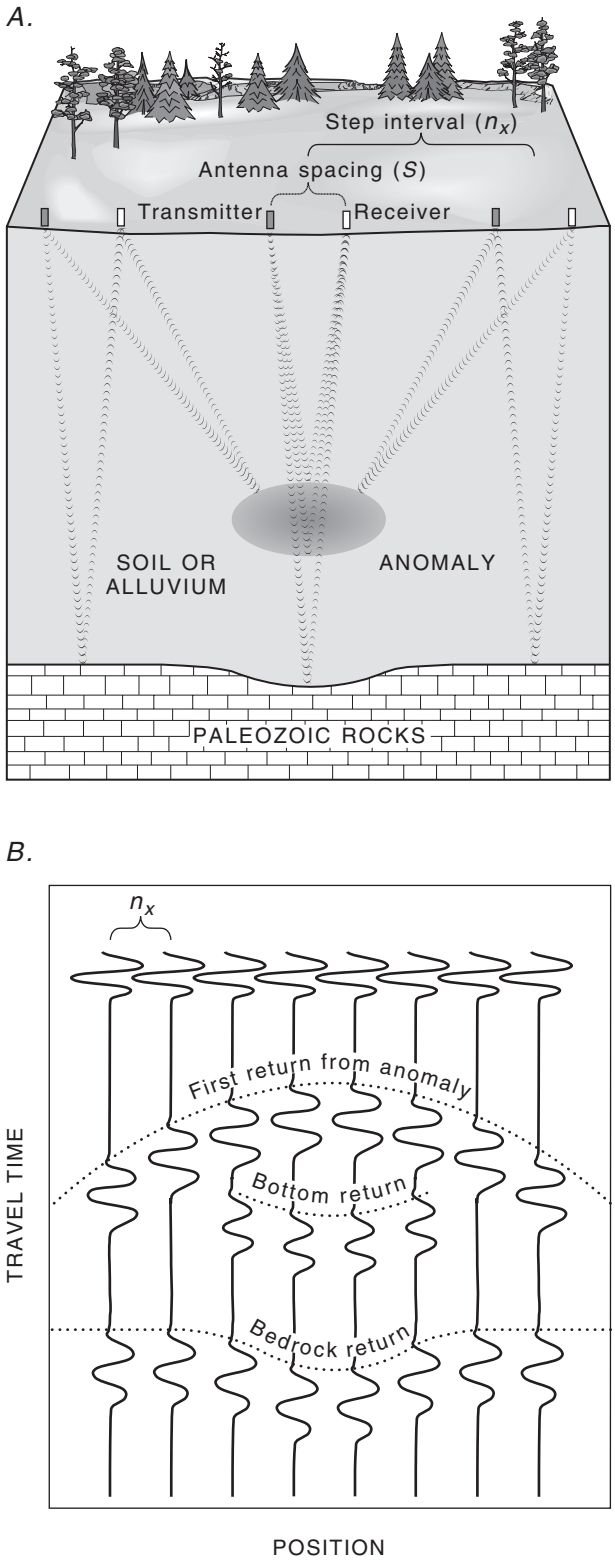

Figure 7. Ground-penetrating radar technique (from Sensors and Software, 1994). *A*, Common-offset single-fold profiling. *B*, Format of reflection section showing interpretation of radar data for features in figure 8A.

Seismic refraction is particularly useful in identifying subsurface fractures because fractures are known to cause appreciable reduction in the seismic velocity relative to the surrounding media (Williams, 1994; R.D. Catchings and W.H.K. Lee, geophysicists, USGS, written commun., 1997). The velocity and amplitude of the shear waves are reduced further where rocks are saturated; however the compressional waves are unaffected under this condition (Nur, 1982).

Two high-resolution, combined seismic-reflection and seismic-refraction profiles were made at the Skunk Canyon, Foxglenn, and Continental sites to obtain images from about 900 to 2,500 ft in depth (**fig. 8**). Major fracture systems inferred at these sites from remotely sensed data and geologic mapping were the targets of investigations (Chavez and others, 1996, 1997; G.M. Mann and Dr. A.E. Springer, geologists, NAU, written commun., 1997). Final location of the seismic lines was facilitated by reconnaissance GPR surveys. One-pound charges of ammonia nitrate buried to depths of about 10 ft were used to generate the seismic energy. The seismic energy was detected by geophones placed about 8.2 ft apart along the survey lines and recorded by multichannel seismographs. The recorded seismic data were processed by computer to generate seismic images of the subsurface. Acquisition and data-processing components are described by Catchings and others (1997) and Jaasma and others (1997).

The seismic-reflection sources and sensors were used to simultaneously acquire seismic-refraction data. Because the distance between the source and sensors is known, the velocity at which seismic energy propagates through the subsurface layers can be calculated. Velocity information is used to determine which areas are underlain by consolidated rock and which are underlain by unconsolidated sediments. Seismic velocities are typically much lower in unconsolidated sediments than in consolidated rock. More importantly, the shallow-velocity information then is used in processing the seismic-reflection image.

The greatest variation in seismic velocities generally occurs near the land surface from lateral variation in the rock or sediment. These lateral variations make it difficult to stack (add) the seismic signal from each energy source into a single seismic section. Because stacking is critical to obtaining a clear image of the subsurface, detailed knowledge of near-surface variations in velocity is necessary for high-resolution imaging. At high frequencies, the shallow sedimentary subsurface in the study area is highly reflective; therefore, lower frequency (<100-Hertz) geophones were used so that the deeper subsurface could be imaged.

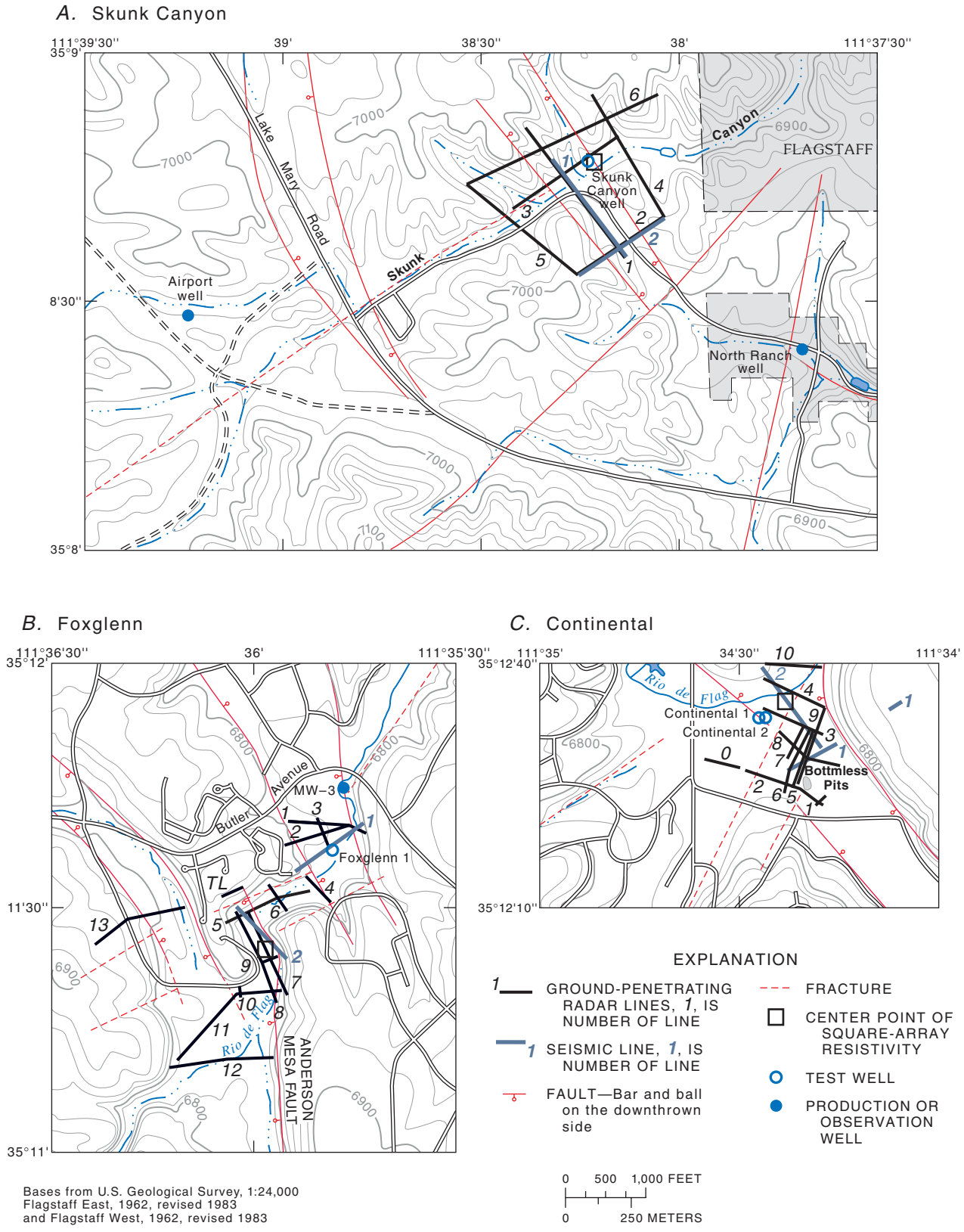

Figure 8. Locations of selected wells and sites where ground-penetrating radar, square-array resistivity, seismic-reflection, and seismic-refraction data were collected near Flagstaff, Arizona. *A*, Skunk Canyon. *B*, Foxglenn. *C*, Continental.

The seismic-reflection images resemble a cross section of the subsurface in which (in theory) shaded portions of the seismic wavelet represent a reflection from the interface between two stratigraphic layers. Because of the layered nature of the rock units in the study area, the subsurface produces abundant reflections that can be traced for several tens to hundreds of feet before they are vertically displaced. Faults on the seismic sections are interpreted where reflectors have been vertically displaced or laterally disrupted.

Square-Array Resistivity

The SAR technique was used to determine the orientation of fractures and the degree of secondary porosity (Lane and others, 1995) and to measure the electrical conductivity of the rock and water. Using this technique, fracture zones generally are indicated by decreased resistivity; water in the fracture zone or a fault further decreases the resistivity.

The SAR technique is much like the Schlumberger or Wenner collinear-array methods. The point of investigation is the center point of the square, and the array size (a) is the length of the side of the square. Electrodes are placed at the corners of the square, and potential and current wires are connected from the transmitter to the electrodes. The array is expanded symmetrically about the center usually in increments of $a\sqrt{2}$, so that the soundings can be interpreted as a function of depth. Three measurements are made for each square setup—two perpendicular (alpha and beta) and one diagonal measurement (gamma; fig. 9A–B). Depth of investigation is roughly equivalent to the size of the square (Habberjam, 1979).

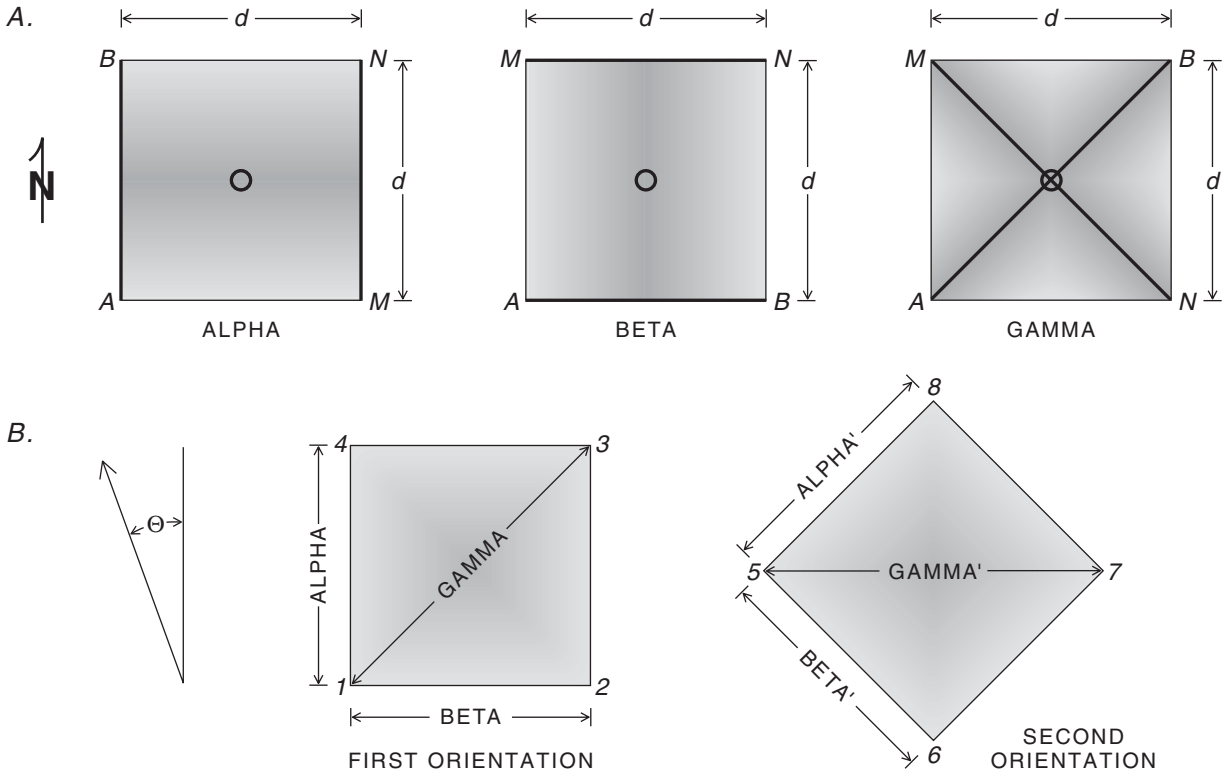

Figure 9. Electrode configurations and crossed array. *A*, Three resistivity measurements: alpha (α), beta (β), and gamma (γ). *AB* are the current electrodes, and *MN* are the potential electrodes in each square-arry setup. Notice in this configuration alpha provides a north-south orientation, and beta provides an east-west orientation if the top of the page is north. The gamma configuration provides a check on alpha and beta. Resistivities (ρ) of homogeneous isotropic material are ργ=0, and ρα=ρβ. Resistivities in heterogeneous anisotropic ground are ρβ=ρα+ργ. *B*, Electrode positions for a crossed array. Habber jam (1972) showed that an apparent fracture-strike value, o for that spacing can be obtained by calculating the geometric mean pm obtained from two square arrays separated by a rotational angle of 45°.

The final size of the square depends on the desired depth of investigation, space limitations, and ability to pull or lay wire through vegetation and over rough terrain. Once the largest square measurements are made, the wires are reeled in and the square is rotated (a 15° rotation was used) and expanded again. Six expansions with 12 directions are required to provide a resistivity measurement every 15° for 180°. The graphical display is mirrored on a polar-coordinate diagram using methods of Taylor and Fleming (1988) to get a 360° plot.

Although the SAR technique has been used successfully in areas with layered sedimentary rocks, the ability of the technique to penetrate the layers of unconsolidated and volcanic material that overlie the sedimentary rocks in much of the study area was unknown. The technique was first tested to verify its utility in the Lake Mary area where faults and other fractures have been previously identified. These fractures are the cause of high well yields in this area. SAR then was applied at the Skunk Canyon, Foxglenn, Continental (**fig. 8**), and Woody Mountain sites. These areas were selected for further study on the basis of available remote-sensing data that indicated a high probability of significant fracturing in the subsurface.

During the summer of 1996, eight SAR soundings were made near or in the city limits of Flagstaff. Soundings were made near existing wells for control, in areas where additional data were needed, where data could be extrapolated from existing wells, or where the City of Flagstaff planned to drill wells. The SAR technique provided several important pieces of information that are not available using other geophysical methods.

1. Polar plots of the azimuthal resistivity that provided a graphical interpretation of fracture orientations with depth. In addition, a strike direction of the major fractures was calculated from crossed square-array apparent-resistivity values.
2. The mean-resistivity curves from the averaged soundings were translated into Schlumberger curves (Schlumberger, 1920) and, in some cases, interpreted to estimate depth to the saturated zone.
3. Coefficients of anisotropy were calculated and plotted against depth of investigation for a crossed array as an indication of rock fracturing.
4. If the conductivity of the ground water at the sounding site was known, estimates of secondary porosity were made by applying the method of Taylor (1984).

Electrical-resistivity methods are the most widely used geophysical methods in ground-water investigations (Keller and Frischknecht, 1966). The reasons are mainly simplicity of instruments and operation, low operational costs, and a feasible depth range, suitability to a wide spectrum of subsurface problems, and easy methods of interpretation. The resistivity of earth materials is measured in units of the ohm-meter, which is the electrical resistance of a cube of material with dimensions of 3.28 ft (1 m) on a side. In the field and under laboratory conditions, earth materials have an observed-resistivity range well over five orders of magnitude. For example, graphitic schists in Chapada Diamantina, Brazil, have a measured-apparent resistivity near 0.25 ohm-meters (D.B. Hoover and H.A. Pierce, hydrologists, USGS, written commun., 1984); whereas, the resistivity of dry rhyolitc rocks in Newberry Crater, Oregon, is as much as 100,000 ohm-meters in some places (A.A.R. Zohdy, emeritus scientist, USGS, oral commun., 1988). The resistivity of a water-bearing rock depends on the salinity, temperature, quantity, and distribution of water through the formation unit (Keller, 1989).

The SAR technique originally was developed as an alternative to the collinear arrays, such as Schlumberger, Werners, and dipole-dipole, when dipping subsurface, bedding, or foliation was present (Habberjam and Watkins, 1967). Habberjam (1972) used a square array and demonstrated that it is more sensitive to anisotropy and requires less surface area than collinear arrays. Lane and others (1995) applied the technique to fractures in crystalline rock and used commercial computer software to provide layered-earth interpretations of the data.

An experimental SAR sounding in a crystalline granite terrain in Payson, Arizona (Pierce, 1996), confirms the utility of the technique and provides valuable joint-trend and substructure information. In addition, Pierce and Hoffmann (1996) presented preliminary results of the SAR soundings for the Flagstaff study area and determined that depth to the semisaturated zone above the regional aquifer could be closely approximated.

Gravity

Previously collected gravity data were evaluated to determine their use in defining local structural trends. The data were reprojected to Universal Transverse Mercator (UTM) from the original Albers projection, and a simple Bouguer gravity map and color image were generated. The UTM grid was then run through BOUNDARY (Blakely and Simpson, 1986), which is a package of computer programs used to locate the horizontal coordinates of the edges of gravity sources from grid data. BOUNDARY uses the principles that state that the maximum horizontal gradient of a gravity anomaly is close to the edge of tabular sources (Cordell, 1979; Grauch and Cordell, 1987). BOUNDARY generates a computer file of maximum horizontal-gradient locations by scanning each grid intersection in four directions— horizontal, vertical, and two diagonals.

Borehole

Borehole-geophysical methods were used in selected wells to verify the results of the surface-geophysical surveys. Acoustic-televiewer, flowmeter, and borehole-video logs provided information on the extent and orientation of water-transmitting fractures in the subsurface near the borehole. Caliper, gamma, electric, and temperature logs were used to infer qualitative information about water-bearing characteristics of the rock units. Neutron and density logs provided in-place information on primary and secondary porosity of the formation.

After surface-geophysical investigations were completed, the City of Flagstaff drilled a total of four wells at Skunk Canyon, Foxglenn, and Continental. Because of difficulty in drilling and maintaining an open borehole at these sites, some of the borehole-geophysical logs are not complete. Video logs were completed for selected intervals at each of the well sites. Acoustic-televiewer logs were completed at Foxglenn and Continental well 2; however, flowmeter logs could only be obtained in the Skunk Canyon well. Gamma and electric logs were completed only at the Skunk Canyon and Continental sites because of the instability of the boreholes at Foxglenn. Lithologic logs for all three sites were constructed from borehole cuttings.

Water Chemistry

Water samples were collected from selected wells and springs and snowmelt to corroborate data from the geophysical methods and contribute data used to determine ground-water movement, ages, and sources and areas of recharge (**fig. 10**). Well selection was based on existing water-chemistry data, accessibility, location, aquifer type, and construction. Selected springs were sampled on the basis of aquifer type and location. Snowmelt samples were collected to represent different altitudes in the study area. Water was collected from 21 wells, 3 springs that discharge from the regional aquifer, and 2 snowmelt sites. In addition, water was collected from four shallow wells, two springs that discharge from perched water-bearing zones above the regional aquifer, and two surface-water sites.

As part of this study, data were collected from some previously sampled wells and springs, and from additional sites to fill in gaps in the data. Existing water-chemistry data also were obtained from records for wells monitored by the City of Flagstaff, from other local water companies, from private well owners, and from studies by Appel and Bills (1981) and McGavock and others (1986). Well-construction data and well logs were used to determine the geologic formation exposed to the screened interval of the well.

Samples were collected from pumped wells or flowing springs through a sampling manifold at land surface to minimize contact with air and other potential sources of contamination. To ensure that collected samples were representative of the aquifer, pH, specific conductance, dissolved-oxygen concentration, and water temperature were monitored until they became stable. When possible, this was done using a Hydrolab Surveyor II, which provided a closed flow-through chamber. Samples of snow were allowed to melt at room temperature, and the snowmelt was processed similar to samples of water from wells and springs.

A 0.45-micrometer pore-size filter was used in a prerinsed filtration apparatus to collect samples for the analysis of dissolved constituents, common ions, trace elements, nutrients, and strontium ($^{87}Sr/^{86}Sr$). Nitric acid (1.0 normal HNO_3) was used on site to acidify samples to a pH of less than 2 as a preservative for trace elements, most cations, and $^{87}Sr/^{86}Sr$.

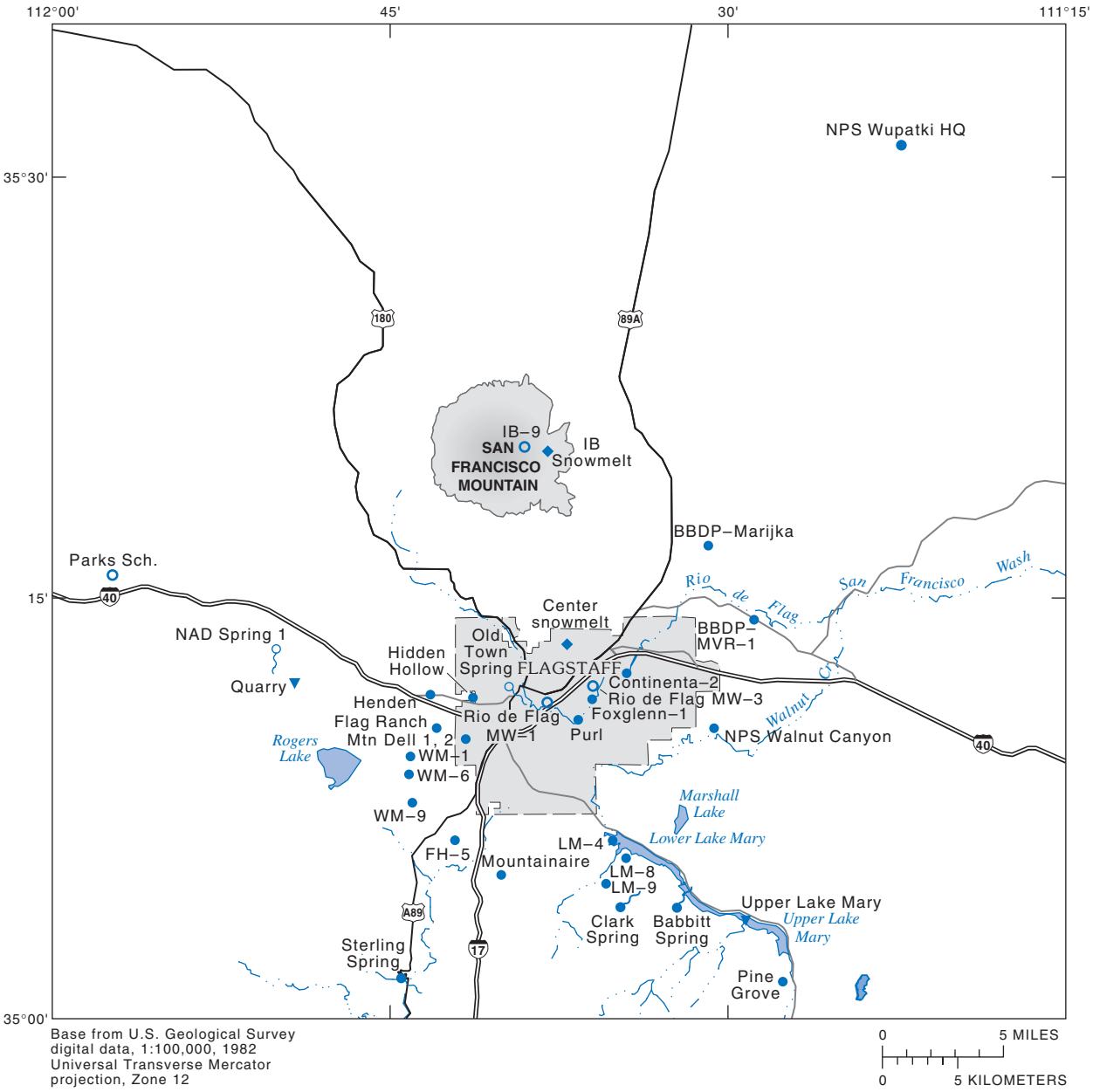

EXPLANATION

- WM–6 REGIONAL-AQUIFER WELL—Annotation, WM–6, denotes city well number
- PERCHED-AQUIFER WELL
- REGIONAL-AQUIFER SPRING
- PERCHED-AQUIFER SPRING
- SURFACE-WATER SITE
- SNOWMELT SITE

Figure 10. Locations of selected wells, springs, and surface-water and snowmelt sites where water samples were collected for chemical and isotope analysis, Flagstaff, Arizona.

Raw unfiltered samples were collected for the determination of isotopes of oxygen ($^{18}O/^{16}O$), hydrogen ($^{2}H/^{1}H$), carbon-14 (^{14}C), carbon-13 ($^{13}C/^{12}C$), tritium (^{3}H), and some common ions and nutrients. Samples for $^{18}O/^{16}O$ and $^{2}H/^{1}H$ analyses were collected in 60-milliliter glass bottles that were filled to the top and sealed to prevent evaporation. Samples for determination of ^{14}C and $^{13}C/^{12}C$ were collected by filling 15.5-gallon containers slowly from the bottom and covering the top to prevent ambient carbon from dust and air mixing with the sample. Samples for ^{3}H analysis were collected in a 1-liter polyethylene bottle. Water for field-alkalinity determination was filtered through a 0.45-micrometer pore-size filter. Some alkalinity determinations were made at the field office in Flagstaff, and some were performed at the site. Alkalinity determinations made at the field office were done within 2 hours of sample collection.

The USGS National Water Quality Laboratory (NWQL) in Arvada, Colorado, analyzed samples for common ions, nutrients, and trace elements, and $^{18}O/^{16}O$, $^{2}H/^{1}H$, and ^{3}H. Analyses for ^{14}C and $^{13}C/^{12}C$ were done by the University of Arizona in Tucson. Analyses for $^{87}Sr/^{86}Sr$ were done by the USGS National Research Program (NRP) laboratory in Denver, Colorado. USGS laboratories in Menlo Park, California, and Reston, Virginia, analyzed samples for $^{18}O/^{16}O$ and $^{2}H/^{1}H$, respectively.

Common Ions, Trace Elements, and Nutrients

Analyses of samples for common ions, trace elements, and nutrients were used to estimate the chemical processes and reactions that determine the chemical composition of the ground water. Variations in water composition can provide information on hydrologic relations between water-bearing units and on ground-water movement.

Stable Isotopes

Stable-isotope data are useful in delineating recharge areas and the hydrologic relations of different water-bearing units. Stable isotopes of an element are measured relative to a standard in which the ratio of the two isotopes (for example $^{18}O/^{16}O$) are known. The standard used is the Vienna Standard Mean Ocean Water (SMOW), prepared and distributed by the International Atomic Energy Agency (1969).

Deviation of the sample from the standard is expressed by a delta (δ) notation, in per mil, which is parts per thousand (‰). The delta notation is computed from the equation

$$\delta = \frac{R_x - R_{std}}{R_{std}} \times 1,000, \qquad (1)$$

where

δ = delta notation,
R_x = ratio of isotopes measured in sample, and
R_{std} = ratio of same isotopes in the standard.

The water molecule, H_2O, typically undergoes a physical fractionation called evaporation. The lighter ^{16}O and ^{1}H molecules will preferentially move from the water phase to the vapor phase leaving behind the heavier ^{18}O and ^{2}H molecules. This action will affect the isotopic signature of the water sample by making it more positive or enriched in the heavier water molecules.

Craig (1961) generated an *x-y* plot of $\delta^{2}H$ and $\delta^{18}O$ for about 400 samples of water from rivers, lakes, and precipitation from various places in the world. Data from these samples fell on a line defined as

$$\delta^{2}H = 8\delta^{18}O + 10 \qquad (2)$$

and called the global meteoric water line. Dansgaard (1964) subsequently studied large bodies of data gathered by the International Atomic Energy Commission (1969) and determined that temperature is the single most important component that directly determines the isotopic signature for precipitation. The composition of precipitation depends on the temperature at which the ocean water is evaporated and more importantly the temperature of the condensation at which clouds and rain or snow are formed. This *temperature effect* is important in determining which regions with summer and winter precipitation may have summer or winter recharge (Mazor, 1991).

Radiogenic Isotopes

The geochemical model NETPATH was used to translate ^{14}C data from percent modern carbon (pmc) to years (Plummer and others, 1991). For the specification of this particular ground-water flow

system, the model by Fonts and Garnier (1979) was used on the assumption of (1) an open system (gas-solution equilibrium) so that the model can back calculate an initial $\delta^{13}C$ for soil CO_2, and (2) 0.0 ‰ $\delta^{13}C$ is the inorganic carbon signature for the carbonate rocks.

Natural background ^{3}H levels are about 5 tritium units (TU); however, anthropogenic ^{3}H was produced from atmospheric thermonuclear tests that began in 1952. Anthropogenic ^{3}H peaked in about 1963 before atmospheric testing was banned (Mazor, 1991). Consequently, semiquantitative age dating of ground water is possible as follows:

- Water having less than 0.5 TU was recharged before 1952,
- Water having more than 10 TU typically can be assumed to have recharged after 1952, and
- Water having more than 0.5 TU and less than 10 TU probably is a mixture of pre-1952 and post-1952 water.

Strontium (Sr) has an ionic radius of 1.13 angstroms (Å), which is only slightly larger than the ionic radius of calcium (Ca, 0.99 Å). This slight difference in size allows Sr to replace Ca in many minerals. The isotopic abundance of the stable isotopes of Sr is variable because of the decay of naturally occurring rubidium (^{87}Rb), which makes the precise isotopic composition of Sr in a rock or mineral dependent on the age of the rock and the $^{87}Rb/^{87}Sr$ ratio of that rock.

HYDROGEOLOGIC SETTING

The study area is at the southern edge of the Colorado Plateau in northern Arizona. Structural warping has caused the repeated advance and withdrawal of oceans across this area resulting in the deposition of several thousand feet of sediments over hundreds of millions of years. Uplift and crustal compression from the late Cretaceous to early Tertiary ages has raised this part of the Colorado Plateau to near its present altitude, created broad regional faults and folds, and resulted in volcanic activity that began in the Paleocene age and has continued to the present. Basin and Range development and its associated crustal extension from the late Tertiary age to the present has resulted in development of many additional faults, joints, and grabens.

The study area is underlain by plutonic and metamorphic rocks, a bedded sequence of sedimentary rocks, and alluvial and volcanic rocks that range in age from Precambrian to Quaternary (**fig. 11**, **pl. 1**). The lithology and hydrologic characteristics of the rocks vary among units and within individual units in the study area. Although more ground water can be contained volumetrically in the fine-grained sediments, ground water moves slowly through these types of sediments. The medium- to coarse-grained sediments contain less water volumetrically, however, they transmit the water more readily through the primary pore spaces in the rock. Secondary physical and chemical alteration of the sedimentary rocks also affect their hydrologic character. Geologic structures, such as folds, faults, and joints affect the regional ground-water flow system in some places.

Hydrogeologic Units

The plutonic and metamorphic rocks are Precambrian in age and are buried deep beneath the study area. The rocks are inferred to be the same rocks of Precambrian age exposed in the Grand Canyon to the north and northwest and consist of plutonic igneous rocks, mafic schist, and gneiss (Barnes, 1989). Where found in oil and gas test wells in the study area, the plutonic and metamorphic rocks typically are massive red granites or granite rubble. Because of their massive crystalline nature, the Precambrian rocks represent the lower confining layer to ground-water flow on the southern Colorado Plateau. Water probably does not penetrate these rocks except where they are extensively fractured.

The Tapeats Sandstone and Bright Angel Shale (Noble, 1922) are Cambrian in age and overlie the plutonic and metamorphic rocks of Precambrian age. The Tapeats Sandstone is a very coarse- to medium-grained, thin-bedded conglomeratic sandstone that is tan to brown to reddish brown in color. The Bright Angel Shale is micaceous shale, siltstone, and minor amounts of fine-grained sandstone that varies in color from green to blue to gray. Because of the lack of deep well data, however, little is known about the water-bearing characteristics of the Tapeats Sandstone or Bright Angel Shale in the study area.

The Muav Limestone, which is Cambrian in age, and the Temple Butte (Martin) Formation, which is Devonian in age (McKee and Resser, 1945), overlie the Tapeats Sandstone and (or) Bright Angel Shale.

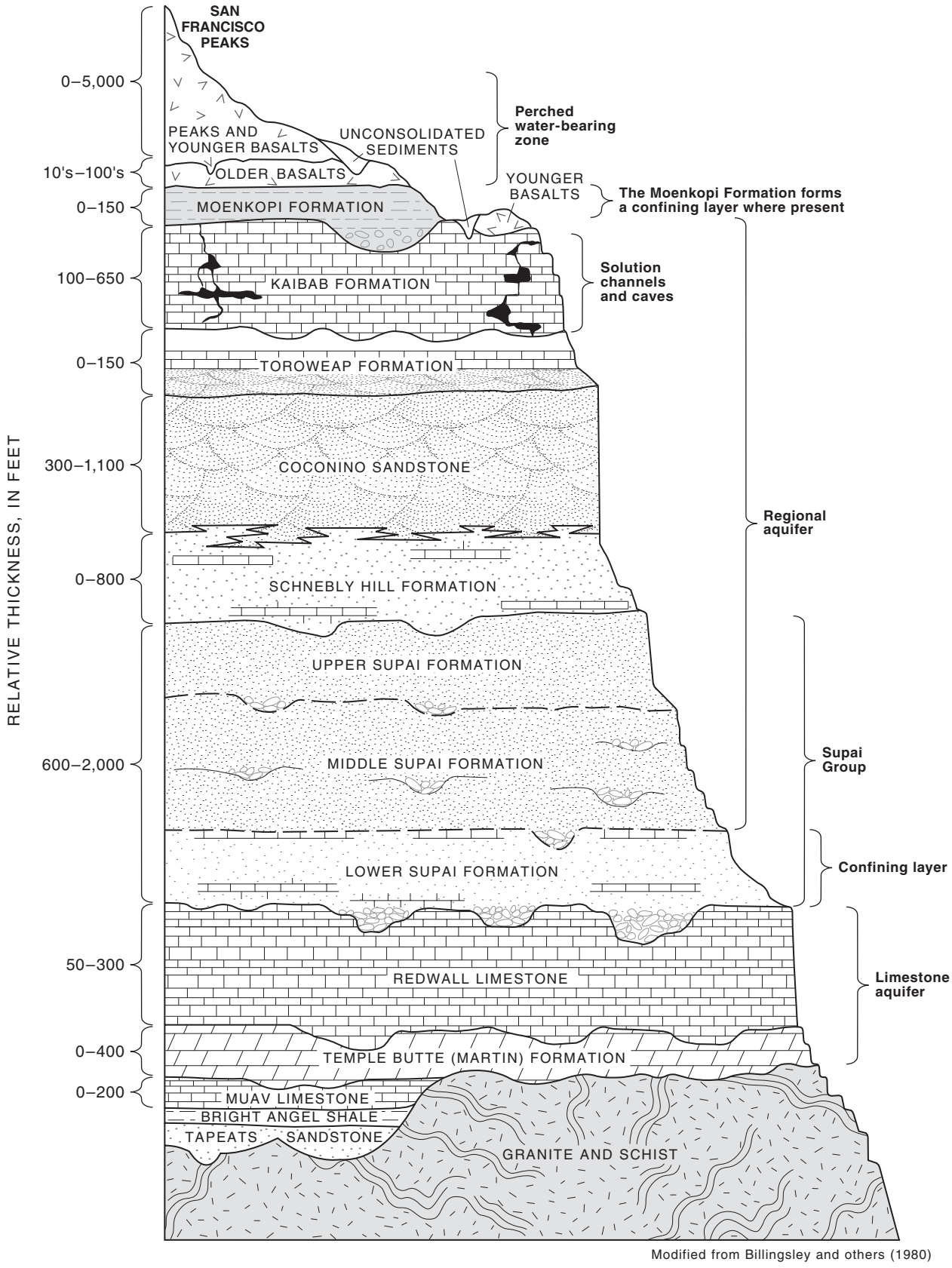

Figure 11. Generalized stratigraphic section of rock units, Flagstaff, Arizona.

In some areas, however, only one of the two formations is present. The Muav Limestone (Noble, 1922) is a thin-bedded, gray, medium- to fine-grained, mottled dolomite; a coarse- to medium-grained grayish-white, sandy dolomite; and a fine-grained limestone. The Temple Butte (Martin) Formation is a grayish-brown to grayish-red to grayish-purple coarse- to medium-grained dolomite and dolomitic limestone with thin interbeds of limey siltstone and shale. The Muav Limestone and (or) the Temple Butte (Martin) Formation typically are zero to as much as 400 ft thick in the study area. These units, where present, are assumed to be fully saturated.

Overlying the Temple Butte (Martin) Formation or the Muav Limestone is the Redwall Limestone of Mississippian age. As found in wells in the study area, the Redwall Limestone is a fine-grained light-gray to gray limestone or dolomite that is occasionally thin bedded and occasionally oolithic (McKee, 1963). The formation typically is from 50 to 300 ft thick in the study area, and, in a few cases, rests directly on top of Precambrian rocks. The Redwall Limestone is fully saturated and is hydraulically connected to the Temple Butte (Martin) Formation and (or) the Muav Limestone.

The Supai Group lies unconformably on and in sharp contrast to the gray limestones of the Redwall Limestone and is divided into three formations—upper, middle, and lower (Blakey, 1990). The Lower Supai Formation is mainly red and purple sandstone and siltstone, and gray limestone and dolomite. In some places, the bottom of the formation contains conglomerate or breccia-type material composed of cherty limestone, chert clasts, and mudstone or claystone. This formation is a confining unit for ground water in the Redwall Limestone. Overlying this unit, is the orange, rounded, very fine-grained calcereous sandstone of the Middle Supai Formation. The Upper Supai Formation is mainly reddish-brown to tan, fine-grained sandstone, red-brown siltstone, occasional thin-bedded mudstone and limestone, hard white to pale-red fine- to medium-grained sandstone, and a complex series of red beds that are mostly fine-grained sandstone, siltstone, and mudstone. The Supai Group is typically 600 to 2,000 ft thick in the study area and is exposed on the east flank of Mount Elden where it is unsaturated (**pl. 1**). The Supai Group is partly to fully saturated throughout the rest of the study area and is hydraulically connected to saturated parts of overlying formations in the southern half of the study area.

The Hermit Formation is Permian in age and, where present north of the study area, overlies the Supai Group. The formation is a red-brown siltstone to silty sandstone to an interbedded sandy mudstone and sandy siltstone and has almost no true shale (Beus and Billingsley, 1989). The similarity in lithology between the Supai Group and Hermit Formation in this part of the Colorado Plateau make the distinction between these units difficult (Blakey, 1990). The Hermit Shale is not recognized in cuttings from wells in the study area; therefore, it is not included in the stratigraphic section shown in **figure 11**.

The Schnebly Hill Formation, which is Permian in age, overlies the Supai Group in the study area and can be seen in the upper part of Oak Creek Canyon at the south end of the study area. Blakey (1990) indicated that the Flagstaff area was near the northwestern limit of deposition of the Schnebly Hill Formation. The Schnebly Hill Formation comprises a sequence of reddish-brown to reddish-orange very fine to silty sandstone, mudstone, limestone, and dolomite (Blakey, 1990). This classification was based on clear stratigraphic, paleontologic, sedimentologic, and tectonic differences between these sediments and adjacent geologic units. Before the new classification, these sandstones and siltstones were either included as part of the lower Coconino Sandstone, which overlies the Schnebly Hill Formation, or were grouped with underlying units. In many cases, they were described as a transitional zone between the Coconino Sandstone and the Supai Group (Pierce and others, 1977; Elston and Dipaolo, 1979). Because there generally is enough information in drillers' logs and well cuttings to make the distinction, the formation is identified in the study area where appropriate. Within the study area, the Schnebly Hill Formation varies in thickness from a few feet to as much as 800 ft and thins and intertongues with the Coconino Sandstone to the west (**pl. 3**). Where the Schnebly Hill Formation is not present, the Coconino Sandstone lies unconformably on top of older units (pl. 3). The Schnebly Hill Formation is partly to fully saturated in the southern half of the study area and is hydraulically connected to the Coconino Sandstone above it and to units below. In the northern half of the study area, the Schnebly Hill Formation is mostly unsaturated.

The Coconino Sandstone (Darton, 1910) is a tan to white to light brown, cross-stratified, nearly pure, eolian, fine-grained quartz sandstone. This formation is Permian in age (Blakey, 1990), ranges from 300 to

1,100 ft thick in the study area, and thins to the west-northwest (**fig. 11**; **pl. 3**). Where faulted, the Coconino Sandstone can be extensively fractured to unconsolidated. Where saturated, the most productive parts of the Coconino Sandstone are in the fracture zones where permeability is greatest. The Coconino Sandstone is fully to partly saturated in the southern half of the study area and unsaturated in the northern half. Outcrops of the Coconino Sandstone are found at the north end of the Lake Mary graben, in Walnut Canyon, on the east flank of Mount Elden, and in Oak Creek Canyon (**pl. 1**). In most of the study area, the regional aquifer is formed by the Supai Group, Schnebly Hill Formation, and Coconino Sandstone. The Coconino Sandstone is the principal water-bearing unit of the aquifer.

The Toroweap Formation, which overlies the Coconino Sandstone, is Late Permian in age (Sorauf and Billingsley, 1991) and comprises carbonate sandstone, red beds, silty sandstone, siltstone, limestone, and thin layers of gypsum. In the Flagstaff area, an abrupt transition occurs from the upper part of the Coconino Sandstone to the Toroweap Formation (Sorauf and Billingsley, 1991). Where distinct, the transition changes from the quartz sandstone of the Coconino Sandstone to the carbonate sandstones and red beds of the Toroweap Formation. In areas where the Toroweap Formation and the Coconino Sandstone cannot be distinguished, the two units generally are described as undifferentiated Coconino Sandstone.

The Kaibab Formation, which is Late Permian in age, overlies the Toroweap Formation on an erosional unconformity (fig. 11, pl. 3). On the basis of more recent stratigraphic and paleontologic information, the Kaibab Limestone (McKee, 1938) was reclassified as the Kaibab Formation by Sorauf and Billingsley (1991). The Kaibab Formation has lower and upper members called the Fossil Mountain and Harrisburg Members, respectively. The Fossil Mountain is a light grey, cherty, thick-bedded limestone to sandy limestone. The chert occurs as nodules, or lenses and layers of intraformational breccia. The Harrisburg Member is an interbedded sequence of light-red to gray limestone, dolomite, siltstone, sandstone, and gypsum (Sorauf and Billingsley, 1991). If enough information is available from drillers' logs or well cuttings, both units can be distinguished in the study area; otherwise, the units are referred to as the Kaibab Formation. The Kaibab Formation ranges from 100 to about 650 ft in thickness. The upper surface of the Kaibab Formation also is erosional and exposed at land surface in much of the southern and eastern parts of the study area (pl. 1). In some cases, the Kaibab Formation has been removed by erosion. Where exposed at land surface, the Kaibab Formation is undulatory. The formation has well-developed joint fractures, many of which are widened by solution, as well as small sinkholes and depressions caused by dissolution of the rock. Near fault zones, the formation is heavily fractured in the subsurface, and many cavities and caverns are widened by dissolution of the rock. Where fully to partly saturated and hydrologically connected to the units below, the Kaibab Formation represents the uppermost geologic unit of the regional aquifer. In other areas, perched water-bearing zones in the Kaibab Formation can be hundreds to more than 1,000 ft above the regional water table (pl. 3).

The Moenkopi Formation is Triassic in age (McKee, 1954) and is composed of red to dark-red to reddish-brown siltstone, silty sandstone, fine- to very fine-grained sandstone, mudstone, and gypsum. The formation occurs as a discontinuous erosional remnant where protected by overlying volcanic rocks (pl. 1). Where present and where not highly fractured or faulted, the Moenkopi Formation generally acts as a confining layer that impedes the downward flow of water. The formation varies in thickness from zero to about 150 ft. If sandstone beds are present, wells completed in this formation may yield small amounts of water.

Overlying the Moenkopi Formation are volcanic rocks of Miocene to Quaternary age (Ulrich and others, 1984; Wolfe and others, 1987; fig. 11, pl. 1, this report). These volcanic rocks are aphanitic basalt and cinder cones; dacite flows and domes; dacite pyroclastic-flow breccia; andesite flows, flow breccia, and tuff breccia; and benmoreitic flows, cinder cones, and domes (pl. 1). These rocks range in thickness from zero to more than 5,000 ft under San Francisco Mountain. Within the study area, the average thickness of the volcanic rocks is about 150 ft. Where sufficiently fractured, or where underlain by clay, the volcanic rocks can be waterbearing. The yield of water from these rocks, however, is small and seasonally variable.

The unconsolidated sediments are the youngest deposits in the study area and consist of alluvium, colluvium, and glacial and landslide material either as a thin veneer or as thicker but discontinuous deposits. The alluvium is thin soils or thicker deposits of silt, clay, and fine sand in stream channels, lakebeds,

grabens, and meadows. The colluvium generally is coarse-grained material that is confined to steep slopes and mountainsides. A few landslide deposits are on the southern flanks of San Francisco Mountain (Wolfe and others, 1987). Glacial outwash occurs in the Inner Basin of San Francisco Mountain and on the east and north slopes. Most of the unconsolidated sediments are waterbearing but because of their limited areal extent and discontinuous character yield only small amounts of water to wells.

Geologic Structure

In the study area, all of the geologic formations have been affected to some degree by tectonic activity on and adjacent to the Colorado Plateau (**pl. 1**). Compressional or tensional stresses can result in folds that change the structure of the lithologic matrix. In general, fractures formed under compressional stress tend to remain fairly tight and closed, which results in little if any increase in ground-water flow. Fractures formed under tensional stress tend to be more open, which results in increases in ground-water flow in places. In some cases, the blocks on either side of a fault can grind the sedimentary rock into a fine powder that fills the fault zone and substantially reduces ground-water flow. Information on displacement of faults also is necessary to determine the continuity of water-bearing zones and confining layers. Fractures can be widened by dissolution of formational material as water moves through them thus increasing ground-water flow in some places. Chemical alteration of the sediments, either by dissolution or precipitation of minerals, also can affect ground-water flow.

The oldest structures, which are pre-Laramide in age, are fractures that strike north and northeast. These fractures are vertical to near vertical and propagate upward from Precambrian basement rocks to the surface. These fractures are inferred to be related to reactivation of Precambrian faults to the west of the study area during a time of tensional stress on the Colorado Plateau (Shoemaker and others, 1978; Wolfe and others, 1987).

The Laramide orogeny, which began in the Late Cretaceous age, resulted in widespread uplift and regional compression of the Colorado Plateau. The flat-lying sedimentary rocks were tilted 1–2° to the east and north. The regional compression resulted in large anticlinal, synclinal, and monoclinal structures throughout the Colorado Plateau (Huntoon, 1989). At least one of these features, the Mormon Mountain anticline south of Lake Mary, trends northwestward through the study area and has imposed local dips of as much as 5° on the sedimentary rocks (pl. 1). Parallel to subparallel fractures are associated with these compressional structures and may be deep seated.

All faults in the study area are younger in age than the pre-Laramide fractures (G.H. Billingsley, geologist, USGS, oral commun., 1997). Most of the faults are normal faults with vertical to near-vertical dips; a few are reverse faults, or strike-slip faults that have little horizontal motion. Some of the normal faults exhibit reverse drag (Dutton, 1882; Davis, 1901; Powell, 1957), which is a downturning of the beds in the downthrown block toward the fault plane in opposition to motion along the fault (**fig. 12**). Reverse drag is an important feature of the local structure because researchers have determined that normal faults develop by displacement under tension of adjacent blocks and create voids that are filled in by the sagging of the downthrown block (Huntoon, 1974). The best example of reverse drag in the study area can be seen in exposures of the Oak Creek Fault in Oak Creek Canyon. Some of the highest yielding wells in the study area are along the north end of the Oak Creek Fault in the Woody Mountain well field.

In the study area, the two principal strikes of faults are north-northeast and north-northwest. The north to northeastward-striking faults are interpreted as reactivation of structure that originates deep in the Precambrian unit by compressional stresses (Shoemaker and others, 1978). The Oak Creek Fault, which is the principal fault of this type, currently has offsets of 200 to 500 ft along the strike of the fault. In the study area, most of the faults strike north to northwest. The north- to northwest-striking faults are one of the youngest structural features on the Colorado Plateau. Some of these faults are the result of basin and range extension that postdates the Laramide orogeny. Many of these features are within the still active Cataract Fault zone. A few of these faults extend through the volcanic rocks and recent alluvial material, which indicates that they are still active. The mechanism for these faults and associated fractures are current extensional stress fields and processes now active on the Colorado Plateau (G.H. Billingsley, geologist, USGS, oral commun., 1997).

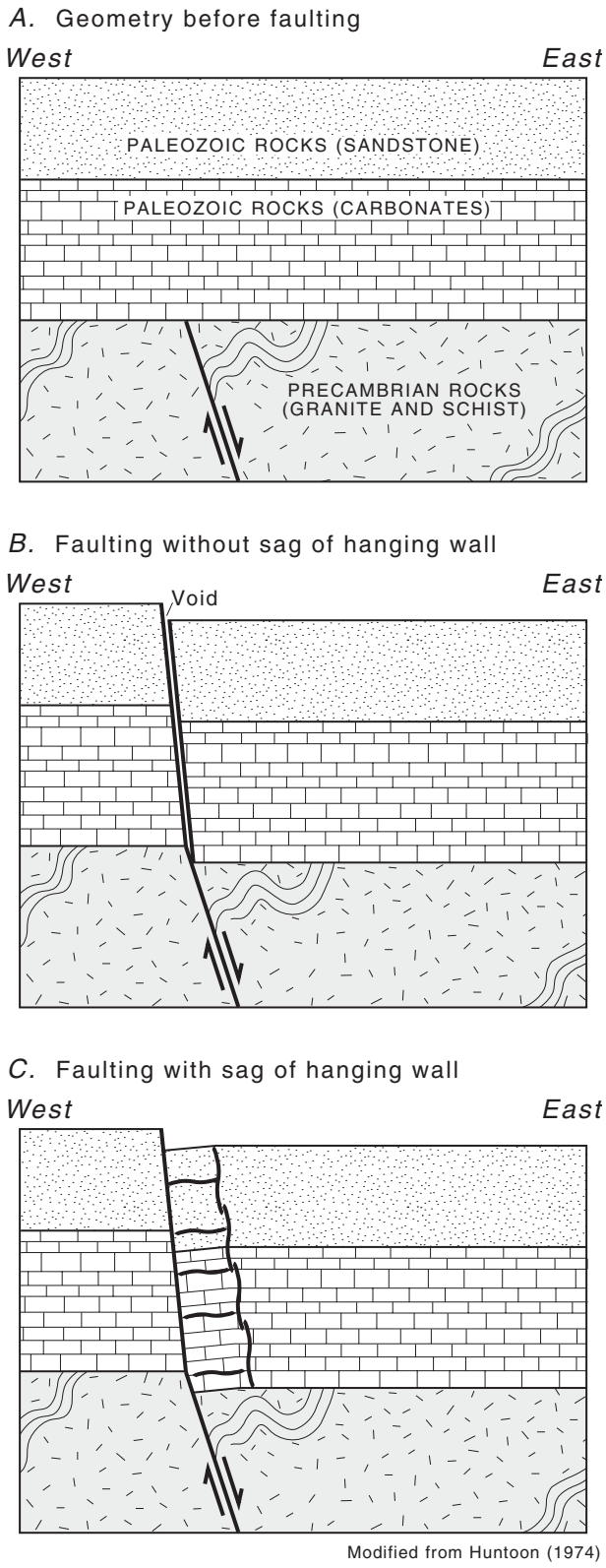

Figure 12. Conceptual model of the development of reverse drag. *A*, Geometry before faulting. *B*, Faulting without sag of hanging wall. *C*, Faulting with sag of hanging wall.

Sedimentary rocks of the regional aquifer are all fractured and folded to varying degrees. Most of the fracturing is related to major fault zones. Although most faults extend through the whole aquifer thickness, other fractures may be formation specific. Thus, these fractures can act as either conduits or barriers to ground-water flow. Shattered rock in these fractured zones is permeable; however, gouge zones, which consist of fine-grained to clay-sized material produced by grinding along the fault plane, are impermeable. In addition, the Kaibab Formation is brittle and contains many joints, solution channels, and other openings that can act as conduits for the flow of water. The lithology of the regional aquifer changes from formation to formation and also vertically and laterally within the formations. The most productive water-bearing material tends to be the fine- to medium-grained sandstones. Because of these structural and lithologic characteristics, the regional aquifer is heterogeneous and anisotropic and has a complex ground-water flow system.

Remote-sensing data and surface-geologic mapping aided in determining the structural framework of the study area. A Thematic-Mapper (TM) image taken on January 15, 1983, was processed at a resolution of about 100 ft (**fig. 3**). Although there is snow cover in this view, many prominent north- and-northwestward striking structures are clearly visible, such as the Oak Creek, Anderson Mesa, and Munds Park Faults, as well as many previously unrecognized enechelon and subparallel features. The area bounded by the northern ends of the Anderson Mesa and Munds Park Faults appears especially fragmented as does the area south of Upper and Lower Lake Mary. The digital-elevation model (DEM) complements the TM image and was used to show structural features unobscured by cultural, vegetation, and soil information (**fig. 4**). The DEM shows structural trends west of the north end of the Anderson Mesa Fault and just to the south and southeast of the airport that are not as apparent in the TM image. A SPOT image pair was made of the Fisher Point-Lower Lake Mary area. SPOT data are similar to TM data; however, SPOT data have much better resolution (about 30 ft) and allow for more detailed images and enlargements. An enlargement was made of part of a SPOT image pair collected on November 7–8, 1995 (**fig. 5**). Pronounced fractures (joints) are evident south of Lower Lake Mary and west of Fisher Point that are not as apparent in the TM image or the DEM. Where needed, the remote-sensing data were

supplemented by additional analysis of low-altitude aerial photographs from the early 1940s. These photographs were used because the forest cover was still fairly open, and development was limited at that time.

G.M. Mann and Dr. A.E. Springer (geologists, NAU, written commun., 1997) found that origin and physiography of the major structural trends near Flagstaff are consistent with origin and physiography proposed by past researchers for the surrounding region (Shoemaker and others, 1978; Ulrich and others, 1984; Wolfe and others, 1987; Huntoon, 1989). These researchers found that (1) north- to northeastward-striking fractures originate from compressional stress, (2) north- to northwestward-striking fractures originate from and are related to tensional stresses, and (3) some northeastward-striking fractures are related to reactivation of deep-seated faults caused by regional extension. Further analysis by G.M. Mann and Dr. A.E. Springer (geologists, NAU, written commun., 1997) suggest that recent and possibly still active tensional stress on the Colorado Plateau results in pull-apart basins that are identified by grabens and enechelon-type normal faulting extending deep into the subsurface. Northeastward-striking fractures generally parallel the direction of ground-water flow and surface drainage. Surface drainage may be better developed along these older structural features, and dissolution of formational material may have increased ground-water flow along these structures.

Gravity data also were used to identify major structural features and trends (**fig. 13**). These data indicated (1) a predominantly northeastward gravity trend that probably represents deep, old, near-vertical faults and (2) a subtle secondary northwestward gravity trend that represents younger structural trends (G.H. Billingsley, geologist, USGS, written commun., 1996).

GEOPHYSICAL INVESTIGATIONS

Lake Mary

The Lake Mary area is south of Flagstaff and contains two of the City of Flagstaff's four main sources of water supply—surface water in Upper Lake Mary and ground water in the regional aquifer that is withdrawn from wells in the Lake Mary well field. Investigation sites in this area were most suited to testing the application of GPR and SAR methods because of the varied surface geology that includes volcanic rocks and alluvium overlying the Kaibab Formation, and exposures of the Kaibab Formation at land surface, and the subsurface information available from well logs for corroboration. Remote-sensing data, photogrammetry, and surface-geologic mapping indicated a significant amount of large and small structural features that previously were unrecognized (**pl. 1**). Two areas of particular interest were the unnamed drainage just to the east of Howard Draw where the City of Flagstaff drilled wells LM-8 and LM-9 and the upper end of Lower Lake Mary (**fig. 6**).

Ground-Penetrating Radar

GPR is well suited for shallow investigations in this type of geologic environment as shown by the results of a survey profile about 65 ft northeast of Lake Mary well 8 (LM-8) in the Lake Mary well field (**fig. 14**A). The survey line was run perpendicular to the northeastward trend of the surface drainage and the surficial-structural features (fig. 6). Interbedding or near-horizontal and bedding-plane fractures in the Kaibab Formation, which is just beneath the alluvial cover and at land surface, are indicated in the survey profile. Interbeds of the Kaibab Formation are disrupted and offset from about 60 to 105 ft from the west end of the survey line. The center of this zone underlies the principal northeastward-striking fracture and the surface drainage. Other high-angle discontinuities are indicated at 210 ft and 230 to 240 ft from the west end of the survey line. Although a single GPR profile may be interpreted in different ways, these data indicate a heavily fractured zone and near-vertical fractures. The lithologic log for well LM-8, which projects into the profile at the west edge of the main fracture zone, shows the alluvium-Kaibab Formation contact is about 24 ft below land surface, which also is indicated by the GPR survey profile.

Data for another GPR profile were collected about 1 mi southeast of LM-8 in a drainage that has similar northeastward and northwestward-striking fractures. This profile indicates a disruption at about 400 to 410 ft from the north end of the survey line (fig. 14B) that closely corresponds to the surface location of a fracture identified photogrammetically and in field reconnaissance. Repositioning of the bedded rock in the fracture zone or minor faulting that extends deeper into the subsurface is shown in the survey profile at 35–40 ft below land surface at 370 and 410 ft from the north end of the survey line. Additional GPR surveys in the Lake Mary area indicated extensive fracturing in the Kaibab Formation and led to the use of GPR as a reconnaissance tool at sites selected for further study as a result of the remote-sensing and geologic investigations.

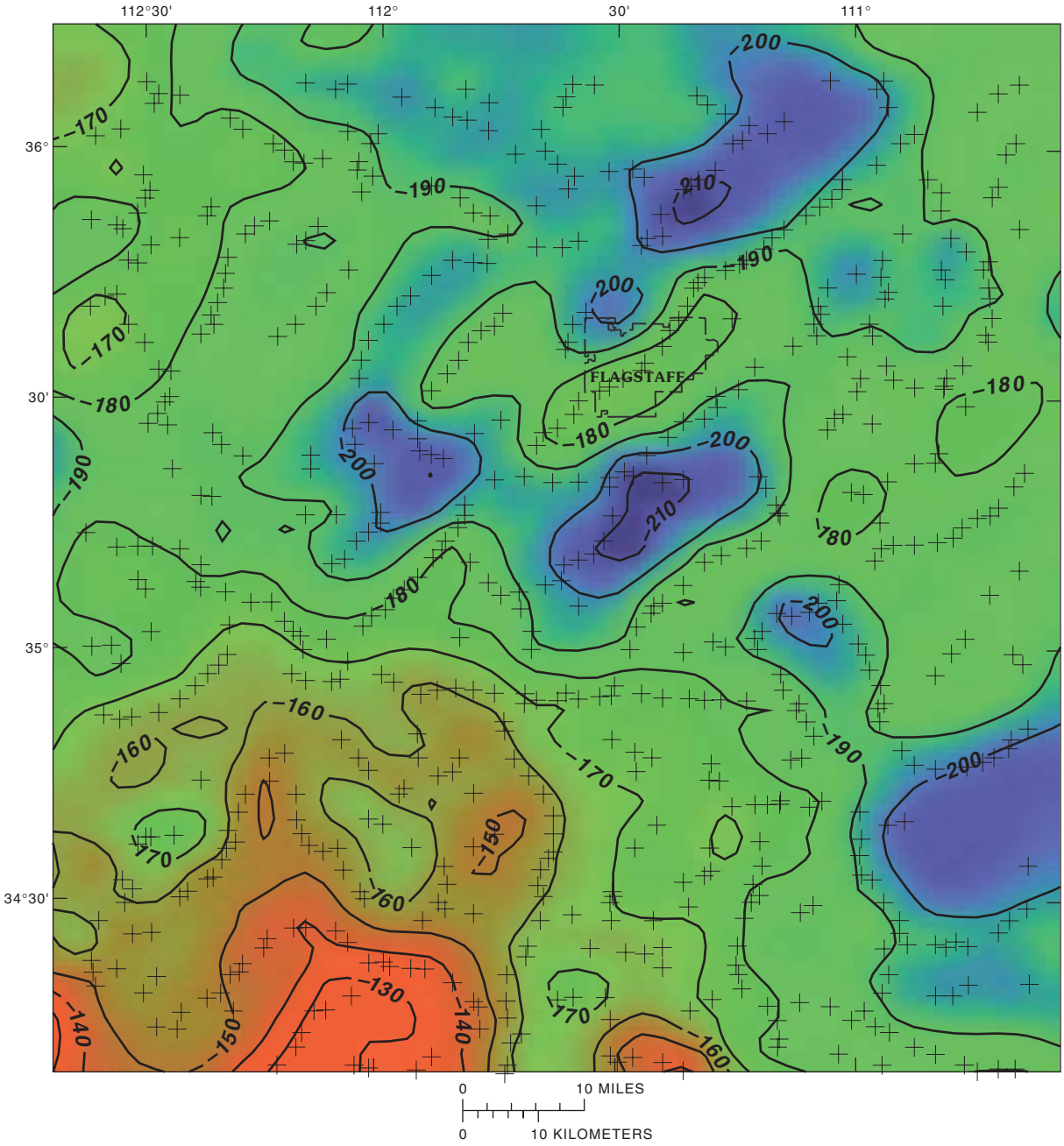

Figure 13. Color edge-enhanced image and simple Bouguer gravity data on a 2.49-mile square grid of the Flagstaff area, Arizona (U.S. Geological Survey, 1993). Universal Transverse Mercator projection. Central meridian = 111°W, and Base latitude = 0°. Note the predominant northeastward trend (N. 45° E.) and a secondary northwestward trend, (N. 45°W.) north of latitude N. 35° and the gravity high in the south west corner of the grid. Due-north trends are evident south of latitude N. 35°. The east-west line at latituede N. 35° may be an artifact of merging the existing grids.

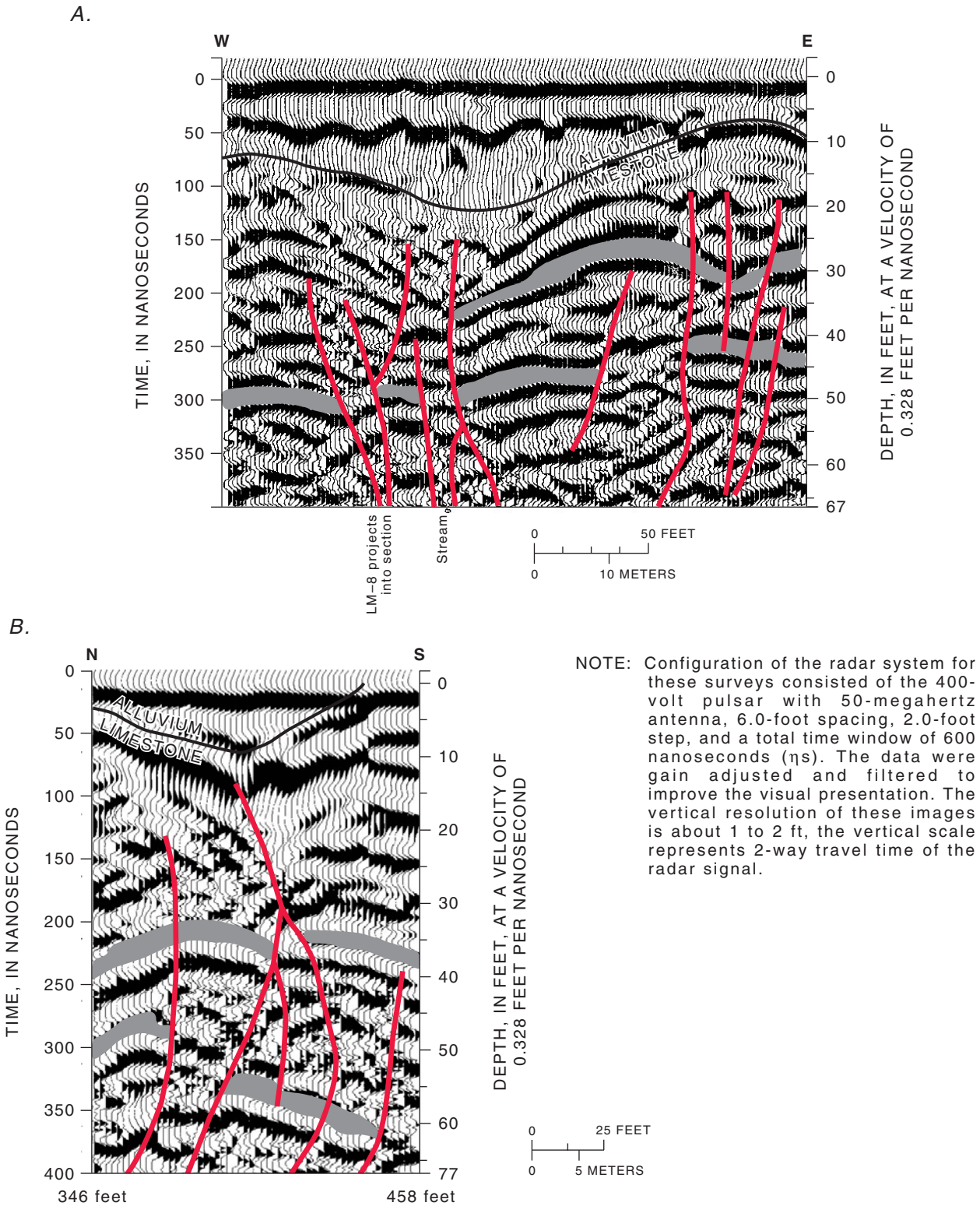

Figure 14. Selected interpreted ground-penetrating radar data for the Lake Mary area. *A*, Radar profile near Lake Mary well 8. *B*, Middle part of the radar profile for site about 1 mile southeast of Lake Mary well 8, 346–458 feet. Interpreted fractures are shown in red and interpreted bedding planes are gray fills. Hyperbolic events are interpreted as airwaves from surface features or openings or open horizontal fractures between bedding planes.

Square-Array Resistivity

The SAR data collected at Lower Lake Mary (LLM; fig. 6; table 1) for the 16.4- to 92.8-foot square arrays form a rough circle (see "**Supplemental Data**, Part A" at the back of the report). This pattern is expected for flat-lying isotropic sediments where the measured apparent resistivity is the same in all horizontal directions. Apparent resistivity data from the 131.2-foot square describes an ellipse when plotted on polar coordinates. The graphically derived apparent strike for fractures at this site is the oblate or the smaller axis of the ellipse (roughly N. 60° W.), which is the primary strike of fractures in the Kaibab Formation and corresponds with one of the predominant structural trends on the Colorado Plateau. The Lake Mary graben is an expression of this structural trend and is exposed on the east side of Lower Lake Mary. Geologic work by Ulrich and others (1984) and maximum horizontal gradients derived from the Bouguer gravity data for the area indicate a similar trend (**fig. 13**). This northwestward trend holds for the 164-, 328.1-, and 492.1 ft square arrays. Because of limited space, the 928.5-ft square array was collected in the crossed-array configuration (Habberjam, 1975) and does not have a corresponding polar plot; however, the calculated apparent strike is N. 58.8° W. (**fig. 15**). Deviations between the graphically derived and calculated apparent-strike directions are less than 15° and typically are less than 5°.

Square-array L8 was in a narrow limestone valley that trends roughly N. 40° E. and is about 262 ft northeast of LM-8 (**figs. 6** and **16**; table 1). The narrow limestone valley limited the square size to 492.1 ft. Polar coordinates for the 16.4- and 32.8-foot square arrays show ellipses with an oblate axis that trends northwestward (N. 60° W.). This trend is similar to the trend seen on the LLM soundings for squares that were greater than 131.2 ft. Unlike the data from Lower Lake Mary, data from even the smallest square sizes at L8 plot as ellipses because the sounding starts on limestone that has no lakebed cover. In addition, the many small fractures described on the structure maps for the area also strike N. 60° W. The strike changes as the depth of investigation increases. The apparent strike of fractures changes to N. 84° E. at 46.3 ft. The northeast fracture orientation indicated by data from the 65.6–492.1-foot square arrays is in line with the northeast orientation of fractures suggested by the valley structure.

Table 1. Data from surface-geophysical investigation sites, Flagstaff, Arizona

[Dashes indicate method not used. SAR, square-array resistivity; GPR, ground-penetrating radar; SEISMIC, seismic reflection or seismic refraction]

Site	Location name	Latitude, in decimal degrees	Longitude, in decimal degrees	Ground-penetrating radar maximum depth, in feet	Maximum square-array size, in feet[1]	Seismic reflection/ seismic refraction maximum depth, in feet	Depth to water, in feet	Specific conductance, in micromhos per centimeter	Methods used
LLM	Lower Lake Mary	35.0922	111.5447	---	928	---	1,153	254	SAR
L8	Lake Mary well 8	35.0950	111.5764	65	492	---	[2]671	488	SAR, GPR
L9	Lake Mary well 9	35.0808	111.5894	65	492	---	226	635	SAR, GPR
W10	Woody Mountain well 10	35.1456	111.7342	---	2,785	---	1,139	199	SAR
W11	Woody Mountain well 11	35.1344	111.7308	---	2,785	---	1,106	233	SAR
SC	Skunk Canyon	35.1458	111.6047	90	2,320	3,600	920	[3]490	SAR, GPR, SEISMIC
FG	Foxglenn	35.1897	111.5997	60	492	3,400	1,312	465	SAR, GPR, SEISMIC
BP	Continental	35.2072	111.5731	140	492	2,400	1,305	450	SAR, GPR, SEISMIC

[1]Depth of investigation is roughly equivalent to size of square array (Habberjam, 1979).
[2]Pumping water level.
[3]Possibly a mixed water. Several days before this sample was collected, the City of Flagstaff pumped several hundred thousand gallons of water from Lake Mary into the well to cause hydrofracting of the formation.

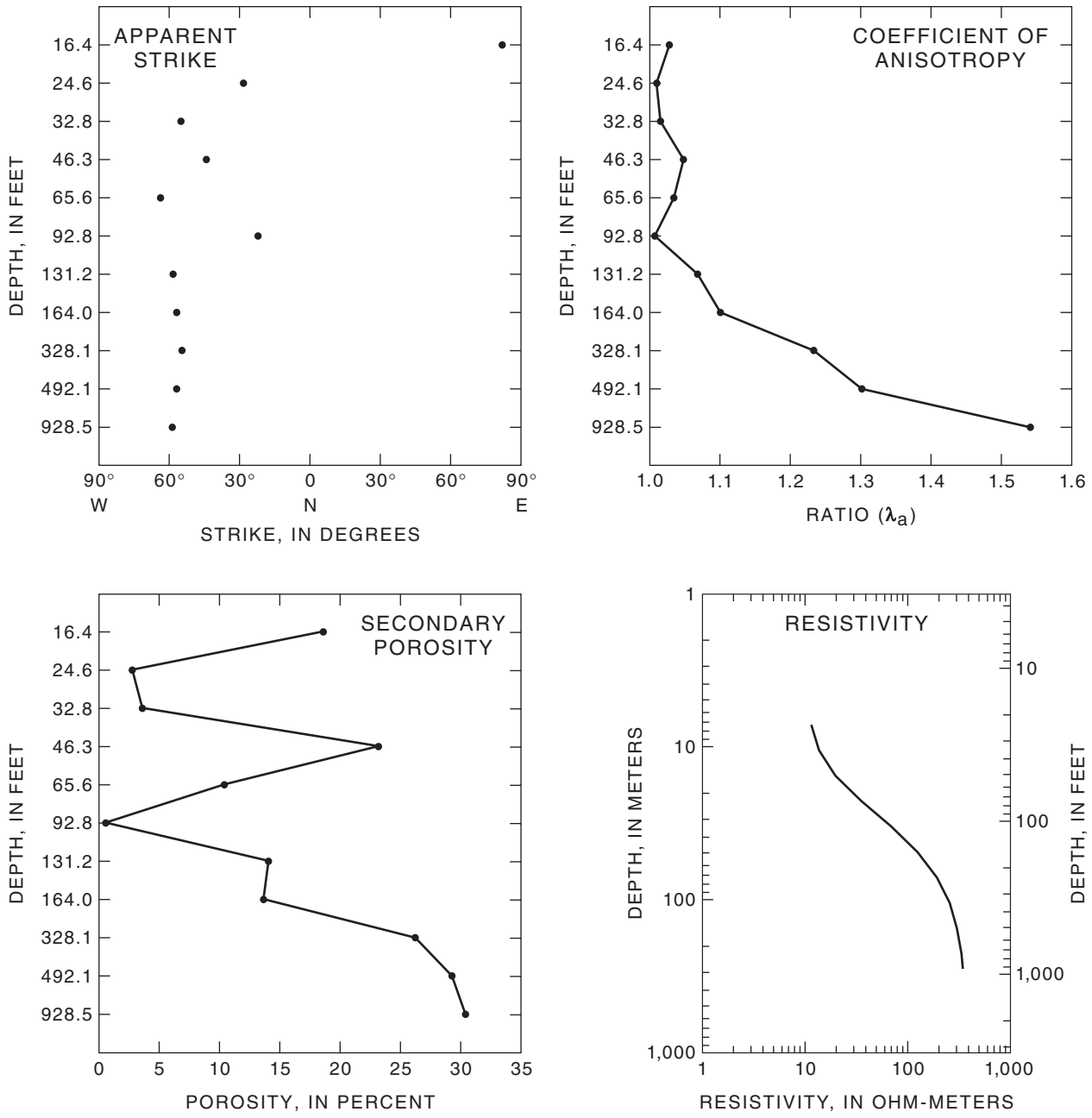

Figure 15. Calculated apparent strike of major fractures, coefficient of anisotropy, secondary porosity, and interpreted resistivity from the square-array sounding data, Lower Lake Mary site (LLM). Apparent strike values are in degrees for each square size (16.4, 24.6, 32.8.....). Coefficient of anisotropy is a dimensionless number where a number larger than one indicates increasing anisotropy. For comparison to the interpreted resistivity curve, depth to water was about 1, 150 feet on the basis of data from Lake Mary wells 6 and 7. Interpretation was done using ATO, which is a vertical electrical-sounding (VES) program by Zohdy (1989).

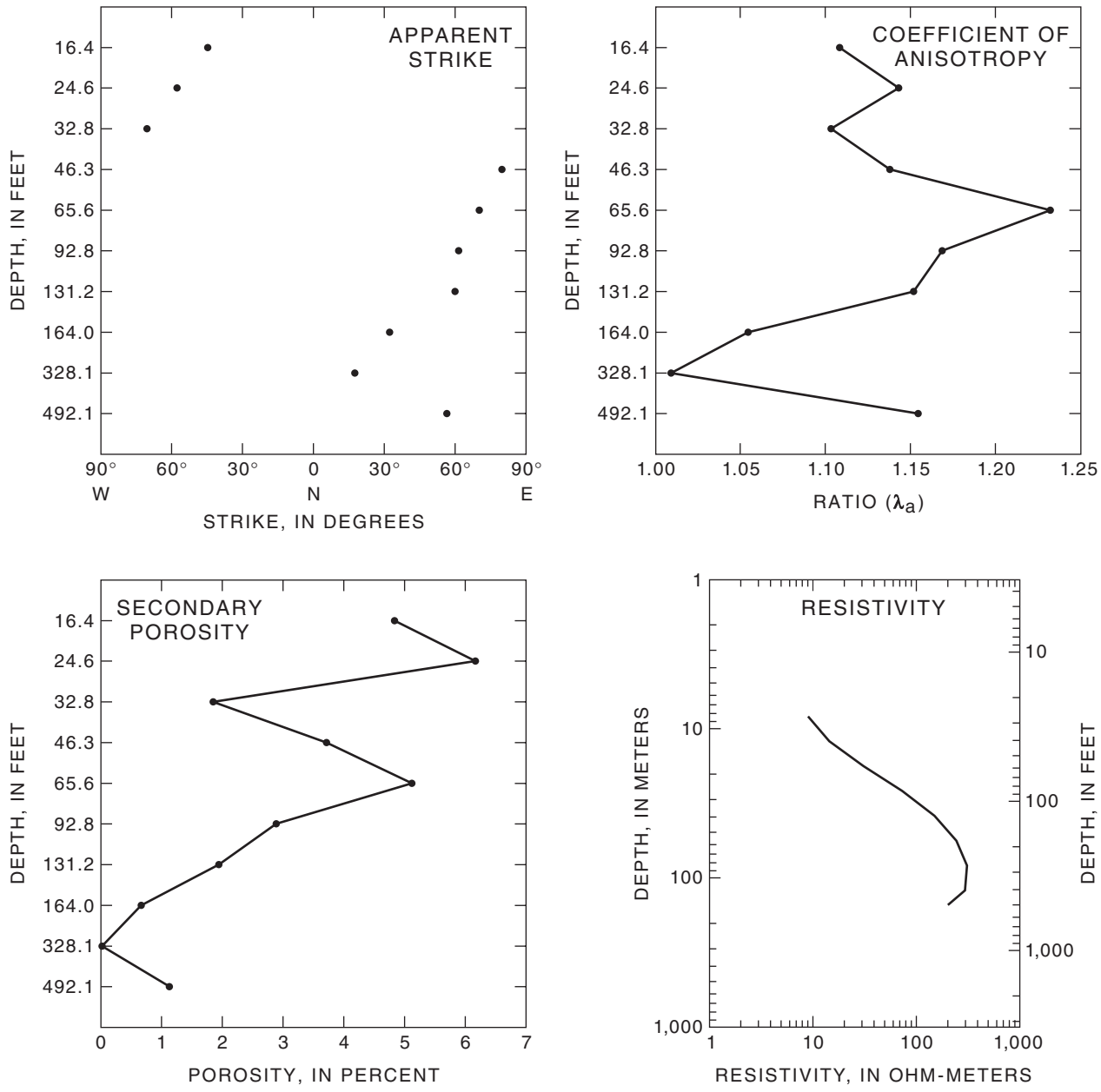

Figure 16. Calculated apparent strike of major fractures, coefficient of anisotropy, secondary porosity, and interpreted resistivity from the square-array sounding data, Lake Mary well 8 site (L8). Apparent strike values are in degrees for each square size (16.4, 24.6, 32.8.....). Coefficient of anisotropy is a dimensionless number where a number larger than one indicates increasing anisotropy. For the interpreted resistivity curve, depth to water was recorded at 671 feet on the day of the sounding (pumping water level). Interpretation was done using ATO, which is a vertical electrical-sounding (VES) program by Zohdy (1989). The interpreted resistivity-curve maxima is at about 312 feet; Lake Mary well 8 was being pumped at about 1,700 gallons per minute, and the pumping water level was about 394 feet.

The strike of major fractures changes with increasing depth from N 60° W. to N. 45° E. Although the sounding did not reach the pumping water level of 671 ft below land surface, the largest square array of 492.1 ft shows increasing coefficient of anisotropy and increasing secondary porosity from 328.1 to 492.1 ft and suggests that there are saturated fractures that provide water to the well (fig. 16).

The square array, L9, near Lake Mary well 9 (LM-9) was about 1.25 mi southwest of LM-8 in the same narrow limestone valley (**figs. 6** and **17**; table 1). The L9 array was about 328 ft southwest of LM-9 and within 328 ft of the intersection of two orthogonal-fracture sets—one that strikes northeastward (N. 45° E.) and one that strikes northwestward (N. 45° W.). The narrow limestone valley and vegetation in the area limited the size of the square array to 492.1 ft; however, the depth of investigation exceeded the depth to water (226 ft) measured at LM-9 on the day of the sounding. Data from the smallest square array (16.4 ft) plots as an ellipse that indicates a predominant fracture strike of roughly west-northwest. Fracture strikes for squares of 24.6 to 131.2 ft change gradually in a clockwise direction to the north. Data for the 164-foot square array indicate a northwestward strike (N. 35° W.), and data for the 328.1-foot square array indicate two apparent strikes—one northwestward (N. 30° W.) and one northeastward (N. 45° E.). The ellipse for the 492.1-foot square array also apparently has two trends—one northwestward (N. 30° W.) and one northeastward (N. 70° E.). Doe and others (1982) describe this type of ellipse as being caused by multiple joint and fracture geometries. Both trends are within the natural variations of the regional trends mapped in the Kaibab Formation. The calculations (Habberjam, 1975) show a low coefficient of anisotropy (<1.06) and a low secondary porosity (<0.5 percent) at square arrays 164, 328.1, and 492.1 ft just above and below the water table (fig. 17). The low secondary porosity may explain why less water is available to well LM-9 than to well LM-8.

Borehole

Wells LM-6 and LM-7 (City of Flagstaff) are near the SAR site near the upper end of Lower Lake Mary (fig. 6). Borehole lithology was the only information collected from these wells (**fig. 18**A–B). As a result, little information is available to correlate with the SAR results collected near here. The plotted resistivity for the LLM site (**fig. 15**) reaches a maximum at the limit of investigation (928.5 ft), which is above the water table (1,150 ft) in this area.

Logs for well LM-8 included lithologic, caliper, gamma, and spontaneous potential (fig. 18C). The hole rugosity indicated by the upper part of the caliper log (350 to 500 ft) correlates well with SAR anisotropy (L8), especially beginning at about 300 ft where the hole size and roughness increase at the transition into the Coconino Sandstone. Secondary porosity as estimated by the SAR data also increases at this point. The plotted interpreted resistivity (fig. 16) reached a maximum at about 312 ft, which is consistent with static water levels in this area at the time of the survey.

Wells LM-8 and LM-9 are in the same drainage that presumably has the same structural trend at each well site; however, LM-9 has considerably different hydraulic properties. Borehole information for this well consists of lithology interpreted from drill cuttings (fig. 18D). The change in SAR anisotropy and secondary-porosity estimates (L9) at about 164 ft is consistent with the change from the Kaibab Formation to the Coconino Sandstone shown in the lithologic log (figs. 17 and 18D). The resistivity at this site reached a maximum at 226 ft, which is consistent with the static water level in LM-9 (210 ft below land surface) at the time of the survey.

Woody Mountain

The Woody Mountain well field is southwest of Flagstaff on the northern end of the Oak Creek Fault. The Oak Creek Fault is uplifted about 300 ft to the west, strikes roughly north-northwest through the area, and is intersected near the middle of the well field by the northwestward-striking Dunnam Fault. Volcanic rocks overlie the consolidated sediments of the Colorado Plateau throughout this area and range from about 300 to 500 ft thick. This area is poorly suited for GPR surveying because of extensive volcanic-rock overburden. The City of Flagstaff drilled two wells near the south end of this well field between 1996 and 1998. The SAR technique was applied to two areas in the south end of the well field to complement the borehole information (**fig. 6**; **table 1**). Lithologic and borehole-geophysical logs correlate with SAR results.

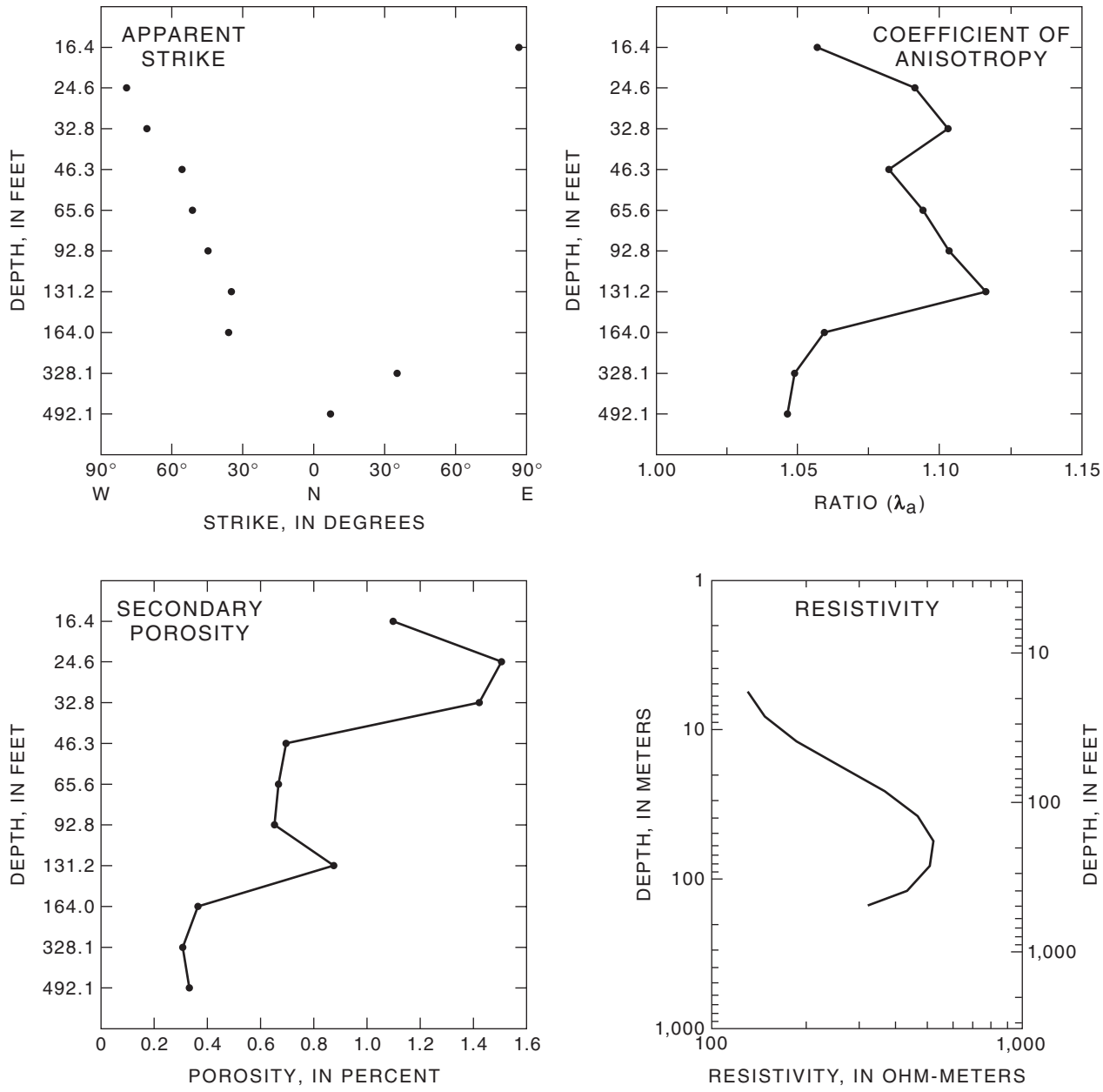

Figure 17. Calculated apparent strike of major fractures, coefficient of anisotropy, secondary porosity, and interpreted resistivity from the square-array sounding data, Lake Mary well 9 site (L9). Apparent strike values are in degrees for each square size (16.4, 24.6, 32.8.....).Coefficient of anisotropy is a dimensionless number where a number larger than one indicates increasing anisotropy. For the interpreted resistivity curve, depth to water was recorded as 226 feet on the day of the sounding (pumping water level). Interpretation was done using ATO, which is a vertical electrical-sounding (VES) program by Zohdy (1989). The interpreted resistivity-curve maxima is at about 207 feet.

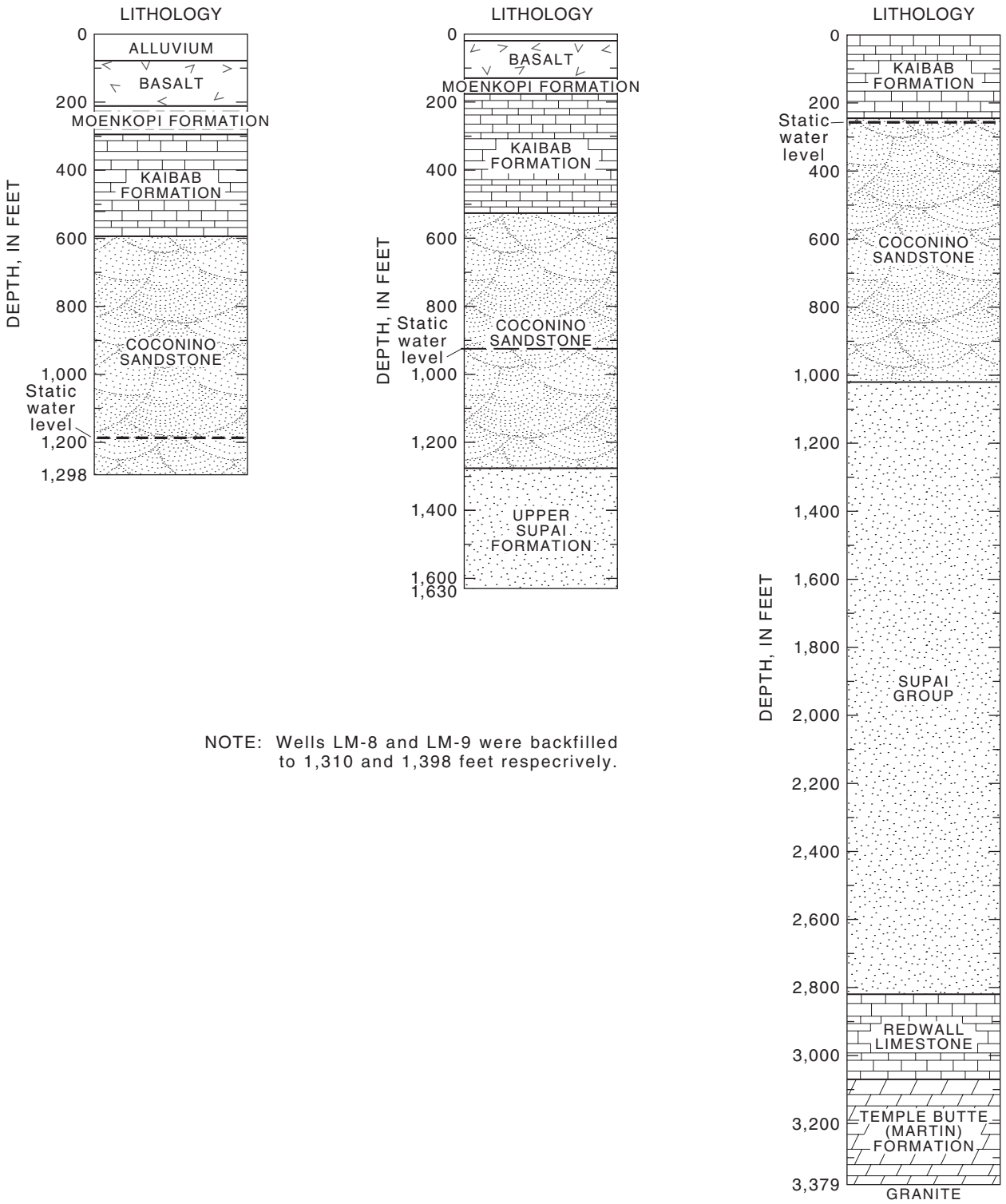

Figure 18. Lithologic and borehole-geophysical logs, Lake Mary sites. *A*, Well LM-6. *B*, Well LM-7. *C*, Well LM-8. *D*, Well LM-9.

C. Lake Mary well LM–8

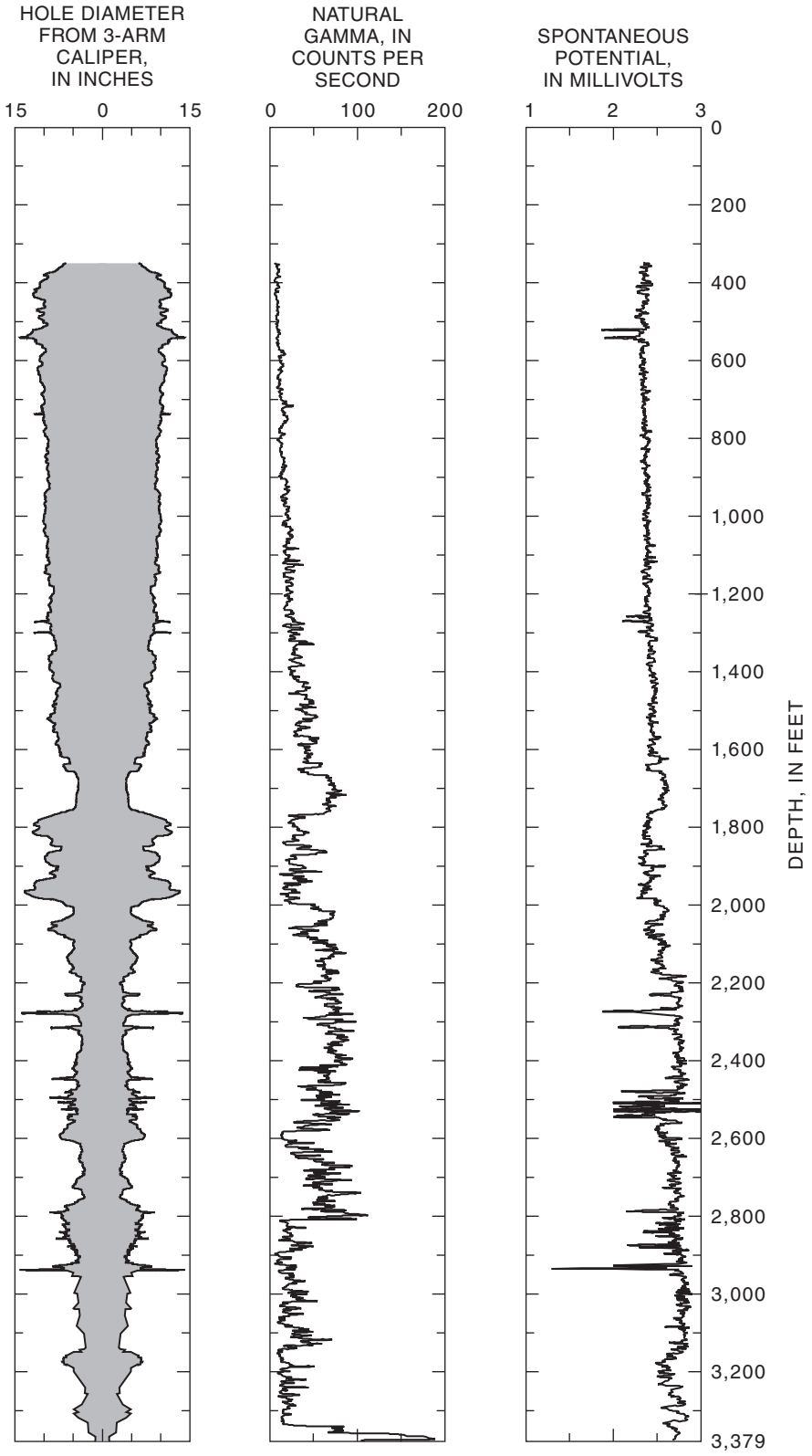

D. Lake Mary well LM–9

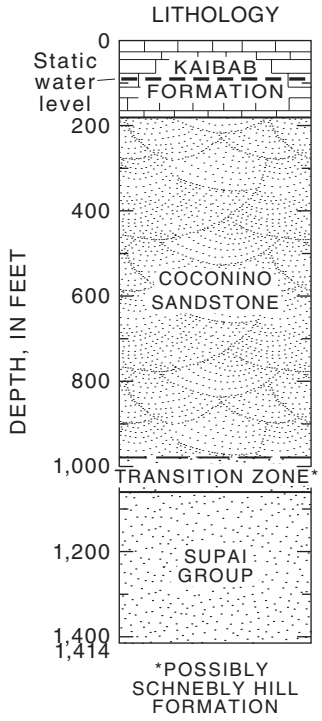

Figure 18. Continued.

Square-Array Resistivity

SAR data at Woody Mountain well 10 (WM-10) for the 32.8- and 65.6-foot square arrays (W10) show a circular pattern that indicates isotropic material that may be volcanic ash or pumice (see "**Supplemental Data**, Part A" at the back of the report). The ellipses for the 65.6- and 164-foot square arrays show a north-northwestward fracture strike (N. 15° W.) that probably is associated with the strike of the Oak Creek Fault. Ellipses for the square arrays of 492.1, 928.5, 1,391.1, and 1,857 ft indicate a northwestward fracture strike (N. 45° W.) that is consistent with the predominant structural trends of the Colorado Plateau. Ellipses for the square arrays of 2,319.6 and 2,785.4 ft indicate a predominant fracture strike of about N. 60° W. This orientation parallels the nearby Dunnam Fault and indicates that the Dunnam Fault is the major structural feature at depth at this site (see "Supplemental Data, Part A" at the back of the report). Variation between the resistivity maxima and depth to water is about 9 percent at this site. The resistivity decreases below the depth of the regional water table (**fig. 19**).

The square array W11 near Woody Mountain well 11 (WM-11) was about 0.75 mi east of the Oak Creek Fault (**figs. 6** and **3**; **table 1**). The data for the 32.8 and 65.6-ft square arrays indicated fracture strikes of N. 45° W. and N. 4° W. (**fig. 20**). Data from the 164-, 328.1-, and 492.1-ft square arrays indicate complex fracture patterns (fig. 20; see section entitled "Supplemental Data, Part A" at the back of the report). The square arrays of 328.1 and 492.1 ft indicate strikes of N. 30° W. and N. 45° W., respectively. The data from the 928.5-, 1,391.1-, 1,857-, 2,319.6-, and 2,785.4-ft square arrays show an increased complexity of fracture patterns at depth. Apparent strike direction at 928.5 ft is N. 2° E., and average strike direction at the 1,391.1-, 1,857-, 2,319.6-, and 2,785.4-ft square arrays is N. 45° W. Fracture strikes vary widely from due west to due north at the 1,391.1- and 2,319.6-ft square arrays, respectively.

The resistivity maxima at 702 ft is shallower than the depth to water (1,103 ft) measured in WM-11 (fig. 20). This relation may indicate locally perched water. A video log showing water pouring past the end of the well casing indicates that ground water enters the borehole above the 800-foot level. The low secondary porosity and coefficient of anisotropy measured using the square arrays of 492.1 and 928.5 ft indicate that rocks at those corresponding depths are less fractured than rocks above and below.

Borehole

Lithologic, caliper, natural gamma, and video logs were made for WM-10 (**fig. 21**A). The natural gamma log correlated well with lithology. The borehole video shows multiple fractures and openings below the bottom of the casing (446 ft; fig. 21A). The fracture density and the number of openings increases downhole to about 950 ft, which is consistent with the caliper log. Most of the fractures are high angle to near vertical with dips that range from 63° to 88°. A significant amount of high-angle fracturing begins to appear at about 1,300 ft in the Coconino Sandstone, and one large, open, near-vertical fracture extends to 1,370 ft where the borehole was collapsed or bridged. The high-angle fractures from 1,300 to 1,370 ft are interpreted to be part of the Oak Creek Fault.

The caliper and video logs for WM-10 compare well with results of the nearby SAR survey. Secondary porosity (fig. 19) was greatest (10.5 percent) at about 330 ft, which is consistent with the presence of fractured basalt in the borehole at this depth. The coefficient of anisotropy (fig. 19) is greatest at a depth of about 930 ft where significant fracturing in the Kaibab Formation was noted in the borehole. The resistivity maxima (fig. 19) at about 1,030 ft is within 10 percent of the static water level for WM-10 (1,139 ft).

Lithologic, natural gamma, and video logs were made for WM-11 (fig. 21B). The natural gamma log correlates well with the lithology to 1,000 ft where the natural gamma log ends. The video log shows multiple fractures and openings from the start of the log at 800 ft to about 1,040 ft. Openings are defined as irregularly shaped cavities that range from less than 1 in. to several feet or more in size and are commonly associated with fractures. The interval from 1,107 to 1,337 ft was not imaged by video because caving and collapse of the borehole necessitated the casing of this interval. The fracture density and number of openings increase with depth from about 950 ft to just above the water level at 1,103 ft. Water enters the hole at 1,103 ft from a large, open, high-angle fracture that extends downhole. The video of the borehole below 1,340 ft (bottom of the casing at the time of the video) also shows an increase in fractures and many horizontal fractures and openings to about 1,550 ft. The fractures range from thin and closed to large and open and vary from horizontal to near vertical. Some fractures are infilled with unconsolidated material or secondary minerals.

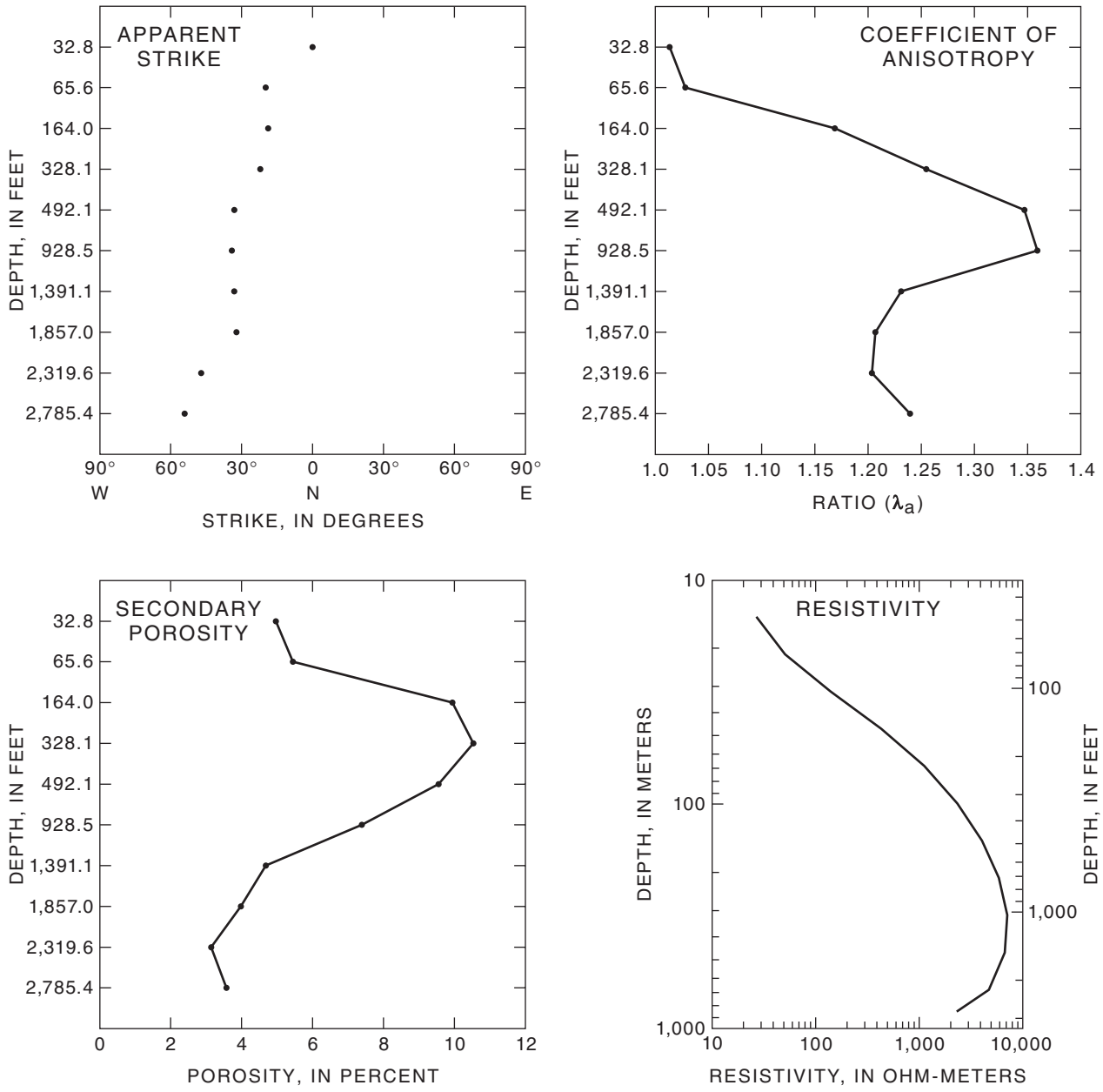

Figure 19. Calculated apparent strike of major fractures, coefficient of anisotropy, secondary porosity, and interpreted resistivity from the square-array sounding data, Woody Mountain well 10 site (W10). Apparent strike values are in degrees for each square size (32.8, 65.6, 164.0.....). Coefficient of anisotropy is a dimensionless number where a number greater than one indicates increasing anisotropy. For the interpreted resistivity curve, depth to water recorded at Woody Mountain well 10 was 1,138 feet. Interpretation was done using ATO, which is a vertical electrical-sounding (VES) computer program by Zohdy (1989). The interpreted resistivity-curve maxima is at about 1,033 feet.

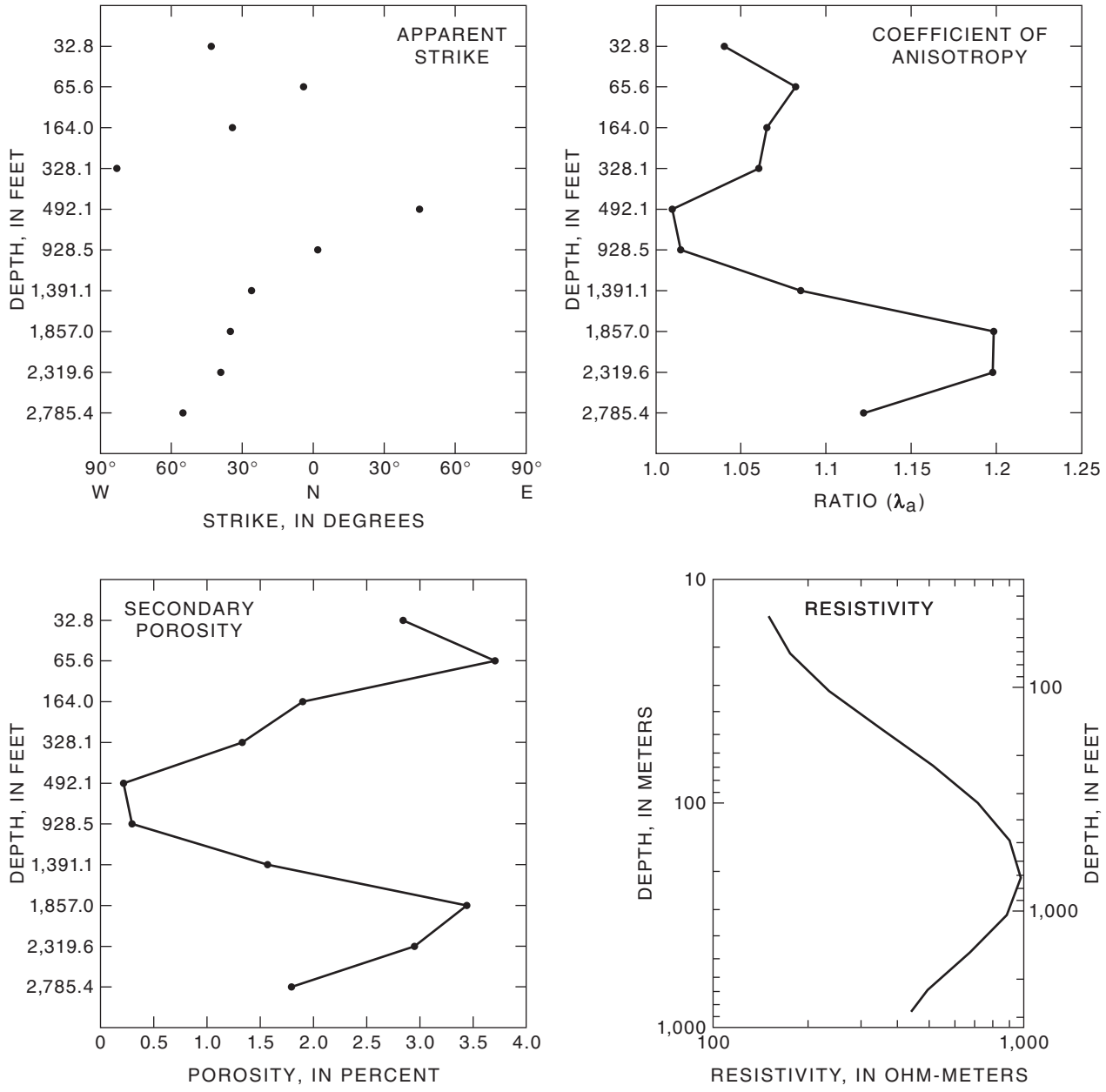

Figure 20. Calculated apparent strike of major fractures, coefficient of anisotropy, secondary porosity, and interpreted resistivity from the square-array sounding data, Woody Mountain well 11 site (W11). Apparent strike values are in degrees for each square size (32.8, 65.6, 164.0.....). Coefficient of anisotropy is a dimensionless number where a number greater than one indicates increasing anisotropy. For the interpreted resistivity curve, depth to water recorded at Woody Mountain well 11 was 1,106 feet. Interpretation was done using ATO, which is a vertical electrical-sounding (VES) computer program by Zohdy (1989). The interpreted resistivity-curve maxima is at about 702 feet.

A. Woody Mountain well WM–10

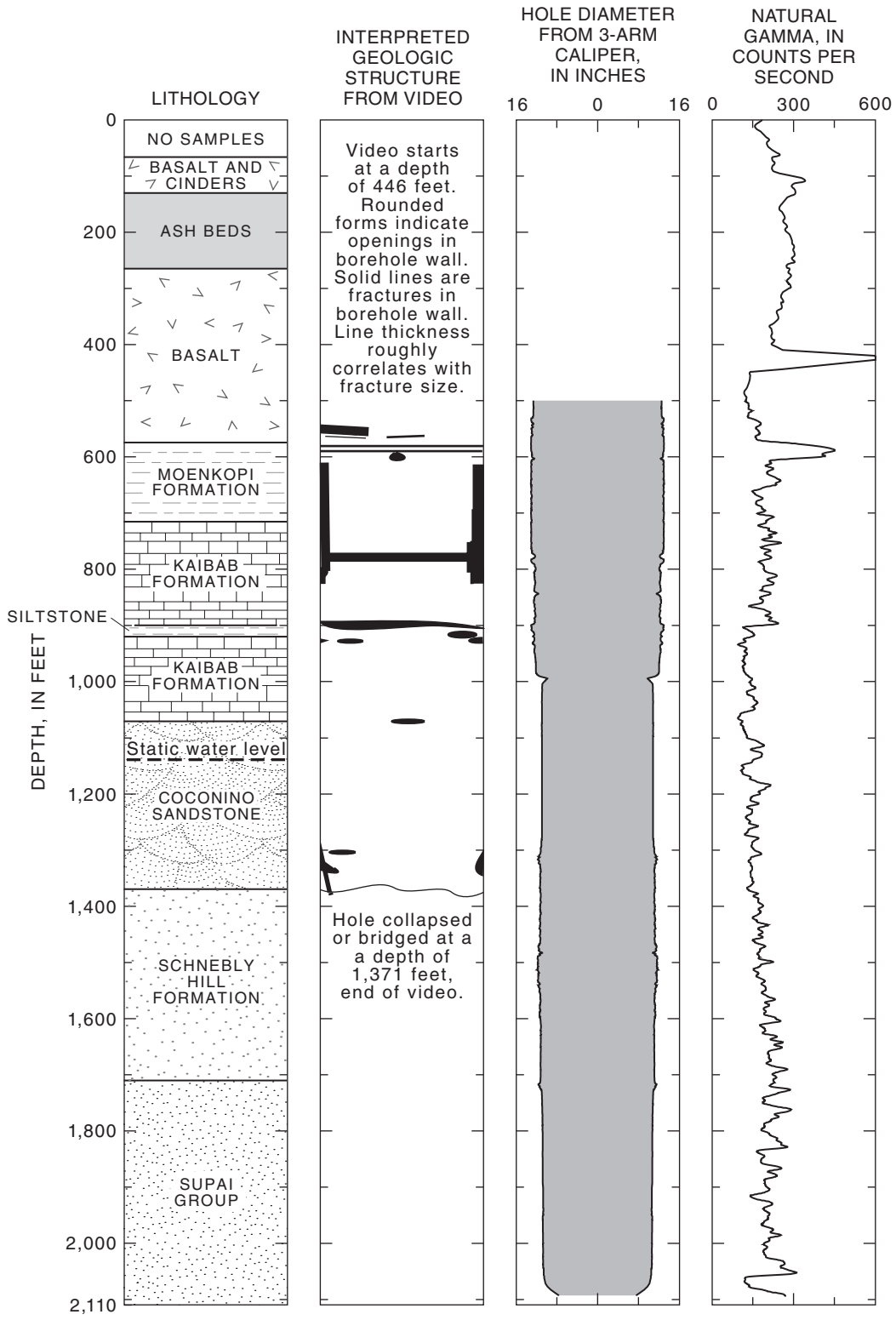

NOTE: Well WM–10 was backfilled to 1,790 feet.

Figure 21. Lithologic and borehole-geophysical logs, Woody Mountain site. *A*, Well 10. *B*, Well 11.

B. Woody Mountain well WM–11

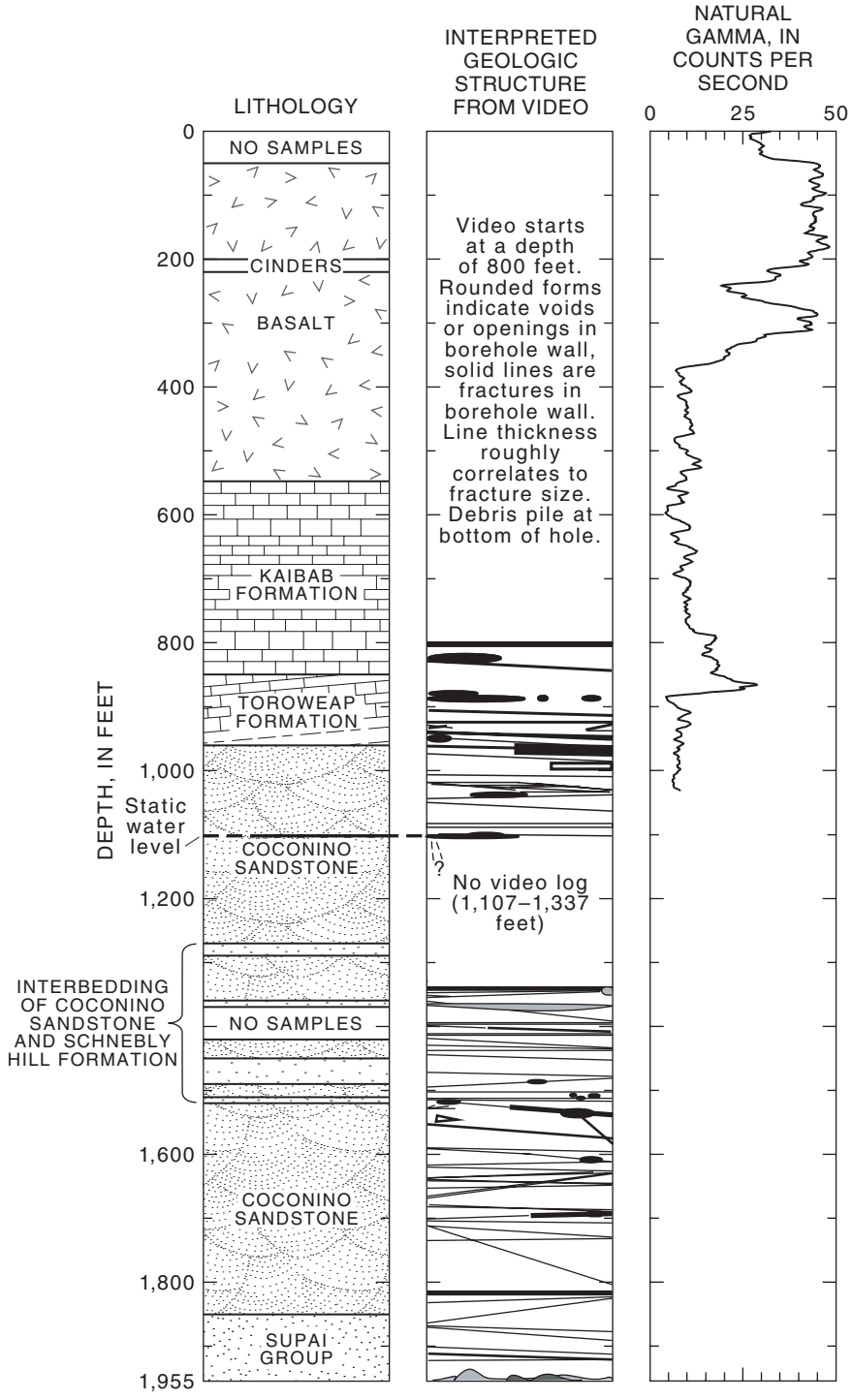

Figure 21. Continued.

No horizontal fractures or openings were observed below 1,550 ft; however, many high-angle fractures occur throughout the remainder of the borehole. Most of the high-angle fractures imaged in WM-11 dip at angles significantly less than high-angle fractures found in other boreholes. The dip of high-angle fractures ranged from 45 to 89° but only averaged 76°. Because this borehole video was not azimuthally referenced, fracture strikes in the subsurface could not be determined for comparison to strikes determined from the SAR survey at this site. The SAR ellipses, however, become much more complex from 1,400 to 1,860 ft where fracture density in the borehole is greatest. Secondary porosity and coefficient of anisotropy begin to increase at about 1,400 ft where video logs show an increase in fracture density, number of openings, and hole rugosity (**figs. 20** and 21 B). Below about 1,860 ft, resistivity, secondary porosity, and coefficient of anisotropy begin to decrease. This decrease corresponds to the decreasing number of fractures shown in the borehole video.

Borehole data for WM-10 and WM-11 indicate that previously unrecognized horizontal to near-horizontal open fractures in the shallow subsurface and below the water table probably are a significant component of the fracture-flow system. Another feature only observed in the video logs is the number of high-angle fractures that have been filled with material washed in from the land surface or with mineral precipitates. The many openings common in limestones, such as the Kaibab Formation, also were imaged in the sandstone and siltstone units of the Coconino Sandstone, Schnebly Hill Formation, and Supai Group. Calcite and other calcareous material are sometimes present as a cementing agent in the Coconino Sandstone, Schnebly Hill Formation, and Supai Group, and the dissolution of this material probably creates some of these openings.

Skunk Canyon

Structural features of Skunk Canyon inferred from remotely sensed data, photogrammetry, and surface-geologic mapping are multiple northwestward-striking fractures intersected by a few minor northeast-striking fractures (**fig. 8**). Outcrops of the Kaibab Formation at this site are well jointed showing significant vertical and horizontal fracturing that probably is not deep seated. The low-lying areas are covered with alluvial material of varied thickness. The principal northwest-trending valley is interpreted as a small graben. GPR, seismic-reflection, seismic-refraction, and SAR surveys were done at this site (**figs. 6** and 8). Data from six GPR surveys and two seismic lines were collected. One SAR survey was completed at about the middle of the site where the two most prominent structures intersect.

Ground-Penetrating Radar

GPR data for Skunk Canyon profile 1 were collected along a northwestward-trending alignment (N. 46° W.) perpendicular to the principal drainage (figs. 8, 22A). The near subsurface appears to be substantially fractured along the entire profile. Multiple fractures with minor bed offsets are indicated by the disruption and offset of the survey profile from 140 to 225 ft from the southeast end of the survey line. Seismic data collected later at this site parallel to profile 1 correlate well with the GPR data. Jaasma and others (1997) indicate that this alignment has extensive faulting along its entire length in the shallow subsurface and at depth.

Data for GPR profiles 2 and 3 were collected perpendicular to profile 1 (figs. 8, 22B and C). Profile 2, similar to profile 1, indicates multiple fractures, minor faults, and inward-dipping beds toward the topographic low centered on the main northwest structural trend. Bedding planes indicated in the profile survey are dipping inward toward the center of the valley to a
70-ft-wide zone of chaotic and disrupted radar signal and are shifted upward in the profile on the northeast side. This shift indicates the inward collapse of the shallow bedrock over a possibly deeper heavily fractured zone. Seismic data collected parallel to profile 2 correlate well with the GPR data. Profile 3 is parallel to and just west of the main drainage, and data from this profile are significantly different from the data from the other two profiles. Interbedded alluvial material is shown in the upper 10 to 30 ft of this survey profile. Below this zone, the chaotic and disrupted character of the profile indicates significantly fractured rock. Several small, broad hyperbolic features occur on this survey profile (**fig. 22**C) that do not appear on the other two profiles shown (fig. 22A–B). Deng and others (1994) proved that hyperbolic features like these can indicate openings or caves in the shallow subsurface in the absence of other surface or subsurface features, such as pipes, powerlines, or trees. Hyperbolic features, such as these, also are produced when fractures are crossed by the radar at acute angles as would be possible with the general northwestward structural trend that is parallel to subparallel to this profile.

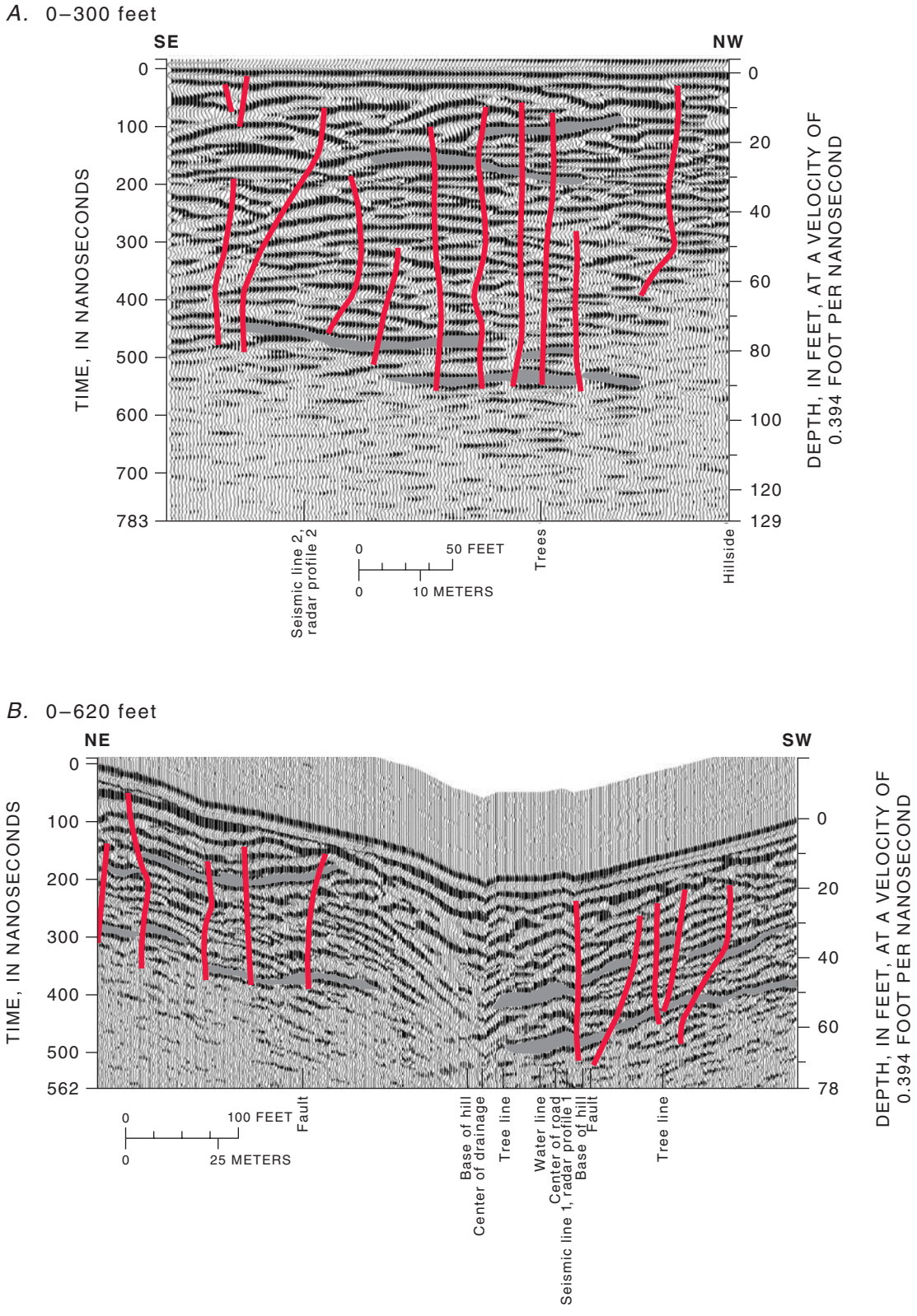

Figure 22. Selected interpreted ground-penetrating radar data for the Skunk Canyon area. *A*, Radar profile 1, 0–300 feet. *B*, Radar profile 2, 0–620 feet. *C*, Radar profile 3, 0–600 feet. Interpreted fractures are show in red, and interpreted bedding planes are gray fills. Hyperbolic events are interpreted as small openings or open horizontal fractues in bewtween bedding planes.

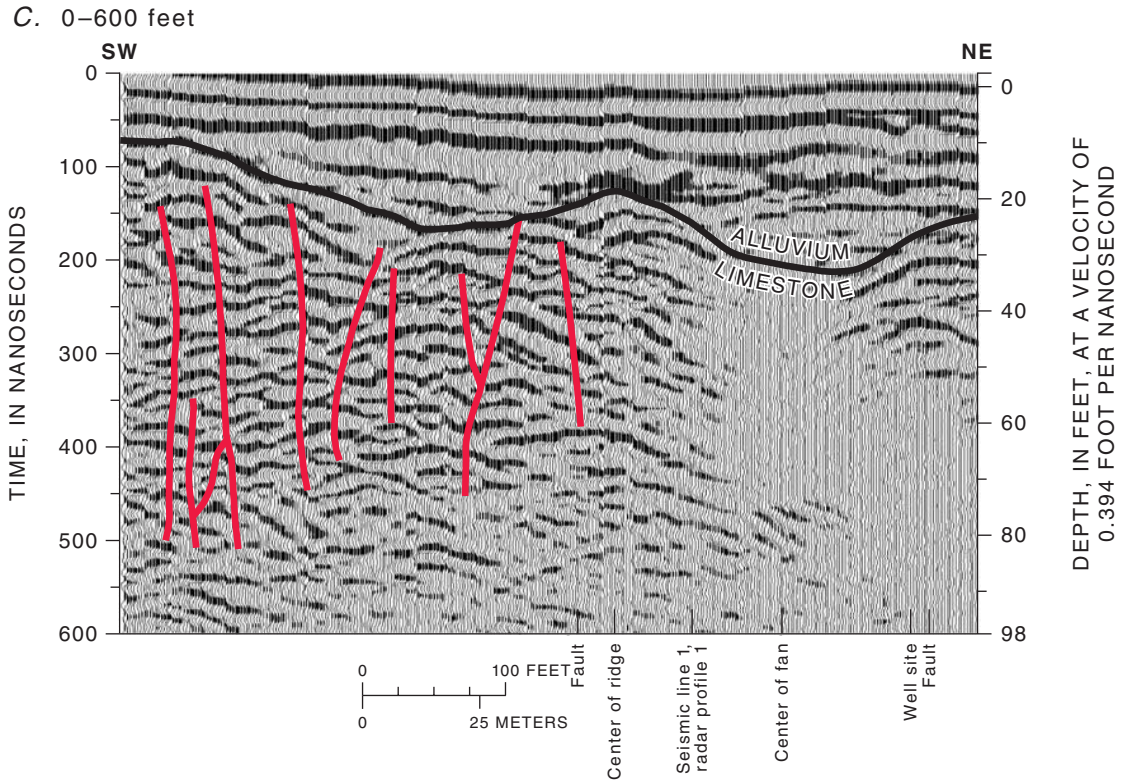

NOTE: Selected GPR data were collected with a 1,000-volt pulsar and 50-megahertz antenna, 12.0-foot spacing, 2.0-foot step, and a total time window of 1,200 nanoseconds (ηs). The data were gain adjusted and filtered to improve the visual presentation, and corrected for elevation changes along the profile. Vertical resolution of these images is about 1.0 to 2.0 ft. The vertical scale represents the two-way travel time of the radar signal.

Figure 22. Continued.

Seismic Reflection and Seismic Refraction

Two seismic-reflection images were collected in the Skunk Canyon area—a northeast-trending image and a northwest-trending image (**fig. 8**). The northwestward-trending image runs roughly down the center of the small graben (**fig. 23**). Many of the fractures observed in this seismic cross section dip at steep angles to near vertical. Only a few of the inferred faults extend along a single plane through the entire depth of the section. Many small zones of disruption extend from a few to several tens of feet. From evidence discussed in more detail in the section on the Continental seismic surveys, these features are inferred to be small caves, large solution openings, or large open fractures that extend well below the surface and would be target zones for water exploration if they extend below the water table. Unlike fractures imaged in other areas, these features do not appear to be well connected.

Square-Array Resistivity

Polar-coordinate graphs for the 32.8 and 65.6-foot square arrays at Skunk Canyon (SC) indicate a northwestward-striking fracture (N. 50° W.; see "**Supplemental Data**, Part A" at the back of the report). Data for the 164-foot square array indicate a north-south fracture pattern, and data for the 328.1- and 492.1-foot square arrays indicate a northwestward-striking fracture (N. 60° W. and N. 75° W., respectively). Data for the square arrays of 928.5 to 2,319.6 ft plotted in polar coordinates show an almost square pattern, which suggests an orthogonal-fracture set (Doe, 1982) that strikes north and west.

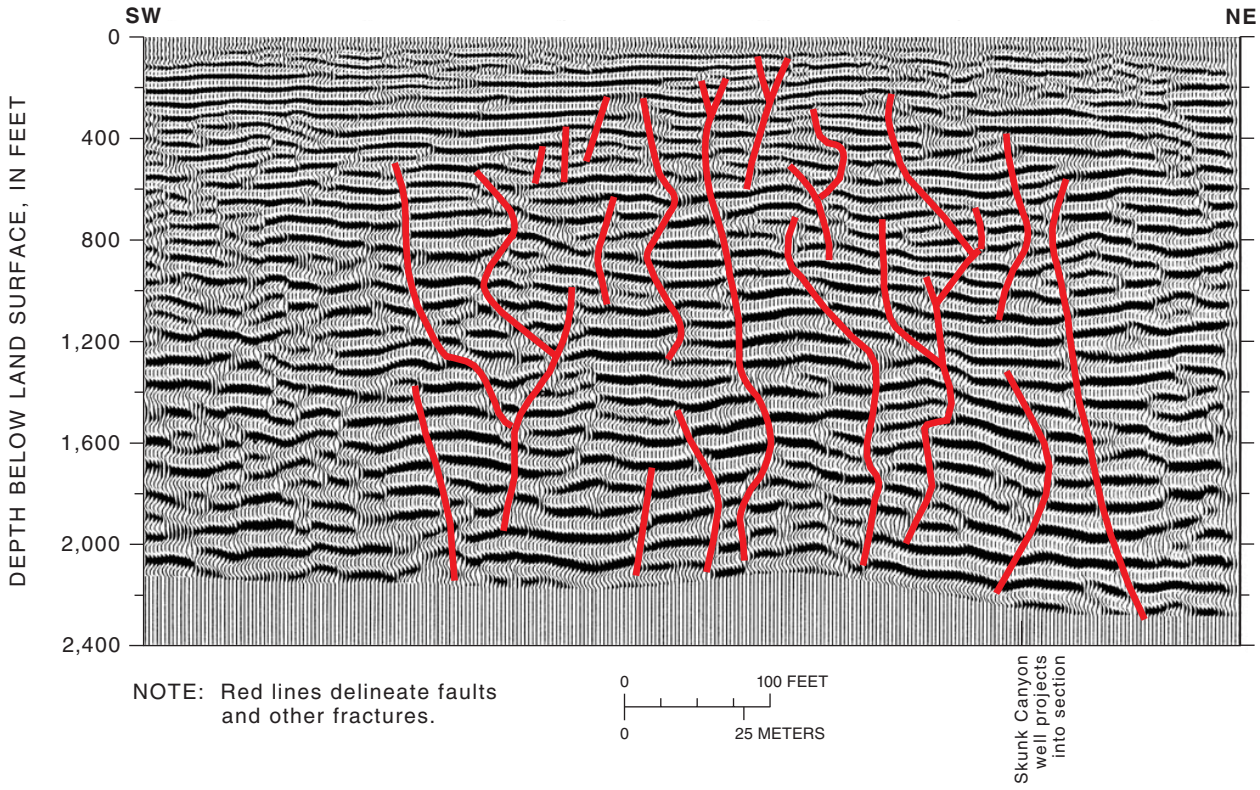

Figure 23. Stacked seismic image of the Skunk Canyon North profile No. 1. Many of the faults in the section are highlighted, but no major, through-going faults are apparent.

The calculated fracture strike for the square arrays of 32.8 and 65.6 ft is northwestward (N. 84° W. and N. 77° W., respectively; **fig. 24**; **table 1**). The strike is due north for the 164-foot square array. The square arrays of 328.1 and 492.1 ft show fracture strikes similar to those shown by the 32.8- and 65.6-foot square arrays. The square arrays of 928.5 to 2,319.6 ft indicate a northwestward strike (about N. 50° W.) that is close to the primary regional trend on the Colorado Plateau. The coefficient of anisotropy generally is flat at a ratio of 1.1:1 with one value of 1.2:1 at the square array of 492.1 ft. Secondary porosity (8.6 percent) is highest at the surface and decreases to less than 1 percent at 2,319.6 ft. Resistivity reached a maximum at 860 ft, which is consistent with the depth to the regional water table (920 ft) at this location (fig. 24).

Borehole

Borehole data for the Skunk Canyon well are correlative with formation lithology and fracturing in the subsurface identified from surface-geophysical surveys (**fig. 25**). The video log shows about 60 fractures above the water table (927 ft below land surface). Most of these fractures occur from 79 to 602 ft in the Kaibab Formation and upper Coconino Sandstone, and only three high-angle fractures are noted from 602 ft to the bottom of the video log at 934 ft. The lowermost of these fractures begins at 925 ft and was discharging water just above the water table in the well. About 34 of the fractures identified on the video log are horizontal to near-horizontal bedding-plane fractures. Most of these fractures are open, and a few are thin to closed. Most of the remaining 26 fractures imaged by the video log are high-angle fractures that dip 76 to 88°, and the rest are lower-angle fractures that dip 40 to 60°. Roughly half of the high-angle fractures are open, and the rest are thin to closed. This video log was not referenced azimuthally; therefore, the orientation of the fractures could not be determined. Data from the caliper logs indicate that additional fracturing occurs from 1,035 to 1,251 ft and from 1,350 to 1,775 ft. Large openings are apparent from the sonic log (not shown) at about 1,200, 1,400 to 1,450, and 1,720 to 1,740 ft.

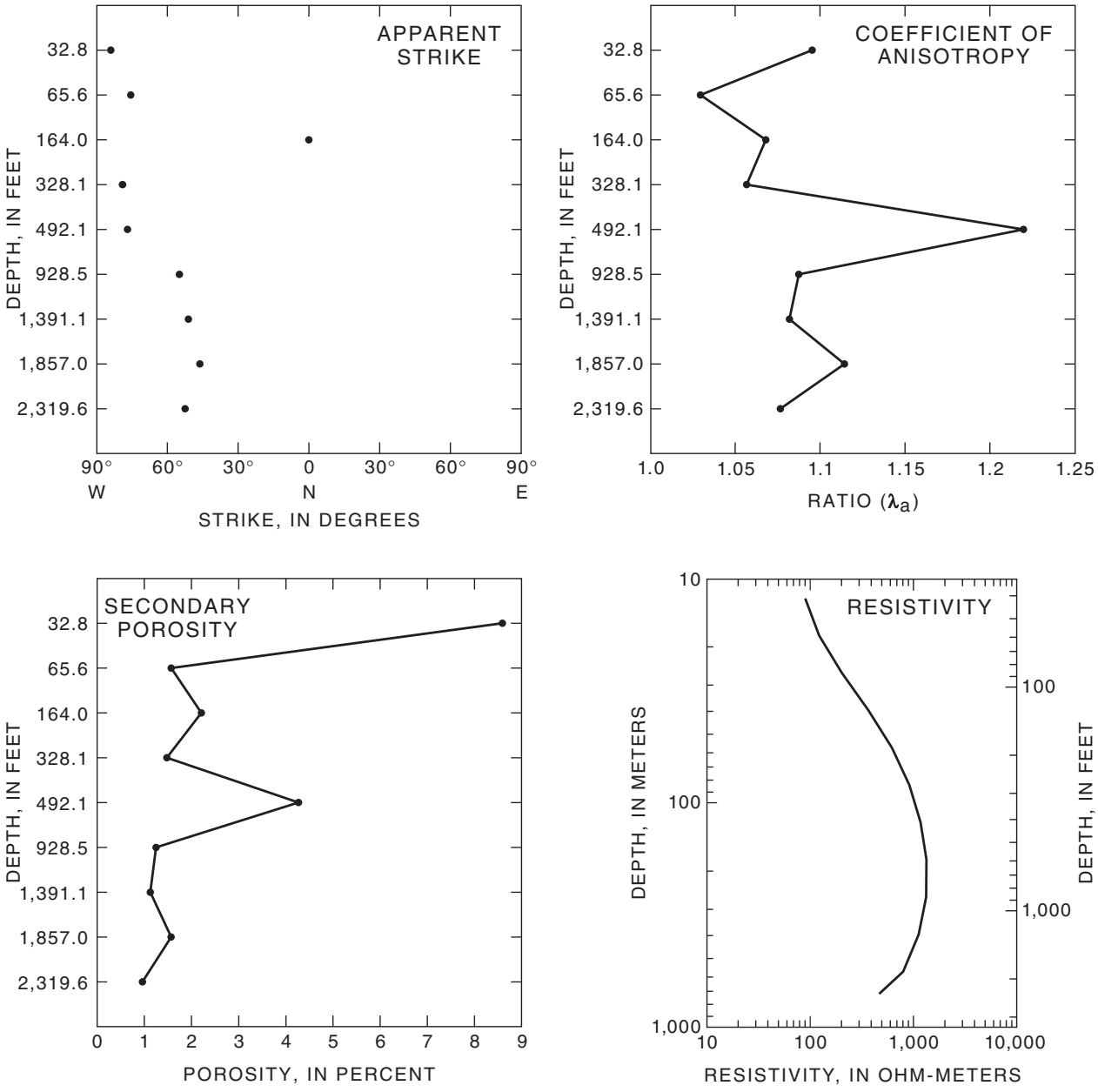

Figure 24. Calculated apparent strike of major fractures, coefficent of anisotropy, secondary porosity, and interpreted resistivity from the square-array sounding data, Skunk Canyon site (SC). Apparent strike values are in degrees for each square size (32.8, 65.6, 164.0.....). Coefficient of anisotropy. For the interpreted resistivity curve, depth to water was recorded as 919 feet. Interpretation was done using ATO, which is a vertical electrical-sounding (VES) computer program by Zohdy (1989). The interpreted resistivity-curve maxima is at about 860 feet.

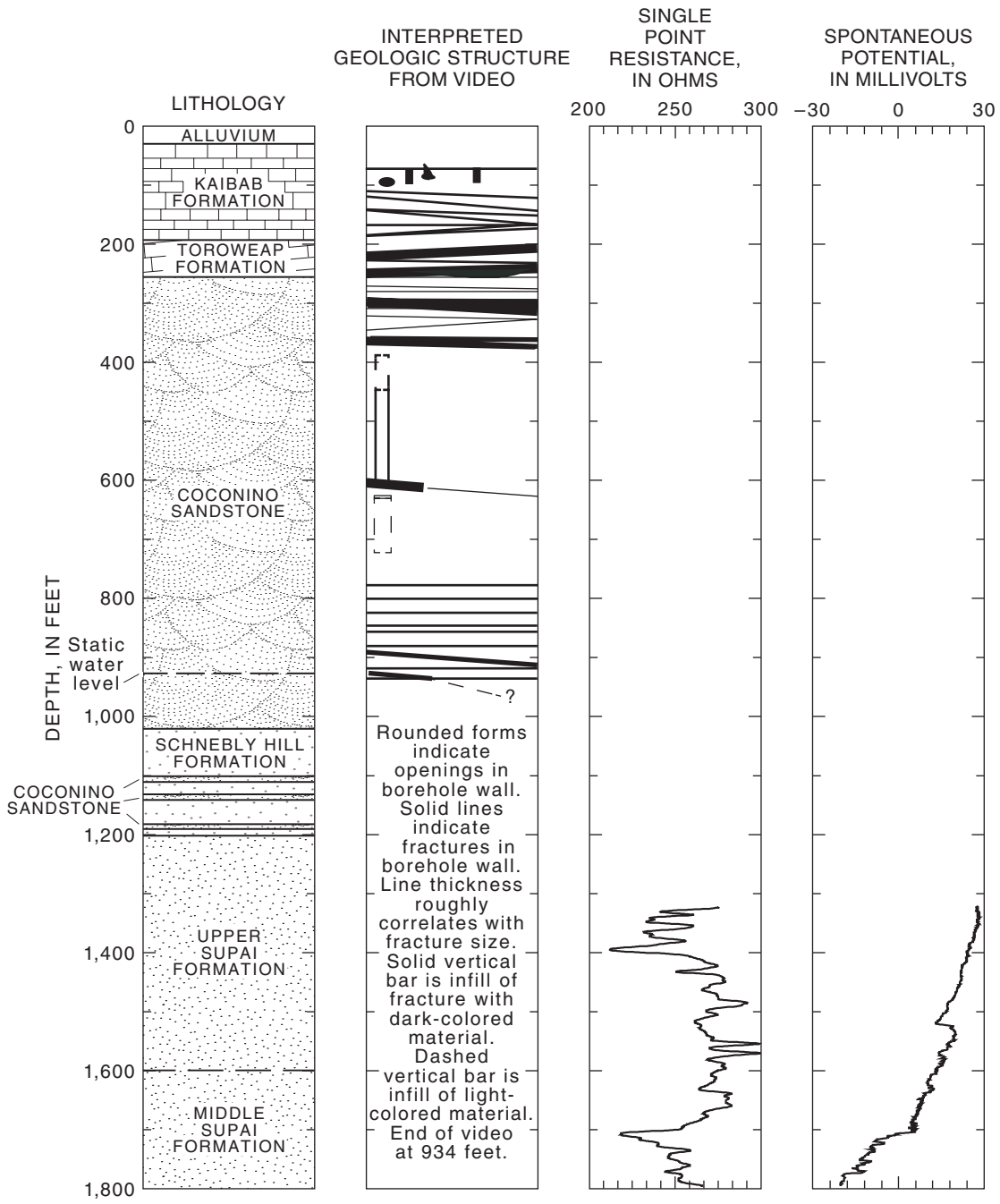

Figure 25. Lithologic and borehole-geophysical logs, Skunk Canyon well.

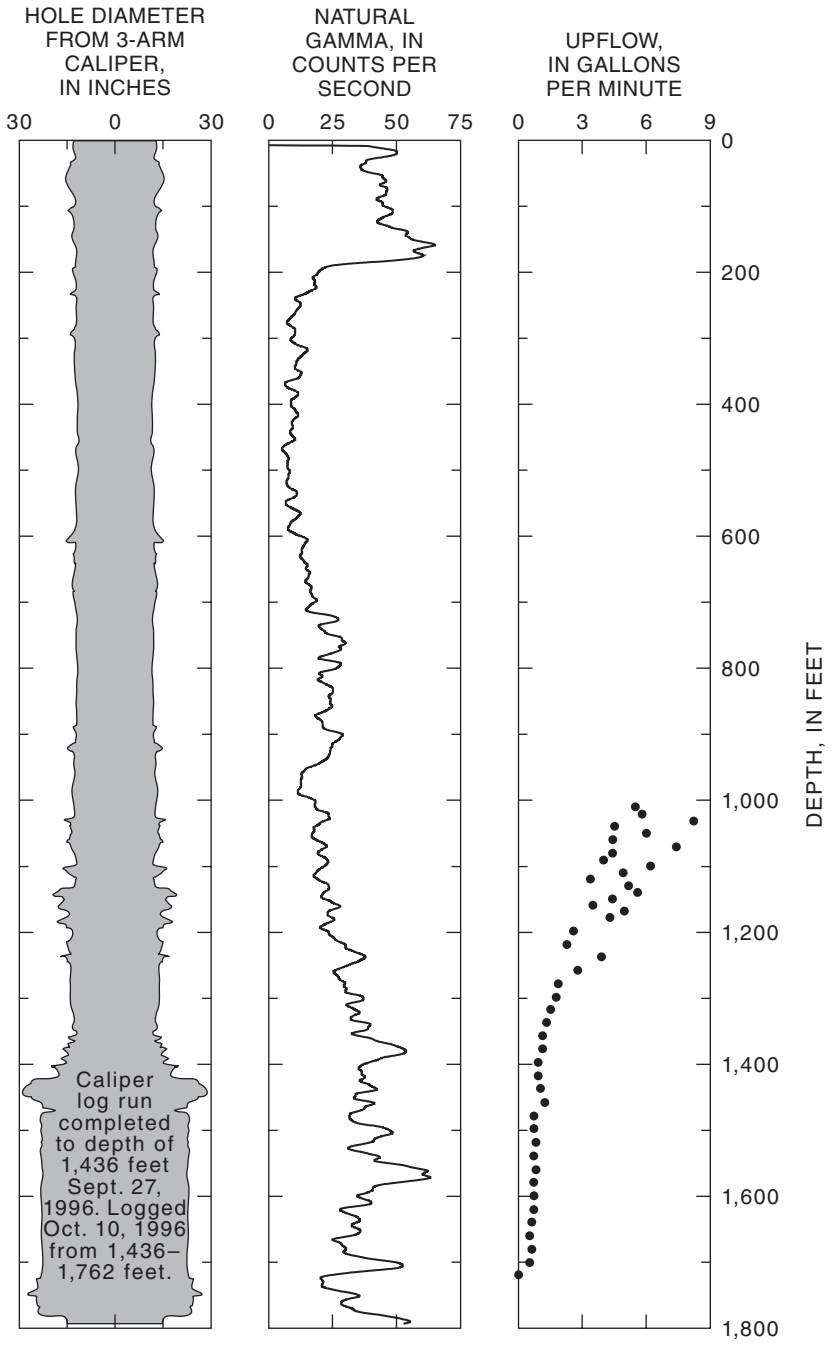

Figure 25. Continued.

In order to determine zones contributing flow to the well, a borehole-flowmeter log was run using a heat-pulse flow-meter while injecting water at a constant 10 gal/min. The flowmeter log indicates that most of the water flowed out of the hole from about 1,000 to 1,300 ft below land surface, and only minor amounts of water flowed out of the borehole from about 1,400 to 1,700 ft. These data correlate well with the location of fractures in the borehole inferred from the caliper and sonic logs. Heavily fractured zones in the borehole documented by the well logs correlate well with the zones of lateral disruption and minor vertical displacement shown on the seismic profile (**fig. 23**).

Peaks in secondary porosity and the coefficient of anisotropy at about 492 ft and at about 1,856 ft (**fig. 24**) correlate with significant disruption of the lithologic units indicated by seismic data from about the same depths (fig. 23) and fractures indicated by borehole-geophysical logs (**fig. 25**).

Foxglenn

Foxglenn is at the north end of the Anderson Mesa Fault, and evaluation of data from surficial investigations indicated the possibility of several structural features that could enhance water-bearing potential in the subsurface (**figs. 6**, **8**, and **26**). Among these features are multiple northwestward-striking faults and grabens intersected by a prominent northeastward-striking fracture. Outcrops of the Kaibab Formation in this area show significant vertical fracturing and horizontal bedding-plane fracturing (**fig. 27**). Fourteen GPR surveys, two seismic surveys, and one SAR survey were completed (fig. 8).

Ground-Penetrating Radar

GPR data for profile 1 were collected along a northwest-southeast line (N. 62° W.) that bends to an east-west line that is nearly perpendicular to the graben and the bounding fault (figs. 8 and 28A). The ends of the profile—from 0 to 120 ft from the east end and from 560 to 912 ft (not shown)—contain a chaotic radar record with short-segment horizontal bedding planes broken and offset several times. This type of chaotic record is consistent with heavily fractured rock that is found in the near-surface portion of a fault zone. The alluvial-bedrock contact on profile 1 at about 20 ft from the east end is consistent with the contact identified from a lithologic log of an observation well (MW-3) about 100 ft to the north (**fig. 28**A).

A short test profile (N. 60° E.) was made directly on bedrock at the north end of the Anderson Mesa Fault (fig. 28B). Three prominent bedding planes are at 2, 22, and 40 ft below land surface in the survey profile, dip shallowly to the east, and are consistent with the trend of the beds exposed at the surface. All three beds are offset downward in step fashion from west to east. At 244 ft from the west end of the profile, the beds are offset as much as 2 to 3 ft and are consistent with the offset on the Anderson Mesa Fault that is exposed downhill from this profile. Also noted deep in the profile are the crossing tails of two hyperbolic features. The location of these features at 60 to 62 ft below land surface suggests that they are not noise from manmade structures on or near the surface but are more likely openings at about 70 to 80 ft from the west end of the profile.

Profile 8 is aligned to the southeast (S. 57° E.) down the west side of the Rio de Flag Valley and is perpendicular to the northeastward-striking fracture zone in this area (fig. 28C). Bedding planes along the north end of the survey line are disrupted, which is consistent with heavy fracturing in the shallow subsurface.

Seismic Reflection and Seismic Refraction

Seismic profile, Foxglenn East, is aligned to the northeast and is set roughly perpendicular to a northwest-trending graben (**figs. 8** and **29**). Seismic profile, Foxglenn North, is roughly in the middle of the area in the flood plain of the Rio de Flag and crosses the Anderson Mesa Fault to the south (fig. 8). Many of the fractures observed on the seismic profile, Foxglenn East, dip at steep to near-vertical angles. Many of the fractures do not extend along a single plane; however, several fractures are interconnected. Three of the more prominent fracture zones extend from the surface or near the surface to as deep as 3,400 ft. Target areas for water exploration would be where these major fracture zones intersect the water table. The seismic-reflection data also appear to have imaged solution openings and caves. In some places, the horizontal layers are disrupted. Such disruption or low-coherence zones extend for tens to hundreds of feet horizontally and vertically throughout the profile above and below the zone of saturation. A well was drilled near the major through-going inferred fault near the center of the section (fig. 29). Well logs show caverns and abundant fractures in the upper 1,640 ft of the borehole where the seismic image is disrupted. The seismic and GPR data show characteristics that are consistent with heavily fractured rocks in the subsurface.

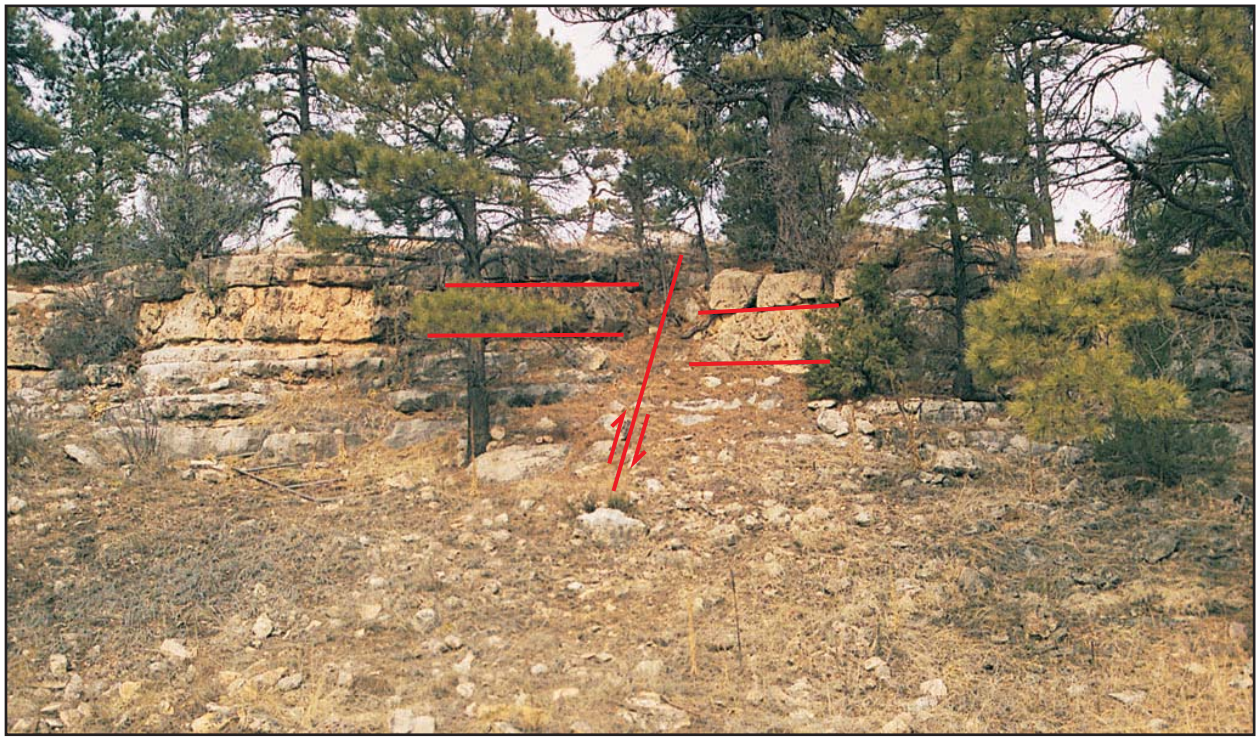

NOTE: Offset is 2–3 feet down to the east.

Figure 26. North end of the Anderson Mesa Fault and bedding-plane fractures in the Foxglenn area.

NOTE: Horizontal fractures in beds to the right and tilt of beds to the left.

Figure 2. Northeastward-striking fracture zone and possible faults in the Foxglenn area.

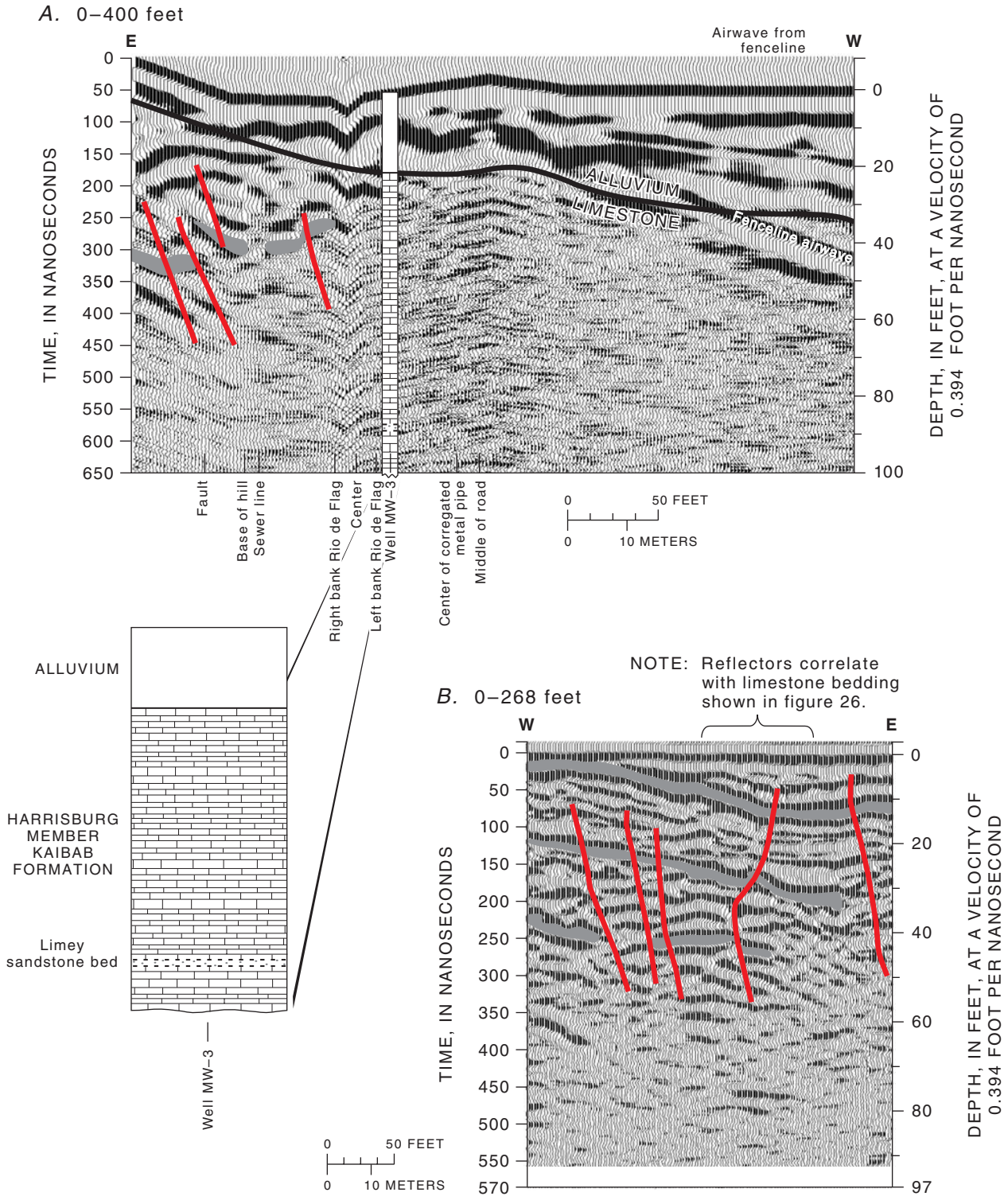

Figure 28. Selected interpreted ground-penetrating radar data for the Foxglenn area. *A*, Radar profile 1, 0–400 feet. *B*, Radar profile, Foxglenn test line, 0–268 feet. *C*, Radar profile 8, 0–500 feet. Interpreted fractures are showin in red, and interpreted bedding planes are gray fills. Hyperbolic events not identified as corregated metal pipe are interpreted as openings or open horizontal fractures.

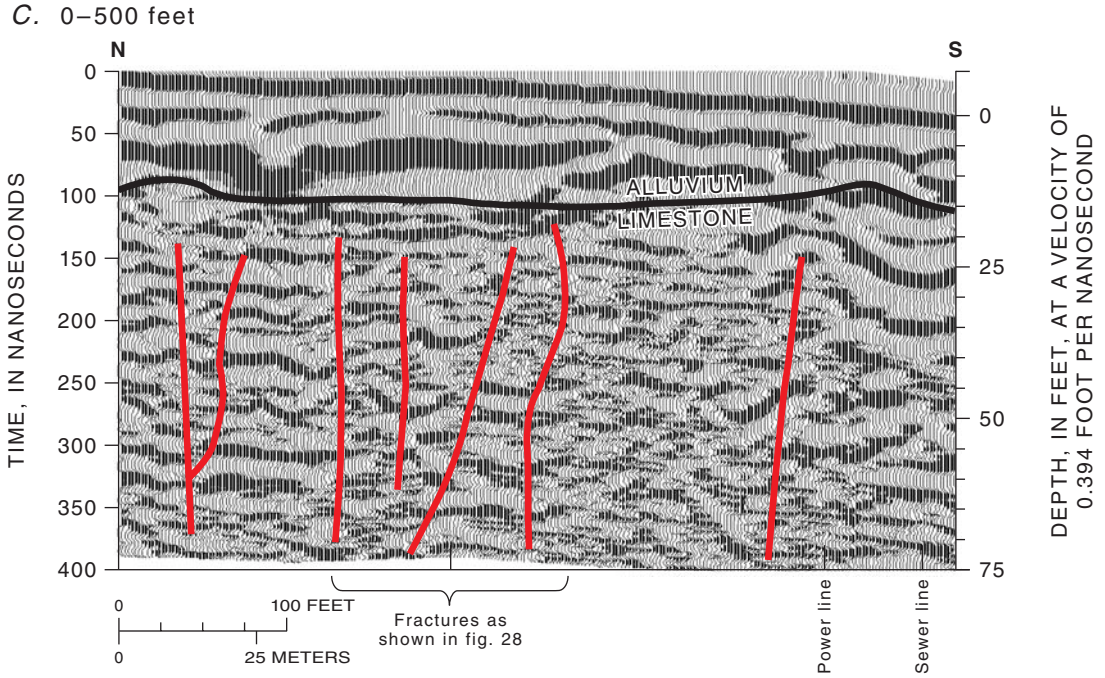

NOTE: Data for GPR were collected with a 1,000-volt pulsar and 50-megahertz antenna, 12.0-foot spacing, 2.0-foot step, and a total time window of 1,600 ηs, except for Foxglenn profile 1. Data for profile 1 were collected with a 25-megahertz antenna and a total time window of 1,800 nanoseconds (ηs). The data were gain adjusted and filtered to improve the visual presentation, and corrected for elevation changes along the profile. Vertical resolution of these images is about 1.0 to 2.0 feet. The vertical scale represents the two-way travel time of the radar signal.

Figure 28. Continued.

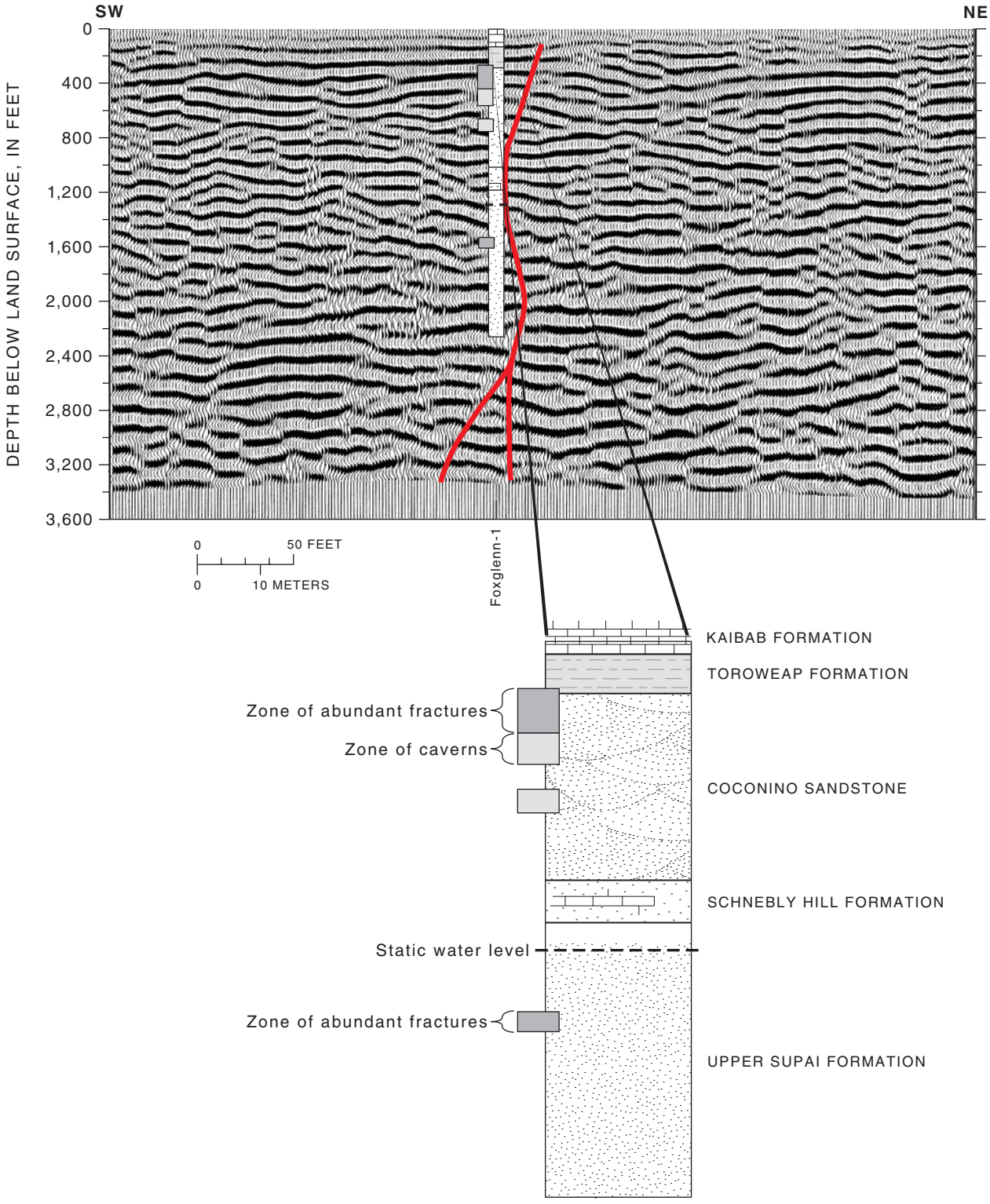

Figure 29. Stacked seismic image of the Foxglenn East profile. The major, through-going fault near the center of the section is shown as a solid red line, but any other faults can be seen on the section where reflectors are offset vertically. A well log also is showin in section. Caverns and other openings were determined from video and borehole-acoustic-teleview logs in the upper 1,640 feet of the borehole. Note that the seismic image shows missing reflections at the depths of caverns and other openings.

Square-Array Resistivity

In the Foxglenn area, the square array (FG) was in a narrow northeastward-trending (N. 15° E.) limestone valley along the Rio de Flag (**figs. 8** and **30**; **table 1**). The narrow limestone valley, vegetation, and cultural features limited the square array to a maximum square size of 492.1 ft (see "**Supplemental Data**, Part A"at the back of the report). The first plot of data from the square array at 32.8 ft shows a rough circular pattern typical of that for valley fill, and data for the 65.6- and 492.1-foot square arrays show that the small axes of the ellipses generally trend east and west.

The trend observed on the polar plots correlates with the calculated fracture strikes (fig. 30; **table 2**). The coefficient of anisotropy generally increases gradually with depth, and secondary porosity generally decreases gradually with depth. The reason for the east-west fracture strike is not clear. Generally, fractures in the Kaibab Formation at Foxglenn have northwestward and northeastward strikes (N. 45° W. and N. 45° E.). The high mean apparent resistivity (7,000 ohm-meters) may indicate open fractures or voids at depth.

Borehole

Video and borehole-acoustic-televiewer logs of the Foxglenn test well imaged about 35 fractures and several large openings from 33 to 1,605 ft below land surface (**fig. 31**). The only other logs available for this well are a lithologic log and a deviation log of the pilot hole. Other logs were not made for this well because collapses and bridging in the borehole during drilling necessitated the placement of casing for stabilization. Fourteen of the fractures imaged were open, horizontal to near-horizontal fractures. The remainder were mostly high-angle fractures that had dips of greater than 80°. A few fractures had dips of 57°. Several large openings also were detected in the borehole. One opening extends as much as 100 ft along the axis of a high-angle fracture from 476 to 582 ft. Another high-angle fracture from 699 to 789 ft was filled with silt and clay that possibly washed in from the surface through interconnected fractures. The video log was not referenced azimuthally; therefore, orientation or strike of the fractures could not be determined.
The borehole-acoustic televiewer imaged five prominent fractures below the water table from 1,545 to 1,605 ft (fig. 31). A large opening extends from about 1,545 to about 1,550 ft. Two open horizontal fractures occur above a washout that extends from about 1,558 to about 1,567 ft. A set of high-angle fractures extends from 1,570 to about 1,582 ft, dips 90°, and strikes northwest (N. 49° W.). One other prominent high-angle fracture is at about 1,590 ft, dips 90°, and strikes northwest (N. 42° W.). Another high-angle fracture is at about 1,600 ft, dips 87°, and strikes northwest (N. 49° W.).

The Foxglenn well is 574 ft from the southwest end of the seismic profile, Foxglenn East (fig. 29).
The fractures and openings in the well correlate with similar features imaged by the seismic profile. The well generally parallels and in places intersects a prominent near-vertical fault inferred from the seismic profile. The bottom of the well is in a zone of lateral disruption in the seismic profile that is similar to zones above that are associated with open fractures and caves. These features may account for bridging, caving, and flowing sand that occurred during the well drilling. The Foxglenn well is in a northwestward-trending graben, and the fractures imaged by the borehole-acoustic televiewer at depth are consistent with this trend.

Continental

The Continental area is at the intersection of two prominent structural trends. The first trend is the Continental graben, which trends northwestward and has been previously mapped by Ulrich and others (1984). The second trend is a series of three previously unmapped lineaments identified photogrammetically and with remotely sensed data that probably are surface fractures overlying deep-seated older northeastward-striking faults similar to those described by Shoemaker and others (1978). The Continental graben appears to be offset laterally to the southwest by the middle of these three lineaments. Displacement on the east-bounding fault of the graben is about 100 ft down to the west. At least two sinkholes are in the Continental graben. One of these sinkholes is referred to locally as the Bottomless Pits, which appear to be a series of northeastward-striking fractures truncated by a minor offset parallel to the main northwestward trend of the graben (**fig. 8**C). All of these fractures have been widened by solution, and the alluvial material overlying the fractures and a minor northwestward-striking fault has slumped and created a depression that is about 30 ft deep. Overflow from Rio de Flag that is intercepted by the Bottomless Pits is diverted under ground. During February and March 1995, runoff from Rio de Flag into the Bottomless Pits continued inter-mittently for 31 days at flow rates of as much as 70 ft^3/s. The estimated total volume of flow during that period was about 610 acre-ft, or about 10 percent of the ground water currently pumped by the City of Flagstaff.

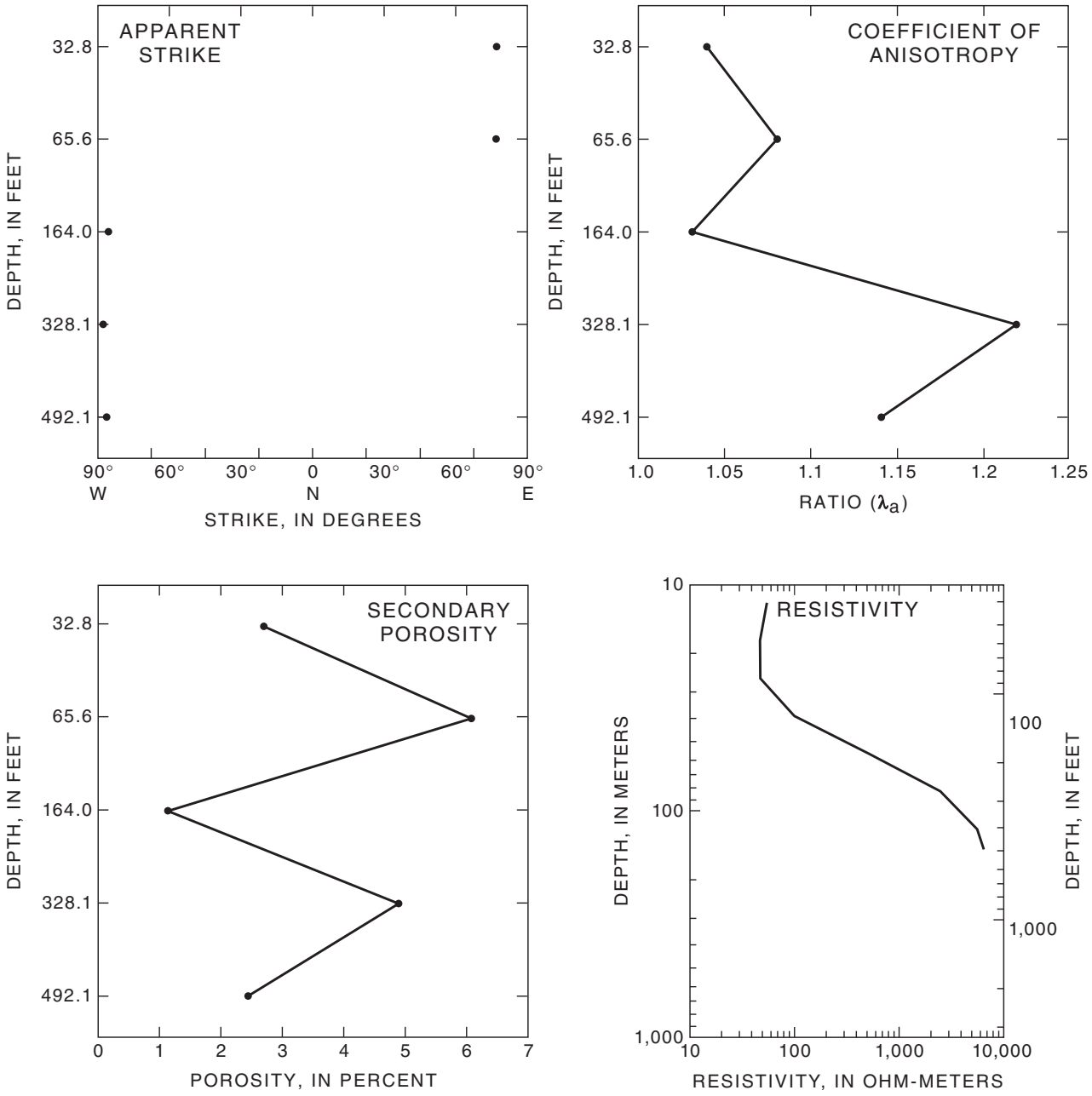

Figure 30. Calculated apparent strike of major fractures, coefficient of anisotropy, secondary porosity, and interpreted resistivity from the square-array sounding data, Foxglenn site (FG). Apparent strike values are in degrees for each square size (32.8, 65.6, 164.0.....). Coefficient of anisotropy is a dimensionless number where any number larger than one indicates increasing anisotropy. For the interpreted resistivity curve, depth to water recorded at the Foxglenn well was 1,312 feet. Interpretation was done using ATO, which is a vertical electrical-sounding (VES) computer program by Zohdy (1989). The interpreted resistivity-curve depth of exploration was 492.1 feet.

Table 2. Physical and chemical data for water from selected wells and springs, for surface water, and for precipitation, Flagstaff, Arizona

[R, regional aquifer; P, perched ground water; S, surface water; SN, snowmelt; deg C, degrees Celsius; mg/L, milligrams per liter; μg/L, micro-grams per liter; μS/cm, microsiemens per centimeter at 25°C; pCi/L, picocuries per liter; TU, tritium units; pmc, percent modern carbon; ^{14}C, carbon-14; ^{13}C, carbon-13; modern, less than 200 years; <, less than. Dashes indicate no data]

Well, spring, or owner name	Site identifier	Latitude	Longitude	Water source	Date	Tempera-ture water (deg C)	pH water whole field (standard units)	Alkalinity wat distot it field (mg/L as $CaCO_3$)	Hardness total (mg/L as $CaCO_3$)	Alkalinity wat dis fix end field (mg/L as $CaCO_3$)	Specific conduct-ance field (μS/cm)
LM-4	(A-20-08)19aba	35°06'25"	111°35'05"	R	07-01-96	11.2	7.8	131	140	130	254
Do.	Do.	Do.	Do.	Do.	02-20-97	11.4	7.9	---	---	---	253
Do.	Do.	Do.	Do.	Do.	08-20-97	11.2	7.9	---	---	---	250
LM-8	(A-20-08)20cca	35°05'47"	111°34'30"	R	07-01-96	11.0	7.3	262	280	258	488
LM-9	(A-20-08)30cda	35°04'51"	111°35'25"	R	07-01-96	10.9	7.2	364	380	359	635
Upper Lake Mary	---	35°04'16"	111°31'02"	S	07-08-96	20.6	7.2	---	---	---	60
WM-1	(A-21-06)35cba	35°09'24"	111°44'01"	R	07-01-96	11.3	8.0	106	100	103	211
WM-6	(A-20-06)02bdb	35°08'47"	111°44'04"	R	07-01-96	12.8	8.1	104	100	103	199
WM-9	(A-20-06)11bdc	35°07'45"	111°43'56"	R	07-01-96	12.8	7.3	118	120	117	233
Do.	Do.	Do.	Do.	Do.	02-25-97	12.2	8.2	---	---	---	209
Do.	Do.	Do.	Do.	Do.	08-26-97	12.6	8.1	---	---	---	212
Continental-2	(A-21-08)17bca2	35°12'23"	111°34'28"	R	04-17-97	11.5	7.8	128	130	128	273
Foxglenn-1	(A-21-07)24aad	35°11'37"	111°35'48"	R	06-01-97	14.5	7.5	227	220	226	428
Pine Grove	(A-19-09)17dcd	35°01'24"	111°27'35"	R	06-10-96	15.0	6.7	254	240	252	475
NPS Walnut Canyon	(A-21-08)26dab	35°10'25"	111°30'37"	R	06-11-96	14.6	7.5	199	200	197	409
Mountainaire	(A-20-07)28bcc	35°05'11"	111°40'00"	R	06-12-96	10.6	6.9	205	200	199	379
Hidden Hollow	(A-21-07)19aca	35°11'30"	111°41'16"	R	06-14-96	19.0	8.1	102	94	103	209
Flag Ranch	(A-21-06)25bcd	35°10'25"	111°42'52"	R	06-13-96	13.2	7.9	---	81	---	187
Purl	(A-21-07)25bbd	35°10'43"	111°36'37"	R	06-18-96	13.1	7.1	247	280	245	450
Henden	(A-21-06)23aad	35°11'35"	111°43'10"	R	06-18-96	14.1	8.0	74	82	77	168
NPS Wupatki HQ[1]	(A-25-10)30bdb	35°31'10"	111°22'20"	R	06-26-96	20.5	7.2	196	450	191	----
Do.[1]	Do.	Do.	Do.	Do.	07-09-96	20.6	7.5	205	450	205	----
IB-9	(A-23-07)33aab2	35°20'27"	111°39'00"	P	07-02-96	5.3	7.6	26	19	25	571
IB snowmelt	---	35°20'27"	111°39'00"	SN	01-29-97	---	---	---	---	---	---
Babbitt Spring	(A-20-08)34cdb	35°04'01"	111°32'16"	R	06-14-96	8.5	7.2	336	350	336	637
Clark Spring	(A-20-08)32cca	35°04'02"	111°34'44"	R	06-13-96	11.0	7.2	261	240	259	462
Rio de Flag MW-1	(A-21-07)23cac	35°11'20"	111°38'00"	P	06-13-96	11.5	6.9	214	270	210	588
FH-5	(A-20-06)24abb	35°06'25"	111°42'03"	R	06-25-96	12.6	7.0	218	220	217	395
Parks Sch.	(A-22-04)27aad	35°15'46"	111°56'58"	P	06-25-96	12.2	7.8	129	110	126	254
Quarry	---	35°12'01"	111°49'31"	S	06-21-96	13.6	---	159	35	161	351
Old Town Spring	(A-21-07)16cdb	35°11'53"	111°39'38"	P	07-08-96	12.5	7.4	108	100	108	244
Rio de Flag MW-3	(A-21-07)25bba2	35°10'52"	111°36'33"	P	06-12-96	11.2	7.3	332	400	326	909
Sterling Springs	(A-19-06)15ddd1	35°01'30"	111°44'22"	R	06-18-96	11.0	7.7	122	140	122	270
NAD-1	(A-21-05)11abc	35°13'15"	111°50'00"	P	06-21-96	8.7	7.3	138	130	136	325
BBDP-MVR-1	(A-21-09)06baa	35°14'16"	111°28'50"	R	06-11-96	17.9	7.7	135	170	132	436
Do.	Do.	Do.	Do.	Do.	04-08-97	18.5	7.8	131	180	131	403
Do.	Do.	Do.	Do.	Do.	08-26-97	18.0	7.7	---	---	---	410
BBDP-Marijka	(A-22-08)23abb	35°16'56"	111°30'52"	R	06-11-96	6.6	6.6	250	250	248	484
Mtn Dell-1	(A-21-07)32bbc1	35°09'46"	111°40'53"	R	06-19-96	12.0	7.1	239	270	234	444
Do.	Do.	Do.	Do.	Do.	03-11-97	10.6	7.2	---	---	---	506
Do.	Do.	Do.	Do.	Do.	08-28-97	11.9	7.3	---	---	---	501
Mtn Dell-2	(A-21-07)32bbc2	35°09'48"	111°40'52"	R	06-19-96	12.0	7.3	184	220	182	370
Center snowmelt	---	34°12'27"	111°37'57"	SN	01-15-97	---	---	---	---	---	---

See footnotes at end of table.

Table 2. Physical and chemical data for water from selected wells and springs, for surface water, and for precipitation, Flagstaff, Arizona—Continued

Well, spring, or owner name	Date	Calcium, dissolved (mg/L as Ca)	Magnesium, dissolved (mg/L as Mg)	Sodium, dissolved (mg/L as Na)	Potassium, dissolved (mg/L as K)	Chloride, dissolved (mg/L as Cl)	Fluoride, dissolved (mg/L as F)	Sulfate, dissolved (mg/L as SO_4)	Silica, dissolved (mg/L as SiO_2)	Arsenic, dissolved (µg/L as As)	Barium, dissolved (µg/L as Ba)
LM-4	07-01-96	27	17	2.0	0.30	0.70	0.20	2.5	7.7	6	66
Do.	02-20-97	---	---	---	---	---	---	---	---	---	---
Do.	08-20-97	---	---	---	---	---	---	---	---	---	---
LM-8	07-01-96	53	36	3.7	.60	2.0	<.10	1.5	9.4	3	380
LM-9	07-01-96	70	49	3.5	.90	2.6	.10	1.3	12	3	650
Upper Lake Mary	07-08-96	---	---	---	---	---	---	---	---	---	---
WM-1	07-01-96	22	12	4.5	1.2	1.7	<.10	2.2	19	4	400
WM-6	07-01-96	20	12	4.8	1.4	1.6	<.10	1.6	19	6	840
WM-9	07-01-96	25	13	4.8	1.2	1.5	<.10	1.5	17	6	580
Do.	02-25-97	---	---	---	---	---	---	---	---	---	---
Do.	08-26-97	---	---	---	---	---	---	---	---	---	---
Continental-2	04-17-97	26	16	5.6	.59	2.0	.19	4.2	9.1	2	505
Foxglenn-1	06-01-97	49	25	4.8	1.1	1.7	<.10	1.5	11	1	480
Pine Grove	06-10-96	52	27	7.4	1.0	---	---	---	24	6	[2]2,000
NPS Walnut Canyon	06-11-96	45	22	4.7	.90	5.8	.10	2.8	11	<1	280
Mountainaire	06-12-96	44	21	3.3	.50	2.9	.20	.80	15	2	36
Hidden Hollow	06-14-96	21	10	4.9	1.5	2.4	<.10	1.7	18	17	160
Flag Ranch	06-13-96	18	8.6	6.4	1.4	1.4	.10	1.8	18	28	210
Purl	06-18-96	56	33	3.1	.90	2.0	<.10	1.4	12	<1	63
Henden	06-18-96	18	8.9	4.9	1.5	1.9	.10	1.9	18	20	660
NPS Wupatki HQ[1]	06-26-96	71	67	260	4.6	430	.30	[3]250	11	<1	22
Do.[1]	07-09-96	71	67	250	4.4	410	.30	220	12	<1	21
IB-9	07-02-96	4.3	2.1	2.7	2.1	.40	.40	1.5	39	2	<2.0
IB snowmelt	01-29-97	---	---	---	---	---	---	---	---	---	---
Babbitt Spring	06-14-96	76	38	8.0	.50	10	.20	3.4	23	<1	25
Clark Spring	06-13-96	49	28	3.3	.50	1.5	.10	2.0	14	<1	46
Rio de Flag MW-1	06-13-96	62	28	17	1.9	52	<.10	22	27	1	38
FH-5	06-25-96	48	25	3.8	1.1	2.3	.10	.80	13	1	950
Parks Sch.	06-25-96	29	9.5	13	2.2	4.7	.10	2.0	29	1	24
Quarry	06-21-96	5.6	5.0	63	12	7.5	.60	3.1	3.2	2	12
Old Town Spring	07-08-96	20	12	11	1.6	6.8	.10	8.6	34	<1	11
Rio de Flag MW-3	06-12-96	78	50	17	1.9	31	.20	24	17	2	46
Sterling Springs	06-18-96	31	14	2.8	.60	1.3	<.10	.50	14	2	120
NAD-1	06-21-96	30	14	14	2.0	4.9	.10	14	23	<1	10
BBDP-MVR-1	06-11-96	36	20	8.2	1.8	29	.10	4.8	13	<1	1,200
Do.	04-08-97	34	23	11	1.9	34	<.10	5.0	13	<1	1,310
Do.	08-26-97	---	---	---	---	---	---	---	---	---	---
BBDP-Marijka	06-11-96	53	28	6.3	1.8	6.1	.20	2.8	19	2	1,200
Mtn Dell-	06-19-96	61	28	4.2	.80	3.1	<.10	2.1	14	3	34
Do.	03-11-97	---	---	---	---	---	---	---	---	---	---
Do.	08-28-97	---	---	---	---	---	---	---	---	---	---
Mtn Dell-	06-19-96	50	22	3.3	.80	5.7	<.10	2.4	15	4	25
Center snowmelt	01-15-97	---	---	---	---	---	---	---	---	---	---

See footnotes at end of table.

Table 2. Physical and chemical data for water from selected wells and springs, for surface water, and for precipitation, Flagstaff, Arizona—Continued

Well, spring, or owner name	Date	Beryllium, dissolved (µg/L as Be)	Boron, dissolved (µg/L as B)	Cadmium, dissolved (µg/L as Cd)	Chromium, dissolved (µg/L as Cr)	Cobalt, dissolved (µg/L as Co)	Copper, dissolved (µg/L as Cu)	Iron, dissolved (µg/L as Fe)	Lead, dissolved (µg/L as Pb)	Manganese, dissolved (µg/L as Mn)	Molybdeum, dissolved (µg/L as Mo)	Nickel, dissolved (µg/L as Ni)
LM-4	07-01-96	<0.50	4.5	<1.0	<5.0	<3.0	<10	<3.0	<10	<1.0	<10	<10
Do.	02-20-97	---	---	---	---	---	---	---	---	---	---	---
Do.	08-20-97	---	---	---	---	---	---	---	---	---	---	---
LM-8	07-01-96	<.50	<4.0	<1.0	<5.0	<3.0	<10	<3.0	<10	<1.0	<10	<10
LM-9	07-01-96	<.50	7.0	<1.0	<5.0	<3.0	<10	<3.0	<10	1.0	<10	<10
Upper Lake Mary	07-08-96	---	---	---	---	---	---	---	---	---	---	---
WM-1	07-01-96	<.50	5.5	<1.0	<5.0	<3.0	<10	3.0	<10	2.0	<10	<10
WM-6	07-01-96	<.50	6.0	<1.0	<5.0	<3.0	<10	<3.0	<10	<1.0	<10	<10
WM-9	07-01-96	<.50	6.0	<1.0	<5.0	<3.0	<10	76	<10	32	<10	<10
Do.	02-25-97	---	---	---	---	---	---	---	---	---	---	---
Do.	08-26-97	---	---	---	---	---	---	---	---	---	---	---
Continental-2	04-17-97	<.50	6.6	<1.0	<5.0	<3.0	<10	<3.0	<10	<1.0	<10	<10
Foxglenn-1	06-01-97	<.50	18.9	<1.0	<5.0	<3.0	<10	13	<10	1.3	<10	<10
Pine Grove	06-10-96	<.50	---	<1.0	<5.0	<3.0	<10	<3.0	<10	<1.0	<10	<10
NPS Walnut Canyon	06-11-96	<.50	9.7	<1.0	<5.0	<3.0	<10	3.0	<10	<1.0	<10	<10
Mountainaire	06-12-96	<.50	6.3	<1.0	<5.0	<3.0	<10	<3.0	<10	<1.0	<10	<10
Hidden Hollow	06-14-96	<.50	10	<1.0	<5.0	<3.0	<10	<3.0	<10	<1.0	<10	<10
Flag Ranch	06-13-96	<.50	8.8	<1.0	<5.0	<3.0	<10	5.0	<10	<1.0	<10	<10
Purl	06-18-96	<.50	15	<1.0	<5.0	4.0	<10	4.0	<10	1.0	10	<10
Henden	06-18-96	.60	17	2.0	<5.0	7.0	<10	6.0	<10	32	<10	<10
NPS Wupatki HQ[1]	06-26-96	<1.5	94	<3.0	<15	<9.0	<30	<9.0	<30	<3.0	<30	<30
Do.[1]	07-09-96	<1.5	96	<3.0	<15	<9.0	<30	14	<30	3.0	<30	<30
IB-9	07-02-96	<.50	5.8	2.0	<5.0	<3.0	<10	<3.0	<10	<1.0	<10	<10
IB snowmelt	01-29-97	---	---	---	---	---	---	---	---	---	---	---
Babbitt Spring	06-14-96	<.50	8.2	<1.0	<5.0	<3.0	<10	<3.0	<10	<1.0	<10	<10
Clark Spring	06-13-96	<.50	10	<1.0	<5.0	<3.0	<10	44	<10	17	<10	<10
Rio de Flag MW-1	06-13-96	<.50	44	<1.0	<5.0	<3.0	<10	8.0	<10	1.0	<10	<10
FH-5	06-25-96	<.50	11	<1.0	<5.0	<3.0	<10	3.0	<10	<1.0	<10	<10
Parks Sch.	06-25-96	<.50	19	<1.0	<5.0	<3.0	<10	20	<10	4.0	<10	<10
Quarry	06-21-96	<.50	42	1.0	<5.0	<3.0	<10	54	<10	7.0	<10	<10
Old Town Spring	07-08-96	<.50	25	<1.0	<5.0	<3.0	<10	<3.0	<10	<1.0	10	<10
Rio de Flag MW-3	06-12-96	<.50	45	<1.0	<5.0	<3.0	<10	17	20	<1.0	<10	<10
Sterling Springs	06-18-96	<.50	4.7	<1.0	<5.0	3.0	20	<3.0	<10	<1.0	<10	<10
NAD-1	06-21-96	<.50	31	<1.0	<5.0	<3.0	<10	<3.0	<10	<1.0	<10	<10
BBDP-MVR-1	06-11-96	<.50	16	<1.0	<5.0	<3.0	<10	5.0	<10	[4]78	<10	<10
Do.	04-08-97	<.50	20	1.1	5.9	<3.0	13	6.9	13	16	<10	15
Do.	08-26-97	---	---	---	---	---	---	---	---	---	---	---
BBDP-Marijka	06-11-96	<.50	19	<1.0	<5.0	<3.0	<10	<3.0	10	<1.0	<10	<10
Mtn Dell-	06-19-96	<.50	13	<1.0	<5.0	<3.0	<10	<3.0	<10	<1.0	<10	<10
Do.	03-11-97	---	---	---	---	---	---	---	---	---	---	---
Do.	08-28-97	---	---	---	---	---	---	---	---	---	---	---
Mtn Dell-	06-19-96	<.50	9.4	<1.0	<5.0	5.0	<10	<3.0	<10	<1.0	<10	<10
Center snowmelt	01-15-97	---	---	---	---	---	---	---	---	---	---	---

See footnotes at end of table.

Table 2. Physical and chemical data for water from selected wells and springs, for surface water, and for precipitation, Flagstaff, Arizona—Continued

Well, spring, or owner name	Date	Silver, dissolved (µg/L as Ag)	Strontium, dissolved (µg/L as Sr)	Vanadium, dissolved (µg/L as V)	Antimony, dissolved (µg/L as Sb)	Lithium, dissolved (µg/L as Li)	Selenium, dissolved (µg/L as Se)	Nitrogen, nitrate dissolved (mg/L as N)	Nitrogen, ammonia dissolved (mg/L as N)	Nitrogen, nitrite dissolved (mg/L as N)	Nitrogen, ammonia+ organic total dissolved (mg/L as N)
LM-4	07-01-96	<1.0	25	<6	2.0	<4	<1	---	0.03	<0.01	<0.20
Do.	02-20-97	---	---	---	---	---	---	---	---	---	---
Do.	08-20-97	---	---	---	---	---	---	---	---	---	---
LM-8	07-01-96	<1.0	62	<6	1.0	<4	<1	---	.03	<.01	<.20
LM-9	07-01-96	<1.0	80	<6	1.0	<4	<1	---	.03	<.01	<.20
Upper Lake Mary	07-08-96	---	---	---	---	---	---	---	---	---	---
WM-1	07-01-96	<1.0	110	<6	2.0	<4	<1	---	.04	<.01	<.20
WM-6	07-01-96	<1.0	91	<6	2.0	<4	<1	---	.03	<.01	<.20
WM-9	07-01-96	<1.0	86	<6	2.0	<4	<1	---	.03	<.01	<.20
Do.	02-25-97	---	---	---	---	---	---	---	---	---	---
Do.	08-26-97	---	---	---	---	---	---	---	---	---	---
Continental-2	04-17-97	<1.0	36	<6	<1.0	<4	<1	---	<.02	<.01	<.20
Foxglenn-1	06-01-97	<1.0	66	<6	<1.0	<4	<1	---	<.02	<.01	<.20
Pine Grove	06-10-96	<1.0	300	<6	1.0	<4	<1	---	.03	<.01	<.20
NPS Walnut Canyon	06-11-96	<1.0	71	<6	<1.0	<4	<1	---	.02	<.01	<.20
Mountainaire	06-12-96	<1.0	110	<6	<1.0	<4	<1	---	.05	<.01	<.20
Hidden Hollow	06-14-96	<1.0	70	<6	2.0	<4	<1	---	.03	<.01	<.20
Flag Ranch	06-13-96	<1.0	77	<6	[5]7.0	<4	<1	---	.02	<.01	<.20
Purl	06-18-96	<1.0	60	<6	<1.0	<4	<1	---	.03	<.01	<.20
Henden	06-18-96	<1.0	70	<6	[5]6.0	<4	<1	---	.03	<.01	<.20
NPS Wupatki HQ[1]	06-26-96	<3.0	1,100	<18	<1.0	26	4	---	<.02	<.01	<.20
Do.[1]	07-09-96	<3.0	1,100	<18	<1.0	23	4	---	.03	<.01	<.20
IB-9	07-02-96	<1.0	18	<6	<1.0	<4	<1	---	.04	<.01	<.20
IB snowmelt	01-29-97	---	---	---	---	---	---	---	---	---	---
Babbitt Spring	06-14-96	<1.0	140	<6	<1.0	<4	<1	---	<.02	<.01	1.1
Clark Spring	06-13-96	<1.0	87	<6	<1.0	<4	<1	---	.120	<.01	<.20
Rio de Flag MW-1	06-13-96	<1.0	160	<6	<1.0	<4	<1	---	.04	<.01	<.20
FH-5	06-25-96	<1.0	110	<6	<1.0	<4	<1	---	<.02	<.01	<.20
Parks Sch.	06-25-96	<1.0	260	15	<1.0	<4	<1	.30	<.02	.01	<.20
Quarry	06-21-96	<1.0	48	<6	1.0	<4	<1	---	.03	.02	.80
Old Town Spring	07-08-96	<1.0	200	<6	<1.0	<4	<1	1.58	.38	.02	<.20
Rio de Flag MW-3	06-12-96	<1.0	130	<6	<1.0	<4	<1	---	.03	<.01	<.20
Sterling Springs	06-18-96	<1.0	80	7	<1.0	<4	<1	---	.02	<.01	<.20
NAD-1	06-21-96	<1.0	320	<6	<1.0	<4	<1	---	.04	<.01	<.20
BBDP-MVR-1	06-11-96	<1.0	120	<6	<1.0	<4	<1	---	.04	<.01	<.20
Do.	04-08-97	1.5	139	<6	<1.0	4	<1	---	<.02	<.01	<.20
Do.	08-26-97	---	---	---	---	---	---	---	---	---	---
BBDP-Marijka	06-11-96	<1.0	160	<6	<1.0	5	1	---	.03	<.01	<.20
Mtn Dell-	06-19-96	<1.0	67	<6	<1.0	<4	<1	---	.04	<.01	<.20
Do.	03-11-97	---	---	---	---	---	---	---	---	---	---
Do.	08-28-97	---	---	---	---	---	---	---	---	---	---
Mtn Dell-	06-19-96	1.0	100	9	1.0	<4	<1	---	.02	<.01	<.20
Center snowmelt	01-15-97	---	---	---	---	---	---	---	---	---	---

See footnotes at end of table.

Table 2. Physical and chemical data for water from selected wells and springs, for surface water, and for precipitation, Flagstaff, Arizona—Continued

Well, spring, or owner name	Date	Nitrogen, NO_2+NO_3 dissolved (mg/L as N)	Phosphorus, total (mg/L as P)	Phosphorus, dissolved (mg/L as P)	Phosphorus ortho, dissolved (mg/L as P)	Solids, sum of constituents, dissolved (mg/L)	Tritium, total (pCi/L)	Tritium, units (TU)	Tritium 2 sigma water, whole total (pCi/L)	δ^2H (per mil)	$\delta^{18}O$ (per mil)
LM-4	07-01-96	0.17	<0.01	0.02	0.03	137	24	7.5	2.0	-72.3	-9.23
Do.	02-20-97	---	---	---	---	---	26	8.2	1.9	-74.5	-9.27
Do.	08-20-97	---	---	---	---	---	24	7.5	1.9	-74.0	-9.27
LM-8	07-01-96	.21	<.01	<.01	.01	265	<1.0	<.31	1.0	-87.5	-12.18
LM-9	07-01-96	.14	.02	<.01	.01	359	<1.0	<.31	1.0	-85.6	-11.77
Upper Lake Mary	07-08-96	---	---	---	---	---	21.4	6.7	1.6	-42.4	-3.18
WM-1	07-01-96	.18	<.01	.01	.02	127	12	3.8	1.0	-86.0	-12.28
WM-6	07-01-96	.16	<.01	<.01	.02	125	2.0	.63	1.0	-83.5	-11.95
WM-9	07-01-96	.14	.07	.06	.07	136	<1.0	<.31	1.0	-85.6	-12.00
Do.	02-25-97	---	---	---	---	---	1.3	<.41	1.0	-85.4	-12.02
Do.	08-26-97	---	---	---	---	---	1.0	<.31	.6	-86.8	-12.13
Continental-2	04-17-97	1.7	.072	.023	.01	153	8.6	2.7	1.0	-90.7	-12.33
Foxglenn-1	06-01-97	.19	.038	<.01	<.01	242	<1.0	<.31	1.0	-90.2	-12.43
Pine Grove	06-10-96	.17	<.01	<.01	.01	---	<1.0	<.31	1.0	-84.4	-11.73
NPS Walnut Canyon	06-11-96	1.6	<.01	<.01	.01	220	<1.0	<.31	1.0	-83.8	-11.88
Mountainaire	06-12-96	.51	.03	<.01	.02	213	7.0	2.2	1.0	-82.8	-11.91
Hidden Hollow	06-14-96	.26	.03	.01	.03	122	<1.0	<.31	1.0	-87.9	-12.38
Flag Ranch	06-13-96	.22	.04	.03	.03	115	<1.0	<.31	1.0	-85.7	-11.87
Purl	06-18-96	.23	<.01	<.01	.01	258	<1.0	<.31	1.0	-85.8	-11.69
Henden	06-18-96	.20	<.01	<.01	.02	102	<1.0	<.31	1.0	-85.5	-11.88
NPS Wupatki HQ[1]	06-26-96	.23	<.01	<.01	<.01	1,220	---	---	---	-73.5	-10.20
Do.[1]	07-09-96	.26	<.01	.01	<.01	1,160	<1.0	<.31	1.0	-75.2	-10.18
IB-9	07-02-96	.11	.04	.04	.05	69	33	10.3	3.0	-93.8	-13.05
IB snowmelt	01-29-97	---	---	---	---	---	---	---	---	-114.1	-15.94
Babbitt Spring	06-14-96	.30	.30	.02	.04	362	27	8.5	2.0	-86.3	-12.12
Clark Spring	06-13-96	<.05	.04	<.01	.02	255	25	7.8	2.0	-68.6	-9.95
Rio de Flag MW-1	06-13-96	1.1	.18	.13	.17	344	19	6.0	2.0	-77.1	-10.38
FH-5	06-25-96	.09	<.01	<.01	.02	226	<1.0	<.31	1.0	-86.9	-11.95
Parks Sch.	06-25-96	.31	.04	.04	.03	169	---	---	---	---	---
Quarry	06-21-96	<.05	.03	.01	.02	152	27	8.5	2.0	-7.9	6.04
Old Town Spring	07-08-96	1.6	.12	.13	.18	167	16	5.0	1.0	-79.3	-10.84
Rio de Flag MW-3	06-12-96	18.0	.06	.06	.06	499	29	9.1	2.0	-86.1	-11.66
Sterling Springs	06-18-96	.14	<.01	<.01	.01	138	2.0	.63	1.0	-82.9	-11.88
NAD-1	06-21-96	3.3	.07	.06	.09	200	31	9.7	2.0	-83.8	-11.44
BBDP-MVR-1	06-11-96	4.6	.01	<.01	.01	216	14	4.4	1.0	-80.8	-11.07
Do.	04-08-97	4.8	<.01	<.01	<.01	230	15	4.7	1.3	-80.4	-10.88
Do.	08-26-97	---	---	---	---	---	16	5.0	1.3	-80.2	-10.82
BBDP-Marijka	06-11-96	1.1	<.01	<.01	.02	274	<1.0	<.31	1.0	-82.8	-11.70
Mtn Dell-1	06-19-96	1.0	.02	<.01	.03	262	3.0	.94	1.0	-87.2	-12.10
Do.	03-11-97	---	---	---	---	---	---	---	---	-86.7	-12.15
Do.	08-28-97	---	---	---	---	---	4.2	1.3	1.0	-87.4	-12.12
Mtn Dell-2	06-19-96	1.8	.01	<.01	.03	218	9.0	2.8	1.0	-86.8	-12.01
Center snowmelt	01-15-97	---	---	---	---	---	---	---	---	-106.9	-15.19

See footnotes at end of table.

Table 2. Physical and chemical data for water from selected wells and springs, for surface water, and for precipitation, Flagstaff, Arizona—Continued

Well, spring, or owner name	Date	^{14}C (pmc)	$\delta^{13}C$ (per mil)	Corrected ground-water age from ^{14}C data[6]
LM-4	07-01-96	76.2	-9.6	MODERN
Do.	02-20-97	---	---	---
Do.	08-20-97	---	---	---
LM-8	07-01-96	113.1	-9.8	MODERN
LM-9	07-01-96	71.4	-9.0	MODERN
Upper Lake Mary	07-08-96	---	---	---
WM-1	07-01-96	44.0	-10.8	2,089
WM-6	07-01-96	46.0	-11.6	2,263
WM-9	07-01-96	41.6	-11.0	2,949
Do.	02-25-97	---	---	---
Do.	08-26-97	---	---	---
Continental-2	04-17-97	52.9	-7.9	MODERN
Foxglenn-1	06-01-97	59.5	-9.2	MODERN
Pine Grove	06-10-96	47.6	-12.4	2,603
NPS Walnut Canyon	06-11-96	58.6	-11.1	230
Mountainaire	06-12-96	50.0	-10.5	830
Hidden Hollow	06-14-96	58.4	-10.7	275
Flag Ranch	06-13-96	35.8	-10.9	4,041
Purl	06-18-96	70.2	-8.3	MODERN
Henden	06-18-96	26.2	-9.7	5,860
NPS Wupatki HQ[1]	06-26-96	18.7	-4.3	5,026
Do.[1]	07-09-96	---	---	---
IB-9	07-02-96	99.4	-15.9	MODERN
IB snowmelt	01-29-97	---	---	---
Babbitt Spring	06-14-96	81.6	-10.8	MODERN
Clark Spring	06-13-96	100.9	-12.6	MODERN
Rio de Flag MW-1	06-13-96	---	---	---
FH-5	06-25-96	62.1	-10.8	MODERN
Parks Sch.	06-25-96	---	---	---
Quarry	06-21-96	110.8	-16.3	MODERN
Old Town Spring	07-08-96	102.3	-12.9	MODERN
Rio de Flag MW-3	06-12-96	---	---	---
Sterling Springs	06-18-96	57.7	-10.9	MODERN
NAD-1	06-21-96	91.0	-12.5	MODERN
BBDP-MVR-1	06-11-96	40.8	-8.6	1,805
Do.	04-08-97	---	---	---
Do.	08-26-97	---	---	---
BBDP-Marijka	06-11-96	28.8	-6.9	3,452
Mtn Dell-1	06-19-96	72.5	-10.4	MODERN
Do.	03-11-97	---	---	---
Do.	08-28-97	---	---	---
Mtn Dell-2	06-19-96	66.5	-9.2	MODERN
Center snowmelt	01-15-97	---	---	---

[1]Water sample may have contained some water from the on-site storage tank. Control valves used to prevent backflow were highly encrusted and may not have been fully closed during sampling.

[2]Maximum Contaminant Level for barium in drinking water is 2 milligrams per liter (2,000 micrograms per liter; U.S. Environmental Protection Agency, accessed June 12, 2000).

[3]Secondary Maximum Contaminant Level for sulfate in drinking water is 250 milligrams per liter (U.S. Environmental Protection Agency, accessed June 12, 2000).

[4]Secondary Maximum Contaminant Level for manganese in drinking water is 0.05 milligrams per liter (50 micrograms per liter; U.S. Environmental Protection Agency, accessed June 12, 2000).

[5]Maximum Contaminant Level for antimony in drinking water is 0.006 milligrams per liter (6 micrograms per liter; U.S. Environmental Protection Agency, accessed June 12, 2000).

[6]Calculated using 100 percent modern carbon for soil gas carbon-14 in model.

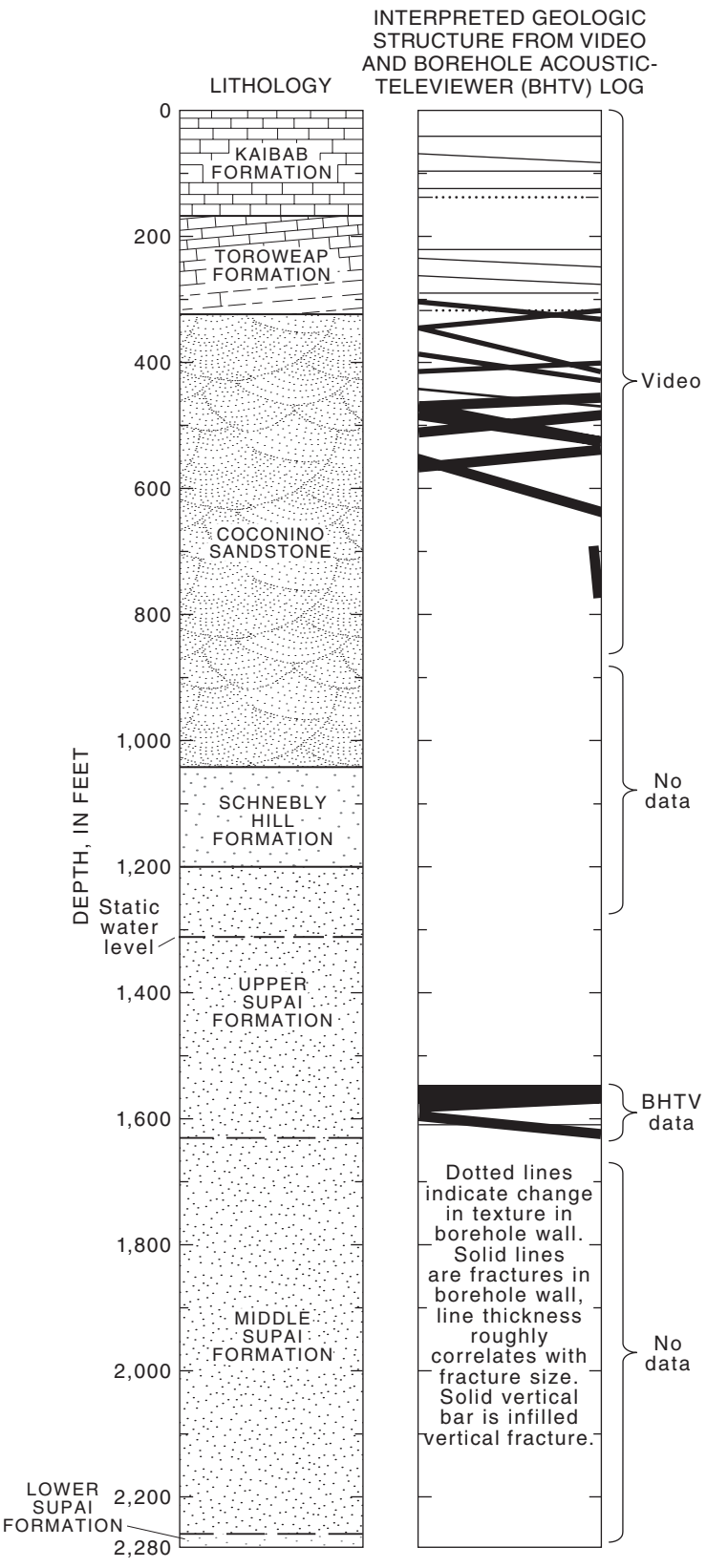

Figure 31. Lithologic, video, and borehole-acoustic-televiewer logs, Foxglenn well.

The other sinkhole is an elongated depression that overlies the east-bounding graben fault. This depression has alluvium throughout its bottom that varies in depth from a few feet to as much as 15 ft. Although the depression is not as well developed as the Bottomless Pits, it is inferred to be a similar feature because of its coincidence with the northwestward-trending structure. These depressions and several other sinkholes that occur throughout the study area represent significant points of periodic recharge to the regional aquifer (**pl. 1**). Eleven GPR surveys, two seismic surveys, and one SAR survey were completed at the site (fig. 8). The two seismic surveys were oriented perpendicular and parallel to principal structural trends in the area.

Ground-Penetrating Radar

GPR was applied to determine the location and orientation of geologic structure in the near-surface bedrock in the interior part of the graben. Profile 2 is just south of the Bottomless Pits (**figs. 8** and **32**A). The image of profile 2 is chaotic indicating highly fractured bedrock near land surface. Three bedding planes about 20, 30, and 40 ft below land surface can be followed laterally across the profile. The Bottomless Pits project into the profile at about 300 ft from the west-northwest end and are seen as a down-dropped block. Other fractures with minor offsets leading into the pits are shown in this profile from 200 to 260 ft from the west-northwest end. Profile 3 is about 600 ft north of the Bottomless Pits and is aligned to the west-northwest roughly parallel to profile 2 between the two principal sinkholes in the area (fig. 32B). The image for profile 3 is chaotic with multiple bedding planes that can be traced for some distance but that are disrupted in several places. At least one prominent zone of offset occurs between 150 and 200 ft from the east-southeast end of the survey line. Profile 9 is aligned to the southwest (S. 18° W.) rough-ly parallel to the bounding graben faults and between the two sinkholes (fig. 32C). Principal zones of disrup-tion along profile 9 occur from 0 to 200 ft and from 700 to 850 ft (not shown) from the northeast end of the survey line where the profile is close to or crosses the bounding graben faults. At these same locations, shallow hyperbolas occur at depths of 120 and 130 ft.

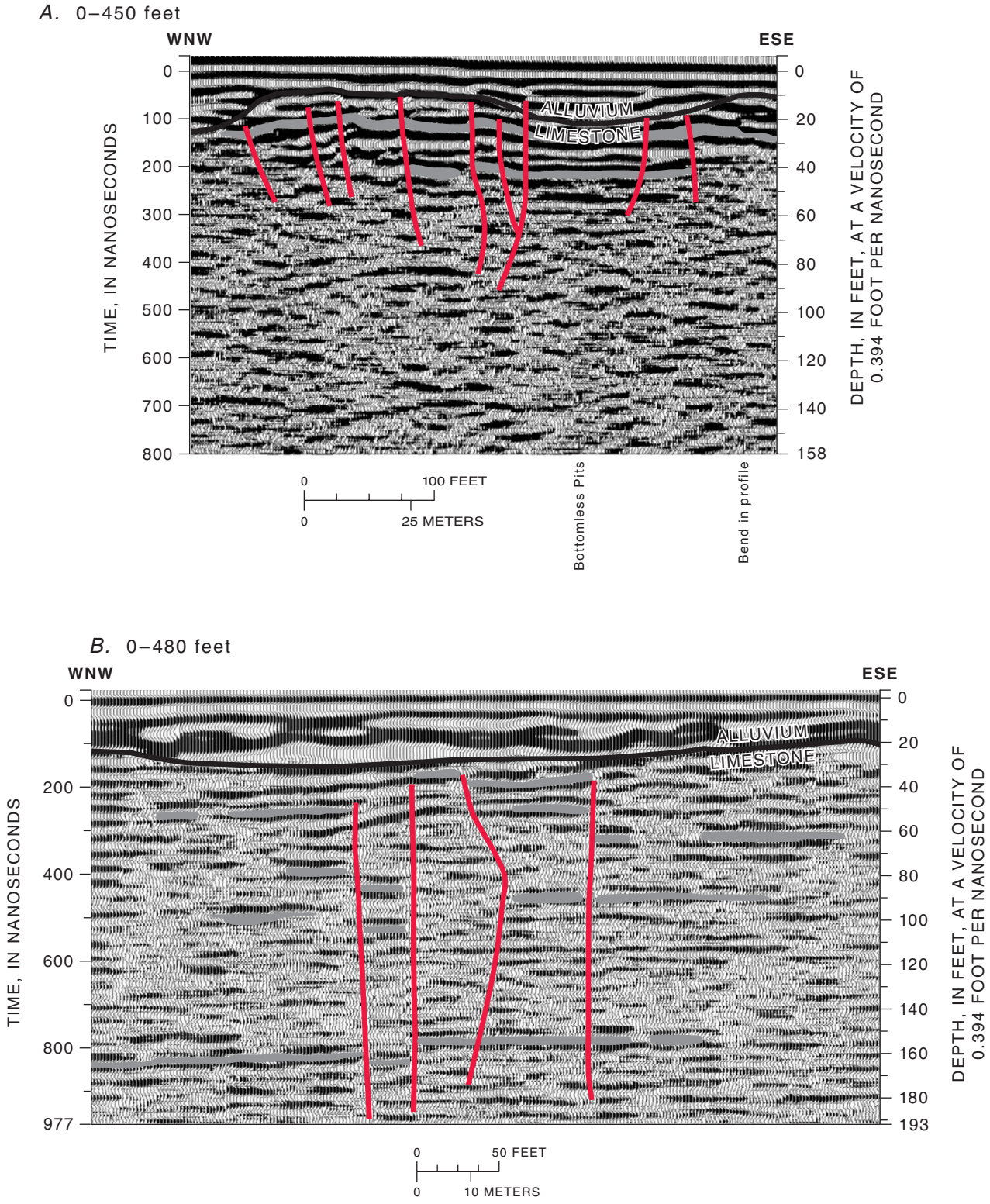

Figure 32. Selected interpreted ground-penetrating radar data for the Continental area. *A*, Radar profile 2, 0–450. *B*, Radar profile 3, 0–480 feet. *C*, Radar profile 9, 0–360 feet. Interpreted fractures are shown in red and interpreted bedding planes are gray fills. Hyperbolic events are interpreted as openings or open horizontal fractures.

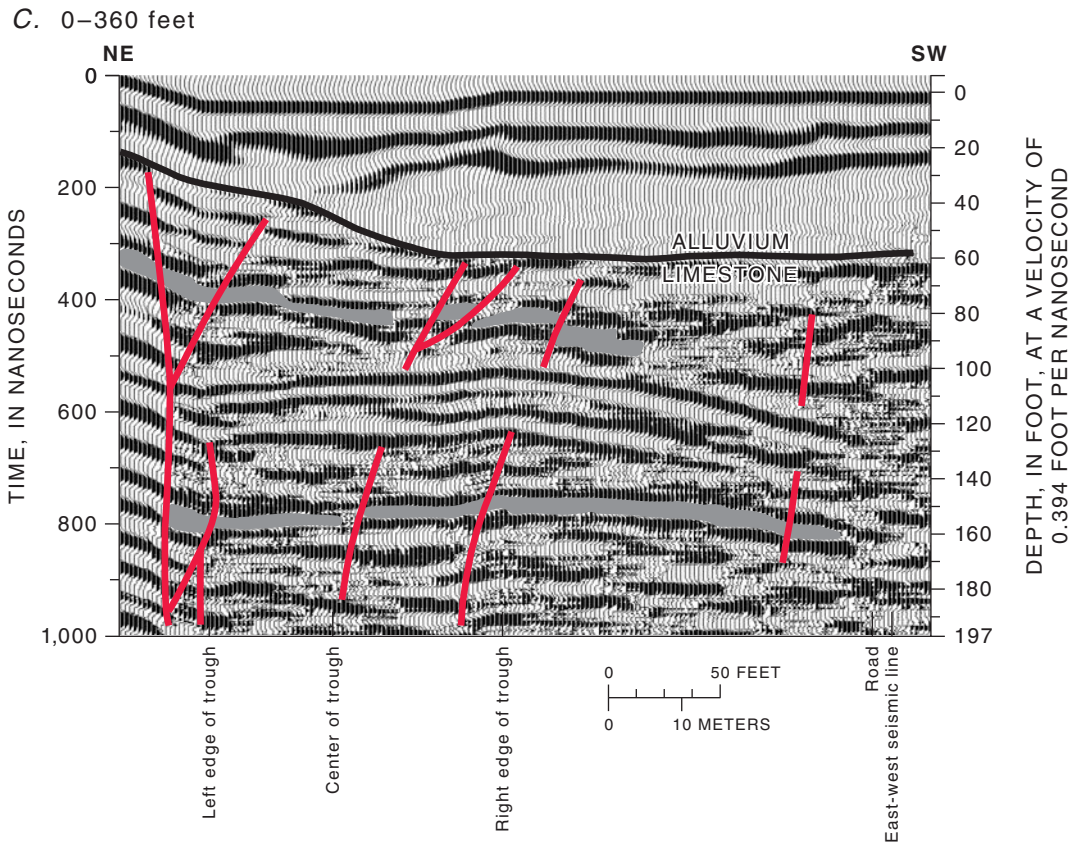

NOTE: Data for GPR were collected with a 1,000-volt pulsar and 50-megahertz antenna, 12.0-foot spacing, 2.0-foot step, and a total time window of 1,600 nanoseconds (ηs). The data were gain adjusted and filtered to improve the visual presentation, and corrected for elevation changes along the profile. Vertical resolution of these images is about 1.0 to 2.0 feet. The vertical scale is the two-way travel time of the radar signal.

Figure 32. Continued.

Because of their proximity to the sinkholes, these hyperbolas probably indicate openings associated with the sinkholes at about 100 feet below land surface.

Seismic Reflection and Seismic Refraction

Two seismic-reflection and seismic-refraction images were collected in the Continental area—one oriented to the northeast (line 1) and one oriented to the northwest (line 2; fig. 8). Many of the faults observed on the seismic sections dip at steep angles; however, some faults have dips as low as 60° (**figs. 33** and **34**). Commonly, the faults intersect or connect with other faults at slightly different angles. Most faults also do not extend to land surface. Some of the more pronounced faults, however, extend from the near surface to depths of more than 2,000 ft and would be the target faults for water exploration (figs. 33 and 34).

In addition to faults, the seismic-reflection data also appear to have imaged subsurface caverns (figs. 33 and 34). In some locations, laterally continuous layers contain zones that did not reflect the seismic energy; low-coherence zones extend for several feet to about 100 feet laterally and vertically and are largest on line 1 of the Continental area. Because these zones of missing reflectors correlate with the surface location of the Bottomless Pits, the extensive zones of missing reflec-tors are inferred to represent subsurface caverns (figs. 33–35).

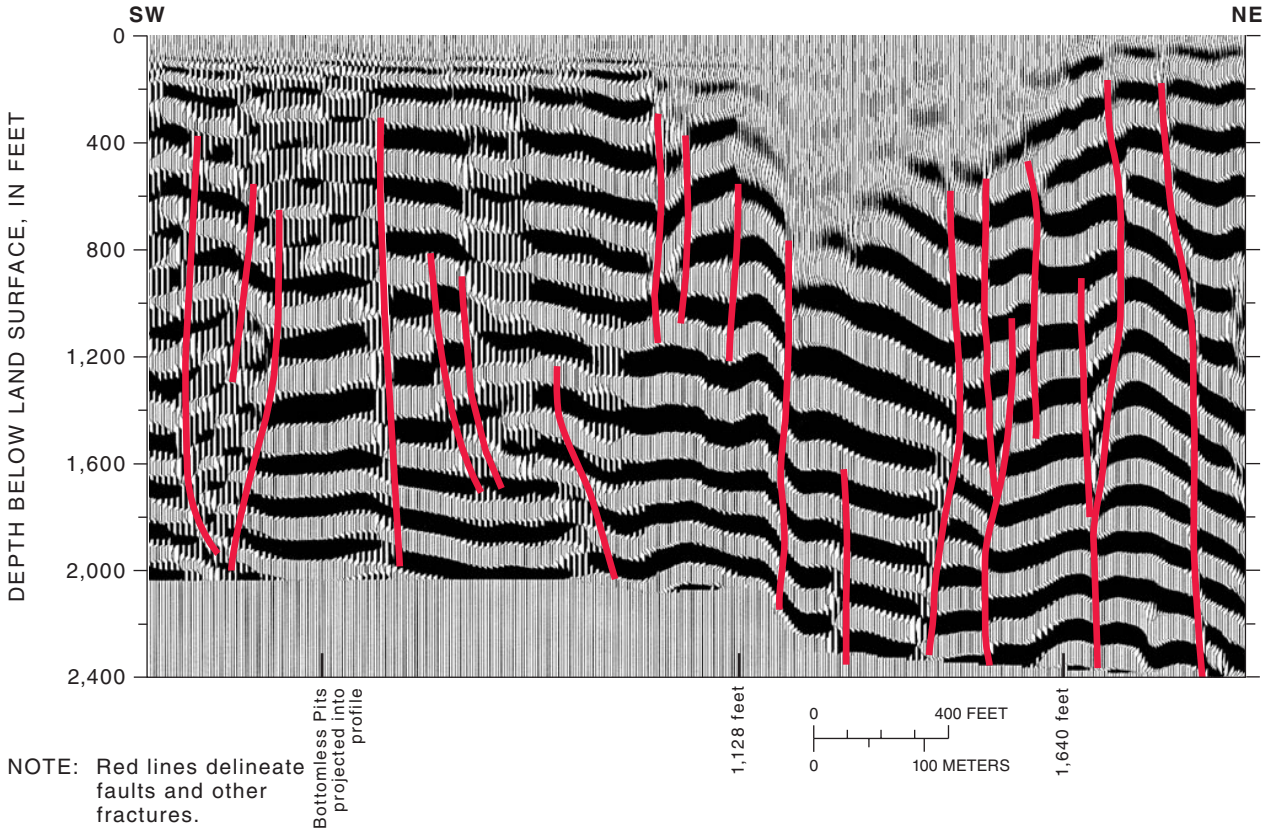

Figure 33. Stacked seismic image along Continental line 1. Low-frequency reflectors continuous over distances of several tens of feet are presumed to correspond to major layers within the subsurface. Vertical offsets in the apparent layers are presumed to be faults. Areas with blurred or missing reflectors in the southwestern half of the section correltate with the location of the Bottomless Pits solution caverns. Missing reflectors in the upper 656 feet from 1,128 to 1,640 feet correspond to an area where surface-shot points were skipped because of locally steep topography.

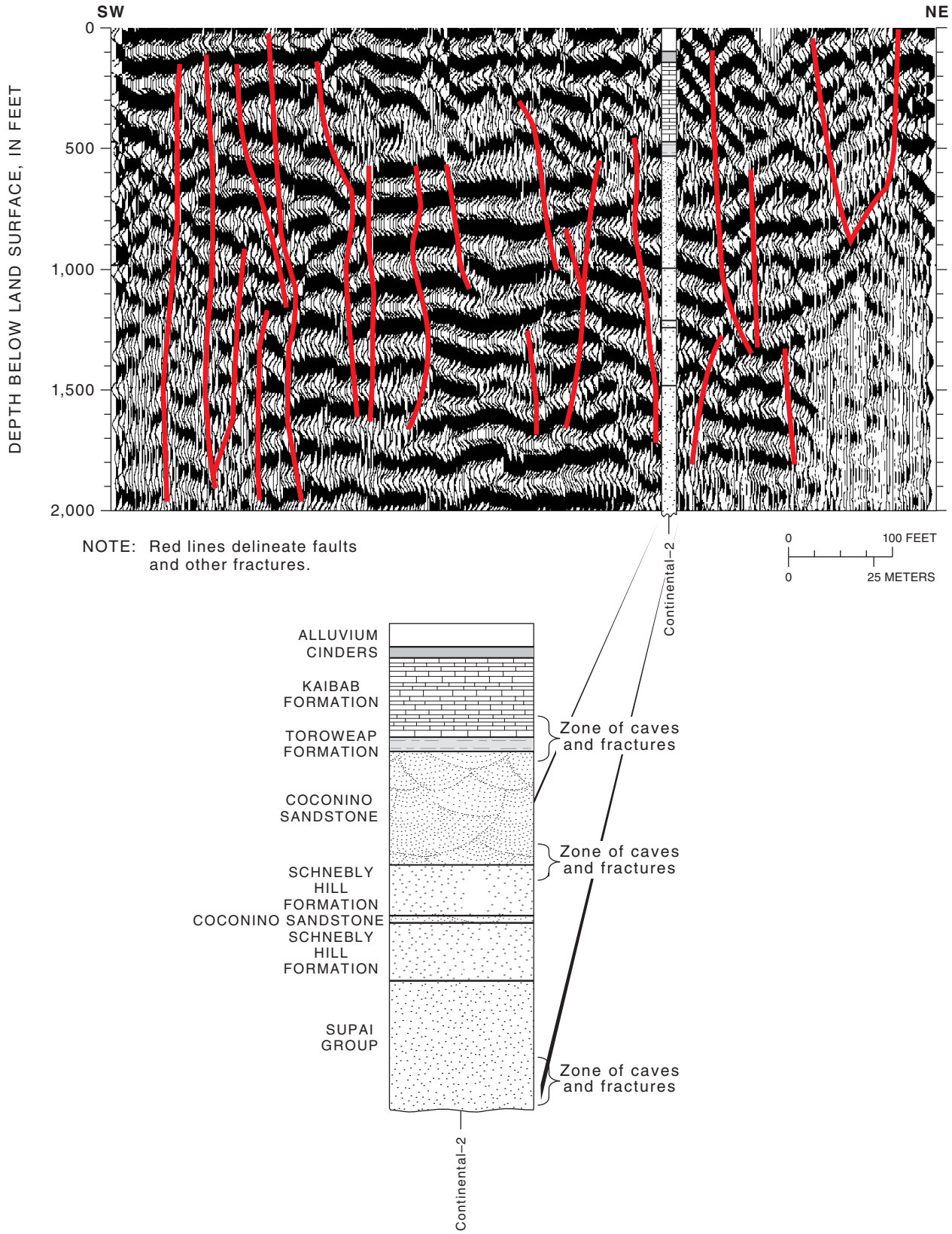

Figure 34. Stacked seismic image along Continental line 2.

NOTE: Offsets in exposed Kaibab Formation. Upthrown side is to the right and unconsolidated alluvium is on the left side of the pit.

Figure 35. Solution-widened fractures, bedding-plane structure, and the Bottomless Pits in the Continental area.

On all other seismic lines, the frequency content of the seismic data is much higher; therefore, the cavern system along line 1 is inferred to be largely responsible for the loss of frequency of the seismic waves. A third line of evidence, which corroborates the idea that the missing zones of reflections correspond to caverns, is in the low seismic velocities (about 2,600 ft/s) of the Kaibab Formation in the shallow subsurface near these zones.

The Kaibab Formation is about 32 ft below land surface at the entrance to the Bottomless Pits and has seismic velocities as low as 2,600 ft/s. On the adjacent hills, however, the Kaibab Formation has a near-surface velocity that ranges from about 7,200 ft/s to about 9,175 ft/s (**fig. 36**). The low velocity is inferred to be the result of seismic waves that travel through the air in the cavern system near the Bottomless Pits.
As compressional-wave velocities in the air are about 1,100 ft/s, velocities as low as 2,600 ft/s near the Bottomless Pits suggest that the near surface includes more open space than rock.

The cavern probably does not extend to 1,000 ft below land surface as inferred on the seismic-reflection sections (**figs. 33** and **34**). The apparent depth on the seismic-reflection section may result from the lower seismic velocity of the air in the caverns relative to the velocity of the adjacent rocks. Seismic-velocity modeling determines an average velocity of the seismic waves as they travel through and around the caverns; therefore, individual cavern depths are not correctly calculated on the seismic-reflection sections. Comparison of the seismic image with the velocity model suggests that the caverns probably extend to only about 130 ft deep because below 130 ft the seismic velocity is consistent with that of the Kaibab Formation on the adjacent hill (fig. 36).

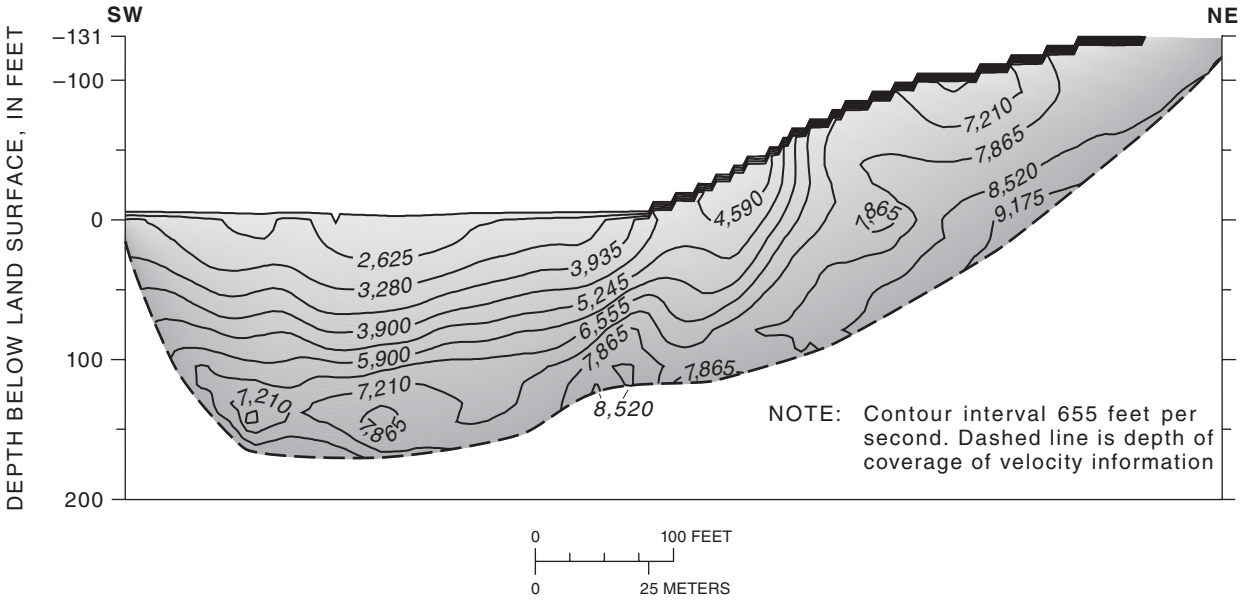

Figure 36. Velocity model for Continental line 1 derived from inversion of seismic-refraction data. Note the low velocities (less than 6,555 feet per second0 within the upper 131 feet in the southwestern half of the velocity model and the high velocities (greater than 7,210 feet per second) at the surface in the northeastern half of the velocity model.

Square-Array Resistivity

The square-array site for Continental (BP) is just south of the Rio de Flag (**figs. 6**, **8**, and **37**; **table 1**). The polar-coordinate plots for the 16.4- to 92.8-foot square arrays are roughly circular and correspond to alluvial material and volcanic rocks in the upper 130 ft (see "**Supplemental Data**, Part A" at the back of the report). The 131.2- to 492.1-foot square arrays show a northwestward trend (N. 45° W.) for the resistivity ellipses consistent with local structural trends in the Kaibab Formation. The depth of investigation at the 492.1-foot square array includes the Toroweap Formation. The strong northwestward trend (N. 45° W.) is supported by a large through-going fault seen on line 1 of the high-resolution seismic-reflection profile (fig. 33).

Fractures at the Continental site strike northwest (fig. 37). The minima in the interpreted resistivity curve at 65.6 ft roughly corresponds to the minimum coefficient of anisotropy and minimum secondary porosity at that depth (fig. 37). The low resistivity values (10–20 ohm-meters) are indicative of a clay layer. Some of the highest secondary-porosity and mean apparent-resistivity values recorded in the study area were measured at this site. The 13-percent secondary-porosity value for the 32.8-foot square array indicates coarse sand or gravel in the upper alluvial interval. Fences and other cultural features limited the depth of investigation to 492.1 ft. The depth to the regional water table is about 1,303 ft at this site.

Borehole

Two wells (wells 1 and 2) were drilled at Continental (fig. 8). Well 1 was drilled to 1,650 ft; however, this hole was abandoned because of a collapse at about 725 ft (**fig. 38**A). Well 2 is 42 ft east of well 1 and was completed to a total depth of 2,160 ft (fig. 38B). The only logs available for well 1 are a lithologic log and a video log (fig. 38A). The video log from well 1 shows extensive fracturing and openings throughout the open part of the hole. Over 55 fractures were imaged, and about 26 of these fractures were horizontal to near horizontal. The vertical to near vertical fractures had dips that ranged from 63° to as much as 87°. A few fractures and many small openings were observed in the Kaibab Formation. Most of the fractures and several large openings were observed in the Coconino Sandstone. Openings at 604 and 708 ft were about 10 and 20 ft deep, respectively, and were developed along fractures. The lateral extent of these openings is unknown.

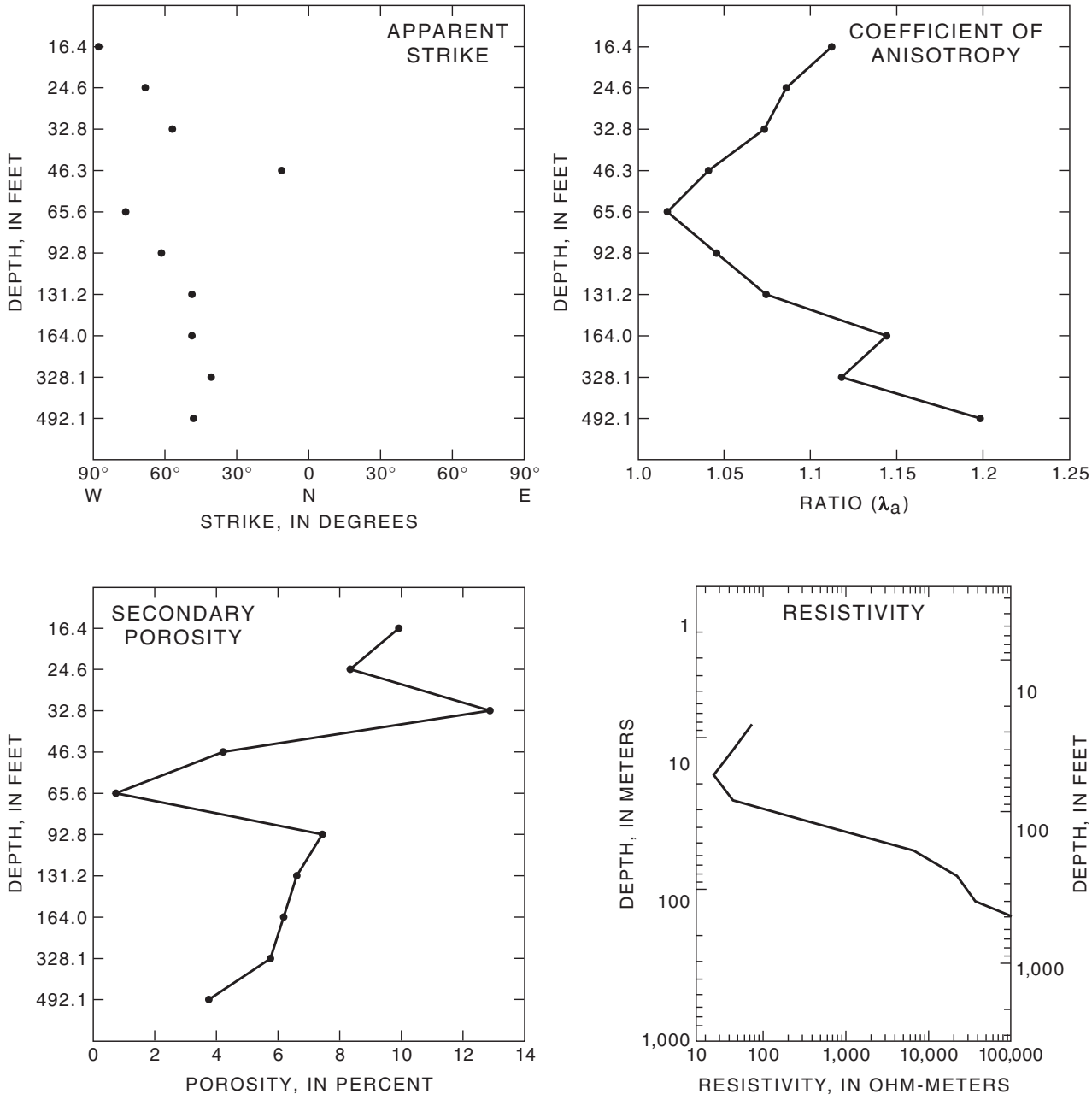

Figure 37. Calculated apparent strike of major fractures, coefficient of anisotropy, secondary porosity, and apparent resistivity for the square-array sounding data, Continental site (BP). Apparent strike values are in degrees for each sqaure size (16.4, 24.6, 32.8.....). Coefficent of anisotropy is a dimensionless number where a number larger than one indicates increasing anisotropy. The interpreted resistivity depth of exploration was 492.1 feet. Interpretation was done using ATO which is a vertical electrical-sounding (VES) computer program by Zohdy (1989). Depth to water recorded at the Continental well 2 was 1,303 feet.

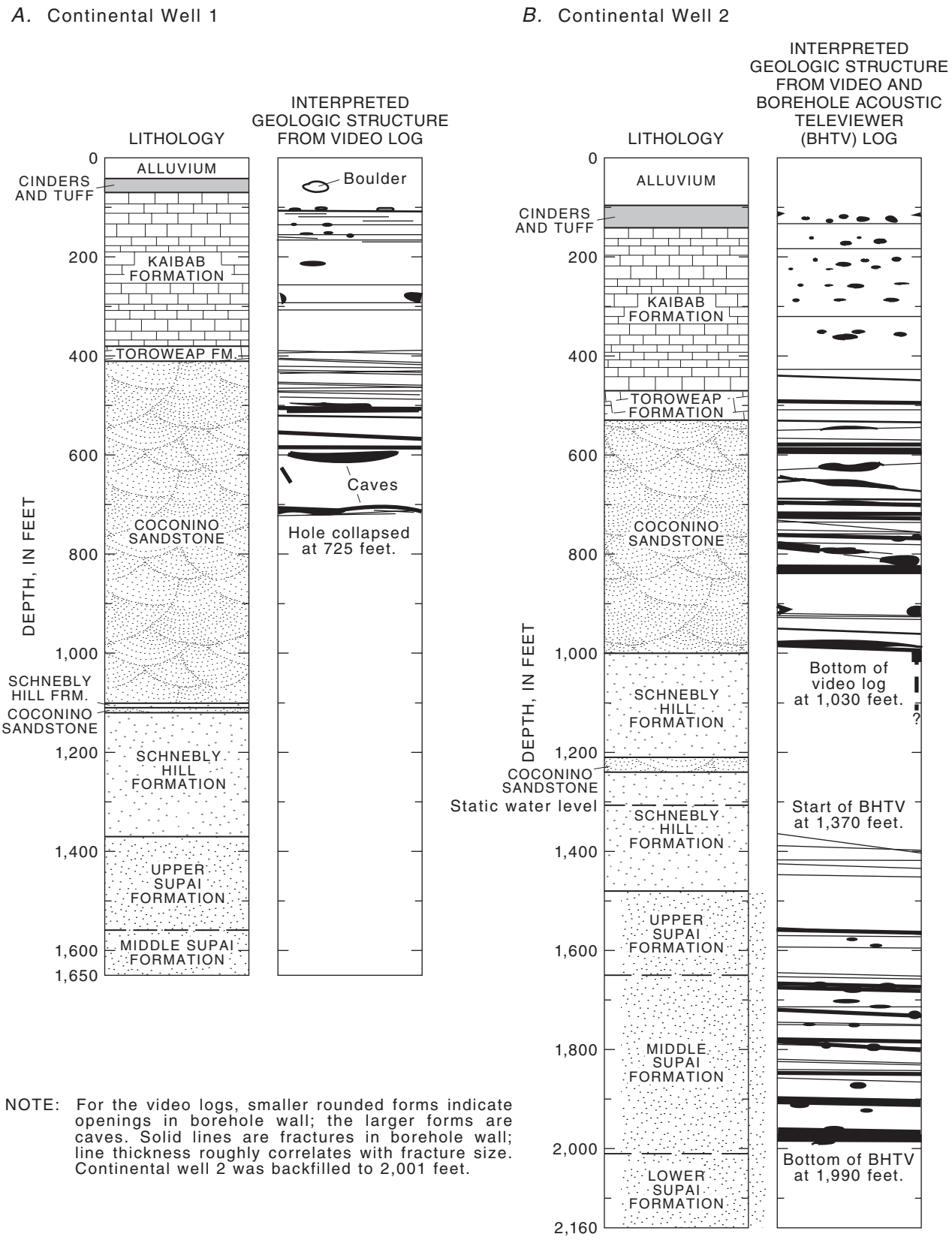

NOTE: For the video logs, smaller rounded forms indicate openings in borehole wall; the larger forms are caves. Solid lines are fractures in borehole wall; line thickness roughly correlates with fracture size. Continental well 2 was backfilled to 2,001 feet.

Figure 38. Lithologic and borehole-geophysical logs, Continental site. *A*, Well 1. *B*, Well 2.

B. Continental well 2 continued

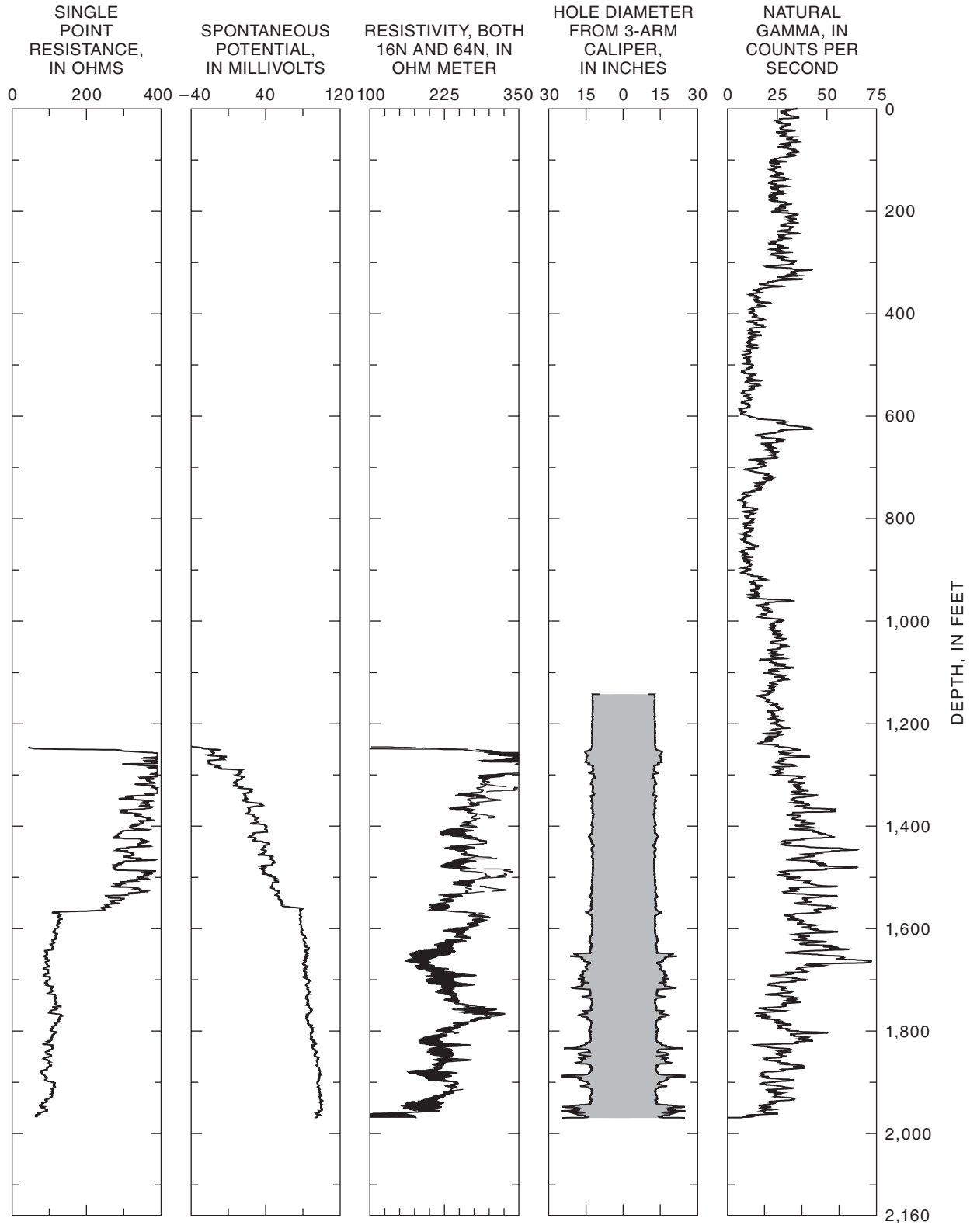

Figure 38. Continued.

Logs of well 2 consist of lithologic, video, borehole-acoustic televiewer, resistivity, spontaneous potential, caliper, and gamma (fig. 38B). The video and borehole acoustic-televiewer log for well 2 imaged about 94 fractures and many small to large openings to a depth of about 2,000 ft. Only 24 of the fractures were horizontal to near horizontal. The vertical to near-vertical fractures had dips that were from 75° to as much as 85°. A few fractures had dips that were from 40 to 60°. As in well 1, the Kaibab Formation in this borehole had many small openings and minor fracturing, and the Coconino Sandstone had several large openings and abundant fracturing. The water level at 1,303 ft is near the bottom of the largely unfractured Schnebly Hill Formation. The most significant fracturing occurs in the Supai Group below 1,640 ft, which is below the water table. Many medium to large open fractures that range from several inches to 8 ft wide are a significant component of the borehole in the Supai Group. The largest openings appear to be horizontal fractures from 1,715 to 1,977 ft below land surface. Comparison of lithology from well 1 to well 2 (**fig. 38** A and B) indicates that the wells are separated by a fault that has a vertical offset of 140 ft. Wells 1 and 2 are on or near the main northeastward-striking fault that crosses the area (**pl. 1**). The structural trend below the water table in well 2 is indicated by the borehole-acoustic-televiewer log. Most of this structure trends to the northwest; a few fractures strike to the northeast. North to northwestward-striking open fractures are at 1,560, and 1,667 ft (N. 2° W. and N. 26° W.), and one northeastward-striking open fracture is at 1,720 ft (N. 30° E.; fig. 38*B*). A few mostly minor fractures strike eastward. The video log was not referenced azimuthally; therefore, the orientation of the fractures higher in the borehole is not known. The wells project into the seismic profile 285 ft to the west at about 537 ft from the southwest end of the seismic survey line (**fig. 34**). The fault zone is observed in the seismic profile from 328 to 381 ft from the southwest end of the seismic survey line (fig. 34). The fractured zones and openings in the wells (fig. 38) are more consistent with the chaotic structure represented from 328 to 381 ft from the southwest end of the seismic line than the more coherent structure at 537 ft from the southwest end. The bottom of the well is just below the zone imaged by seismic methods.

HYDROGEOLOGY OF THE REGIONAL AQUIFER

Ground water occurs in three general zones throughout the study area: (1) perched ground water that is close to the land surface, (2) ground water in the regional-aquifer system, and (3) ground water in a deep limestone aquifer that underlies the regional-aquifer system. Perched ground water is found close to land surface in unconsolidated alluvium and volcanic rocks and in the interbedded sandstones in either the Moenkopi or the Kaibab Formations (Appel and Bills, 1981; McGavock and others, 1986). These perched zones generally are small and discontinuous. As a result, they are not suitable for the long-term high-yield withdrawals that are needed by large municipal water systems. One exception to these conditions is the perched water-bearing zone in glacial outwash and volcanic rocks in the Inner Basin of San Francisco Mountain. Although this water-bearing zone yields from 150 to as much as 800 gal/min to wells, it has limited areal extent and is seasonally dependent on recharge from snowmelt. This water-bearing zone is already fully developed by the City of Flagstaff for public supply (Harshbarger and Associates and John Carollo Engineers, 1974). Other, smaller perched water-bearing zones in Flagstaff have been outgrown by the City of Flagstaff.

Ground water in the regional-flow system is in the fine-grained to medium-grained sediments of the Kaibab Formation, Coconino Sandstone, Schnebly Hill Formation, and Supai Group (**pl. 3**). These formations are hydraulically connected and generally function as one water-bearing zone.

In previous studies, this aquifer system has been referred to as the Coconino aquifer (Mann, 1976; McGavock and others, 1986), C-aquifer system (Cooley and others, 1969), or the regional aquifer (Levings, 1980; Owen-Joyce and Bell, 1983). This aquifer system is referred to as the regional aquifer in this report. The regional aquifer is the most extensive and productive aquifer underlying the study area and is the source of most of the municipal and public ground-water supply. Regional studies indicate that water recharges the regional aquifer from precipitation and runoff throughout the area and along the Mogollon Rim (McGavock, 1968; Levings, 1980; Owen-Joyce and Bell, 1983; McGavock and others, 1986). Water that does not infiltrate directly to the regional water table is contained for a time in the perched water-bearing zones mainly in the volcanic rocks close to land surface. The water moves downgradient along the fracture

zones underlying the volcanic rocks or to discharge points at land surface. After reaching the regional water table, the water then moves laterally and vertically until it discharges as springs along the Little Colorado and Colorado Rivers to the north, Oak Creek to the south, or is pumped out of the ground to wells. Areas of greater permeability in the water-bearing units and concentrated flow in rocks that are highly fractured or faulted affect this general flow of ground water. On the basis of information obtained from recent drilling, the most productive part of the regional aquifer appears to be in a zone of medium to coarse flowing sand in fracture zones near the lower part of the Middle Supai Formation at depths of 2,200 to 2,600 ft. Because of drilling difficulties, information is limited on the hydraulic properties of this water-bearing zone.

The underlying Redwall and Muav Limestones and the Martin Formation form a confined limestone aquifer (J.M. Montgomery Consulting Engineers, Inc., 1982). Little is known about the occurrence and movement of ground water in this aquifer. Ground water in the deep limestone aquifer is separated from the overlying regional aquifer by siltstones and mudstones in the Lower Supai Formation. Coarser-grained material in the Redwall and Muav Limestones functions as the water-bearing zone. Movement of water depends on fracture and solution-channel openings in the formation to facilitate ground-water flow. Well-test data for LM-8 and an oil and gas test well (Federal 1) indicate that this aquifer has hydraulic heads comparable to those in the regional aquifer (J.M. Montgomery Consulting Engineers, Inc., 1982). Few well-yield data, however, are available for the limestone aquifer. Because of the depth of this aquifer and the productivity of the overlying regional aquifer, the Redwall and Muav Limestones are not used as a source of water supply in the study area.

Water Levels and Saturated Thickness

A map of potentiometric contours was constructed using static water levels measured in wells and altitude data from springs from 1994 through 1997 (**pl. 2**). Additional wells are shown on plate 2 for which water-level measurements precede 1994 (**pl. 4**). In some areas, particularly those outside the main areas of ground-water pumping, historical water levels at these additional wells could be representative of conditions during 1994–97.

Two mounds of ground water are indicated by the potentiometric-contour data (pl. 2). One of these mounds is south of Lake Mary and has a peak altitude of about 7,000 ft. The other less well-defined mound is west of Woody Mountain and has a peak altitude of about 6,100 ft. A small area of confined ground water is south of Lake Mary coincident with the southern ground-water mound. This area is overlain by several hundred feet of basalt that forms the upper confining layer. The ground-water mound is south of the Lake Mary graben coincident with the Mormon Mountain anticline. Data on the confined part of the aquifer are from a few private wells and observation wells and from springs south of Lake Mary that discharge at the contact between the volcanic rocks and the upper part of the regional aquifer.

From depth-to-water and lithologic information, the saturated thickness of the regional aquifer is estimated to vary from 600 ft in the northern part of the study area to 2,200 ft in the southern part. The average thickness is about 1,200 ft. Hydrographs of selected observation wells completed in the regional aquifer (figs. 39–41) are indicative of the types of water-level changes that occur. The saturated thickness of the aquifer at these sites ranges from 110 ft (Henden well) to 914 ft (LM-8; figs. 39–41). LM-8 and Federal 1 are the only wells in the study area that fully penetrate the regional aquifer.

Ground-water withdrawals and seasonal recharge can cause fluctuations in the water table of as much as several hundred feet in some places. Hydrographs for wells WM-5, LM-2, and LM-8 show several hundred feet of decline when several other wells in the City of Flagstaff well fields are being pumped (**fig. 39**). These hydrographs also show a general decline in the water level of about 100 ft in the Lake Mary area and several tens of feet in the Woody Mountain area in the last 20 to 40 years. The hydrograph for the Forest Highlands 1 well to the southeast of the Woody Mountain well field shows about 85 ft of decline in the water level since 1985 (fig. 39). The hydrograph for the Henden well north of the Woody Mountain well field is variable and shows no discernible trend (fig. 39); however, the period of record is short. The water level in the Navajo Army Depot well (NAD-1) at the west end of the study area responds quickly to seasonal recharge in the area. Measured flow in the sinkhole about 800 ft east of this well in 1996 was directly correlated to a 35-foot rise in the water level in the well (Randy Wilkerson, geology student, NAU, written commun., 1997; **fig. 40**, this report). Hydrographs for Little America well 1, Black Bill-Doney Park- Sunset well, and ADOT-Winona well in the northeastern part of the study area show fluctuating water levels and no discernible trend despite withdrawals of about 1,000 acre-ft annually in this area for public supply (**fig. 41**).

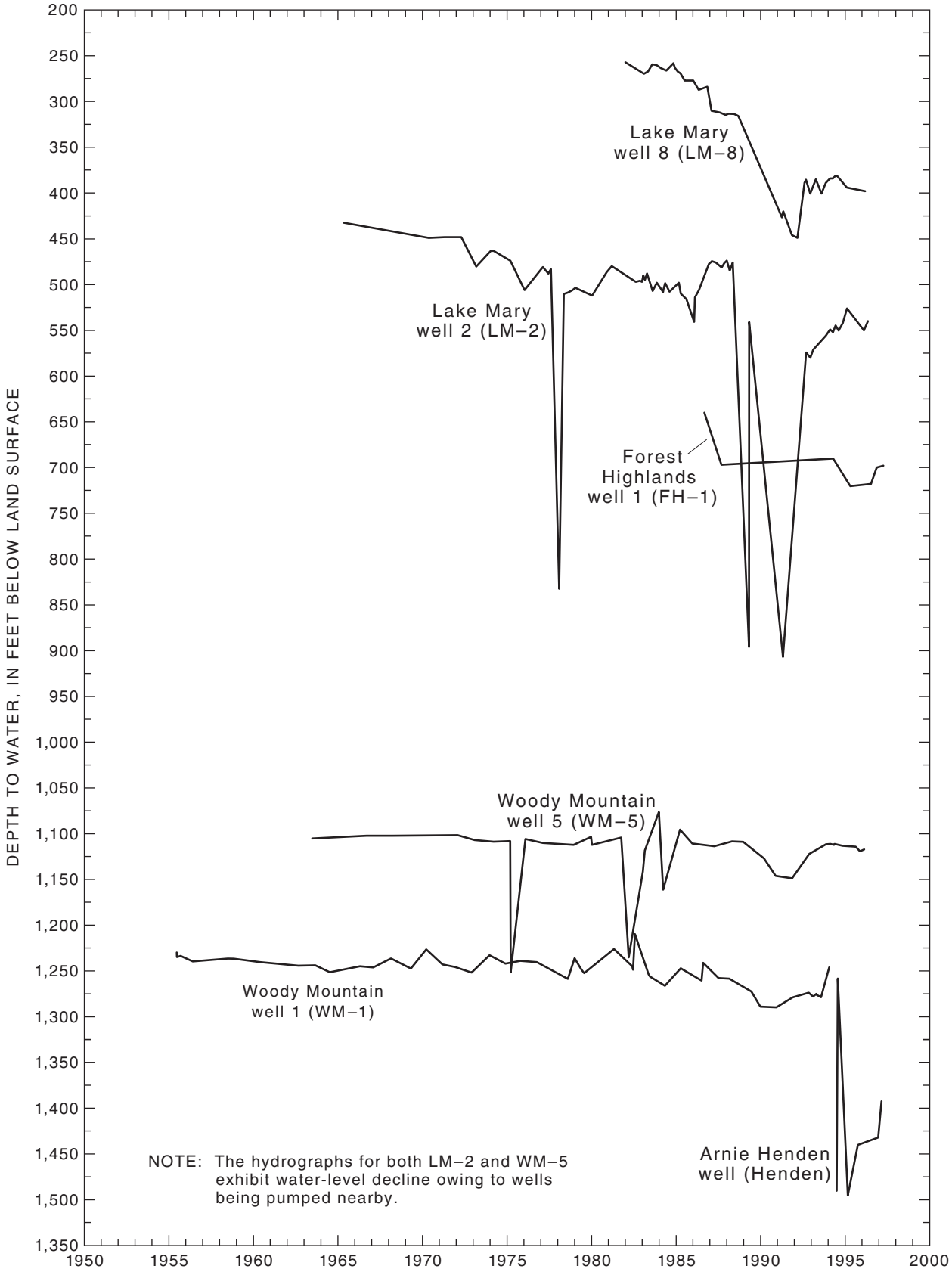

Figure 39. Water levels in selected observation wells, Flagstaff, Arizona.

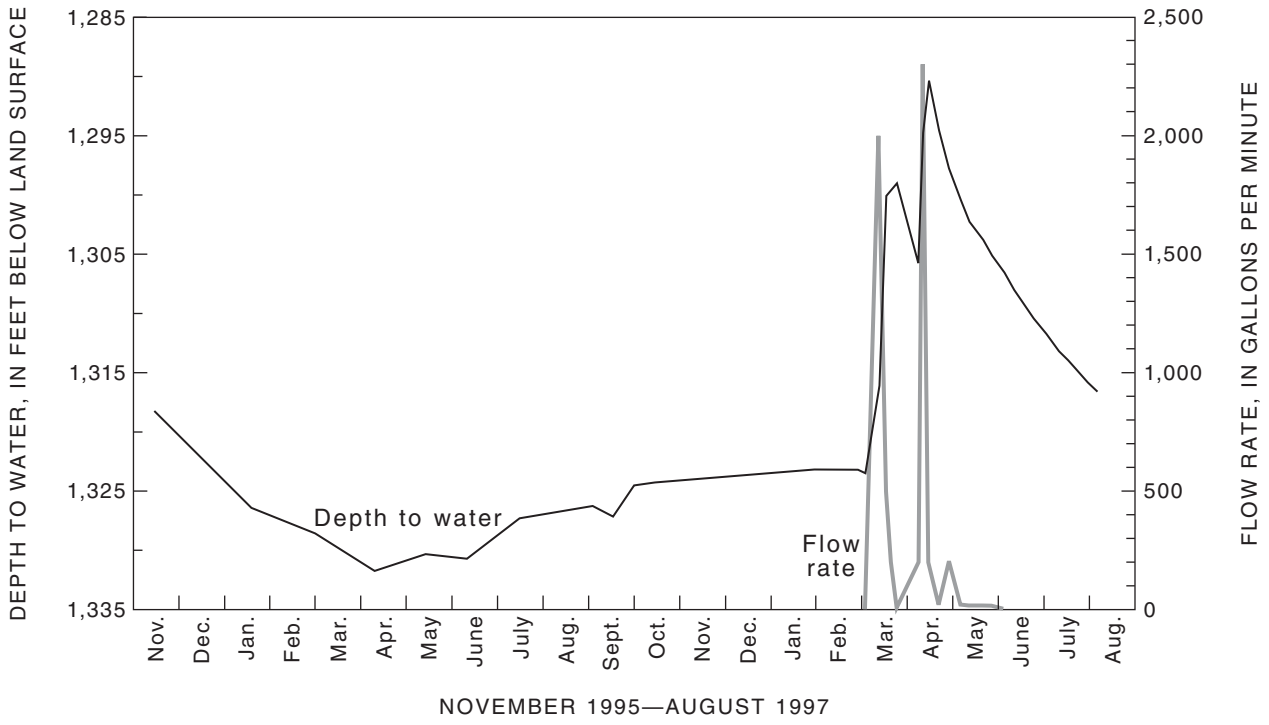

Figure 40. Relation of water level in the Navajo Army Depot well (NAD–1) to the flow rate of Lake Atherton into a nearby sinkhole (Randy Wilkerson, geology student, Northern Arizona University, written commun., 1997).

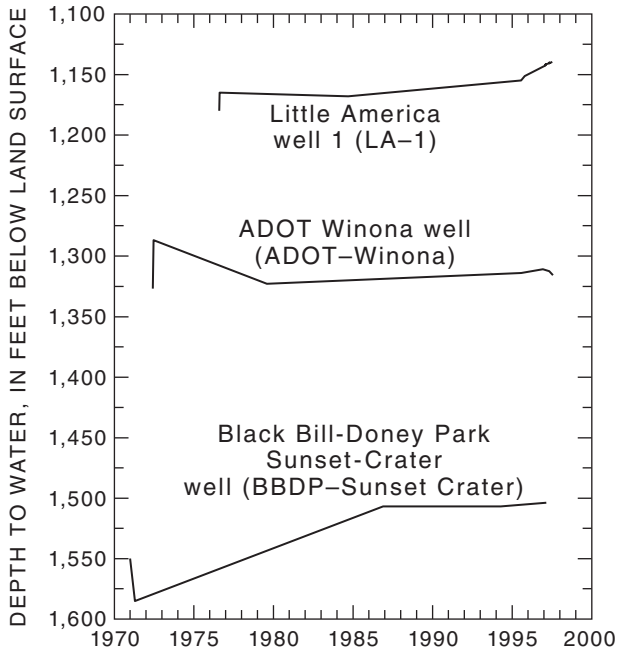

Figure 41. Water levels in selected observation wells in the northeastern part of the study area near Flagstaff, Arizona.

Well Yield and Specific Capacity

Well yields were determined from well and aquifer tests for 76 wells in the study area (**pl. 4**). Several other tests were completed for wells in the study area; however, the pumping periods were too short and often the pumping rates were too low to produce accurate well-yield estimates. In other cases, pumping rates were high for short time periods also leading to inaccurate well-yield estimates.

For the 76 wells with usable well or aquifer test data, well yields vary from 4 to 1,700 gal/min and average 175 gal/min. Several factors contribute to this large range in values: (1) formation lithology, (2) degree and type of fracturing, (3) degree of secondary mineralization of the aquifer, (4) penetrated saturated thickness, (5) well efficiency, and (6) pump design and lift. Degree and type of fracturing probably has the greatest effect on well yield. Wells yielding less than 100 gal/min typically are not completed in or near faults or other fractures; whereas, wells yielding more than 100 gal/min typically are completed in or near known faults or fractures.

Specific capacity, which is a useful indicator of well and aquifer performance, was calculated for 58 wells by dividing well discharge by measured drawdown (**fig. 42**D). Specific-capacity values range from 0.014 to 13.0 (gal/min)/ft of drawdown and average 2.16 (gal/min)/ft (pl. 4). In conjunction with well yield and other hydraulic properties, specific-capacity data can be useful in analyzing well performance in relation to aquifer characteristics. Specific capacity was used to estimate transmissivity for 17 single well tests. Because these data reflect well and pump efficiencies and effects of casings in addition to aquifer characteristics, this information needs to be evaluated carefully. These data also are affected by transient conditions in the well that cast additional doubt on the use of this data as indicators of hydraulic properties.

A general relation exists between specific capacity and geology (**pl. 1**). Specific capacity is highest for wells completed in the Coconino Sandstone and (or) Supai Group close to fractures. Wells generally have a low specific capacity when developed in the Coconino Sandstone and (or) the Supai Group where fractures are not apparent at land surface. One exception to this general relation is the Black Bill-Doney Park Marijka (BBDP-Marijka) well that was developed in the Upper and Middle Supai Formations where no apparent fractures are visible on the land surface. Well logs, however, show significant horizontal and bedding-plane fracturing in the water-bearing units at this site. Specific capacities are lowest for wells developed in the water-bearing units of the Kaibab or Schnebly Hill Formations regardless of whether or not the wells are close to fractures.

Hydraulic Properties

The hydraulic properties—transmissivity, hydraulic conductivity, and storage coefficient—are important components of aquifer assessments because they provide information that is useful for the development of wells and for predicting aquifer response to stress. Formation lithology and the type and degree of fracturing affect hydraulic properties. Faults may be areas of high permeability because of the heavily fractured nature of the rock in the fault zone. Faults also may be areas of low permeability surrounded by areas of more heavily fractured rocks that have higher permeability. Consequently, wells drilled along faults do not always have high well yields. Hydraulic properties of the regional aquifer for this study were developed from historical information and the analysis of field data collected for this study.

Transmissivity and Hydraulic Conductivity

Transmissivity values were calculated from 43 of the 76 well and aquifer tests. Twenty-two of these values were from previously published or reported tests, 17 values were estimated from specific-capacity values for single-well tests re-evaluated for this study, and 4 values were determined from single-well tests completed during this study. The typical response to pumping of wells in the study area indicates that the regional aquifer is anisotropic and unconfined. Well tests in parts of the aquifer unaltered by fractures have drawdown responses consistent with radial flow to a well from fine-grained porous media. This condition is indicated by semilog-drawdown curves plotted as straight lines with steep slopes out to 48 hours. Forty-eight hours is the maximum length of most of the well tests. Many of the well tests were terminated at 24 to 48 hours before equilibrium was reached and where delayed yield to the well may have affected the drawdown response. Some of the drawdown data for longer well tests indicated that declining water levels reached aquifer boundaries related to lithology or geologic structure. These boundary conditions were typically indicated by a change in the slope of the drawdown data (**fig. 43**). Where the aquifer was extensively fractured or faulted, two types of drawdown response were typically measured. In some cases, the semilog-drawdown curves resulted in stepped or multiple-slope drawdown curves in response to constant pumping. This type of response is characteristic of fractured rock that has only a few prominent fractures. Early in the pumping of wells, flow from fractures causes the rate of drawdown to increase with time. As pumping continues and fractures are dewatered, flow from the rock matrix into fractures results in slower drawdown. As pumping continues, the drawdown increases again as flow to the wells is from both fractures and the rock matrix. Where the aquifer is extensively fractured and the fractures are well connected, the drawdown response to constant pumping is consistent with that of unfractured porous media. The response curve of drawdown on a semilog plot is a straight line but with a much shallower slope.

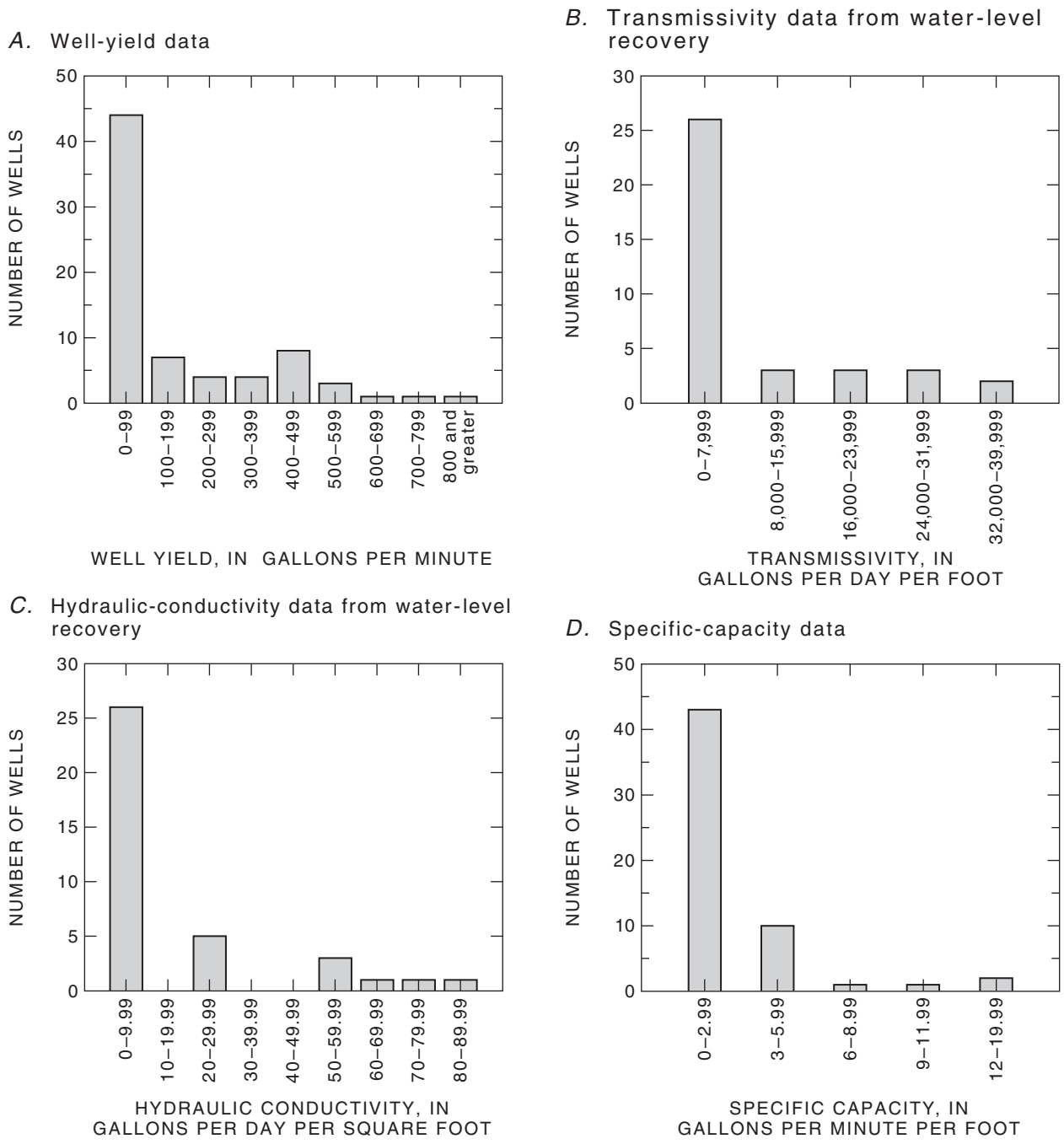

Figure 42. Distribution of data from well and aquifer tests, Flagstaff, Arizona. *A*, Well-yield data. *B*, Transmissivity data from water-level recovery. *C*, Hydraulic-conductivity data from water-level recovery. *D*, Specific-capability data.

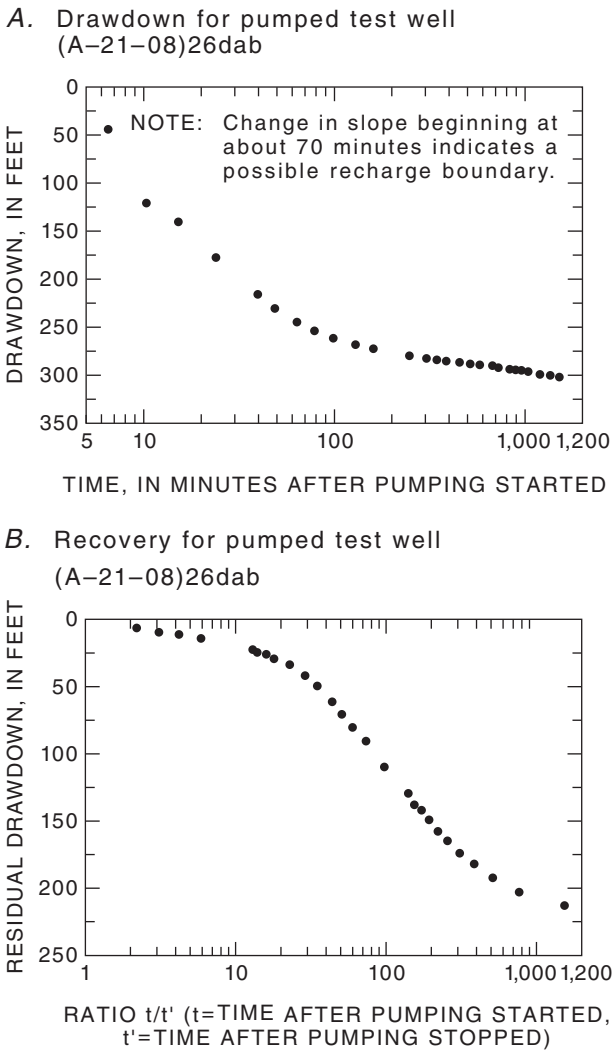

Figure 43. Drawdown and recovery data for a typical well test in the Flagstaff area. *A*, Walnut Canyon well. *B*, Recovery, Wlanut Canyon well.

Several general relations are noted when comparing transmissivity and hydraulic-conductivity data to lithology and geologic structure. Transmissivity and hydraulic conductivity generally are higher at wells developed in the Coconino Sandstone and the Supai Group, especially in areas that are extensively fractured. Transmissivity and hydraulic conductivity are low at wells developed in the Kaibab and Schnebly Hill Formations even where these units are extensively fractured. Transmissivity and hydraulic conductivity generally are higher where extensive fracturing occurs regardless of lithology. The lowest transmissivity and hydraulic-conductivity values have been obtained from parts of the aquifer that are far removed from any observed fracturing in the surface or subsurface.

From the drawdown data, transmissivity values range from about 100 to 31,200 (gal/d)/ft and average 6,400 (gal/d)/ft (**pl. 4**). Transmissivity values from the recovery data range from 100 to 35,000 (gal/d)/ft and average 8,600 (gal/d)/ft (pl. 4). Factors contributing to the wide range of values are (1) short-duration or low-discharge single well tests that do not fully define the hydraulic characteristics of the aquifer, (2) the different volumes of aquifer tested (use of wells that only partially penetrate the water-bearing units), and (3) fracture flow that substantially enhances the aquifer characteristics contributing flow to the well.

Hydraulic-conductivity values were calculated from 41 of the 42 transmissivity values derived from drawdown data and range from 0.14 to 51.5 (gal/d)/ft^2 and average 11.9 (gal/d)/ft^2 (pl. 4). Hydraulic-conductivity values also were calculated from the 30 transmissivity values derived from recovery data and range from 0.14 to 79.1 (gal/d)/ft^2 and average 17.4 (gal/d)/ft^2 (pl. 4). Hydraulic-conductivity values calculated from transmissivity values determined from well and aquifer tests lasting two or more days probably are more reliable than hydraulic-conductivity values determined from shorter tests.

Data for transmissivity and hydraulic conductivity show a distribution similar to that of the well-yield data (**fig. 42**A–C). Most of the transmissivity data are less than 5,000 (gal/d)/ft, and nine values were greater than 10,000 (gal/d)/ft. Most hydraulic-conductivity values are less than 10 (gal/d)/ft^2, and 13 values were greater than 10 (gal/d)/ft^2 (fig. 42C).

Regression plots were made of transmissivity, hydraulic conductivity, and specific capacity as functions of well yield (**fig. 44**A–C). A good correlation exists between low well yield and low hydraulic conductivity; however, the variability and scatter in the data increases with increasing yield and hydraulic conductivity (fig. 44A–B). These data indicate possible effects on the wells from formation grain size and (or) secondary permeability from fractures that cause greater scatter and variability in the data at higher well yields. Well construction also may influence results.

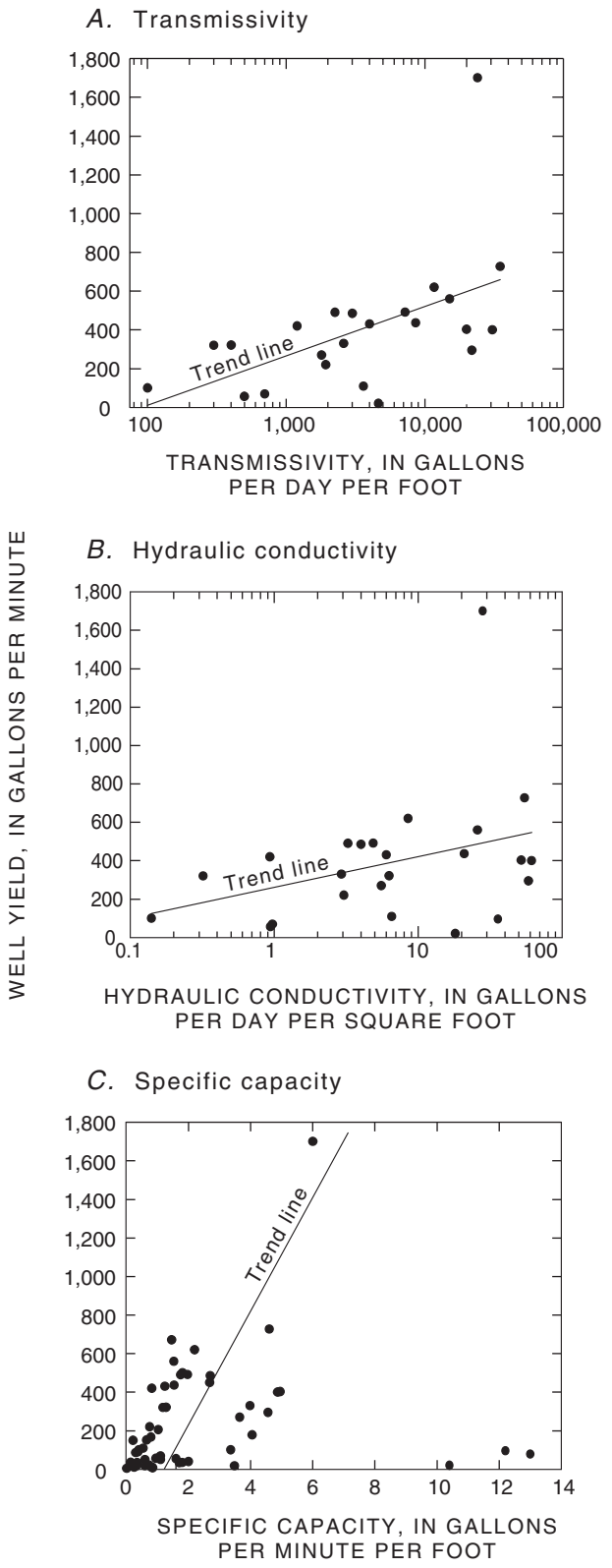

Figure 44. Relation of well yield to transmissivity, hydraulic conductivity, and specific capability, Flagstaff, Arizona. *A*, Transmissivity. *B*, Hydraulic conductivity. *C*, Specific capacity.

Storage Coefficients and Aquifer Storage

Specific storage, and specific yield are related to geologic structure and the potentiometric surface of the regional aquifer (**pl. 2**). Three values of specific storage average 0.023 and range from 0.00023 to 0.05. Eight specific-yield values average 0.077 and range from 0.0002 to 0.14. Although there are few data to define a relation of storage to lithology and geologic structure, some general trends are apparent. Storage coefficients generally are greatest in the Coconino Sandstone. Specific yields also are high in the Supai Group and are lowest in the Kaibab and Schnebly Hill Formations. Storage coefficients for the regional aquifer are consistent with values calculated for the C aquifer that underlies the Navajo and Hopi Reservations (Cooley and others, 1969) and parts of southern Coconino County (McGavock and others, 1986) and comprises rock units contemporaneous with the regional aquifer. On the basis of the average specific yield and average saturated thickness, the water in storage in the study area is estimated to be about 4,800,000 acre-ft.

Ground-Water Flow System

North of the ground-water divide coincident with the two ground-water mounds to the south and southwest of Flagstaff, ground water moves laterally and vertically to the north, northeast, and northwest toward the Grand Canyon and the Little Colorado River (pl. 2). South of the divide, ground water generally moves laterally and vertically to the south and southwest toward Oak Creek and Verde Valley. Locally, ground-water flow is diverted, disrupted, reduced, or enhanced by subsurface changes in lithology and geologic structure. Both of the main pumping centers near Flagstaff are on or just north of the ground-water divide.

The rate and direction of ground-water movement is partly a function of the hydraulic gradient derived from the slope of the potentiometric surface (pl. 2). Hydraulic gradients in the regional aquifer near Flagstaff vary from about 40 to 1,000 ft/mi. The varied hydraulic gradient indicates that ground-water flow does not flow uniformly from topographically high areas to topographically low areas and that the flow is controlled in some places by fractures. This condition is evinced by the moderate to low gradients between the Woody Mountain and Lake Mary well fields and north of the Lake Mary well field coincident with the Anderson Mesa Fault. Faults also can impede the

lateral movement of ground water as shown by the steep gradient to the northeast of the Lake Mary well field (**pls. 2** and **3**). Anderson Mesa is uplifted several hundred feet by the fault to the northeast of the Lake Mary well field and has positioned fine-grained sediments of the lower part of the Supai Group into contact with water-bearing units of the regional aquifer in the Lake Mary graben. As a result, flow across the fault in this area is slow and results in steep hydraulic gradients. With the exception of Oak Creek, ground water does not discharge to streams in the study area. The direction of lateral ground-water flow, therefore, is not necessarily toward streams in the study area.

Recharge and Discharge

Recharge to the regional aquifer occurs throughout the study area in the form of (1) infiltration of precipitation (rain and snowmelt) through unsaturated soil and rocks to the water table, (2) infiltration of surface water from significant storms into stream channels, solution channels, and sinkholes, (3) infiltration of treated effluent into the Rio de Flag, (4) seepage from lakes, and (5) downward leakage and overflow from perched water-bearing zones above the regional aquifer. Rio de Flag has one of the lowest calculated runoff values (0.04 in./yr) in Arizona (McGavock and others, 1986). Lateral movement of ground water from outside the study area into the study area (underflow) is not likely because of the location of the ground-water mounds at the south end of the study area.

Most of the recharge occurs near areas of highest precipitation at altitudes above 7,000 ft to the south of Lake Mary and on San Francisco Mountain. Infiltration and recharge are greater in the winter months when the ground is saturated for prolonged periods as a result of snowmelt and minimal evapotranspiration. Summer recharge generally is from intense thunderstorms that produce runoff into streams, solution channels, and sinkholes that direct the water rapidly to the water table. High evapotranspiration rates during the summer generally limit the amount of precipitation that reaches the water table.

Average annual precipitation for the City of Flagstaff is about 21.1 in. (Sellers and others, 1985). Evaporation and infiltration rates have been estimated, mainly for the Lake Mary area, by Blee (1988). Blee determined that evaporation losses of 27 percent of the average annual precipitation are possible, and as much as 45 percent of the average annual runoff into Lake Mary seeps out of the bottom of the lake. Errol L. Montgomery and Associates (1993) estimated that from 4 to 17 percent of the average annual precipitation is recharged to the regional aquifer in the area that contributes recharge to the Lake Mary well field. If 17 percent of the average precipitation (21.1 in./yr) is used as an estimate of recharge for the whole study area, then as much as 94,400,000,000 gallons or 290,000 acre-ft is recharged to the regional aquifer annually. Many of the other natural and manmade lakes in the area are suspected to have high seepage rates because of porous or highly fractured material underlying the lakes.

Most of this recharge is balanced by outflow from the aquifer to discharge areas outside the study area. The main points of natural discharge to the south of the study area are springs along Oak Creek, interformational flow downgradient into the Verde Valley, and springs in the Verde Valley (Levings, 1980; Owen-Joyce and Bell, 1983). To the north, ground water flows downgradient to discharge points along the Little Colorado and Colorado Rivers (McGavock and others, 1986). As of 1998, discharge from all regional aquifer wells and springs in the study area is about 7,500 acre-ft/yr. The combined natural discharge to areas north and south of the study area (about 400,000 acre-ft/yr; R.J. Hart, hydrologist, USGS, written commun., 1996) is greater than the estimated recharge to the study area, but these discharge areas receive additional ground-water flow from outside the study area. Some ground water also may be flowing out of the study area to the northwest in the direction of the Havasu Basin. Evapotranspiration of water directly from the regional aquifer is minimal and restricted to a few small areas to the south of Lake Mary and the upper part of Oak Creek where springs discharge. Vertical leakage to underlying water-bearing zones is likely to be restricted in most of the area by confining beds in the lower part of the Supai Group. Some ground-water exchange probably does occur along fault zones that propagate all the way to basement rocks. Little net exchange of water, however, is likely to occur because of high hydraulic pressure in the underlying limestone aquifer (J.M. Montgomery Consulting Engineers, Inc., 1982).

Water Chemistry

The distribution of dissolved chemical constituents in the regional aquifer is mainly the result of naturally occurring processes. Dissolved-solids concentrations in ground water in the regional aquifer are small near recharge areas and increase downgradient as the water reacts with aquifer materials. Recharge from treated effluent along the Rio de Flag may be providing additional nutrients and chloride to some parts of the regional aquifer.

Common Ions, Trace Elements, and Nutrients

In the study area, ground water is predominantly a calcium (Ca2+) magnesium (Mg2+) bicarbonate (HCO3-) type (fig. 45). Water from wells, Black Bill-Doney Park MVR-1 (BBDP-MVR-1), Continental-2, Rio de Flag MW-1, and MW-3, has higher concentrations of chloride (Cl; **figs. 45** and **46**), which indicates that recharge may be occurring from the Rio de Flag. The Rio de Flag receives treated effluent from the wastewater-treatment plants. Ground water that discharges from Old Town Spring, NAD-1, Inner Basin well 9 (IB-9), and the well at Parks School that are developed in perched water-bearing units in the volcanic rocks yielded higher concentrations of sodium (Na+) and potassium (K+; fig. 45), which indicates dissolution of volcanic glass (Hearne and others, 1985; table 2, this report).

Major-ion data for wells and springs that discharge ground water from the regional aquifer generally fall into one of two groups—the Woody Mountain group or the Lake Mary group (**fig. 47**). The groupings represent, in part, certain water-rock reactions as water passes through the unsaturated zone (see "Supplemental Data, Part C" at the back of the report). Ground water in the Woody Mountain group receives recharge from infiltration of precipitation through volcanic rocks and yields lower concentrations of Ca^{2+} and Mg^{2+} (**fig. 48**A–B) and higher concentrations of silica (SiO_2; **fig. 49**) than the water in the Lake Mary group, which receives recharge from infiltration of precipitation through limestones and volcanic rocks (fig. 49).

Chemistry of ground water from perched water-bearing zones generally plots either in the Woody Mountain or Lake Mary group. Perched ground water in the Kaibab Formation (Rio de Flag MW-1 and MW-3) yields concentrations of Ca and Mg similar to those in water from regional-aquifer wells in the Lake Mary group (fig. 48). Chemistry of perched water in volcanic rocks (Parks School well, IB-9, Old Town Spring, and NAD-1) plot with water from wells in the regional aquifer in the Woody Mountain group (fig. 48).

Barium (Ba) was the only trace metal present in significant concentrations in water from the regional aquifer. Concentrations of Ba in ground water from Pine Grove (2.0 mg/L) were at the Maximum Contaminant Level (MCL) for drinking water (U.S. Environmental Protection Agency, 1999). BBDP-MVR-1 (1.2 mg/L), BBDP-Marijka (1.2 mg/L), and Mtn Dell-1 (1.2 mg/L) also contained high concentrations of Ba, but were below the MCL (**table 2**). The high concentrations of Ba probably are the result of the dissolution of evaporites in the Supai Group (Appel and Bills, 1981; McGavock and others, 1986).

Concentrations of nitrate NO^-_2+NO^-_3) as N in ground water from most of the wells and springs were below the MCL of 10 mg/L (U.S. Environmental Protection Agency, 1993a, b). Ground water from Rio de Flag MW-3 contained 8.0 mg/L of NO^-_2+NO^-_3. BBDP-MVR-1 and Continental-2 along the Rio de Flag contained 4.6 and 1.7 mg/L of NO^-_2+NO^-_3, respectively, and NAD-1 contained 3.3 mg/L of NO^-_2+NO^-_3. Sites that have measureable concentrations of NO^-_2+NO^-_3 may indicate recent local recharge from effluent sources. Water from the rest of the wells and springs contained less than 1.0 mg/L of NO^-_2+NO^-_3.

Stable Isotopes

Ground-water samples collected from 23 wells and 3 springs that discharge water from the regional aquifer were analyzed for stable isotopes of oxygen and hydrogen. Samples from three wells and two springs that discharge water from perched water-bearing zones and two snowmelt samples also were analyzed. The small range of $\delta^{18}O$ and δ^2H in water from the regional aquifer and from perched ground-water zones indicate a common recharge source for the study area (**fig. 50**). Little or no evaporation occurs in most of the ground-water system; however, water from wells—LM- 4, BBDP-MVR-1, and Rio de Flag MW-1—have isotopic compositions that are indicative of local recharge from surface water that had undergone evaporation (fig. 50).

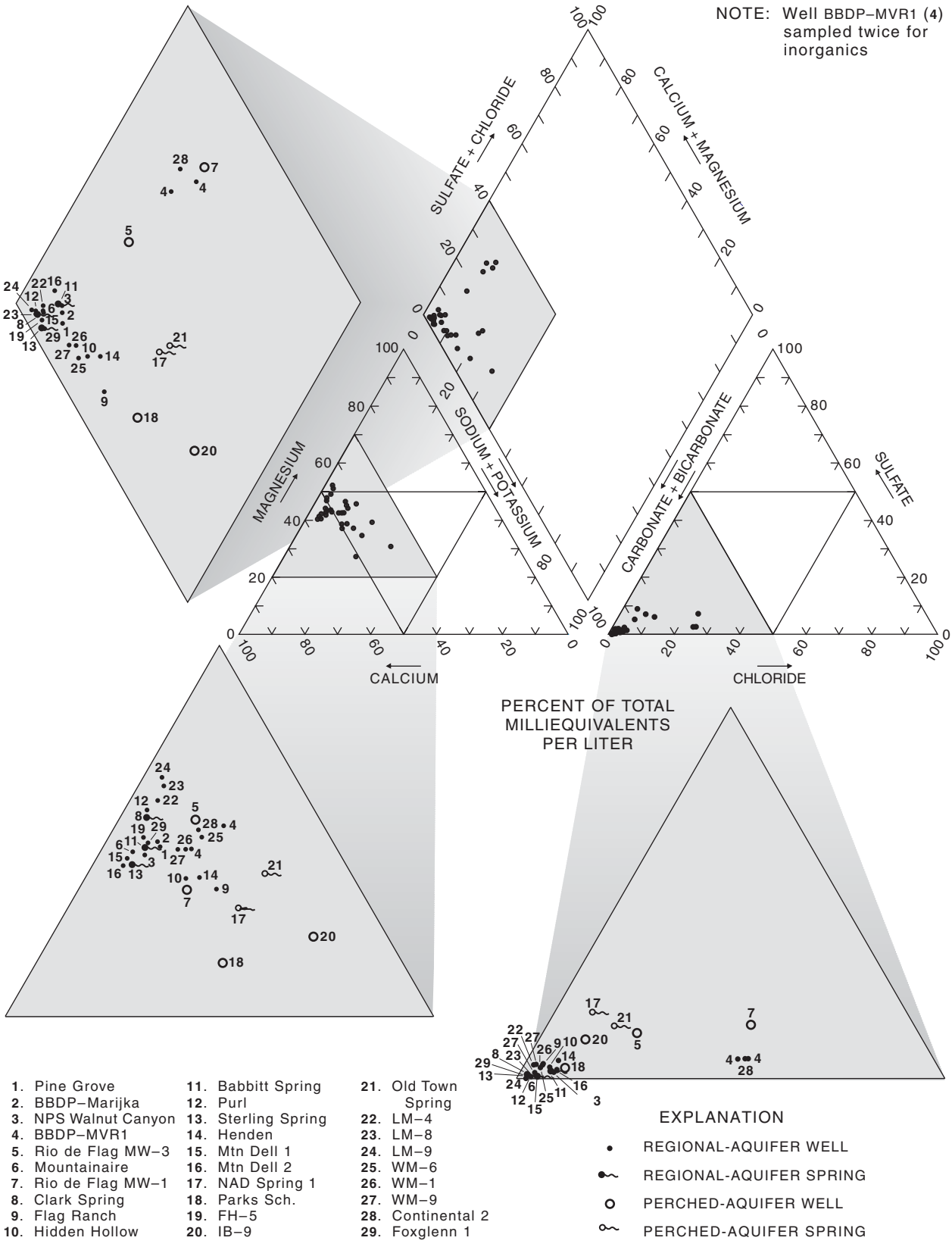

Figure 45. Relative composition of ground-water samples from the regional aquifer and perched water-bearing zones, Flagstaff, Arizona, 1995–97.

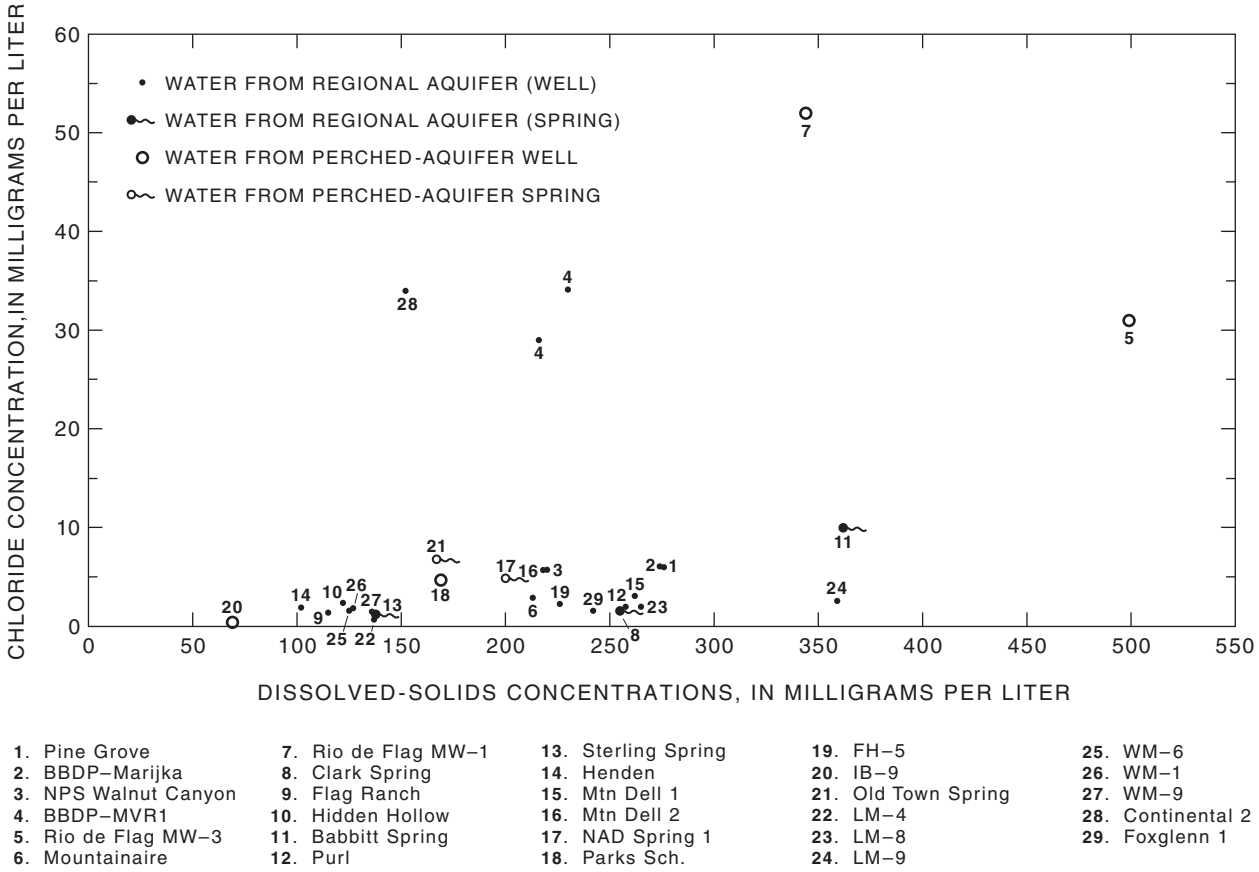

1. Pine Grove
2. BBDP–Marijka
3. NPS Walnut Canyon
4. BBDP–MVR1
5. Rio de Flag MW–3
6. Mountainaire
7. Rio de Flag MW–1
8. Clark Spring
9. Flag Ranch
10. Hidden Hollow
11. Babbitt Spring
12. Purl
13. Sterling Spring
14. Henden
15. Mtn Dell 1
16. Mtn Dell 2
17. NAD Spring 1
18. Parks Sch.
19. FH–5
20. IB–9
21. Old Town Spring
22. LM–4
23. LM–8
24. LM–9
25. WM–6
26. WM–1
27. WM–9
28. Continental 2
29. Foxglenn 1

Figure 46. Concentrations of chloride as a function of concentrations of dissolved solids in water from the regional aquifer and perched water-bearing zones, Flagstaff, Arizona, 1995–97.

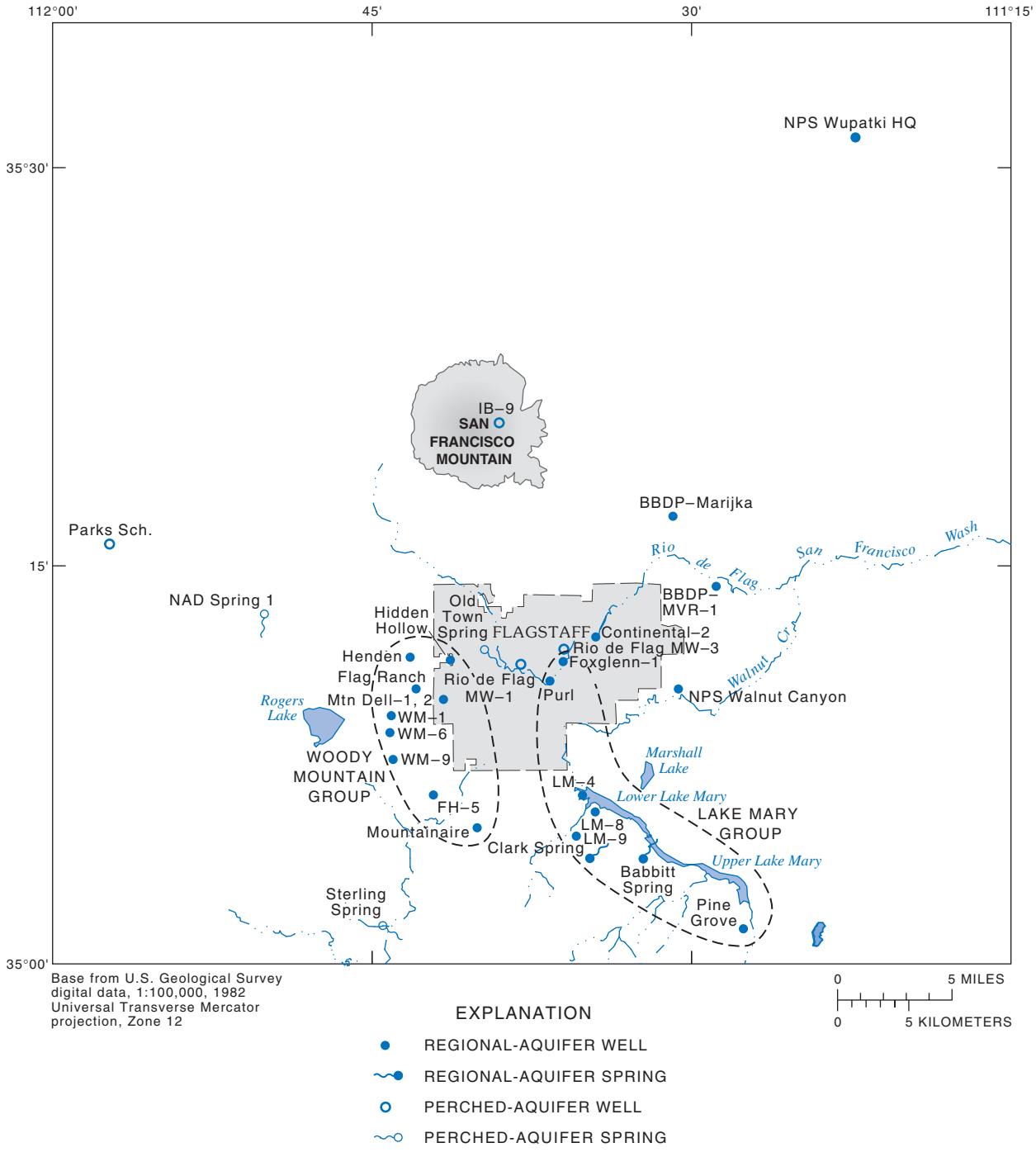

Figure 47. Areas of the regional aquifer in which wells and springs have similar water-chemistry characteristics, Flagstaff, Arizona, 1995–97.

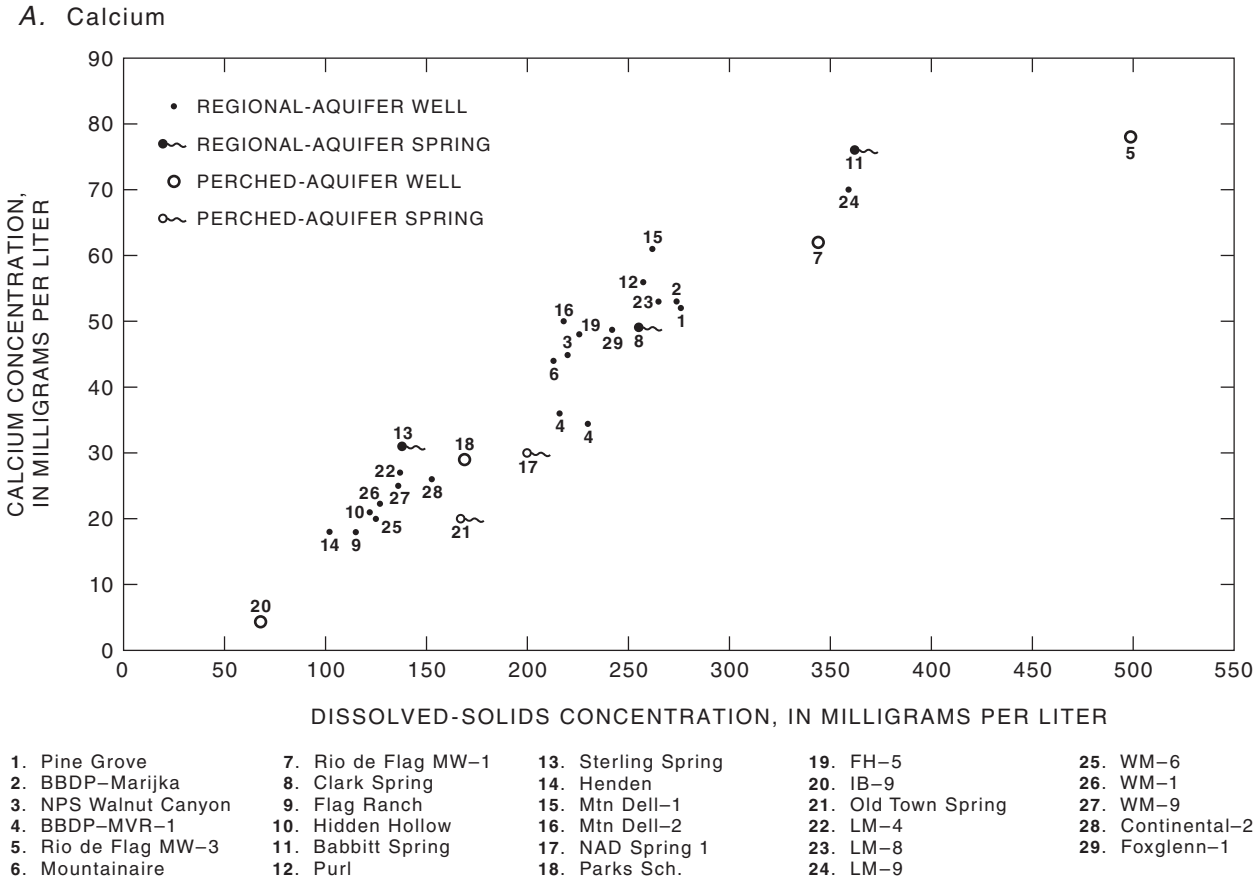

Figure 48. Concentrations of calcium and magnesium as a function of concentrations of dissolved solids in water from the regional aquifer and perched water-bearing zones, Flagstaff, Arizona, 1995–97. *A*, Calcium. *B*, Magnesium.

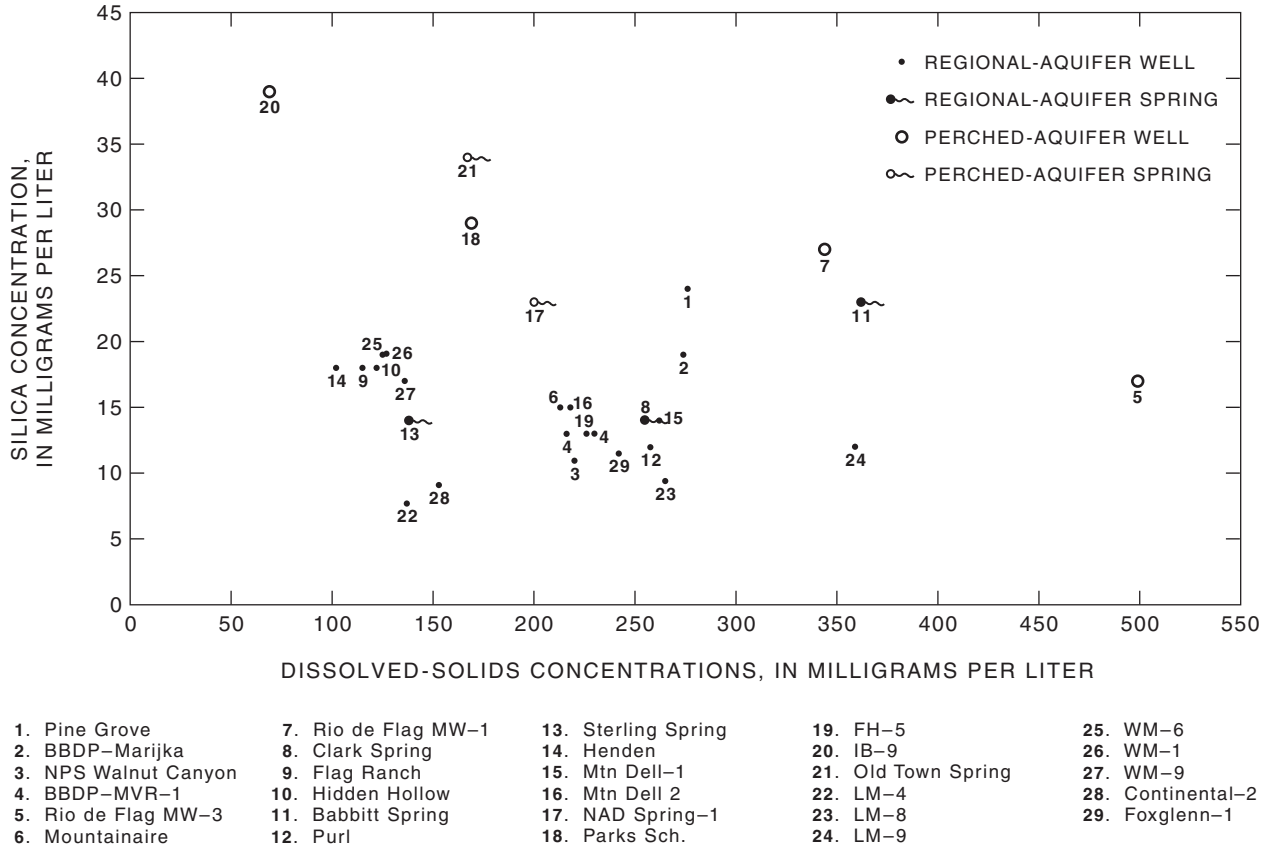

1. Pine Grove
2. BBDP–Marijka
3. NPS Walnut Canyon
4. BBDP–MVR–1
5. Rio de Flag MW–3
6. Mountainaire
7. Rio de Flag MW–1
8. Clark Spring
9. Flag Ranch
10. Hidden Hollow
11. Babbitt Spring
12. Purl
13. Sterling Spring
14. Henden
15. Mtn Dell–1
16. Mtn Dell 2
17. NAD Spring–1
18. Parks Sch.
19. FH–5
20. IB–9
21. Old Town Spring
22. LM–4
23. LM–8
24. LM–9
25. WM–6
26. WM–1
27. WM–9
28. Continental–2
29. Foxglenn–1

Figure 49. Concentrations of silica as a function of concentrations of dissolved solids in water from the regional aquifer and perched water-bearing zones, Flagstaff, Arizona, 1995–97.

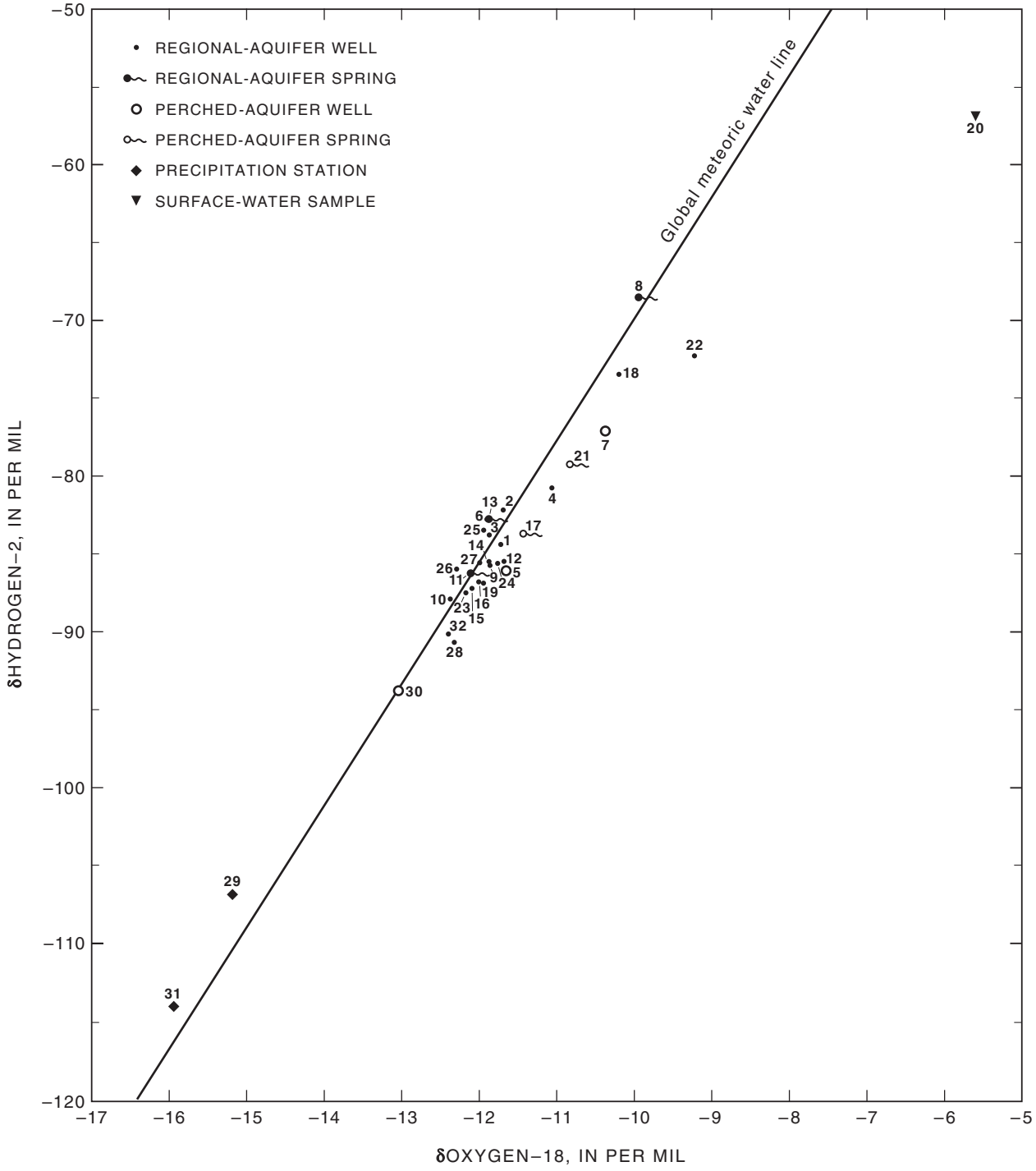

1. Pine Grove
2. BBDP–Marijka
3. NPS Walnut Canyon
4. BBDP–MVR–1
5. Rio de Flag MW–3
6. Mountainaire
7. Rio de Flag MW–1
8. Clark Spring
9. Flag Ranch
10. Hidden Hollow
11. Babbit Spring
12. Purl
13. Sterling Spring
14. Henden
15. Mtn Dell–1
16. Mtn Dell–2
17. NAD Spring 1
18. NPS Wupatki HQ
19. FH–5
20. Upper Lake Mary (surface water)
21. Old Town Spring
22. LM–4
23. LM–8
24. LM–9
25. WM–6
26. WM–1
27. WM–9
28. Continental–2
29. Center snowmelt (precipitation)
30. IB–9
31. IB snowmelt (precipitation)
32. Foxglenn–1

Figure 50. Oxygen and hydrogen isotopes in water from the regional aquifer and perched water-bearing zones, and from surface-water and precipitation sites, Flagstaff, Arizona, 1995–97.

All three sites are near surface water. LM-4 is near Lower Lake Mary, and BBDP-MVR-1, and Rio de Flag MW-1 are near parts of the Rio de Flag where treated effluent is discharged. The shallow well, Rio de Flag MW-3, and the deep Purl well are within 0.5 mi of each other along the Rio de Flag and yield water having similar isotopic compositions. The similarity in isotopic composition of water from all wells sampled indicates that recharge occurred at a similar altitude and temperature, which is consistent with a common source (fig. 50). Old Town Spring and NAD-1 discharge ground water from perched zones in the volcanic rocks, and this ground water has an isotopic composition that indicates evaporation of source water; whereas, none of the springs that discharge from the regional aquifer have this composition (fig. 50). Clark Spring, which discharges from the regional aquifer, has a distinctly different isotopic composition than that of Babbitt and Sterling Springs, which also discharge ground water from the regional aquifer. The different compositions indicate a different source of recharge (fig. 50). Repeat samples of ground water from BBDP-MVR-1, Mtn Dell-1, LM-4, and WM-9 showed no seasonal shifts in isotopic composition (table 3).

Radiogenic Isotopes

Samples of water from 20 wells and 2 springs that discharge water from the regional aquifer were collected for analysis of ^{13}C and ^{14}C (table 2). Samples also were collected from Old Town Spring, NAD-1, and IB-9 that discharge perched ground water from the volcanic rocks. Estimated ages of the ground water in the regional aquifer indicate areas of modern waters (less than 200 years) and areas of older waters (greater than 5,000 years ±3,000 years; table 2). Estimated ground-water ages indicate modern water in the Lake Mary area and older water (2,000 to greater than 5,000 years) in the Woody Mountain area (**pl. 1**). Differences in estimated ground-water ages between the two areas may reflect depth to ground water, travel times for ground-water movement, and (or) pumping effects that draw deeper, older waters from wells. Ground water is 200 to 900 ft below land surface in the Lake Mary area and is as much as 1,200 ft below land surface in the Woody Mountain area. Estimated ground-water ages for the Lake Mary area, Woody Mountain area, and Wupatki National Monument are in agreement with the ground-water flow directions as determined from the potentiometric surface.

Uncertainties for the estimated ages of ground water from selected wells were determined by a sensitivity analysis (**table 4**) for all the estimated components in the model calculation (Fonts and Garnier, 1979). Two components—the initial 14C for soil gas and the δ13C of carbonate—were the unknowns that would directly affect the estimated ages. The 14C for soil gas used in the model was 100 percent modern carbon (pmc). Sensitivity analysis was run for 115 pmc and 85 pmc (table 4). The δ13C of carbonates held constant at 0.0 ‰ for the models. The sensitivity was run using +1‰ and -1‰ for δ13C (table 4). The estimated uncertainty generated by the model is ±3,000–4,000 years.

Table 3. Temporal data for oxygen, deuterium, and tritium in water from selected wells that discharge water from the regional aquifer, Flagstaff, Arizona

[Isotope-composition values are in per mil. Dashes indicate no data. <, less than; ^{18}O, oxygen-18; δ^2H, deuterium]

Well name	Temporal samples								
	Oxygen and deuterium						Tritium, in tritium units		
	Summer 1996		Winter 1996/ Spring 1997		Summer 1997				
	$\delta^{18}O$	δ^2H	$\delta^{18}O$	δ^2H	$\delta^{18}O$	δ^2H	Summer 1996	Spring 1997	Summer 1997
BBDP-MVR-1	-11.07	-80.8	-10.88	-80.4	-10.82	-80.2	4.4	4.7	5.0
Mtn Dell-1	-12.10	-87.2	-12.15	-86.7	-12.12	-87.4	.94	---	1.3
LM-4	-9.23	-72.3	-9.27	-74.5	-9.27	-74.0	7.5	8.2	7.5
WM-9	-12.00	-85.6	-12.02	-85.4	-12.13	-86.8	<.31	<.41	<.31

Table 4. Sensitivity analysis for calculations of carbon-14 ages

[^{14}C, carbon-14; ^{13}C, carbon-13]

Well site	^{14}C soil gas at 85 percent modern carbon		^{14}C soil gas at 115 percent modern carbon	
	$\delta^{13}C$ of carbonate, in per mil	Estimated age of ^{14}C, in years	$\delta^{13}C$ of carbonate, in per mil	Estimated age of ^{14}C, in years
WM- 6	-1	370	-1	2,800
Do.	+1	1,400	+1	2,900
Henden	-1	3,900	-1	7,700
Do.	+1	5,200	+1	6,400
BBDP-Marijka	-1	1,400	-1	5,200
Do.	+1	2,700	+1	3,900
NPS Wupatki HQ	-1	2,000	-1	7,400
Do.	+1	4,900	+1	4,500
Pine Grove	-1	820	-1	4,100
Do.	+1	1,600	+1	3,300
NPS Walnut Canyon	-1	-1,700	-1	1,900
Do.	+1	-640	+1	770

Samples of water for analysis of 3H were collected from 22 wells and 3 springs that discharge water from the regional aquifer (**table 2**). Samples also were collected at three wells and three springs that discharge water from volcanic rocks and from Upper Lake Mary and Quarry. Activities of 3H in water from the regional aquifer ranged from less than 0.31 tritium units (TU; detection limit) to 8.5 TU (table 2). The highest activities occurred at LM-4, BBDP-MVR-1, and Babbitt Spring. Activities of 3H at LM-4 (7.5, 8.2) suggest a component of recent recharge to the site or a possible connection to water from Lake Mary. Activity of 3H in water from BBDP-MVR-1 probably is related to infiltration of effluent along the Rio de Flag.

Samples of perched ground water generally had higher activities of 3H (range 5.0 to 10.3 TU) than samples from the regional aquifer. The highest activities of 3H were 9.1 TU for Rio de Flag MW-3, 9.7 TU for NAD-1, and 10.3 TU for IB-9. Older estimated 14C ground-water ages and measurable activity of 3H in the Woody Mountain area and other locations including Doney Park, Mountainaire, and Continental indicated mixing of deep older water and shallow recharge water throughout the regional aquifer.

Water samples were collected from 14 ground-water sites that yield water from the regional aquifer and 3 springs—Clark Spring, Babbitt Spring, and Sterling Spring—that yield water from the regional aquifer for analysis of Sr (**table 5**). Values of δ87Sr indicate recharge is occurring locally throughout the study area. The stable-isotope ratio δ87Sr in these samples (**fig. 51**A–B; table 5) correlates with the ratio found in carbonate rocks deposited in the Late Permian age (Peterman and others, 1970). This ratio is indicative of water-rock reactions that mainly occur in the unsaturated zone as water recharges the deeper regional aquifer. Chemical influence from the young volcanic rocks (Faure, 1977) is evident by the 87Sr/86Sr of 0.702 to 0.704 for wells near San Francisco Mountain (table 5, this report; M.M. Ort, associate professor, NAU, written commun., 1997). Ground water that recharges through volcanic rocks yields the lighter composition as found in water from Sterling Spring, WM-9, WM-1, Henden well, and the well in Hidden Hollow (Group A in fig. 51A–B). Water that recharges primarily through limestone yields the heavier composition as found in water from LM-4, LM-9, and the Purl well (Group C in fig. 51–B). Groups A and C partially coincide with the Woody

Mountain and Lake Mary areas, respectively (**fig. 47**). The δ87Sr values that plot in Group B—Babbitt Spring, Clark Spring, BBDP-Marijka, BBDP-MVR-1, Mountainaire, Mtn Dell-1, FH-5, Foxglenn-1, and Pine Grove—suggest a mixture of ground water from the volcanic rock and limestone recharge areas (fig. 51A–B).

Effects of Geologic Structure on Ground-Water Flow

A large scatter exists in the orientation of surface-structural features (**fig. 52**); however, two trends are dominant. A northwestward trend (N. 58° W.) accounts for 71 percent of the total structure, and a weaker north-northeastward trend accounts for 24 percent of the total structure. Weaker structural trends are concentrated north to south and east to west.

Acoustic-televiewer logs from selected wells verified multiple near-vertical fractures that, in many cases, did not correlate with the surface alignment of the associated structure. This change in the orientation of structural features with depth was further verified by the square-array resistivity data (see "**Supplemental Data**, Part A" at the back of the report). Many horizontal to near-horizontal fractures that had no surface expression were identified from the borehole data. These types of structural features, however, are not uncommon. Exposures of bedrock in steep-walled canyons, such as Walnut Canyon and some parts of the Rio de Flag, have prominent horizontal fractures along bedding planes in the Kaibab Formation (**fig. 53**); it does seem unusual that these horizontal fractures buried below 1,000 ft or more of overburden would be as large as indicated by the borehole-geophysical logs.

The most productive wells associated with structural trends have significant high-angle or horizontal fracturing (**fig. 54**). These wells include LM-8, WM-10, Foxglenn-1, Continental-2, and the BBDP-Marijka well. The least productive wells (LMEX-2, LMEX-6, BBDP-Cosnino, and ADOT-Winona) yield water from water-bearing zones that have not been altered by structural deformation. Available data are insufficient to define the dimensions of interconnected fracture-flow zones as of 1998; even in the Lake Mary well field where there is a wide distribution of wells and data, extended aquifer tests of as much as 90 days fail to show consistent response to pumping (Errol L. Montgomery and Associates, 1992).

Table 5. Stable-isotope data for strontium in water from selected wells and springs that discharge water from the regional aquifer, Flagstaff, Arizona

[Sr, strontium; ^{87}Sr, strontium-87; ^{86}Sr, strontium-86]

Well or spring site	Sr, in micro grams per liter[1]	$^{87}Sr/^{86}Sr$	$\delta^{87}Sr$, in per mil	Well or spring site	Sr, in micrograms per liter[1]	$^{87}Sr/^{86}Sr$	$\delta^{87}Sr$, in per mil
Babbitt Spring	140	0.70748	-2.43	Sterling Spring	84	0.70648	-3.84
Clark Spring	96	.70706	-3.02	WM-9	93	.70655	-3.74
BBDP-Marijka	163	.70731	-2.66	WM-1	110	.70588	-4.68
BBDP-MVR-1	125	.70693	-3.20	FH-5	100	.70702	-3.07
Purl	63	.70816	-1.47	Foxglenn-1	68	.70785	-1.90
Hidden Hollow	72	.70663	-3.62	Henden	73	.70632	-4.06
LM-4	27	.70814	-1.49	Mtn Dell-1	79	.70751	-2.38
LM-9	82	.70882	-.54	Pine Grove	292	.70707	-3.00
Mountainaire	110	.70723	-2.78				

[1]Concentrations determined by U.S. Geological Survey National Research Program Laboratory and do not necessarily match concentrations listed in table 2 as determined by U.S. Geological Survey National Water-Quality Laboratory.

A. Strontium

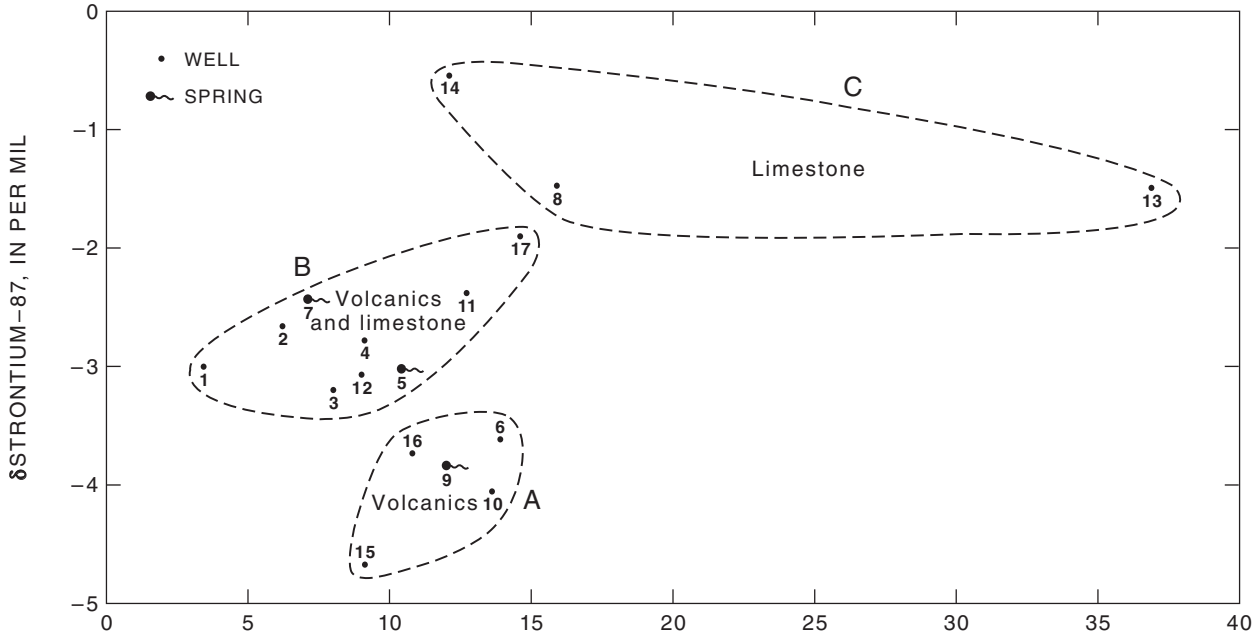

1. Pine Grove
2. BBDP–Marijka
3. BBDP–MVR–1
4. Mountainaire
5. Clark Spring
6. Hidden Hollow
7. Babbitt Spring
8. Purl
9. Sterling Spring
10. Henden
11. Mtn Dell–1
12. FH–5
13. LM–4
14. LM–9
15. WM–1
16. WM–9
17. Foxglenn–1

NOTE: Groupings indicate wells and springs that receive ground-water recharge through similar rock types.

B. Strontium-isotope data as a function of cation activity

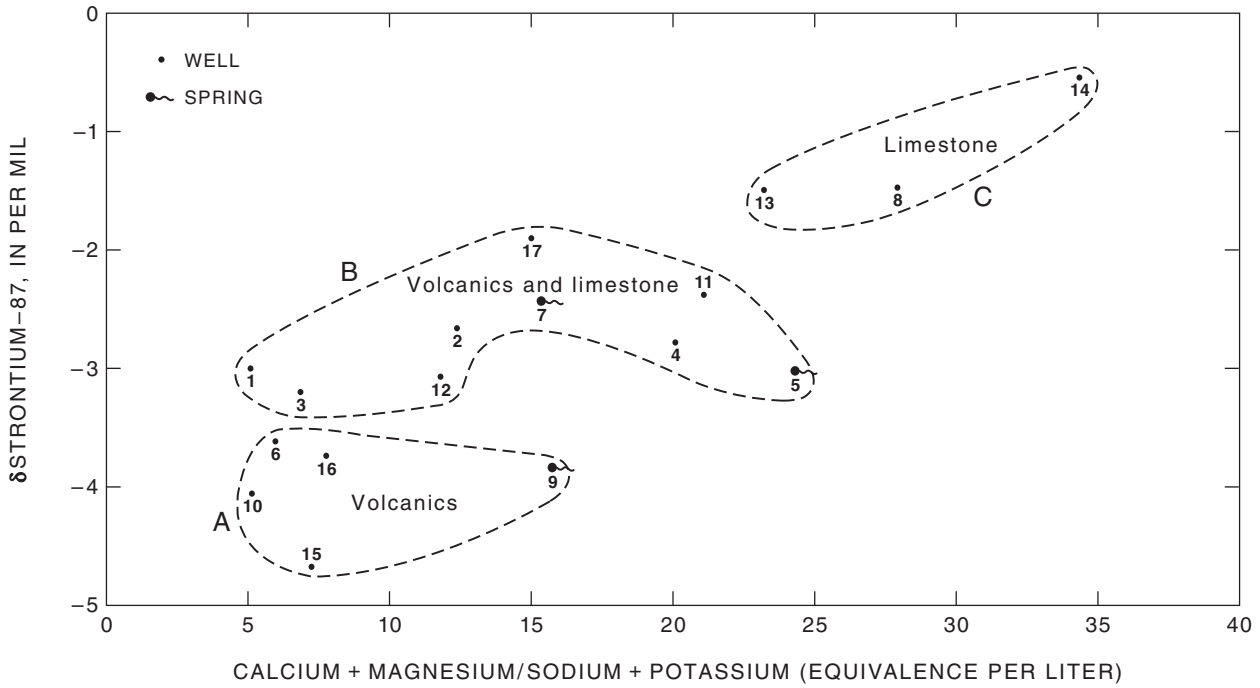

Figure 51. Strontium-isotope data for water from the regional aquifer, Flagstaff, Arizona, 1995–97. *A*, Strontium. *B*, Strontium-isotope data as a function of cation activity.

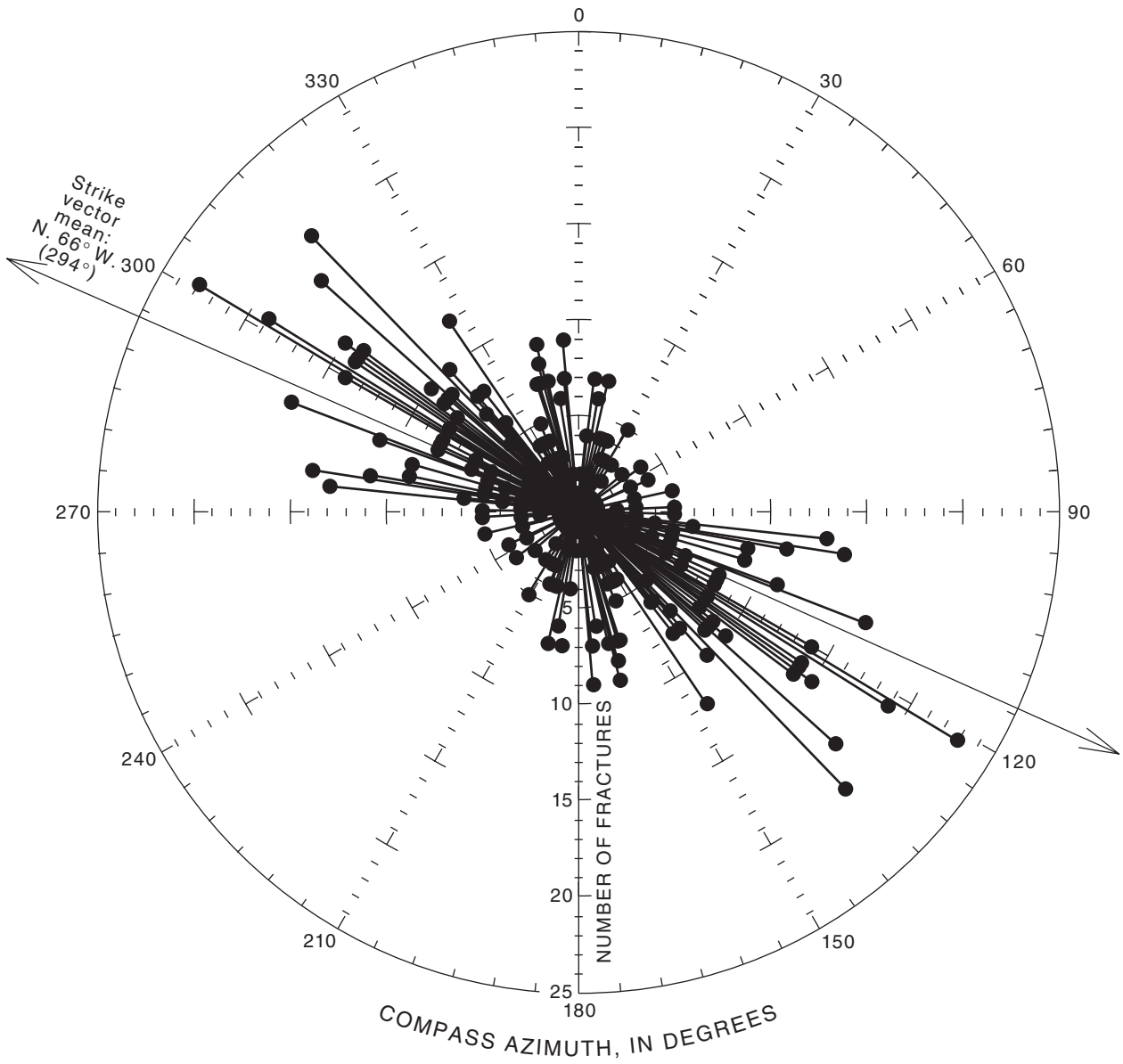

Figure 52. Orientation of documented surface fractures, Flagstaff, Arizona, 1995–97.

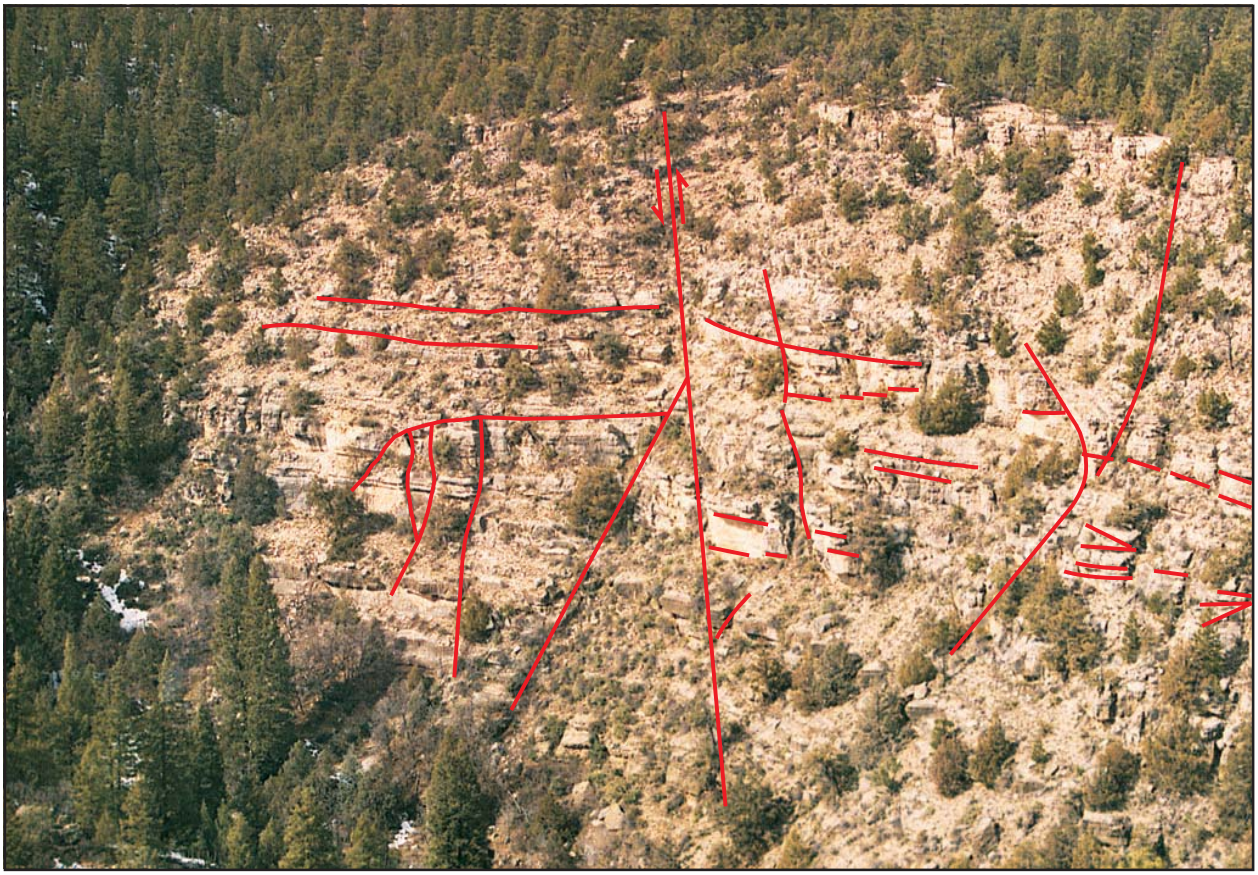

Figure 53. Horizontal and bedding-plane fracturing in Walnut Canyon, Flagstaff, Arizona.

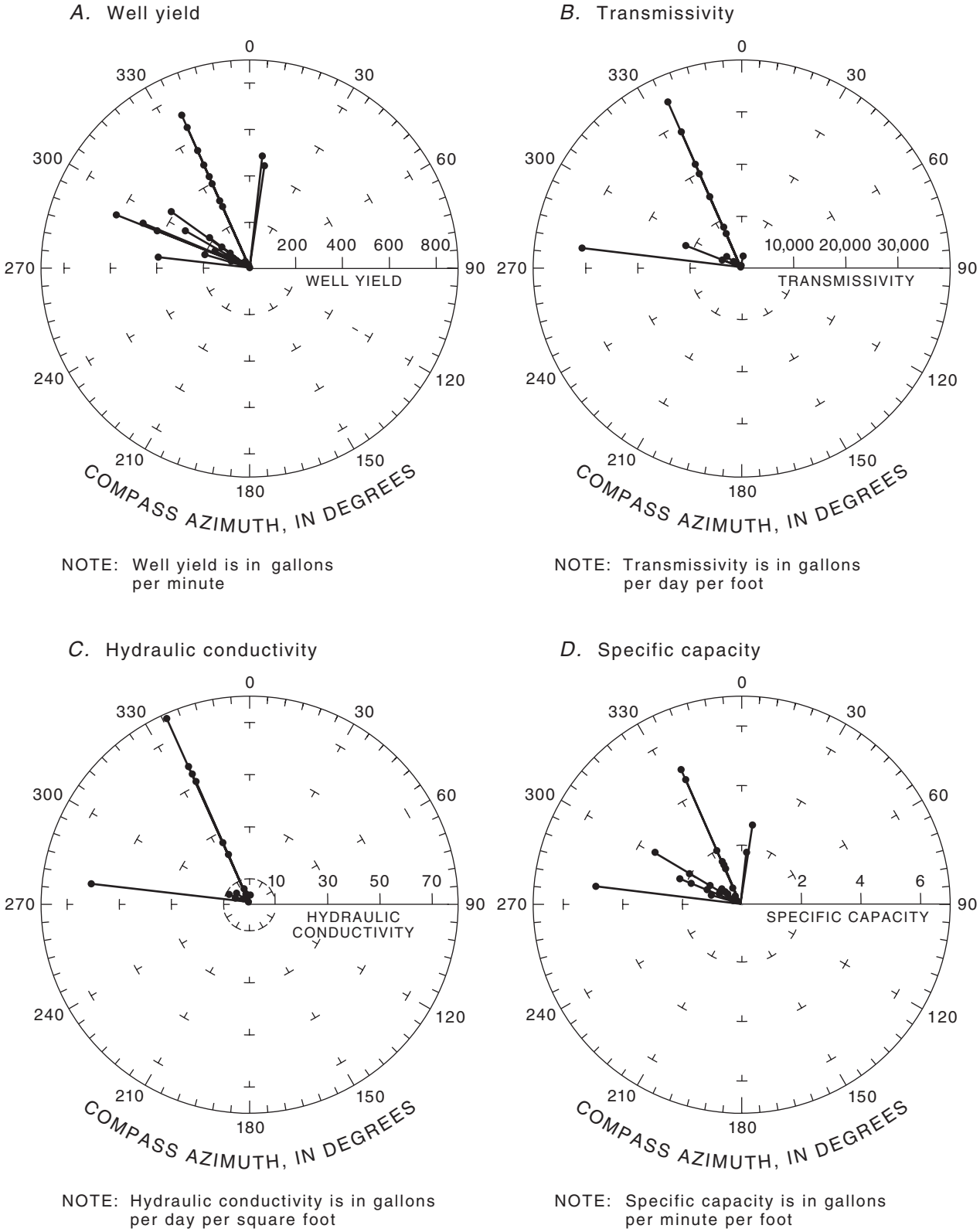

Figure 54. Relation of data from well and aquifer tests to structural orientation of surface geology, Flagstaff, Arizona. *A*, Well yield. *B*, Transmissivity. *C*, Hydraulic conductivity. *D*, Specific capacity.

Regional Structure

Well yield and hydraulic properties indicate a relation between ground-water flow and geologic structure on a regional scale. Well yields are greatest and hydraulic properties are most favorable near regional-scale structural deformation, such as the Oak Creek and Anderson Mesa Faults, and are lowest and least favorable in areas with no structural deformation. The range of hydraulic-conductivity values spans the general range of values reported for well-cemented and lithified sedimentary rocks and for rocks that are fractured and friable (fig. 55). The range of hydraulic-conductivity values is somewhat higher than the range reported for sandstone and unjointed crystalline limestone, which indicates fractures have an effect on hydraulic properties of the regional aquifer. Ground water moves from areas of high hydraulic head to areas of low hydraulic head generally along the path of least resistance; therefore, ground water will flow more easily and rapidly through those portions of an aquifer that have increased permeability due to fracturing. The direction of ground-water flow generally is parallel to subparallel to major structural trends in the Woody Mountain, Lake Mary, Foxglenn, and Continental areas (**pl. 2**). In wells that are near structural deformations, water-level fluctuations can be indicators of recharge from precipitation and runoff directly through fractures, sinkholes, and (or) solution-channel openings (**fig. 40**).

Average ground-water flow velocities were calculated as a product of the hydraulic conductivity, hydraulic gradient, and effective porosity after Lohman (1979) as a means of evaluating the effect of geologic structure on ground-water flow. As Lohman (1979) indicates, the average velocity does not necessarily equal the actual velocity between any two points in an aquifer. Average-flow velocities should not be used to predict the velocity and distance of water movement (travel time); however, they can be useful as estimates of flow (**table 6**). The estimated travel time from the Lake Mary area to the Continental area is much shorter than from the Woody Mountain area to Continental (table 6). Ground-water flow from Lake Mary to Continental is parallel to regional structure (Anderson Mesa Fault); whereas, flow from Woody Mountain to Continental is perpendicular to mostly local structural trends (**pl. 1**).

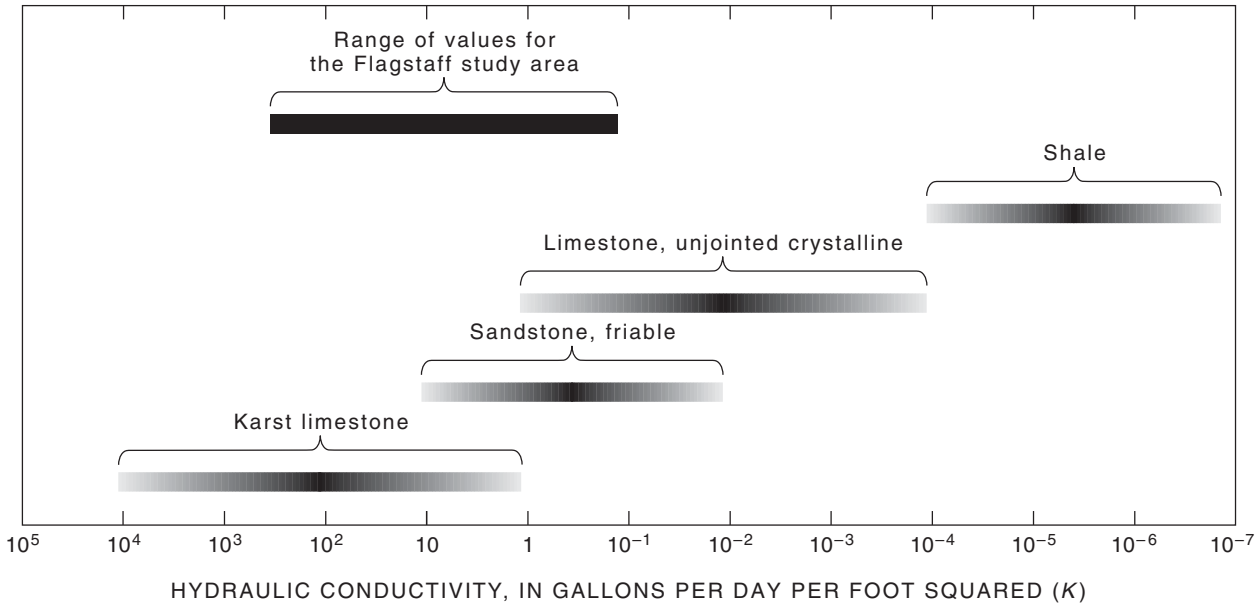

Figure 55. Comparison of hydraulic-conductivity data in the Flagstaff area with hydraulic-conductivity data for similar consolidated rocks (modified from Davis, 1969; Dunn and Leopold, 1978; and Freeze and Cherry, 1979).

Table 6. Average ground-water flow velocity and estimated travel times for ground water in selected parts of the study area, Flagstaff, Arizona

Area	Average flow velocity, in feet per year	Distance, in feet	Estimated travel time, in years
Lake Mary to Woody Mountain	57.5	57,000	990
Lake Mary to Continental	33.1	54,920	1,700
Woody Mountain to Continental	14.1	53,860	3,800
Continental to Doney Park	15.3	31,680	2,100
Continental to Wupatki	25.7	141,500	5,500

These travel times roughly correlate with ground-water ages in these areas after the influences of more recently recharged waters and mixing are considered. Storage-coefficient and specific-yield data were not correlated with structural trends as transmissivity and hydraulic conductivity were because few storage-coefficient and specific-yield data exist for the study area. Storage-coefficient and specific-yield data obtained during the study are considered to be representative of aquifer conditions because they are similar to values determined in previous studies (Cooley and others, 1969; McGavock and others, 1986) and fall within the ranges given for similar geologic materials throughout the continental United States (table 7). The calculated secondary porosity from SAR surveys ranged from 0 to about 30 percent and compares well with the range of expected values for similar consolidated rocks (table 7) and the few measured porosities available (**pl. 4**). The calculated secondary porosity from the SAR surveys compares well with data from the seismic surveys and borehole-geophysical logs; for example, the calculated secondary porosity and coefficient of anisotropy and the resistivity maxima of the Foxglenn site had significant peaks at 328 to 492 ft (**fig. 30**). These data correlate well with the seismic-image disruption and the multiple fractures in the same depth range. Data from the 164- to 492-foot range at the Continental site are similarly correlated to subsurface fractures (**figs. 18**, **37**, **39**). These fractures are well above the water table at the Foxglenn and Continental areas.

Specific capacity was compared with transmissivity to determine if specific capacity could be used to estimate aquifer properties. A correlation could not be made because well losses and well and pump efficiencies introduced errors in specific-capacity and transmissivity estimates. In the study area, transmissivity values are reflective of the screened interval open to the aquifer and may represent multiple rock formations. Specific capacity and hydraulic properties derived from pumped wells are affected by well radius, pumping period, and saturated thickness.

Local Structure

Well yield and hydraulic conductivity for wells in the Woody Mountain and Lake Mary well fields are similar and are affected by nearby faults and other fractures (pl. 4). For these areas, well yields generally range from about 300 to 700 gal/min.

Table 7. Porosity and specific yield for common consolidated rocks and for rock units of the regional aquifer near Flagstaff, Arizona

[Data from Driscoll (1996) except for data for rock units of the regional aquifer near Flagstaff, Arizona. <, less than. Dashes indicate no data]

Geologic unit	Porosity, in percent	Specific yield, in percent
Sandstone	5–30	5–15
Limestone/dolomite (original and secondary porosity)	1–20	---
Shale	0–10	.5–5
Limestone	---	0.5–5
Dense, solid rock	<1	---
Rock units of the regional aquifer near Flagstaff, Arizona	4–50	1.6–33

The wells in the Woody Mountain well field are near the Oak Creek Fault. WM-7, which is near the junction of the Oak Creek and Dunnam Faults, has the highest well yield in the well field (pls. 2 and 4). Well yields for the Lake Mary well field range from 57 gal/min to 1,700 gal/min. Most of the high-yield wells at Lake Mary are near either Anderson Mesa or the Lake Mary Faults (**pl. 2**). LM-8, which is the most productive well in the study area, is near north-eastward-striking fractures that are connected to the Lake Mary graben (pl. 2). LM-3 and LMEX-6 have well yields of 167 and 57 gal/min, respectively, and are not near fractures. Well LMEX-2 has a well yield of only 69 gal/min even though the well is near surface fractures. Hydraulic conductivity for the Woody Mountain well field ranges from 20 to about 80 (gal/d)/ft^2. WM-9 is anomalous because it has a well yield of 521 gal/min and the hydraulic conductivity was 2.33 (gal/d)/ft^2; however, the data may be suspect because pumping rates were not stable for any of the test periods. The well was pumped only at high rates, and recovery data were collected for only a short time. Hydraulic conductivity for the Lake Mary well field ranges from 0.14 to 28.8 (gal/d)/ft^2.

In other areas, well yield and hydraulic conductivity generally are less than well yield and hydraulic conductivity at the Woody Mountain and Lake Mary well fields but still correlate with nearby faults and other fractures. The wells at Forest Highland have well yields of 200 to 300 gal/min, and the hydraulic conductivity in this area ranges from 3.0 to 6.5 (gal/d)/ft^2. These wells are associated with a moderately fractured zone north and west of the Munds Park graben (pl. 2). The wells at Little America, Foxglenn, and Continental have well yields of 100 to 490 gal/min, and the hydraulic conductivity ranges from 1.84 to 6.9 (gal/d)/ft^2 (pl. 2). The yield of the Little America well is limited by well design, and the aquifer in this area may be capable of a greater yield as indicated by the hydraulic properties. These wells are in northwestward-trending grabens intersected by northeastward-striking fractures (pl. 2).

A few high-yield wells have no apparent surface-structure relation, such as the BBDP-Marijka well, which is in the northeastern part of the study area. Data from this well indicate significant secondary permeability from fracturing at depth related to horizontal bedding-plane fractures. These same features were observed in video logs of the wells at Foxglenn and Continental.

Some wells near major surface fractures have unexpectedly low yields such as Skunk Canyon and LM-9. Data from remote-sensing and surface-geophysical surveys indicated that Skunk Canyon was an optimal site for a high-yield well. Borehole data indicated many open fractures above and below the water table; however, the well yield of 150 gal/min was less than expected. A possible explanation for the low yield is a lack of connectivity of the fractures that contribute flow to the well. LM-9 is a low-yield well drilled along a northeastward-striking fracture alignment that should have had a high yield on the basis of data from previous drilling in the area. This well was located by referencing the surface structure and topography only. As a result, the open interval of the well may not be in the main fracture-flow zone at depth or may be in a low-permeability gouge zone along the structure at depth.

Many of the low-yield wells (less than 100 gal/min) have no apparent relation to surface structure. These wells generally are northeast of Flagstaff and in the area that is west of the city and east of Oak Creek Fault (pl. 2).

Data from the NAD-1 are indicative of how local structure can have a significant effect on the occurrence and movement of regional ground water. The NAD-1 responded to rainfall and runoff into adjacent fractures and sinkholes with a nearly immediate 35-foot rise in water level that declined to the previous level during the following two or three dry months (**fig. 40**).

In the Rio de Flag area, water-level changes indicate an increase in ground-water storage from the late 1980s to the mid-1990s (pl. 2). This area is heavily fractured and faulted at the surface allowing effluent along the Rio de Flag to recharge the regional aquifer. Near-continuous discharge of effluent began in the mid-1980s and continues to date. In addition, discharge along the Rio de Flag increased in the early to mid-1990s because of periods of above-normal rainfall.

POTENTIAL FOR FUTURE GROUND-WATER DEVELOPMENT

Remotely sensed data, surface-geologic mapping, and surface-geophysical methods proved to be effective methods of determining potential high permeability at the depth of the regional aquifer. Areas of the aquifer that include northward- and northwestward-trending geologic structures, particularly where the structures

intersect, have been shown to be more productive than areas of the aquifer that include other structures. Some parts of the aquifer (Continental, Foxglenn, and Doney Park areas) were shown to have significant horizontal and bedding-plane fractures that also result in higher permeabilities and greater aquifer productivity.

The east side of the Oak Creek Fault north and south of the Woody Mountain well field are areas where well yields could be similar to well yields in the Woody Mountain well field (about 300 to 750 gal/min). The Oak Creek Fault in this area is substantially fractured below the regional water table where encountered in wells. Recent geophysical surveys at the southern end of the Woody Mountain well field indicate that these trends continue in that area. Well data subsequently verified the results of the geophysical surveys. Small-diameter wells penetrating just the upper few hundred feet of the aquifer just to the south and east at the Woody Mountain well field where the Dunnam Fault and the Munds Park graben converge (**pl. 2**) consistently yield 100 to 200 gal/min.

The Lake Mary well field probably is fully developed as indicated by water-level declines over the last decade (**fig. 39**; pl. 2). Two areas of the regional aquifer near the Lake Mary well field, however, have geologic and hydrologic characteristics similar to areas of the aquifer in the Lake Mary well field. One of these areas is the lower end of Upper Lake Mary, which is bounded on the east by the Anderson Mesa Fault and to the west by the Lake Mary Fault.The other area is in Newman Canyon, which is intersected by a series of northwestward-striking faults and grabens (pl. 2).

North of the Lake Mary area near Fisher Point along Walnut Canyon, northwestward-trending grabens intersect the Anderson Mesa Fault (pl. 2). This intersection of geologic structure has substantially fractured rock in the subsurface. These structural trends continue to the north into the Foxglenn and Continental areas where test drilling has verified the extent and orientation of fractures and faults below the regional water table. Just to the west of Foxglenn is a series of parallel to intersecting northwestward-striking faults and grabens that may provide increased permeability and aquifer productivity.

Additional site-specific analysis of remotely sensed data and the collection and analysis of additional geophysical data could be used to locate other areas of potential increased permeability. Borehole logging to identify the extent, orientation, and direction of fractures, and the collection of additional aquifer-test data would provide the information necessary to continue to correlate well yields and hydraulic properties with geologic structure in the Flagstaff area.

SUMMARY AND CONCLUSIONS

In recent years, the City of Flagstaff has become more dependent on ground water from the regional aquifer. Water use in the study area increased about 30 percent from the mid-1980s to the mid-1990s, and the use of ground water has surpassed the use of surface water. In 1995, the population of Flagstaff was 58,500. Recent studies of community growth and development project a population of about 100,000 by the year 2020. Long-range resource-management plans foresee the need to secure additional dependable water supplies to meet the future demands of an increasing population and a developing commercial environment. In September 1995, the USGS, in cooperation with the City of Flagstaff, began a study to improve the understanding of the occurrence and movement of ground water and the relation between hydrogeologic characteristics and well productivity in the regional aquifer.

The study area is at the southern edge of the Colorado Plateau in northern Arizona and is underlain by unconsolidated sediments and volcanic rocks, a bedded sequence of sedimentary rocks, and plutonic and metamorphic rocks that range from Quaternary to Precambrian in age. The unconsolidated sediments occur as thin to thick discontinuous deposits on top of either the volcanic rocks or the Kaibab Formation. Both the unconsolidated sediments and the volcanic rocks can be waterbearing in small localized areas. Because of the limited areal extent of these water-bearing zones, the unconsolidated sediments and volcanic rocks yield only small amounts of water to wells. Volcanic rocks overlie either the Moenkopi or Kaibab Formations. The Moenkopi Formation is not highly fractured and acts as a confining layer where present. Where not overlain by volcanic rocks and (or) the Moenkopi Formation, the Kaibab Formation is exposed at land surface. Where fully to partly saturated and hydraulically connected to formations below, the Kaibab Formation represents the uppermost part of the regional aquifer. In other areas, perched water-bearing zones in the Kaibab Formation can be hundreds to more than 1,000 ft above the regional water table.

The Kaibab Formation overlies the Toroweap Formation and the Coconino Sandstone. The Coconino Sandstone, where fully to partly saturated in the southern half of the study area, is considered to be the principal water-bearing unit of the regional aquifer. The Coconino Sandstone overlies and intertongues with the Schnebly Hill Formation. The Schnebly Hill Formation, where present, is fully to partly saturated and hydraulically connected to the Coconino Sandstone above it and the Supai Group below it. Where the Schnebly Hill Formation is not present, the Coconino Sandstone lies unconformably on top of the Supai Group. The Supai Group is composed of the Upper, Middle, and Lower Supai Formations. The Supai Group is fully to partly saturated throughout the study area and is the bottommost geologic unit of the regional aquifer. The Supai Group overlies the Redwall Limestone, which in turn overlies the Temple Butte (Martin) Formation or the Muav Limestone where the Temple Butte Formation is not present. The Redwall Limestone, Temple Butte Formation, and (or) Muav Limestone are fully saturated and confined by the overlying Lower Supai Formation. Little is known about their hydraulic characteristics and they are not used as a water source locally. The plutonic and metamorphic rocks that underlie the study area have little or no water-bearing potential and represent the lower limit of ground-water flow in this part of the Colorado Plateau.

Remote sensing and geologic mapping indicate that there are many significant surface structural features that include folds, faults, grabens, joints, and other fractures that were not previously identified. These structural features were shown to have a significant effect on the occurrence and flow of ground water in the regional aquifer. Surface-geophysical and borehole surveys indicate that many of these surface-structure alignments extend deep into the regional aquifer. Combined high-resolution seismic-reflection and seismic-refraction imaging in the study area was successful in imaging details of the fracture system from the near surface to well below the regional water table. These data provide information on the dip of rock units that can be used to calculate offsets from surface-structural features before drilling. The seismic images also may be used to avoid large shallow-depth faults that interfere with drilling.

The SAR method provided information on fracture strike, porosity, and anisotropy of rock units that can be used in the same manner as the seismic-reflection and seismic-refraction methods previously described. Such methods can be used to locate potential well sites.

Borehole-geophysical data and video-log data for selected test wells also indicated that the surface-structural trends typically are present within the water-bearing zone. Borehole data in conjunction with the surface-geophysical data indicate that fracture orientation changes with depth but is in general agreement with surface-structure trends. The borehole data also identified near-horizontal to horizontal fractures and bedding-plane fractures that are not as apparent in the surface-geophysical data but are a significant component of the fracture-flow environment in the wells.

Water levels fluctuate in response to local short-term rainfall, snowmelt, local pumping and longer-term climatic variations. Water levels in a few observation wells respond abruptly to significant rainfall and runoff. These wells are near open fractures and sinkholes that direct surface water directly to the regional aquifer. In the Woody Mountain and Lake Mary well fields, data from observation wells show a seasonal response and long-term trends related to pumping. In the Woody Mountain well field, water levels in observation wells declined 100 ft or more when many of the production wells were pumped for extended periods. The average decline of water levels in the Woody Mountain well field over the last 42 years is about 35 ft. In the Lake Mary well field, water levels in some observation wells declined as much as 400 ft when production wells were pumped for extended periods. Water levels in some parts of the Lake Mary well field have declined about 100 ft in the last 34 years, and most of the decline occurred in the last 10 years. Water levels in these areas do recover to varying degrees depending on the amount and timing of precipitation and pumping by the city. Water levels in several observation wells that are measured quarterly to annually in parts of the regional aquifer that have minimal or no structural deformation had no apparent response to short-term climate variability or pumping.

Well yields vary considerably within the study area; some of this variability is due to the quality and duration of well tests. In most cases, these well tests are done to verify the minimally acceptable yield rather than to determine actual hydraulic properties of the aquifer near the well. Most high-yield wells are near

fractures or other surface-structural features and show a bias for northwestward-trending structure and secondary north-northeastward-trending structure. The most productive wells are near or on structural features connected with grabens that trend northwestward through the area. In several high-yield wells, there is significant horizontal to near-horizontal fracturing in addition to near-vertical fractures that substantially improve the well yield. Low-yield wells have no significant relation to surface geologic structure. Some of the variability in wells that yield less than 100 gal/min probably is related to horizontal and vertical lithologic changes within the water-bearing zone. A few wells drilled near structural features had low yields. Most of these wells were located without the benefit of surface-geophysical data to identify a potential target zone. As a result, these wells which are near a structural trend at land surface, may be completed some distance from the structural trend at depth.

Although hydraulic properties of wells in the study area are variable, they do exhibit an apparent relation to geologic structure. Transmissivity, hydraulic conductivity, storage coefficient, and (or) specific yield were estimated or determined from available well and aquifer tests of 43 regional-aquifer wells in the study area. Many of the remaining well tests were not usable for determining hydraulic properties because the pumping rate of the well was too low or the duration of the test was too short to provide meaningful information. Estimated transmissivity values range from 100 to 35,000 (gal/d)/ft. Hydraulic-conductivity values calculated from transmissivity values range from 0.14 to 81.5 (gal/d)/ft^2. Some of the variability in specific-capacity and aquifer-test results appear to be related to the design and development of the wells and to the quality and duration of the well or aquifer tests. Physical factors affecting well yield and aquifer performance are grain size and type and degree of cementation of the rock units, type and degree of fracturing of the formation, and interconnectivity of fractures. Although the population of data is small and there is a fair amount of variability, there appears to be a fair relation between well yield, hydraulic properties, and surface-geologic structure. Favorable hydraulic properties are associated with northwestward-trending surface structure. A weaker relation of favorable hydraulic properties exists with the north-northeastward-trending structure.

Storage coefficients and specific yields of the regional aquifer were determined for 11 sites in the study area, and porosity was determined for three sites. Storage coefficients for three wells drilled in the confined part of the regional aquifer varied from 0.00023 to 0.05. Specific yield for eight wells in the unconfined part of the regional aquifer ranged from 0.0002 to 0.14 and averaged 0.077. Although limited, the broad range of storage characteristics suggests a structural influence to the primary water-bearing characteristics. On the basis of the average specific yield and the average saturated thickness, the water in storage in the regional aquifer in the study area is estimated to be 4,800,000 acre-ft. Porosity, which was estimated from well logs, ranges from 4 to 50 percent.

On the basis of the average annual precipitation and estimates of infiltration, the estimated annual average recharge is 290,000 acre-ft. Fractures and sinkholes probably provide direct conduits for precipitation and surface flow to the regional aquifer. A mound of ground water had developed in the Rio de Flag area as a result of localized recharge from consistently available effluent. As of 1998, discharge from wells in the regional aquifer was about 7,500 acre-ft/yr. This value is 2.6 percent of the estimated annual recharge to the aquifer and 0.16 percent of the estimated amount of water in storage.

Common-ion data for water from the regional aquifer generally plot into one of two groups—the Woody Mountain group or the Lake Mary group. The Woody Mountain group is characterized by water that has recharged through the volcanic rocks and has higher concentrations of SiO_2. The Lake Mary group is characterized by water that has recharged through the limestone sediments and has higher concentrations of Ca and Mg.

Data for $^{18}O/^{16}O$ and $^{2}H/^{1}H$ indicate a common recharge source with limited evaporation occurring for most of the recharge waters. Isotope data from a few wells indicates recharge is occurring from surface water such as Lake Mary and the Rio de Flag. Estimated ^{14}C ground-water ages coincide with ground-water movement from the Lake Mary area northwest to the Woody Mountain area and northeast toward Wupatki. Sites with measurable ^{3}H and older estimated ^{14}C ages indicate mixing of older and younger ground water in the aquifer. These data corroborate the interpreted relation of ground-water flow and geologic structure in the study area.

Average flow velocities from hydraulic conductivity, hydraulic gradient, and effective porosity data indicate ground water takes about 1,000 years to flow from the main recharge area to the south of Lake Mary downgradient toward the Woody Mountain area. Ground water flows faster from Lake Mary to the Continental area parallel to regional structures such as the Anderson Mesa Fault. But flow from Woody Mountain to the Continental area appears to be slowed by local structural features that cross the flow path at near perpendicular angles. Velocities of ground water flowing north out of the area result in travel times that are consistent with carbon ages of ground water along the flow path.

Remotely sensed data, surface-geologic mapping, and surface-geophysical methods proved to be effective methods of determining potential high permeability at the depths of the regional aquifer without the need for exploratory drilling. On the basis of information gathered from these methods, three of four wells located by the City of Flagstaff were capable of long-term yields of about 500 gal/min. The fourth well yielded about 200 gal/min. The relatively low yield may be due to a lack of interconnectivity of fractures. Seven areas of potential high well yield were identified on the basis of information gathered in this study.

Some additional work could be useful in developing a more complete understanding of the fracture-flow system in the regional aquifer in the Flagstaff area. The collection of specific-capacity and aquifer-test data from new wells that are drilled and developed in the area would provide information that will refine the correlation of well yield and hydraulic properties with geologic structure. Sufficient borehole logging to identify the extent, orientation, and direction of fractures would be useful to continue development of the fracture-flow relation. These data also will provide useful information in the proper design and construction of high-yield wells. Additional observation wells in outlying areas would provide water-level data necessary to determine local variations in ground-water flow direction. Additional temporal analysis of selected isotopes in ground water can be used to refine the relation of water chemistry to geologic structure and ground-water flow developed in this study. As the base of data develops and expands, future attempts at more accurate water budgets will provide more detailed information on the effects of water use on the available ground-water resources. A mathematical model of the fracture-flow system in the regional aquifer may be needed to predict future responses of the ground-water system to natural and anthropogenic stresses.

SELECTED REFERENCES

Akers, J.P., 1962, Relation of faulting to the occurrence of ground water in the Flagstaff area, Arizona, *in* Geological Survey Research 1962: U.S. Geological Survey Professional Paper 450–B, p. 97–100.

Akers, J.P., Cooley, M.E., and Dennis, P.E., 1964, Synopsis of ground-water conditions on the San Francisco Plateau near Flagstaff, Coconino County, Arizona: U.S. Geological Survey open-file report, 30 p.

Aldrich, L.T., Wetherill, G.W., Tilton, G.R., and Davis, G.L., 1956, The half life of rubidium-87: Physics Review, v. 104, p. 1045–1047.

Anning, D.W., and Duet, N.R., 1994, Summary of ground-water conditions in Arizona, 1987–90: U.S. Geological Survey Open-File Report 94–476, 1 sheet.

Appel, C.L., and Bills, D.J., 1980, Map showing ground-water conditions in the Canyon Diablo area, Coconino and Navajo Counties, Arizona–1979: U.S. Geological Survey Open-File Report 80–747, 1 sheet.

———1981, Map showing ground-water conditions in the San Francisco Peaks area, Coconino County, Arizona–1979: U.S. Geological Survey Open-File Report 81–914, 2 sheets.

Barnes, C.W., 1989, Early Proterozoic rocks on Grand Canyon, Arizona, *in* Elston, D.P., Billingsley, G.H., and Young, R.A., eds., Geology of Grand Canyon, northern Arizona: Washington, D.C., American Geophysical Union, 28th International Geological Congress Field Trip Guidebook T115/315, p. 90–93.

Beres, M., and Haeni, F.P., 1991, Application of ground-penetrating radar methods in hydrogeologic studies: Ground Water, v. 29, no. 3, p. 375–386.

Beus, S.S., 1973, Devonian stratigraphy and paleo-geography along the western Mogollon Rim, Arizona: Flagstaff Museum of Northern Arizona Bulletin 49, 36 p.

Beus, S.S., and Billingsley, G.H., 1989, Paleozoic strata of the Grand Canyon, Arizona, *in* Elston, D.P., Billingsley, G.H., and Young, R.A., eds., Geology of Grand Canyon, northern Arizona: Washington, D.C., American Geophysical Union, 28th International Geological Congress Field Trip Guidebook T115/315, p. 122–127.

Billingsley, G.H., Breed, W.J., and Beasley, D., 1980, Geologic cross section along Interstate 40—Kingman to Flagstaff, Arizona: Chandler, Arizona, Pagosa Press, Petrified Forest Museum Association in cooperation with Museum of Northern Arizona map sheet.

Blakey, R.C., 1979, Stratigraphy of the Supai Group (Pennsylvanian-Permian), Mogollon Rim, Arizona, *in* Beus, S.S., and Rawson, R.R., eds., Carboniferous stratigraphy in the Grand Canyon Country, northern Arizona and southern Nevada: Falls Church, Virginia, American Geological Institute Guidebook Series No. 2, Ninth International Congress of Carboniferous Stratigraphy and Geology, p. 89–104.

———1990, Stratigraphy and geologic history of Pennsylvanian and Permian rocks, Mogollon Rim region, central Arizona and vicinity: Geological Society of America Bulletin, v. 102, no. 9, p. 1189–1217.

Blakey, R.C., and Knepp, R., 1989, Pennsylvanian and Permian geology of Arizona, *in* Jenney, J.P., and Reynolds, S.J., eds., Geologic Evolution of Arizona: Arizona Geological Society Digest 17, p. 313–347.

Blakely, R.J., and Simpson, R.W., 1986, Approximating edges of source bodies from magnetic or gravity anomalies: Geophysics, v. 51, no. 7, p. 1494–1498.

———1987, Approximating edges of source bodies from magnetic or gravity anomalies—Discussion and reply by author: Geophysics, v. 54, no. 9, p. 1214.

Blee, J.W.H., 1988, Determination of evaporation and seepage losses, upper Lake Mary near Flagstaff, Arizona: U.S. Geological Survey Water-Resources Investigations Report 87–4250, 39 p.

Catchings, R.D., Jaasma, N.M., Goldman, M.R., and Rymer, M.J., 1997, Seismic images beneath the Continental (Bottomless Pits) area, Flagstaff, Arizona: U.S. Geological Survey Open-File Report 97–76, 29 p.

Chavez, P.S., Jr., 1984, U.S. Geological Survey mini-image processing system (MIPS): U.S. Geological Survey Open-File Report 84–880, 12 p.

———1992, Comparison of spatial variability in visible and near-infrared spectral images: Photogrammetric Engineering and Remote Sensing, v. 58, no. 7, p. 957–964.

Chavez, P.S., Jr., and Bowell, J., 1988, Comparison of the spectral information content of Landsat thematic mapper and SPOT for three different sites in the Phoenix, Arizona region: Photogrammetric Engineering and Remote Sensing, v. 54, no. 12, p. 1699–1708.

Chavez, P.S., Jr., Velasco, M., and Sides, S.C., 1996, Ground-water resources evaluation, Flagstaff, Arizona—Remote-sensing component: U.S. Geological Survey Open-File Report 96–739, 27 p.

Chavez, P.S., Jr., Velasco, M., Soltesz, D.L., and Sides, S.C., 1997, Terrestial remote sensing: U.S. Geological Survey Open-File Report 96–739, available on World Wide Web at URL http://terraweb.wr.usgs.gov/TRS/about.html, accessed February 12, 1998.

City of Flagstaff, 1996, Flagstaff 2020—A community profile: Flagstaff, Arizona, City of Flagstaff report, 106 p.

Cooley, M.E., 1960a, Physiographic map of the San Francisco Plateau—Lower Little Colorado River area, Arizona: Tucson, University of Arizona, Geochronology Laboratory report.

———1960b, Structural sections of the San Francisco Plateau—Lower Little Colorado River area, Arizona, showing the relationship of the volcanic rocks of the San Francisco volcanic field with the erosion surfaces along the Little Colorado River: Tucson, University of Arizona, Geochronology Laboratory report.

———1963, Hydrology of the Plateau upland province, *in* White, N.D., and others, Annual report on ground water in Arizona, spring 1962 to spring 1963: Phoenix, Arizona State Land Department Water-Resources Report 15, p. 27–38.

Cooley, M.E., Harshbarger, J.W., Akers, J.P., and Hardt, W.F., 1969, Regional hydrogeology of the Navajo and Hopi Indian Reservations, Arizona, New Mexico, and Utah, *with a section on Vegetation* by O.N. Hicks: U.S. Geological Survey Professional Paper 521–A, 61 p.

Cooper, H.H., Jr., and Jacob, C.E., 1946, A generalized graphical method for evaluating formation constants and summarizing well-field history: Washington, D.C., American Geophysical Union Transactions, v. 27, no. 4, p. 526–534.

Cordell, Lindrith, 1979, Gravimetric expression of graben faulting in Santa Fe Country and the Espanola Basin, New Mexico, *in* Ingersoll, R.V., ed., Santa Fe Country: Santa Fe, New Mexico Geological Society Guidebook, 30th Field Conference, October 4–6, 1979, p. 59–64.

Cosner, O.J., 1962, Ground water in the Wupatki and Sunset Crater National Monuments, Coconino County, Arizona: U.S. Geological Survey Water-Supply Paper 1475–J, p. 357–374.

Craig, H., 1961, Standard for reporting concentrations of deuterium + oxygen-18 in natural waters: Science, v. 133, no. 3467, p. 1833–1834.

Damon, P.E., Shafiqullah, Mohammed, and Leventhal, J.S., 1974, K-Ar chronology for the San Francisco volcanic field and rate of erosion of the Little Colorado River, *in* Karlstom, T.N.V., Swann, G.A., and Eastwood, R.L., eds., Part 1 of Geology of Northern Arizona: Geological Society of America Guidebook for Rocky Mountain Section Meeting, Flagstaff, Arizona, v. 6, no. 5, p. 221–235.

Dansgaard, W., 1964, Stable isotopes in precipitation: Tellus, v. 16, no. 4, p. 436–469.

Darton, N.H., 1910, A reconnaissance of parts of northwestern New Mexico and northern Arizona: U.S. Geological Survey Bulletin 435, 88 p.

Davis, G.H., 1978, Monoclinal fold patterns of the Colorado Plateau, *in* Matthews, V., III, ed., Laramide Folding Associated with Basement Block Faulting in the Western United States: Geological Society of America Memoir 151, p. 215–233.

Davis, S.N., 1969, Porosity and permeability of natural materials, *in* DeWiest, R.J.M., ed., Flow Through Porous Media: New York, Academic Press, p. 54–90.

Davis, W.M., 1901, An excursion to the Grand Canyon of the Colorado: Harvard College, Museum of Comparative Zoology Bulletin, v. 38, p. 107–201.

Davis, J.L, and Annan, A.P., 1989, Ground-penetrating radar for high-resolution mapping of soil and rock stratigraphy: Geophysical Prospecting, v. 37, no. 5, p. 531–551.

Deng, S., Zhengrong, Z., and Wang, H., 1994, The application of ground-penetrating radar to detection of shallow faults and caves: Ontario, Canada, University of Waterloo, Waterloo Centre for Ground-Water Research, Fifth International Conference on Ground-Penetrating Radar Proceedings, Kitchener, Ontario, Canada, v. 3, p. 115–120.

Driscoll, F.G., 1986, Groundwater and wells, second edition: St. Paul, Minnesota, Johnson Division, 1108 p.

Doe, T.W., Long, J.C.S., Endo, H.K., and Wilson, C.R., 1982, Approaches to evaluating the permeability and porosity of fractured rock masses, *in* Goodman, R.E., and Hueze, F.E., eds., Issues in Rock Mechanics: New York, American Institute of Mining, Metallurgical, and Petroleum Engineers, Inc., Proceedings of the Twenty-Third Symposium on Rock Mechanics, Berkeley, California, August 25–27, 1982, p. 30–38.

Dunn, T., and Leopold, L.B., 1978, Water in environmental planning: San Francisco, California, W.H. Freeman and Company, 818 p.

Duren Engineering, Inc., 1983, Yield analysis for the Lake Mary and Woody Mountain well fields, City of Flagstaff, Arizona: Duren Engineering, Inc., unpublished report, 100 p.

Dutton, C.E., 1882, The Tertiary history of the Grand Canyon district with atlas: U.S. Geological Survey Monograph 2, 264 p.; atlas, 23 sheets.

Elston, D.P., 1989, Middle and Late Proterozoic Grand Canyon Supergroup, Arizona, *in* Elston, D.P., Billingsley, G.H., and Young, R.A., eds., Geology of Grand Canyon, northern Arizona: Washington, D.C., American Geophysical Union, 28th International Geological Congress Field Trip Guidebook T115/315, p. 94–105.

Elston, D.P., and DiPaolo, W.D., 1979, Pennsylvanian-Permian stratigraphy of the Sedona area and environs, central and northern Arizona, *in* Baars, D.L., ed., Permianland: Santa Fe, New Mexico, Four Corners Geological Society, Ninth Field Conference, A Field Symposium—Guidebook of the Four Corners Geological Society, September 27–30, 1979, p. 131–141.

Elston, D.P., and Scott, G.R., 1976, Unconformity at the Cardenas-Nankoweap contact (Precambrian), Grand Canyon Supai Group, northern Arizona: Geological Society of America Bulletin 87, no. 12, p. 1763–1772.

Faure, Gunter, 1977, Principles of isotope geology: New York, John Wiley and Sons, p. 97–137.

Fenneman, N.M., and Johnson, D.W., 1946, Physical divisions of the United States: U.S. Geological Survey, scale, 1:1,000,000, 1 sheet.

Feth, J.H., 1953, A geologic and geophysical reconnaissance of the Doney Park-Black Bill Park area, with reference to ground water, *with a section on Geophysics* by C.B. Yost, Jr.: U.S. Geological Survey Circular 233, 11 p.

Feth, J.H., and Hem, J.D., 1963, Reconnaissance of headwater springs in the Gila River drainage basin, Arizona: U.S. Geological Survey Water-Supply Paper 1619–H, 54 p.

Fetter, C.W., 1980, Applied hydrogeology: Columbus, Ohio, Charles E. Merrill Publishing Company, 488 p.

Founts, J.C., and Garnier, J.M., 1979, Determination of the initial ^{14}C activity of the carbon—A review of the existing models and a new approach: Washington, D.C., American Geophysical Union, Water Resources Research, v. 15, no. 2, p. 399–413.

Freeze, R.A., and Cherry, J.A., 1979, Groundwater: Englewood Cliffs, New Jersey, Prentice-Hall, 604 p.

Gilbert, G.K., 1875, Report on the geology of portions of Nevada, Utah, California, and Arizona, examined in the years 1871 and 1872, *in* U.S. Army Corps of Engineers, Report upon geographical and geological explorations and surveys west of the 100th Meridian, v. 3, Geology: Washington, D.C., U.S. Government Printing Office, p. 17–187.

Grauch, V.J.S., and Cordell, Lindrith, 1987, Limitations of determining density or magnetic boundaries from the horizontal gradient of gravity or pseudogravity data (short note): Geophysics, v. 52, no. 1, p. 118–121.

Habberjam, G.M., 1972, The effects of anisotropy in square-array resistivity measurements: Geophysical Prospecting, v. 20, no. 2, p. 249–266.

———1975, Apparent resistivity, anisotropy, and strike measurements: Geophysical Prospecting, v. 23, no. 2, p. 211–247.

———1979, Apparent resistivity observations and the use of square-array techniques: Berlin, Germany, Bebruder Borntraeger, Geoexploration Monograph Series 1, no. 9, 152 p.

Habberjam, G.M., and Watkins, G.E., 1967, The use of a square configuration in resistivity prospecting: Geophysical Prospecting, v. 15, no. 3, p. 445–467.

Hantush, M.S., 1962, Aquifer test on partially penetrating wells: American Society of Civil Engineering Transcripts, v. 127, part I, p. 268–283.

Harshbarger and Associates, 1976, Lake Mary aquifer report, City of Flagstaff, Arizona: Tucson, Arizona, Harshbarger and Associates duplicated report, 89 p.

———1977, Hydrogeological and geophysical report on the Lake Mary area, City of Flagstaff, Arizona: Tucson, Arizona, Harshbarger and Associates duplicated report, 74 p.

Harshbarger and Associates, and John Carollo Engineers, 1972, Water resources report, City of Flagstaff, Arizona: Tucson, Arizona, Harshbarger and Associates, and John Carollo Engineers duplicated report, 124 p.

———1973, Woody Mountain aquifer report, City of Flagstaff, Arizona: Tucson, Arizona, Harshbarger and Associates, and John Carollo Engineers duplicated report, 96 p.

———1974, Inner Basin aquifer report, City of Flagstaff, Arizona: Tucson, Arizona, Harshbarger and Associates, and John Carollo Engineers duplicated report, 85 p.

Hearn, P.P., Steinkampf, W.C., Bortelson, G.C., and Drost, B.W., 1985, Geochemical controls on dissolved sodium in basalt aquifers of the Columbia Plateau, Washington: U.S. Geological Survey Water-Resources Investigations Report 84–4304, 38 p.

Hem, J.D., 1985, Study and interpretation of the chemical characteristics of natural waters, 3rd ed.: U.S. Geological Survey Water-Supply Paper 2254, 263 p.

Hodgson, R.A., 1961, Reconnaissance of jointing in Bright Angel area, Grand Canyon, Arizona: American Association Petroleum Geologists Bulletin, v. 45, no. 1, p. 95–97.

Holm, R.F., and Cloud, R.A., 1990, Regional significance of recurrent faulting and intracanyon volcanism at Oak Creek Canyon, southern Colorado Plateau, Arizona: Geology, v. 18, no. 10, p. 1014–1017

Huntoon, P.W., 1974, Synopsis of Laramide and post-Laramide structural geology of the eastern Grand Canyon, Arizona, *in* Karlstrom, T.N.V., Swann, G.A., and Eastwood, R.L., eds., Geology of Northern Arizona, *with Notes on Archaeology and Paleoclimate—Regional Studies*: Geological Society of America, Rocky Mountain Section Meeting, Flagstaff, Arizona, part 1, p. 317–335.

———1989, Phanerozoic tectonism, Grand Canyon, Arizona, *in* Elston, D.P., Billingsley, G.H., and Young, R.A., eds., Geology of Grand Canyon, northern Arizona: Washington, D.C., American Geophysical Union, 28th International Geological Congress Field Trip Guidebook T115/315, p. 76–89.

International Atomic Energy Agency, 1969, Environmental isotope data—World survey of isotope concentration in precipitation, 1953–1963: Vienna, Austria, International Atomic Energy Agency, Technical Report 165, v. 1.

Jacob, C.E., 1950, Flow of ground water, *in* Rouse, Hunter, ed., Engineering Hydraulics: New York, John Wiley and Sons, Proceedings of the Fourth Hydraulics Conference, Iowa Institute of Hydraulic Research, June 12–15, 1949, chap. 4, p. 321–386.

Jaasma, N.M., Catchings, R.D., Goldman, M.R., and Rymer, M.J., 1997, Seismic imaging in the Skunk Canyon and Foxglenn areas of Flagstaff, Arizona, U.S. Geological Survey Open-File Report 97–147, 48 p.

Kaehler, C.A., and Hsieh, P.A., 1991, Hydraulic properties of a fractured-rock aquifer, Lee Valley, San Diego County, California: U.S. Geological Survey Open-File Report 90–592, 94 p.

Karlstrom, T.N.V., Swann, G.A., and Eastwood, R.L., eds., 1974, Geology of Northern Arizona *with Notes on Archaeology And Paleoclimate—Regional Studies*: Geological Society of America Rocky Mountain Section Meeting, Flagstaff, Arizona, part 1, 407 p.

——— 1974, Geology of Northern Arizona *with Notes On Archaeology And Paleoclimate—Area Studies And*

Field Guides: Geological Society of America Rocky Mountain Section Meeting, Flagstaff, Arizona, part 2, 398 p.

Keller, G.V., 1989, Electrical properties, *in* Carmichael, R.S., ed., Practical Handbook of Physical Properties of Rocks and Minerals: Boca Raton, Florida, CRC Press, section V, p. 359–427.

Keller, G.V., and Frischknect, F.C., 1966, Electrical methods in geophysical prospecting: London, Great Britain, Pergamon Press, 519 p.

Lane, J.W., Jr., Haeni, F.P., and Watson, W.M., 1995, Use of a square-array direct-current resistivity method to detect fractures in crystalline bedrock in New Hampshire: Groundwater, v. 33, no. 3, p. 476–485.

Levings, G.W., 1980, Water resources in the Sedona area, Yavapai and Coconino Counties, Arizona: Phoenix, Arizona Water Commission Bulletin 11, 37 p.

Lohman, S.W., 1979, Ground-water hydraulics: U.S. Geological Survey Professional Paper 708, 70 p.

McGavock, E.H., 1968, Basic ground-water data for southern Coconino County, Arizona: Phoenix, Arizona State Land Department Water-Resources Report 33, 48 p.

McGavock, E.H., Anderson, T.W., Moosburner, Otto, and Mann, L.J., 1986, Water resources of southern Coconino County, Arizona: Phoenix, Arizona Department of Water Resources Bulletin 4, 53 p.

McKee, E.D., 1938, The environment and history of the Toroweap and Kaibab Formations of northern Arizona and southern Utah: Carnegie Institution of Washington Publication 492, 268 p.

———1954, Stratigraphy and history of the Moenkopi Formation of Triassic age: Geological Society of America Memoir 61, 133 p.

———1963, Nomenclature for lithologic subdivisions of the Mississippian Redwall Limestone, Arizona: U.S. Geological Survey Professional Paper 475–C, p. C21–C22.

———1982, The Supai Group of Grand Canyon: U.S. Geological Survey Professional Paper 1173, 504 p.

McKee, E.D., and Resser, C.E., 1945, Cambrian history of the Grand Canyon region: Carnegie Institution of Washington Publication 563, 232 p.

Manera, Incorporated, 1987, Data and results of well and aquifer tests for Forest Highlands, Flagstaff, Arizona: Manera Incorporated Technical Report, December 9, 1987, 88 p.

Mann, L.J., 1976, Ground-water resources and water use in southern Navajo County, Arizona: Phoenix, Arizona Water Commission Bulletin 10, 106 p.

Mazor, E., 1991, Applied chemical and isotopic groundwater hydrology: New York, John Wiley and Sons, 274 p.

Mears, B., 1950, Faulting in Oak Creek Canyon and a discussion of contrary bending: Plateau, v. 23, no. 2, p. 26–31.

Montgomery, Errol L., and Associates, 1992, Results of drilling, construction, and testing City of Flagstaff Lake Mary regional aquifer exploration wells and shallow aquifer monitor wells, Coconino County, Arizona: Tucson, Arizona, Errol L. Montgomery and Associates report prepared for the City of Flagstaff, 185 p.

———1993, Results of 90-day aquifer test and groundwater flow model projections for long-term groundwater yield for the Coconino-Supai aquifer Lake Mary well field, Coconino County, Arizona: Tucson, Arizona, Errol L. Montgomery and Associates report prepared for the City of Flagstaff, 123 p.

Montgomery, J.M., Consulting Engineers, Inc., 1982, Results of Redwall-Martin testing program at Lake Mary well No. 8: Flagstaff, Arizona, James M. Montgomery Consulting Engineers, Inc., report to the City of Flagstaff, Arizona Utilities Department, 10 p.

Montgomery, Watson, 1996, City of Flagstaff well completion report—Woody Mountain-10: Montgomery Watson, Project Number 528700, June 1996, 22 p.

Moore, R.B., and Wolf, E.W., 1987, Geologic map of the east part of the San Francisco volcanic field, north-central Arizona: U.S. Geological Survey Miscellaneous Field Studies Map MF–1950, scale, 1:50,000.

Moore, R.B., Wolfe, E.W., and Ulrich, G.E., 1976, Volcanic rocks of the eastern and northern parts of the San Francisco volcanic field, Arizona: Journal of Research of the U.S. Geological Survey, v. 4, no. 5, p. 549–560.

Moore, R.T., Wilson, E.D., and O'Hare, R.T., 1960, Geologic map of Coconino County, Arizona: Arizona Bureau of Mines Map M-3-2, scale 1:375,000.

National Oceanic and Atmospheric Administration, 1998, Climatological data, annual summary—Arizona, 1997: Asheville, North Carolina, U.S. Department of Commerce, National Oceanic and Atmospheric Administration, National Climatic Data Center, v. 1997, no. 13.

Noble, L.F., 1922, A section of the Paleozoic formations of the Grand Canyon at the Bass Trail, *in* Shorter Contributions to General Geology, 1922: U.S. Geological Survey Professional Paper 131–B, p. 23–73.

Nur, Amos, ed., 1982, Stanford rock physics progress report, January 1982: Stanford, California, Stanford Junior University, v. 13, 121 p.

Ohm, G.S., 1827, Die galvanische Kettle, mathematisch 1st ed.: Berlin, Germany, T.H. Reimann, 245 p.

———1969, The galvanic circuit investigated mathematically, 102 *of* Van Nostrand Science Series [translation of Ohm, G.S., 1827]: New York, Kraus, 269 p.

Owen-Joyce, S.J., and Bell, C.K., 1983, Appraisal of water resources in the upper Verde area, Yavapai and Coconino Counties, Arizona: Phoenix, Arizona Department of Water Resources Bulletin 2, 219 p.

Peterman, Z.E., Hedge, C.E., Tourtelot, H.A., 1970, Isotopic compositions of strontium in sea water throughout Phanerozoic time: Geochemica et Cosmochimica Acta, v. 34, no. 1, p. 105–120.

Pierce, H.A., 1996, Ground-water availability in the Town of Payson, Arizona—Transition zone between the Colorado Plateau and Basin and Range, Gila County, Arizona, *in* Wanted: Water for Arizona [abs.]: Phoenix, Arizona, Arizona Hydrological Society, 9th Annual Meeting, Proceedings, September 12–14, 1996, Prescott, Arizona, p. 103–105.

Pierce, H.A., and Hoffmann, J.P., 1996, Use of square-array direct-current resistivity method to detect fractures in consolidated sedimentary rocks in the Colorado Plateau near Flagstaff, Arizona [abs.]: Washington, D.C., American Geophysical Union, 1996 Fall Meeting, Supplement to EOS Transactions, v. 77, no. 46, November 12, 1996, abstract H31A-1, p. F184.

Peirce, H.W., Jones, Nile, and Rodgers, Ralph, 1977, A survey of uranium favorability of Paleozoic rocks in the Mogollon Rim and Slope region, east-central Arizona: Tucson, Arizona, Arizona Bureau of Geology and Mineral Technology Circular 19, 71 p.

Plummer, L.N., Prestemon, E.C., Parkhurst, D.L., 1991, An interactive code (NETPATH) for modeling NET geochemical reactions along a flow path: U.S. Geological Survey, Water-Resources Investigations Report 91–4078, 227 p.

Powell, J.W., 1957, The exploration of the Colorado River: Chicago, Illinois, University of Chicago Press, abridged from the first edition of 1875, 138 p.

Reynolds, S.J., 1988, Geologic map of Arizona: Tucson, Arizona Geological Survey Map M-26, scale, 1:1,000,000.

Robinson, H.H., 1913, The San Franciscan volcanic field, Arizona: U.S. Geological Survey Professional Paper 76, 213 p.

Roscoe Moss Co., 1990, Handbook of ground-water development: New York, John Wiley and Sons, 493 p.

Schlumberger, Conrad, 1920, Essais de prospection electrique du sous-sol: Academie Science Comptes Rendus, v. 170, no. 9, p. 519–521.

Sellers, W.D., Hill, R.H., and Sanderson-Rea, Margaret, eds., 1985, Arizona climate—The first hundred years: Tucson, University of Arizona Press, 143 p.

Sensors and Software, 1994, Pulse EKKO 100 user's guide, version 1.1: Sensors and Software, Inc. Technical Manual 25, 204 p.

Shoemaker, E.M., Squires, R.L., and Abrams, M.J., 1978, Bright Angel and Mesa Butte Fault systems of northern Arizona, *in* Smith, R.B., and Eaton, G.P., eds., Cenozoic tectonics and regional geophysics of the western Cordillera: Geological Society of America Memoir 152, p. 341–367.

Smiley, T.L., 1958, The geology and dating of Sunset Crater, Flagstaff, Arizona, *in* Guidebook of the Black Mesa Basin: New Mexico Geological Society 9th Field Conference, Gallup, New Mexico, October 16–18, 1958, p. 186–190.

Sorauf, J.E., and Billingsley, G.H., 1991, Members of the Toroweap and Kaibab Formations, Lower Permian, Northern Arizona, and Southwestern Utah: Rocky Mountain Association of Geologists, The Mountain Geologist, v. 28, no. 1, p. 9–24.

Taylor, R.W., 1984, The determination of joint orientation and porosity from azimuthal resistivity measurements, *in* Nielsen, D.M., and Curl, Mary, eds., Proceedings of the National Water Well Association and U.S. Environmental Protection Agency Conference on Surface and Borehole Geophysical Methods in Ground-Water Investigations: Worthington, Ohio, National Water Well Association, San Antonio, Texas, February 7–9, 1984, p. 37–49.

Taylor, R.W., and Fleming, A.H., 1988, Characterizing jointed systems by azimuthal resistivity surveys: Groundwater, v. 26, no. 4, p. 464–474.

Theis, C.V., 1935, The relation between the lowering of the piezometric surface and the rate and duration of discharge of a well using ground-water storage: Washington, D.C., American Geophysical Union Transactions., 16th Annual Meeting, part 2, p. 519–524.

Thorstenson, D.J., and Beard, L.S., 1998, Geology and fracture analysis of Camp Navajo, Arizona Army National Guard, Arizona: U.S. Geological Survey Open-File Report 98–242, 42 p.

Twenter, F.R., and Metzger, D.G., 1963, Geology and ground water in Verde Valley—The Mogollon Rim region, Arizona: U.S. Geological Survey Bulletin 1177, 132 p.

Ulrich, G.E., Billingsley, G.H., Hereford, Richard, Wolfe, E.W., Nealey, L.D., and Sutton, R.L., 1984, Map showing geology, structure, and uranium deposits of the Flagstaff 1°x2° quadrangle, Arizona: U.S. Geological Survey Miscellaneous Investigations Series Map I–1446, scale, 1:250,000.

Ulriksen, P.F., 1982, Application of impulse radar to civil engineering: Lund, Sweden, Lund University of Technology, doctoral thesis, 179 p.

U.S. Environmental Protection Agency, 1993a, National revised drinking-water regulations—Maximum contaminant levels: Washington, D.C., U.S. Environmental Protection Agency, U.S. Code of Federal Regulations, Title 40, Part 141, July 1, 1993, p. 592–732.

———1993b, National revised drinking-water regulations—Secondary contaminant levels: Washington, D.C., U.S. Environmental Protection Agency, U.S. Code of Federal Regulations, Title 40, Part 143, July 1, 1993, p. 774–777.

———1999, Current drinking-water standards: U.S. Environmental Protection Agency, Office of Ground Water and Drinking Water, URL http://www.epa.gov/safewater/mcl.html, accessed June 12, 2000.

U.S. Geological Survey, 1985, Annual summary of ground-water conditions in Arizona, spring 1983 to spring 1984: U.S. Geological Survey Open-File Report 85–410, 1 sheet.

———1993, National geophysical data grids—Gamma ray, gravity, magnetic, and topographic data for the conterminous United States: U.S. Geological Survey Digital Data Series DDS-9, CD-ROM.

Waterloo Hydrogeologic, Inc., 1999, User's manual for aquifer test—The intuitive aquifer test analysis package: Waterloo, Ontario, Canada, Waterloo Hydrogeologic, Inc., 176 p.

Weir, G.W., Ulrich, G.E., and Nealey, D.L., 1989, Geologic map of the Sedona 30°x60° quadrangle, Yavapai and Coconino Counties, Arizona: U.S. Geological Survey Miscellaneous Investigations Series Map I–1896, scale 1:100,000.

Williams, T., 1994, Three-dimensional shallow structure of Cienega Valley, California: Berkeley, California, University of California-Berkeley, masters thesis, 56 p.

Wolfe, E.W., Ulrich, G.E., Holm, R.F., Moore, R.B., and Newhall, C.G., 1987, Geologic map of the central part of the San Francisco volcanic field, north-central Arizona: U.S. Geological Survey Miscellaneous Field Studies Map MF–1959, scale, 1:50,000.

Yost and Gardner Engineers, 1961, City of Flagstaff, Arizona, 1961 water report: Flagstaff, Arizona, Yost and Gardner Engineers unpublished report to the City of Flagstaff, 32 p.

Zohdy, A.A.R., 1973, A computer program for the automatic interpretation of Schlumberger sounding curves over horizontally layered media: Springfield, Virginia, U.S. Department of Commerce, National Technical Information Service PB–232–703/AS, 25 p.

———1989, A new method for the automatic interpretation of Schlumberger and Wenner sounding curves: Geophysics, v. 54, no. 2, p. 245–253.

SUPPLEMENTAL DATA

A. Azimuthal Plots of Apparent Resisitivity from Square-Array Resistivity Data

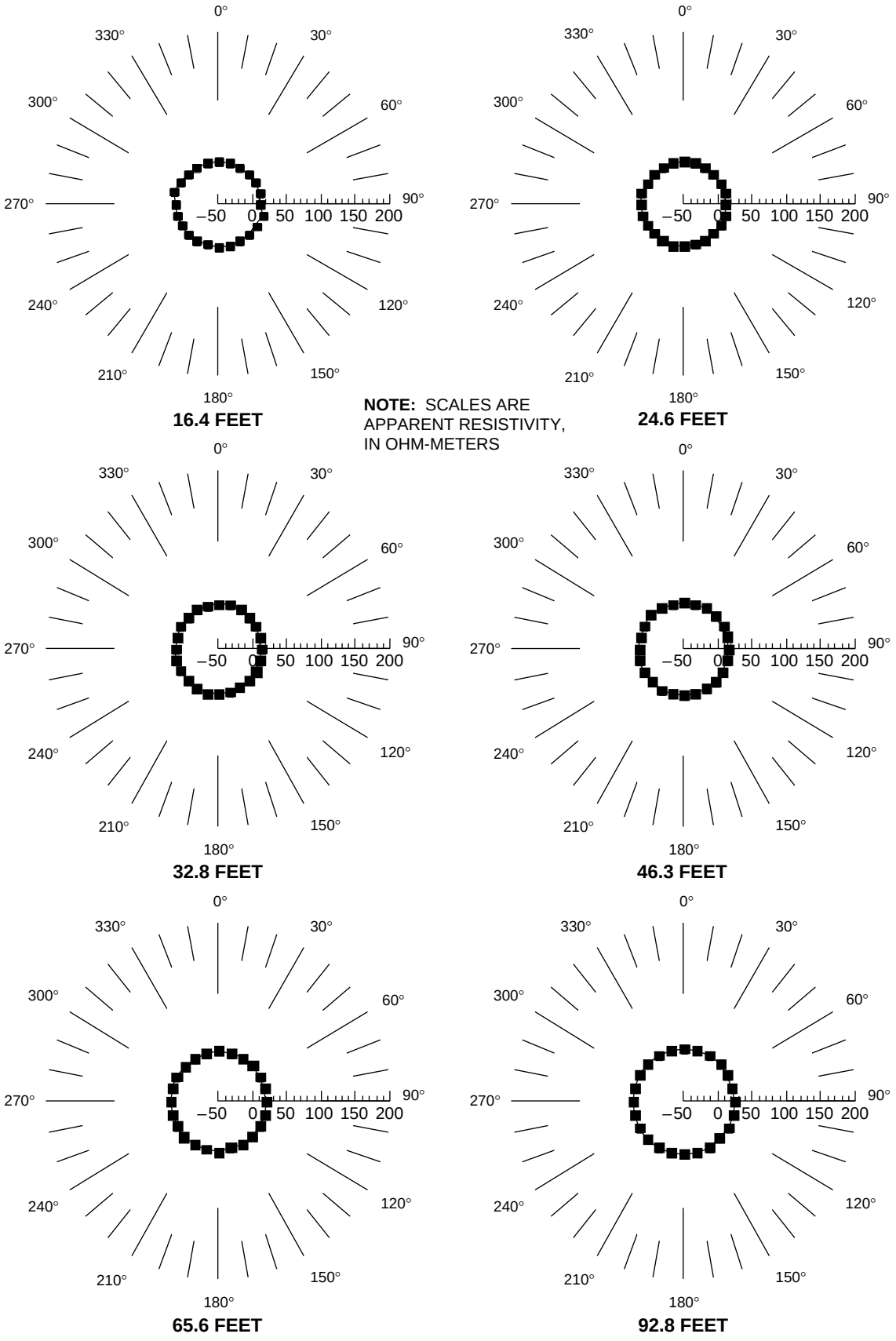

Part A. Lower Lake Mary (LLM).

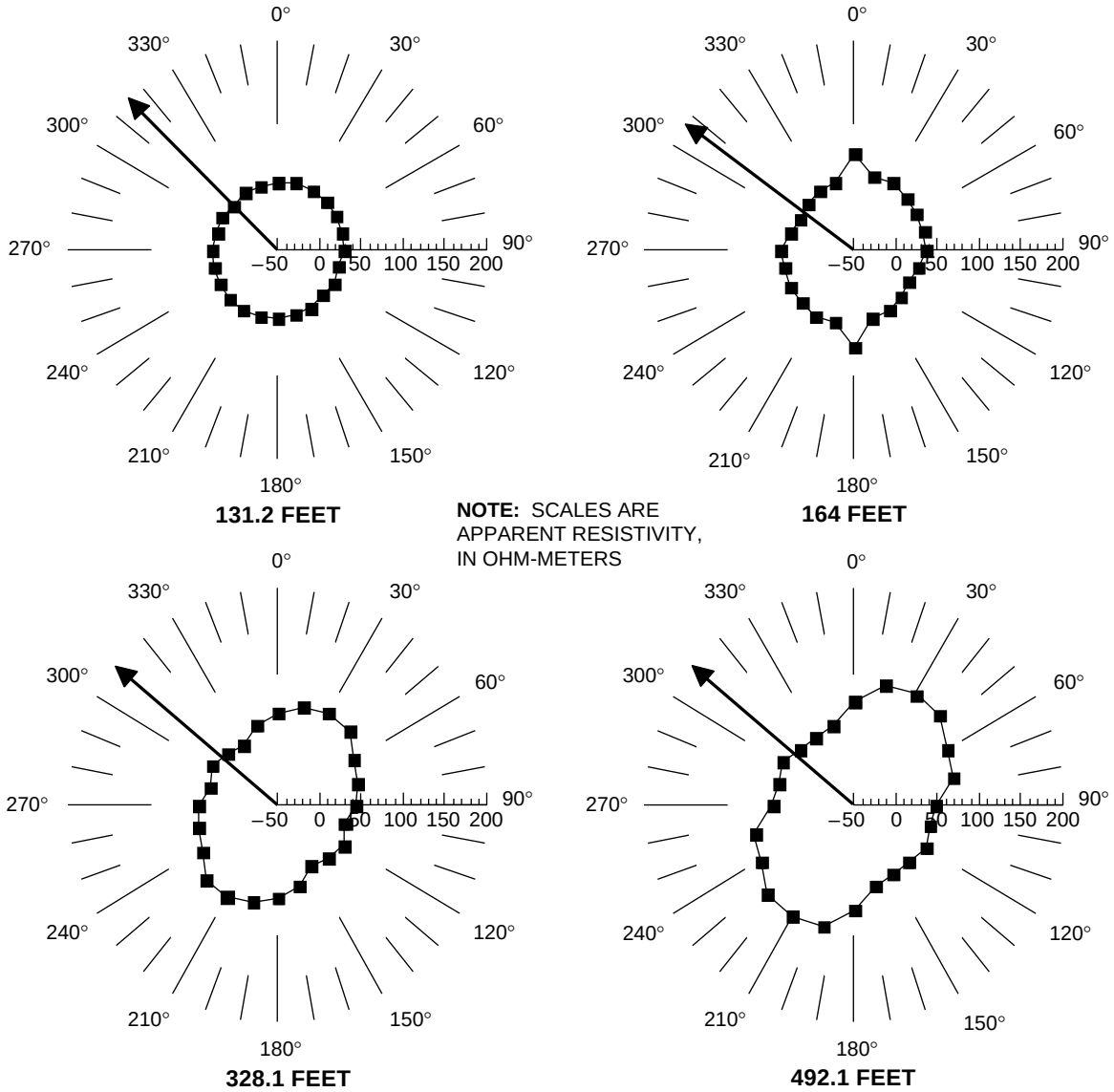

Part A. Continued. Lower Lake Mary (LLM).

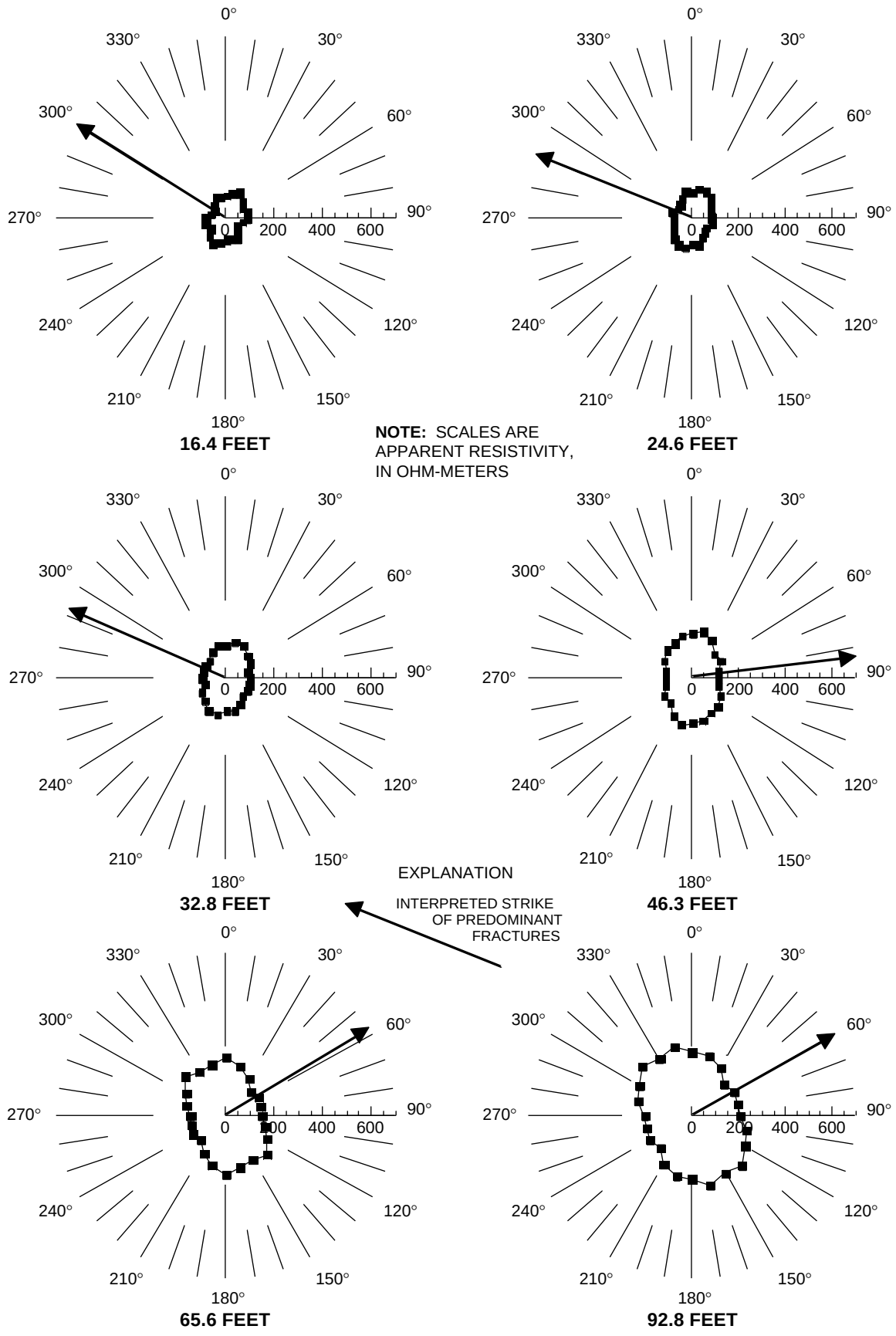

Part A. Continued. Lake Mary well 8 site (L8).

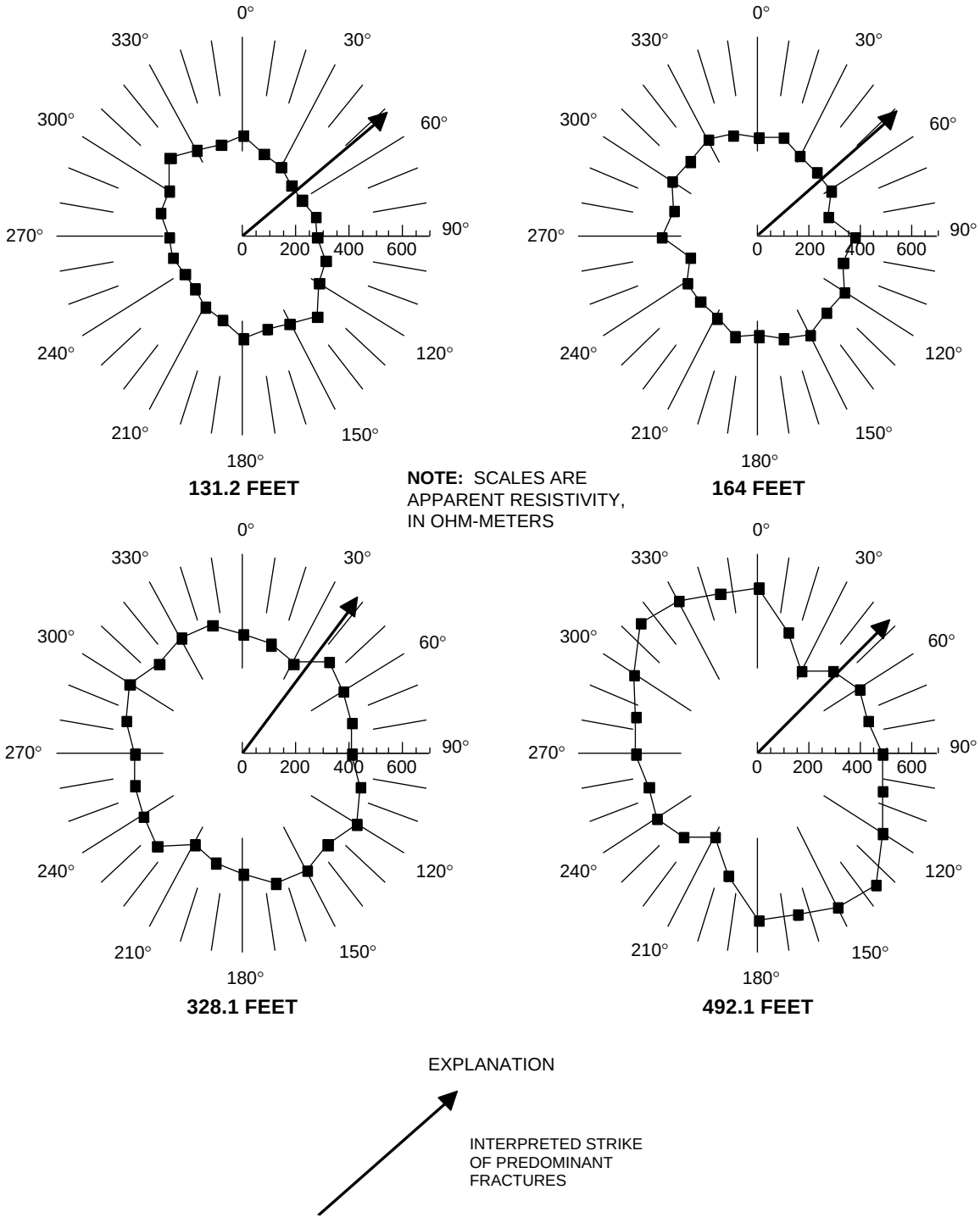

Part A. Continued. Lake Mary well 8 site (L8).

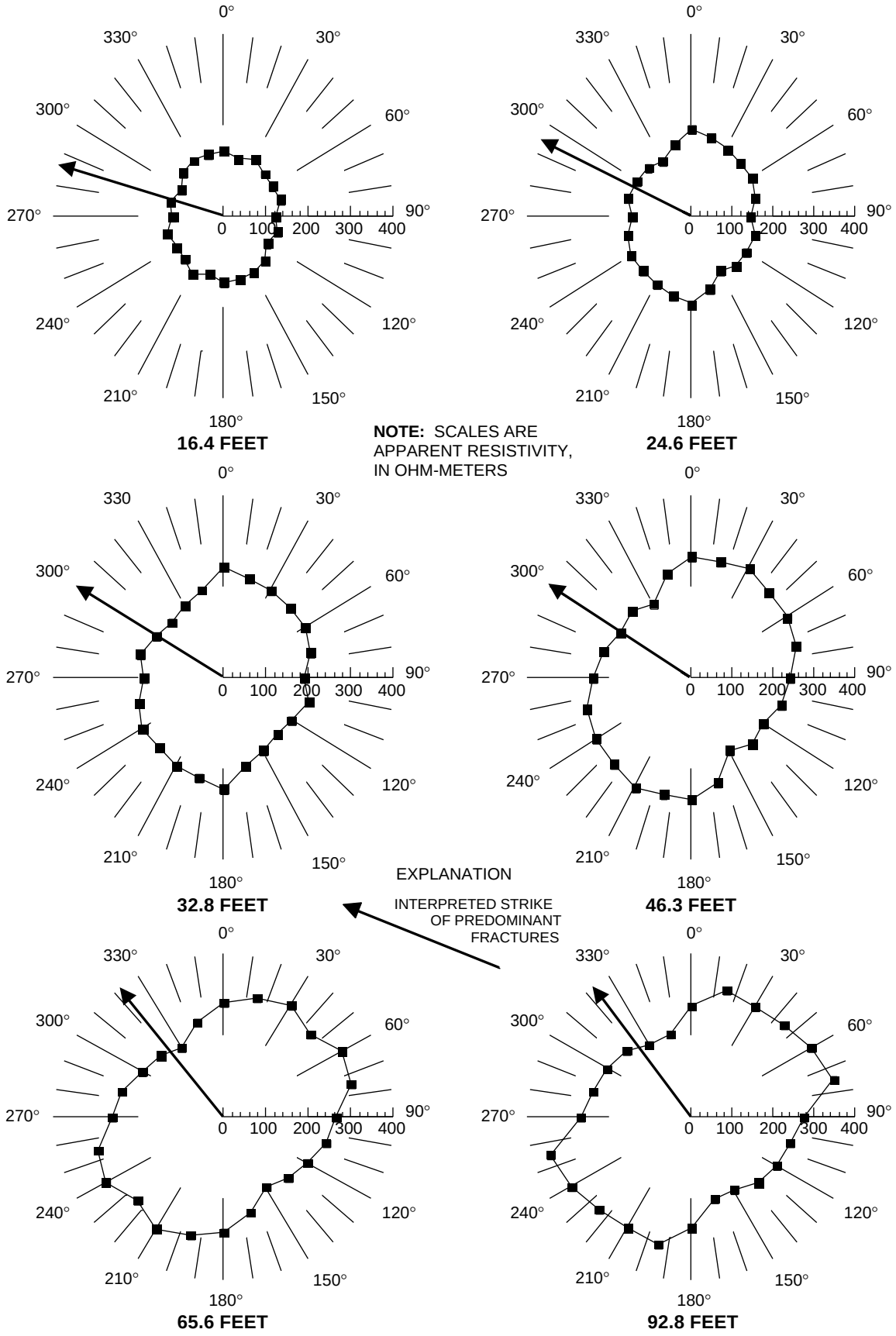

Part A. Continued. Lake Mary well 9 site (L9)

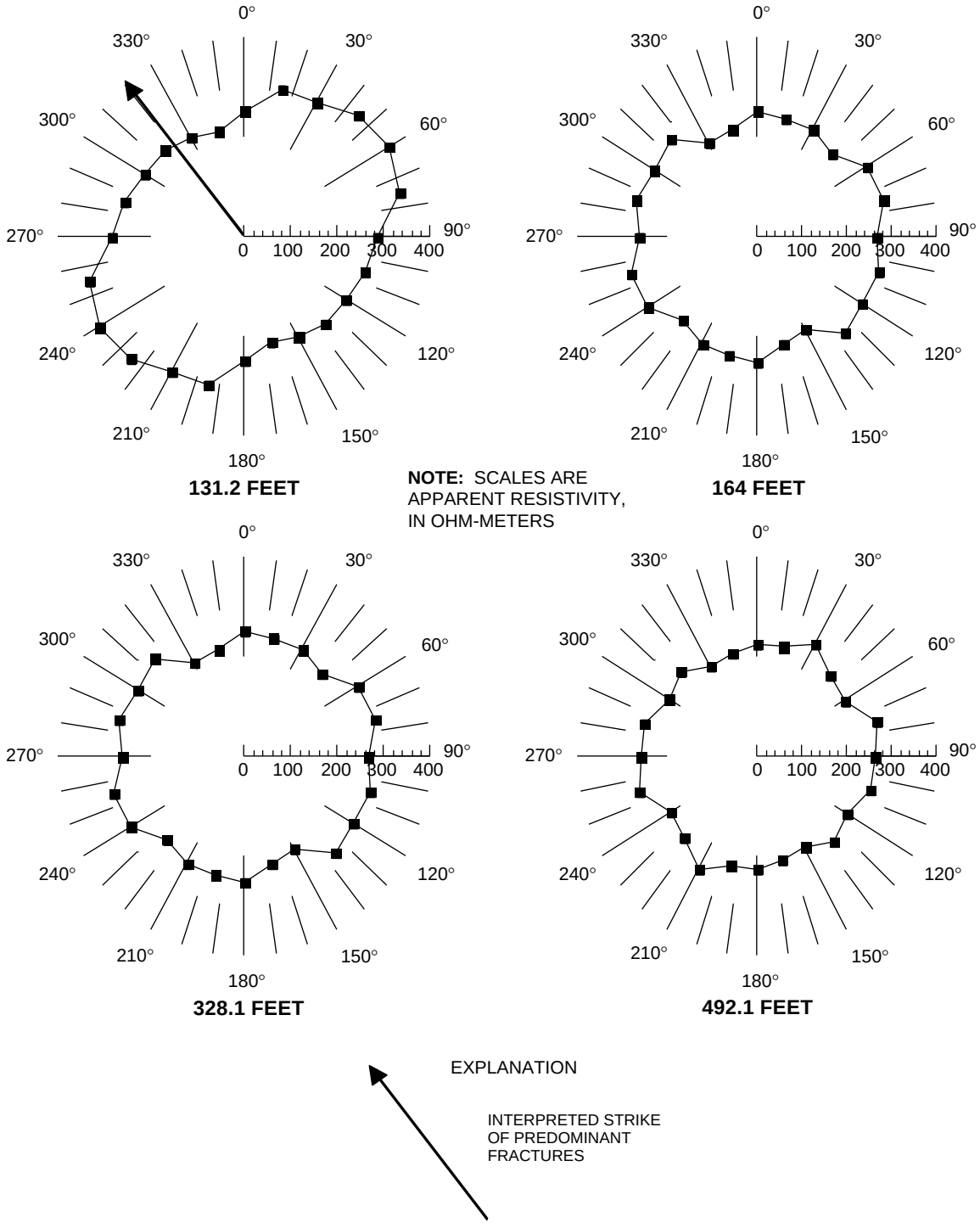

Part A. Continued. Lake Mary well 9 site (L9).

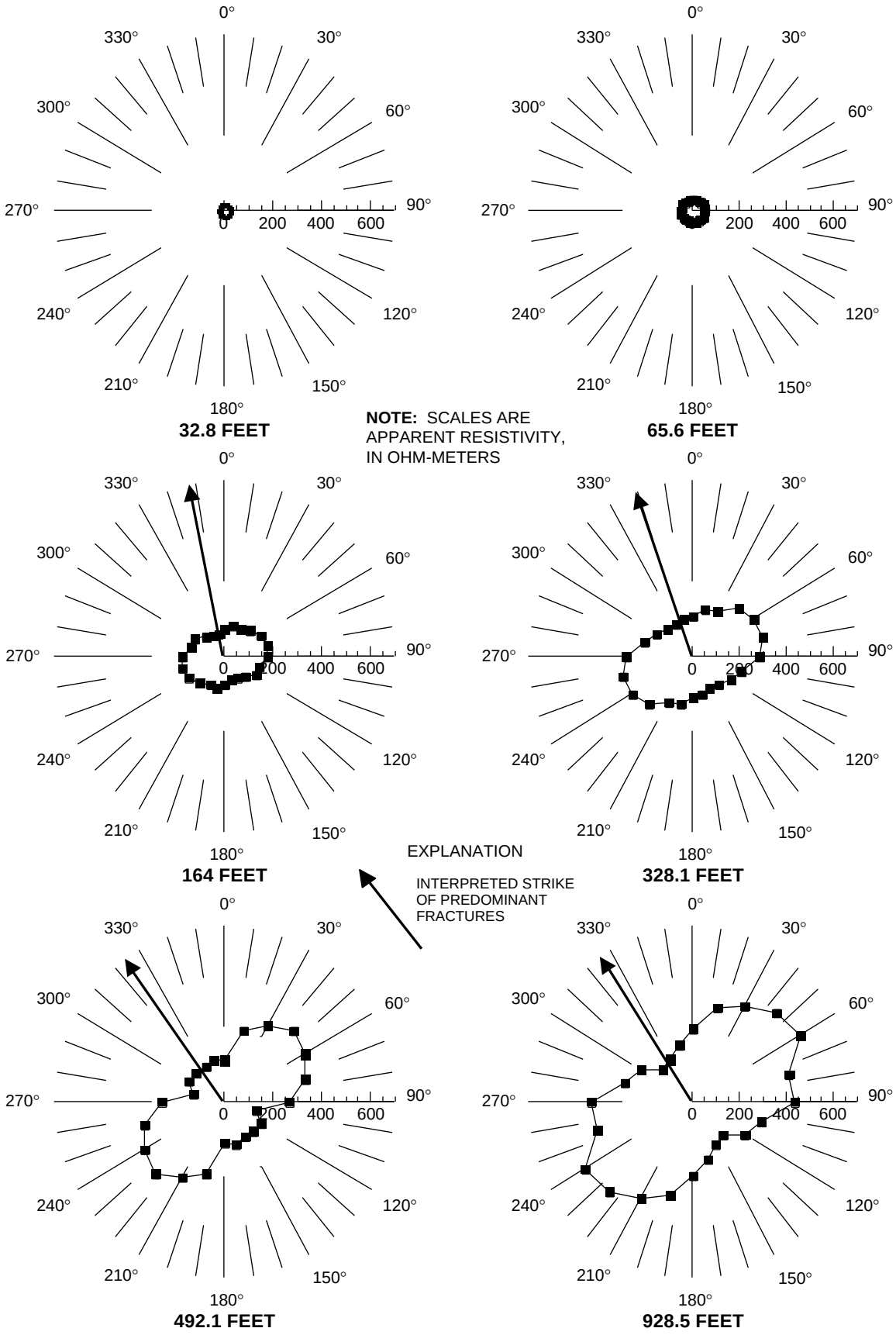

Part A. Continued. Woody Mountain at well 10 (W10).

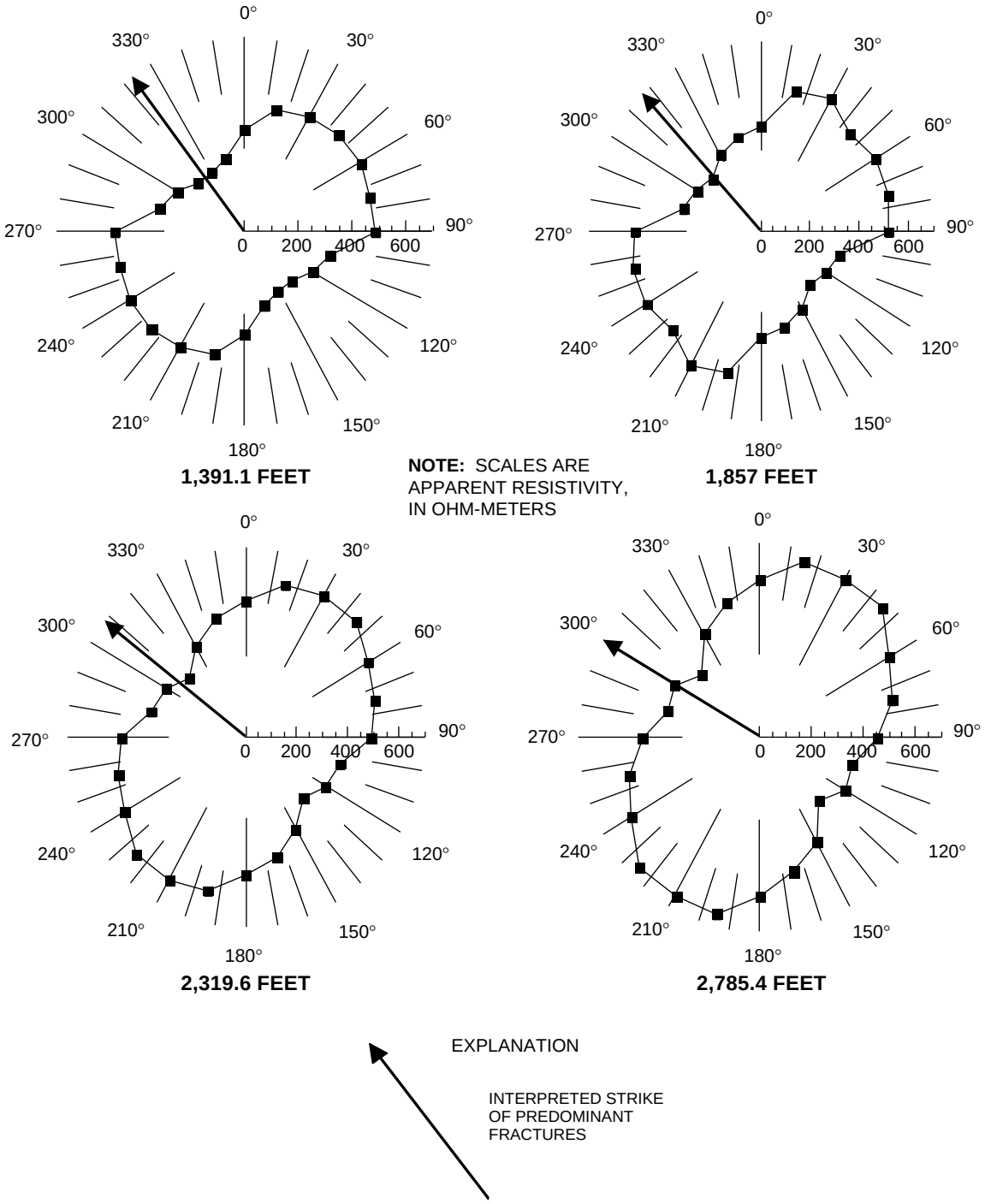

Part A. Continued. Woody Mountain at well 10 (W10).

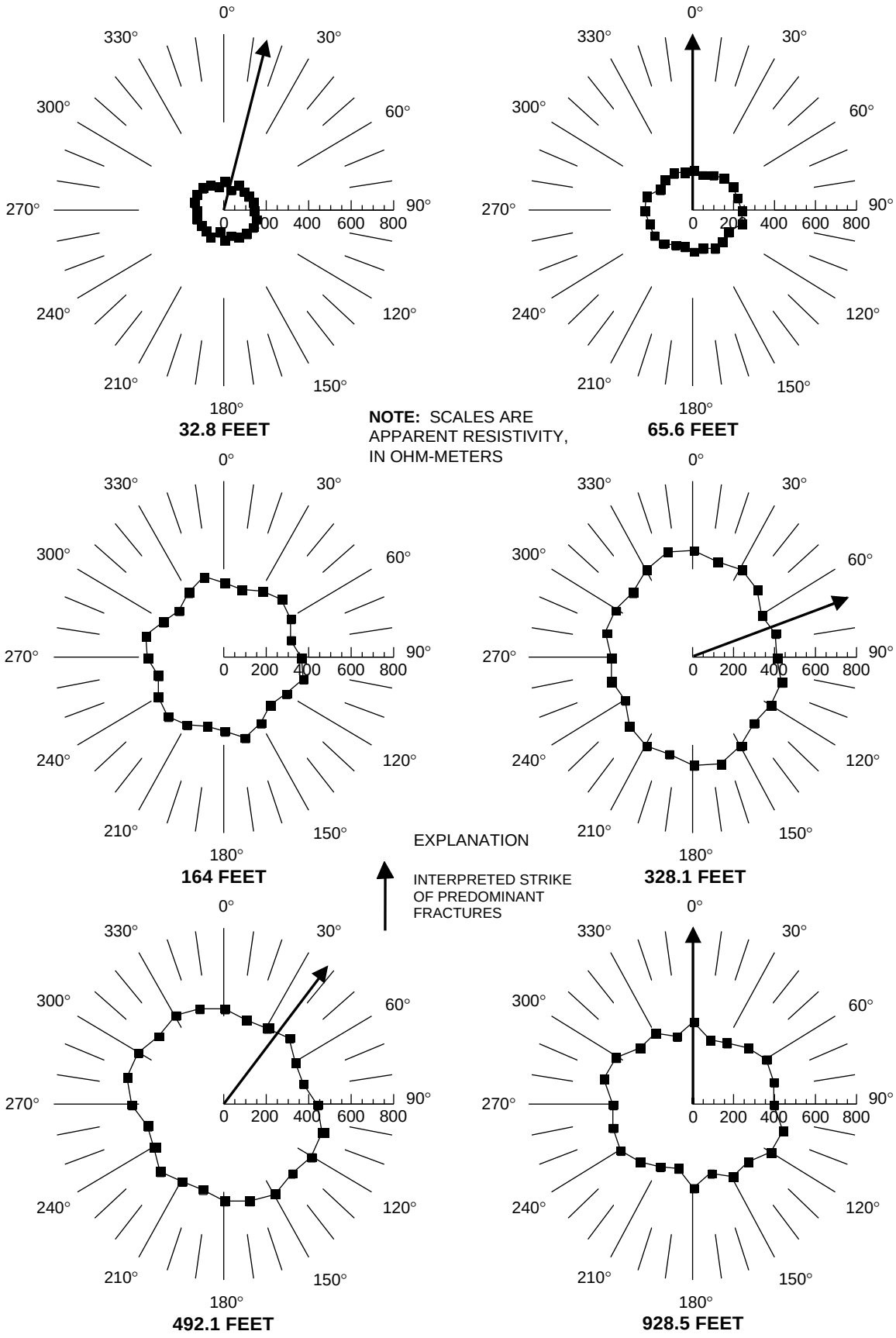

Part A. Continued. Woody Mountain at well 11 (W11).

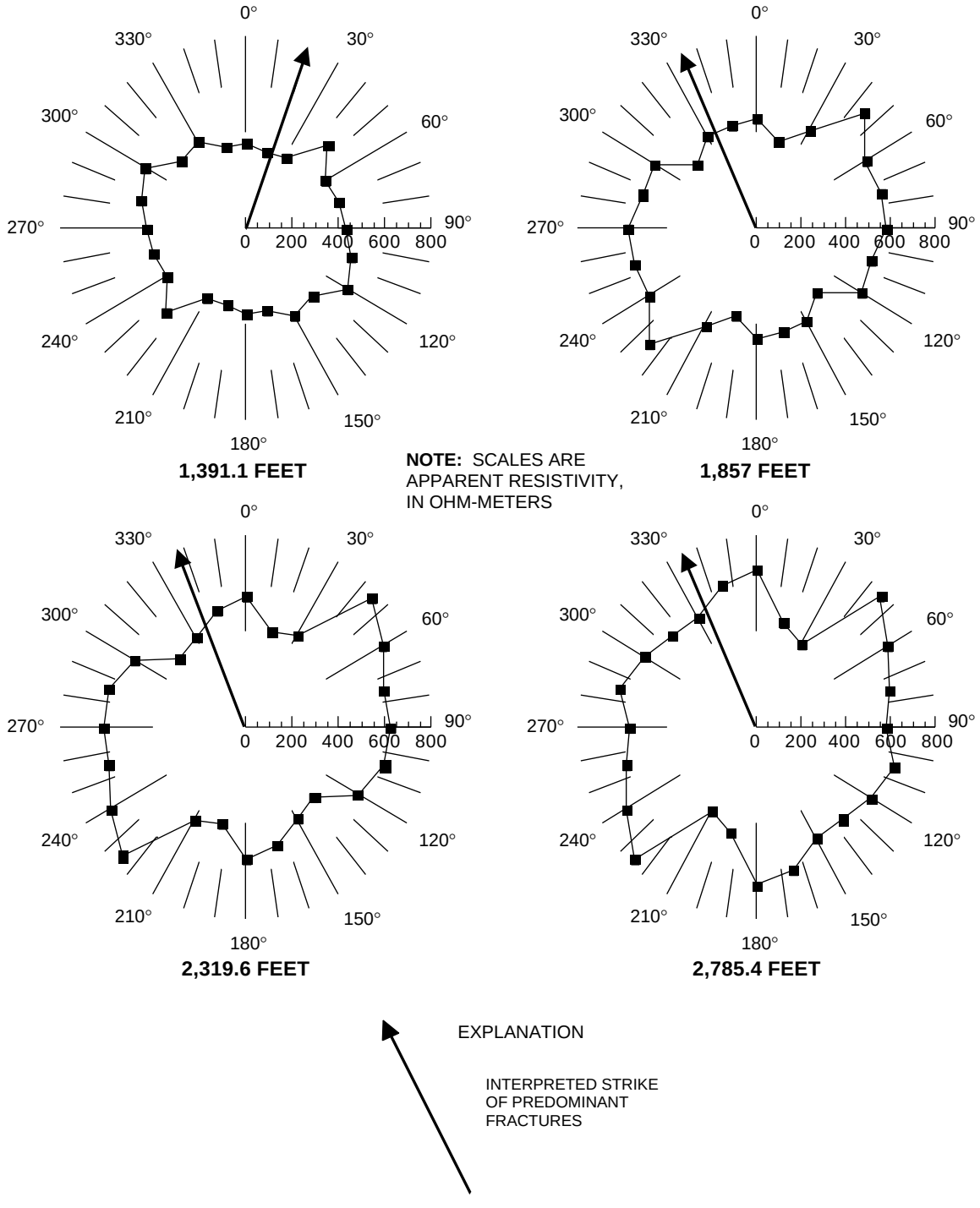

Part A. Continued. Woody Mountain at well 11 (W11).

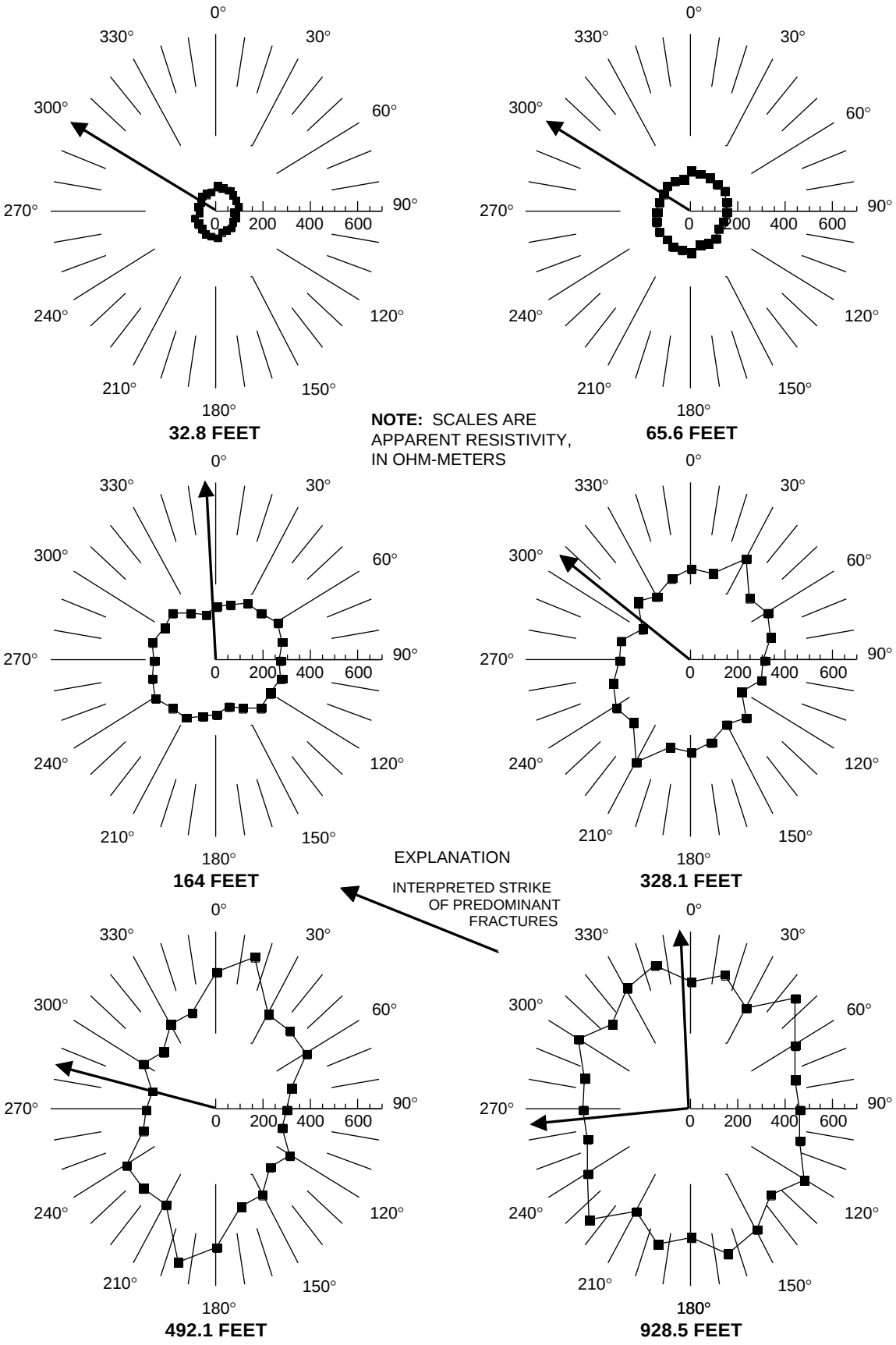

Part A. Continued. Skunk Canyon (SC).

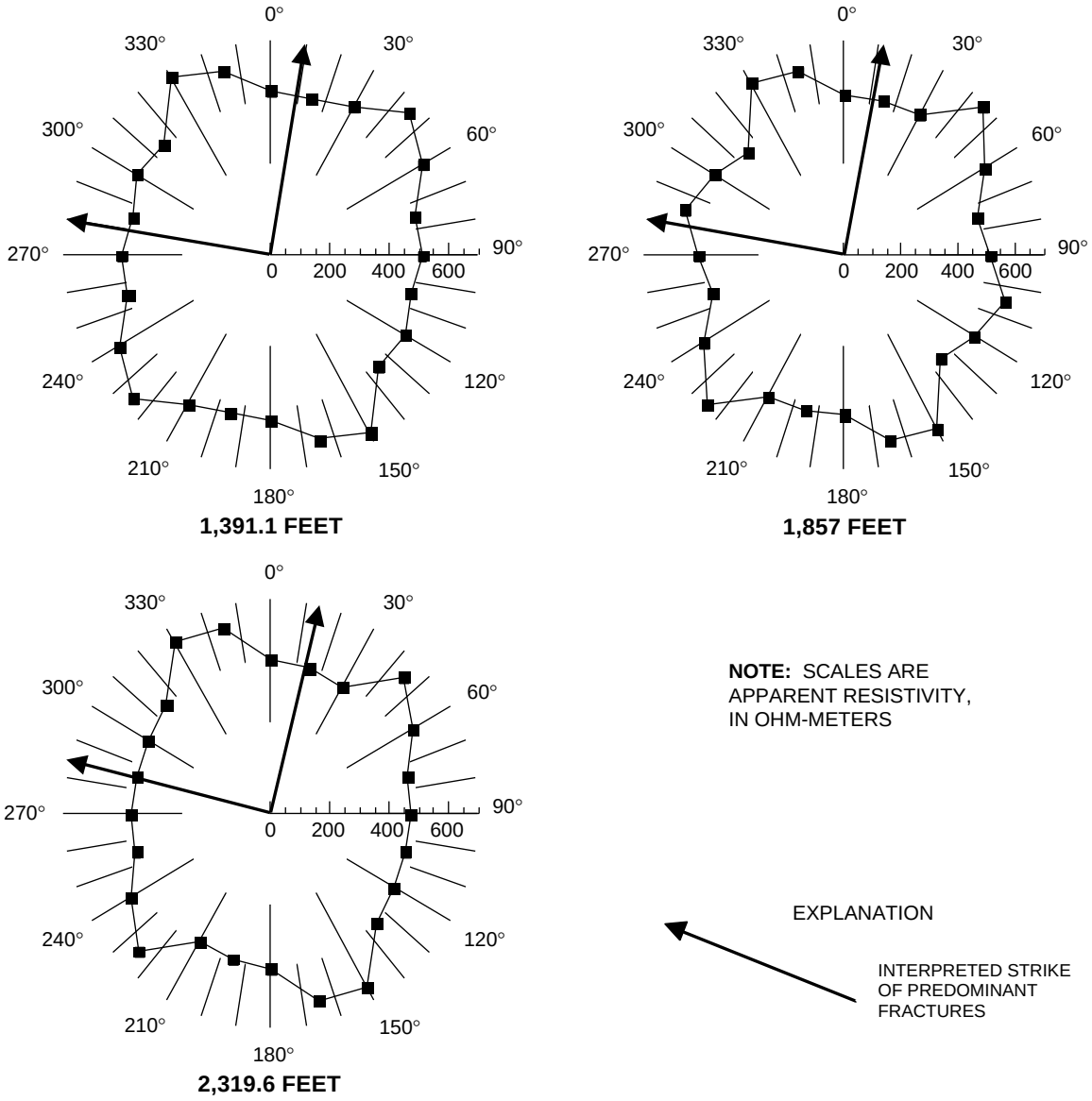

Part A. Continued. Skunk Canyon (SC).

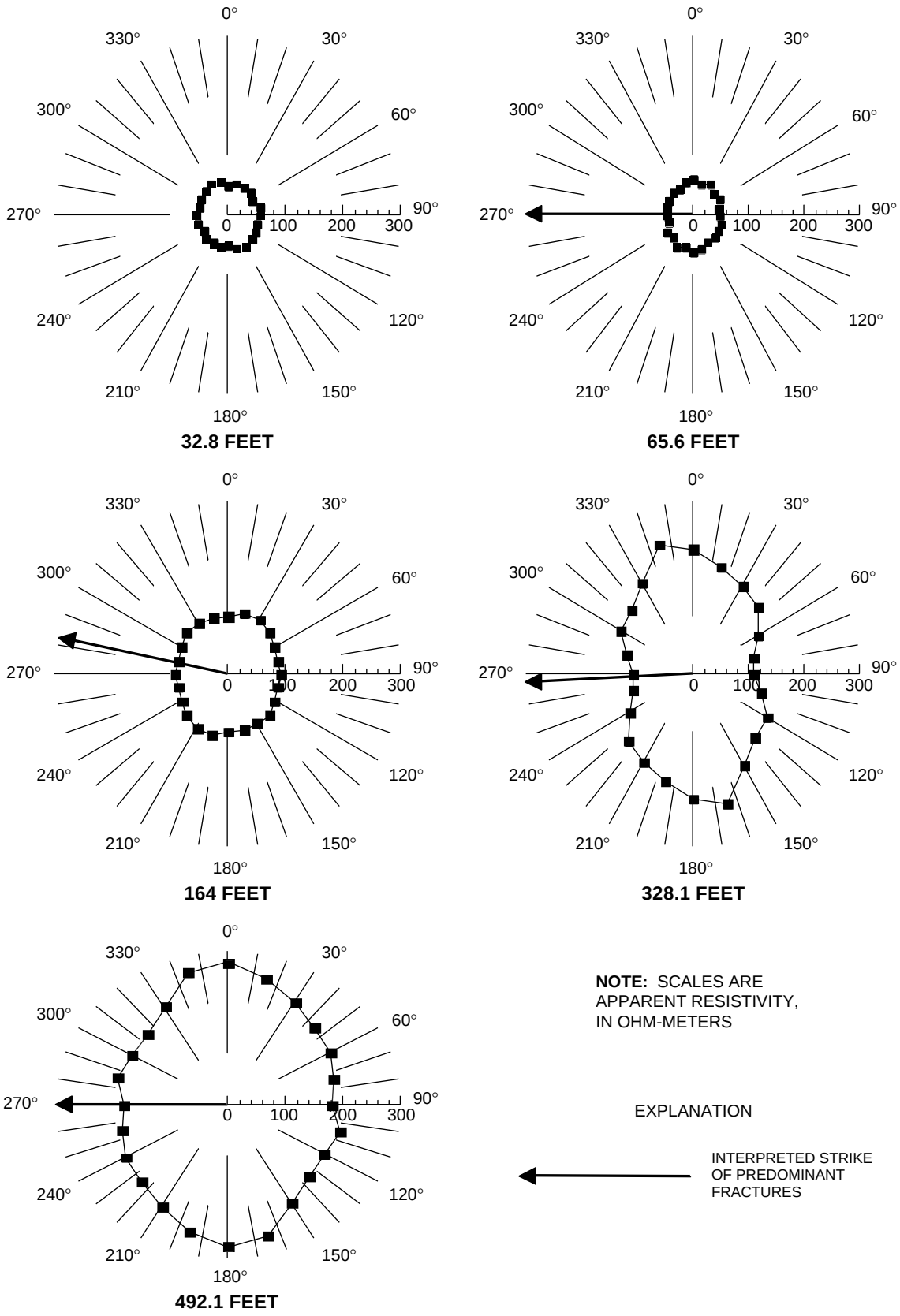

Part A. Continued. Foxglenn (FG).

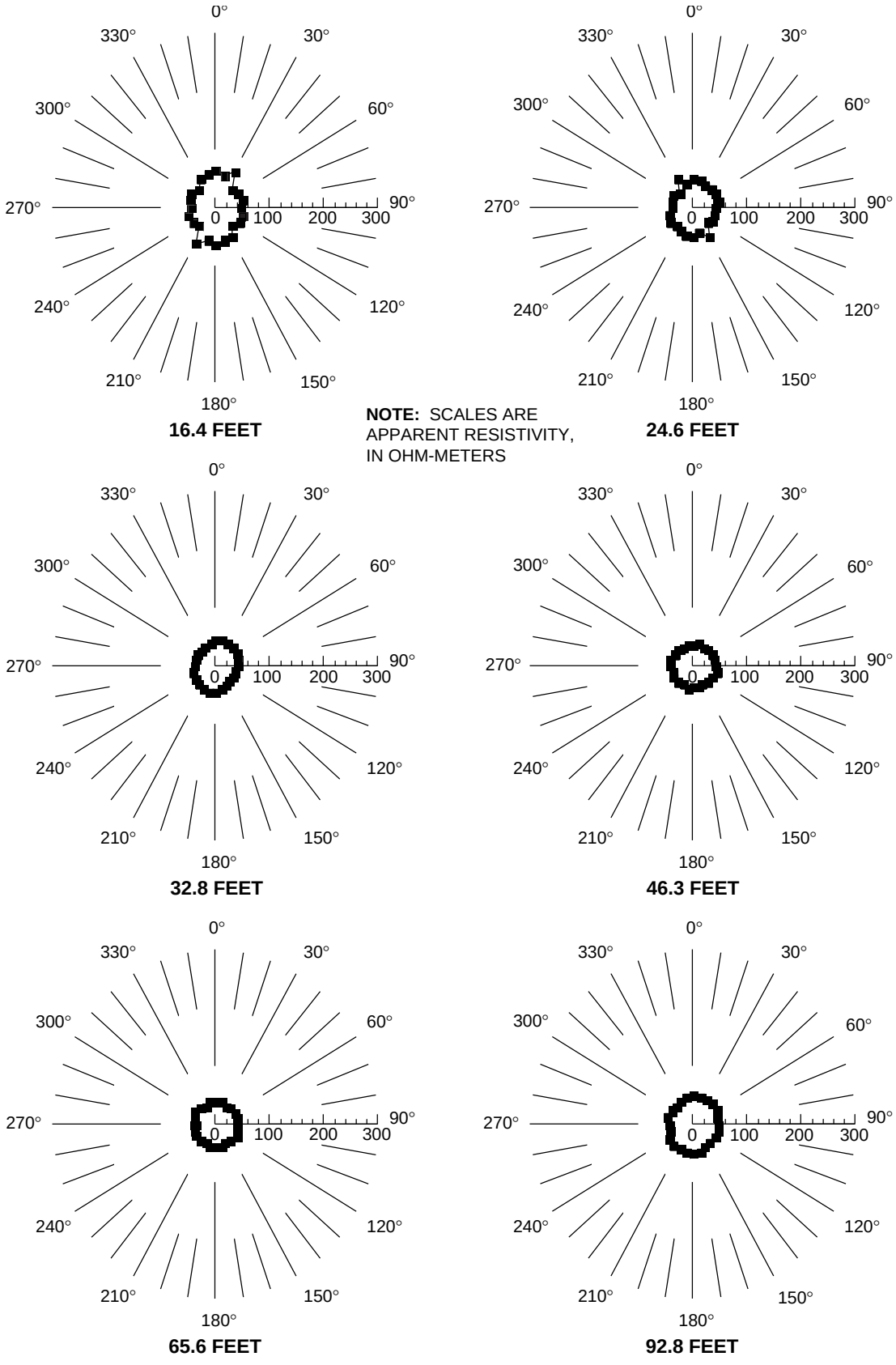

Part A. Continued. Continental (BP).

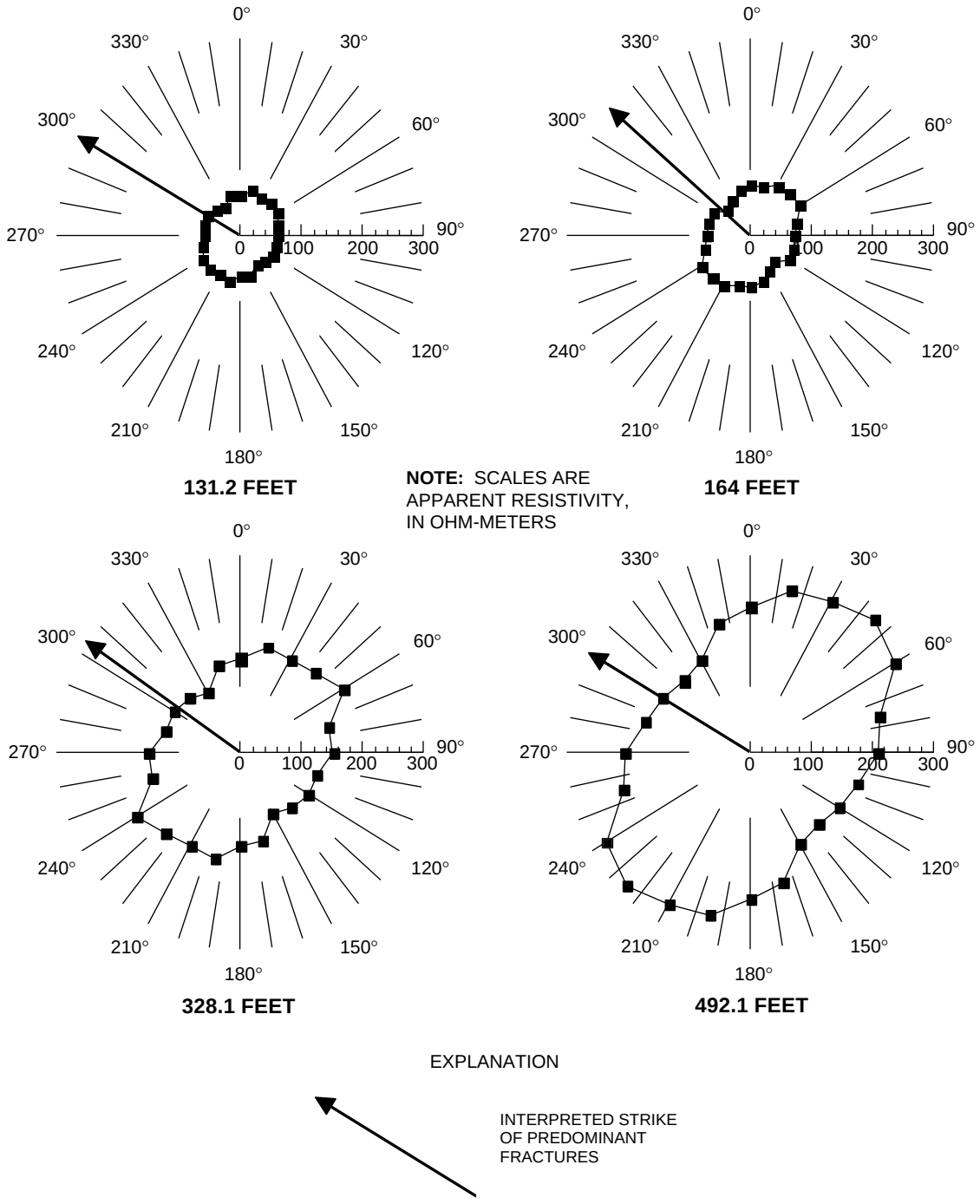

Part A. Continued. Continental (BP).

SUPPLEMENTAL DATA—CONTINUED
B. Hydrologic Data for Wells and Springs in the Regional Aquifer and Miscellaneous Sites, Flagstaff, Arizona

Well name or owner	Site identifier	Latitude	Longitude	Well name or owner	Site identifier	Latitude	Longitude
Riddle 3-A	(A-17-04)03aac2	34°53'19"	111°55'13"	FH-3	(A-20-07)19aba	35°06'26"	111°41'26"
Harless 27A	(A-17-04)04bbd1	34°53'20"	111°57'01"	FH Test WelL	(A-20-07)19cbb1	35°06'00"	111°42'05"
Harless 27B	(A-17-04)04bbd2	34°53'20"	111°57'00"	FH-1	(A-20-07)19cbb2	35°05'58"	111°42'05"
Yucc (A-Crary 1)	(A-17-04)05caa	34°52'55"	111°57'49"	Kachina-3	(A-20-07)20cca	35°05'47"	111°40'57"
Tupper Farm	(A-17-05)05bdc	34°53'04"	111°51'33"	LMEX-6	(A-20-07)23dca	35°05'45"	111°37'10"
Hopkins #1	(A-17-05)08bcb	34°52'18"	111°51'50"	LMEX-4	(A-20-07)25dcb1	35°04'55"	111°36'15"
Cathedral 1	(A-17-05)16cad	34°51'04"	111°50'25"	Mountainaire	(A-20-07)28bcc	35°05'11"	111°40'00"
Hancock	(A-18-04)15dbc	34°56'16"	111°55'36"	Kachina-1	(A-20-07)30bbc	35°05'33"	111°42'05"
Red Cyn Ranch	(A-18-04)25bcb	34°54'55"	111°53'59"	Kachina-2	(A-20-07)30bdb	35°05'16"	111°41'50"
Bradshaw Fee-1	(A-18-04)34abb	34°54'14"	111°55'32"	TH 4	(A-20-07)35bac	35°04'33"	111°37'34"
Rudy Buuch 1	(A-18-05)27abb	34°55'04"	111°49'13"	LM-1	(A-20-08)18bbb	35°07'16"	111°35'44"
Rudy Buuch 2	(A-18-05)27abc	34°54'57"	111°49'16"	LM-2	(A-20-08)18bcc	35°07'00"	111°35'47"
Hopkins 28-1	(A-18-05)28ada	34°54'53"	111°49'52"	Whitley-1	(A-20-08)18cac1	35°06'48"	111°35'27"
Marsland 1	(A-18-05)29adc	34°54'49"	111°51'05"	Whitley-2	(A-20-08)18cac2	35°06'50"	111°35'35"
Gillett 1	(A-18-05)31bcd	34°53'55"	111°52'45"	LM-4	(A-20-08)19aba	35°06'25"	111°35'05"
Hallermund 1	(A-18-05)31ddb	34°53'32"	111°52'05"	Schnieder	(A-20-08)19dac	35°05'55"	111°34'59"
Hopkins 34-2	(A-18-05)34bac	34°54'10"	111°49'27"	Suiter	(A-20-08)19dda	35°05'50"	111°34'50"
Hopkins 34-1Y	(A-18-05)34bca1	34°53'57"	111°49'39"	LMO-3	(A-20-08)20acd	35°06'10"	111°34'10"
Hopkins 34-1X	(A-18-05)34bca2	34°53'58"	111°49'39"	LM-8	(A-20-08)20cca	35°05'47"	111°34'30"
Christensen	(A-18-07)08ddc	34°57'06"	111°40'13"	LMO-1	(A-20-08)20cca2	35°05'50"	111°34'30"
AZWC-5	(A-18-07)15ccc2	34°56'16"	111°38'54"	LM-5	(A-20-08)20dbc	35°05'53"	111°34'07"
AZWC-10	(A-18-07)22baa2	34°56'08"	111°38'27"	LM-6	(A-20-08)27bbb	35°05'37"	111°32'32"
Ltl Antelope	(A-18-07)27cbb	34°54'51"	111°38'47"	LM-7	(A-20-08)27caa	35°05'07"	111°32'10"
Oil Discovery 1	(A-19-06)17dac	35°01'47"	111°46'32"	Old LM-9	(A-20-08)28cba	35°05'10"	111°33'25"
ADOT-89A	(A-19-06)W14bab	35°02'00"	111°43'55"	LMO-2	(A-20-08)29bbb	35°05'32"	111°34'43"
Pine Flats	(A-19-06)W27aaa	35°00'35"	111°44'18"	Garrison	(A-20-08)30abb	35°05'35"	111°35'15"
Federal 1	(A-19-07)01ddd1	35°03'06"	111°35'55"	Bathen	(A-20-08)30abc	35°05'30"	111°35'10"
Henson	(A-19-08)04bbb	35°03'50"	111°33'35"	Wahlers	(A-20-08)30bdb	35°05'20"	111°35'30"
Tilley	(A-19-08)04bbd	35°03'43"	111°33'37"	Cook-1	(A-20-08)30bdc	35°05'15"	111°35'30"
Walter	(A-19-08)05add	35°03'30"	111°33'50"	Cook-2	(A-20-08)30cba2	35°05'10"	111°35'40"
LMEX-1	(A-19-08)05ddd1	35°03'05"	111°33'50"	LM-9	(A-20-08)30cda	35°04'51"	111°35'25"
Pine Grove	(A-19-09)17dcd	35°01'24"	111°27'35"	TH-3	(A-20-08)30cdd1	35°04'50"	111°35'25"
Soshone OW	(A-19-10)05dba	35°03'22"	111°21'19"	LMEX-3	(A-20-08)32cab1	35°04'15"	111°34'25"
Anderson 1	(A-19-10)23ddb	35°00'35"	111°18'00"	LMEX-2	(A-20-08)33cdb	35°04'05"	111°33'20"
EPNG 1	(A-19-10)24bdd	35°01'00"	111°17'20"	Slayton	(A-20-09)22acb	35°06'14"	111°25'38"
Flowalt 1	(A-19-10)24cdb	35°00'35"	111°17'25"	Pickett OT	(A-20-10)26dbc	35°05'00"	111°18'15"
Potter-1	(A-20-05)24bbd	35°06'16"	111°49'24"	Drye	(A-20-10)S01aaa	35°09'08"	111°16'48"
WM-5	(A-20-06)02bbb	35°08'55"	111°44'15"	Babbitt	(A-20-11)07add	35°07'54"	111°15'40"
WM-10	(A-20-06)02bcb	35°08'43"	111°44'17"	R Owens OT	(A-20-11)12baa	35°08'15"	111°10'55"
WM-6	(A-20-06)02bdb	35°08'47"	111°44'04"	Crockett	(A-21-05)01acc3	35°13'55"	111°48'50"
WM-11	(A-20-06)11baa	35°08'05"	111°43'50"	NAD-1	(A-21-05)11cbc	35°12'45"	111°50'30"
WM-7	(A-20-06)11bab	35°08'08"	111°44'01"	Burns	(A-21-06)10daa	35°13'00"	111°44'15"
WM-9	(A-20-06)11bdc	35°07'45"	111°43'56"	Fried	(A-21-06)22bab	35°11'40"	111°44'55"
WM-8	(A-20-06)11bdd	35°07'50"	111°43'50"	Henden	(A-21-06)23aad	35°11'35"	111°43'10"
Morrison	(A-20-06)19bbb	35°06'25"	111°48'25"	Saskan Ranch	(A-21-06)24bcb	35°11'27"	111°43'03"
FH-5	(A-20-06)24abb	35°06'25"	111°42'03"	Flag Ranch	(A-21-06)25bcd	35°10'25"	111°42'52"
FH-4	(A-20-06)24adb	35°06'10"	111°42'25"	Flag Ranch Test	(A-21-06)25bcd2	35°10'25"	111°42'55"
North Ranch	(A-20-07)02cca	35°08'25"	111°37'40"	WM-Test	(A-21-06)34cca	35°09'10"	111°45'05"

Well name or owner	Site identifier	Latitude	Longitude
Skunk Canyon	(A-20-07)03aca	35°08'48"	111°38'17"
Airport Well	(A-20-07)04dac	35°08'28"	111°39'15"
Kimmerly	(A-20-07)07aaa1	35°08'10"	111°41'10"
Tyrrell	(A-20-07)07aaa2	35°08'10"	111°41'10"
Roaldstad	(A-20-07)07adb	35°07'55"	111°41'20"
Heckathorne	(A-20-07)12bba	35°08'10"	111°36'40"
LM-3	(A-20-07)12ddb	35°07'36"	111°36'02"
Riordan	(A-21-07)20bdb	35°11'30"	111°40'40"
Ponderosa Paper-1	(A-21-07)22aad	35°11'35"	111°37'50"
Ponderosa Paper-2	(A-21-07)22ada	35°11'30"	111°37'50"
Rio de Flag MW-1	(A-21-07)23cac	35°11'20"	111°38'00"
LA-3	(A-21-07)23dcc	35°10'58"	111°37'17"
Foxglenn-1	(A-21-07)24aad	35°11'37"	111°35'48"
Potter	(A-21-07)24ccd	35°10'55"	111°36'30"
Rio de Flag MW-3	(A-21-07)25bba2	35°10'52"	111°36'33"
Purl	(A-21-07)25bbd	35°10'43"	111°36'37"
LA-2	(A-21-07)26abb	35°10'53"	111°37'12"
LA-1	(A-21-07)26abd	35°10'45"	111°37'05"
Mtn Dell-1	(A-21-07)32bbc1	35°09'46"	111°40'53"
Mtn Dell-2	(A-21-07)32bbc2	35°09'48"	111°40'52"
Kohner	(A-21-07)34baa	35°09'50"	111°38'20"
Continental-1	(A-21-08)17bca1	35°12'24"	111°34'27"
Continental-2	(A-21-08)17bca2	35°12'23"	111°34'28"
NPS Walnut Canyon	(A-21-08)26dab	35°10'25"	111°30'37"
BBDP-Flowers	(A-21-09)05ddd	35°13'30"	111°27'15"
BBDP-MVR-1	(A-21-09)06baa	35°14'16"	111°28'50"
BBDP-Cosnino	(A-21-09)08bcc	35°13'05"	111°28'10"
Wilbur	(A-21-09)10bbd	35°13'20"	111°26'00"
Foster	(A-21-09)11bbb	35°13'25"	111°25'00"
Pill	(A-21-09)14acc	35°12'10"	111°24'30"
Porter	(A-21-09)15dda	35°11'55"	111°25'05"
ADOT-Winona	(A-21-09)17acc	35°12'15"	111°27'40"
CVWC	(A-21-09)23cba	35°11'15"	111°24'55"
WM-3	(A-21-06)35bcc	35°09'35"	111°44'10"
WM-1	(A-21-06)35cba	35°09'24"	111°44'01"
WM-2	(A-21-06)35ccb	35°09'16"	111°44'08"
WM-4	(A-21-06)35ccc	35°09'05"	111°44'08"
Ritland	(A-21-07)09acc	35°13'05"	111°39'25"
Pugh	(A-21-07)09bac	35°13'22"	111°39'37"
Hidden Hollow	(A-21-07)19aca	35°11'30"	111°41'16"
Moody	(A-21-10)16bdc	35°12'30"	111°20'15"
Drye	(A-21-11)19bcb	35°11'45"	111°16'10"
Poore	(A-21-11)31cdd	35°09'25"	111°15'50"
EPNG-3	(A-22-04)08dac1	35°17'55"	111°59'10"
EPNG-5	(A-22-05)26acd	35°15'35"	111°49'50"
Parks Sch.	(A-22-04)27aad	35°15'46"	111°56'58"
EPNG-6	(A-22-05)26adc2	35°15'35"	111°49'40"
Fort Valley	(A-22-06)26aaa	35°16'06"	111°46'08"
Garrett-Bacon	(A-22-07)34dda	35°14'33"	111°37'54"
AT&T	(A-22-08)16dad	35°17'20"	111°32'35"
BBDP-Sunset	(A-22-08)23aab	35°17'00"	111°30'35"
BBDP-Marijka	(A-22-08)23abb	35°16'56"	111°30'52"
Cromer School	(A-22-08)26bbb	35°16'08"	111°31'18"
Koch Field	(A-22-08)27caa	35°15'40"	111°32'05"
Mitchell	(A-22-08)35aac	35°15'10"	111°30'35"
US Grisp	(A-22-09)29baa	35°16'00"	111°27'50"
Oil Test	(A-22-10)03acd	35°19'30"	111°18'45"
Kuttkuhn	(A-22-10)15bdc	35°17'40"	111°19'10"
Salt Well	(A-22-11)19ccc	35°16'25"	111°16'20"
IB-9	(A-23-07)33aab2	35°20'27"	111°39'00"
NPS Sunset Ctr-2	(A-23-08)21aad	35°22'05"	111°32'35"
Rhoten Spr	(A-23-10)01bbb	35°25'05"	111°17'20"
Ranch Well	(A-23-10)24abb	35°22'25"	111°16'50"
NPS-Citadel	(A-25-09)06ccd	35°34'10"	111°28'45"
NPS Wupatki HQ	(A-25-10)30bdb	35°31'10"	111°22'20"

[Method of construction: A, air rotary; B, bored or augered; C, cable tool; H, hydraulic rotary; P, air percussion; R, reverse rotary; D, dug.

Type of log available: C, caliper; D, drillers; E, electric logs; F, fluid conductance; G, geologist; I, induction; J, gamma ray; L, lateral log; M, microlog; N, neutron; P, Photographic video; S, sonic; T, temperature; U, gamma gamma; V, fluid viscosity; Z, other.

Aquifer code: 120VLCC, volcanic rocks; 310KIBB, Kaibab Formation; 310CCNN, Coconino Sandstone; 310SUPI, Supai Group; 330RDLL, Redwall Limestone; 341MRTN, Martin Formation.

Other available data: QW, water quality; HP, hydrologic properties.

Dashes indicate no data]

Well name or owner	Site identifier	Date well constructed	Depth of well (feet)	Altitude of land surface (feet)	Water level (feet)	Date water level measured	Diameter of casing (inches)	Top of open interval (feet)	Bottom of open interval (feet)
Riddle 3-A	(A-17-04)03aac2	01-29-69	1,242	4,480	---	---	7.00	827	1,242
Harless 27A	(A-17-04)04bbd1	02-10-64	1,294	4,415	---	---	10.75	104	1,294
Harless 27B	(A-17-04)04bbd2	04-22-64	1,958	4,415	---	---	5.00	1,713	1,868
Yucc (A-Crary 1)	(A-17-04)05caa	10-09-64	1,663	4,365	733	03-19-74	10.00	108	1,663
Tupper Farm	(A-17-05)05bdc	05-22-76	1,209	4,650	917	05-22-76	10.80	969	1,209
Hopkins #1	(A-17-05)08bcb	04-25-69	1,195	4,430	723	03-07-75	7.00	1,060	1,195
Cathedral 1	(A-17-05)16cad	04-14-71	1,015	4,410	600	06-00-71	6.00	858	1,015
Hancock	(A-18-04)15dbc	00-00-61	1,300	4,740	400	03-05-74	6.00	20	1,300
Red Cyn Ranch	(A-18-04)25bcb	00-00-50	1,120	4,760	760	06-02-67	8.00	5	1,120
Bradshaw Fee-1	(A-18-04)34abb	04-28-71	3,203	4,480	329	08-22-74	9.00	90	3,203
Do.	Do.	---	---	---	---	---	---	---	---
Rudy Buuch 1	(A-18-05)27abb	00-00-49	1,200	4,700	709	06-02-67	8.00	20	1,200
Rudy Buuch 2	(A-18-05)27abc	---	1,200	4,650	---	---	---	---	---
Hopkins 28-1	(A-18-05)28ada	08-08-68	1,308	4,665	688	03-07-75	4.50	1,233	1,238
Do.	Do.	---	---	---	---	---	4.50	1,271	1,277
Do.	Do.	---	---	---	---	---	4.50	1,300	1,302
Marsland 1	(A-18-05)29adc	03-00-64	852	4,555	679	05-31-67	6.00	480	852
Gillett 1	(A-18-05)31bcd	00-00-65	1,050	4,600	925	03-19-74	6.00	1,000	---
Hallermund 1	(A-18-05)31ddb	02-09-69	1,215	4,540	850	04-09-69	6.00	1,071	1,215
Hopkins 34-2	(A-18-05)34bac	05-00-69	1,217	4,480	---	---	13.00	51	1,217
Hopkins 34-1Y	(A-18-05)34bca1	12-00-68	1,150	4,450	---	---	6.25	1,051	1,083
Do.	Do.	---	---	---	---	---	6.25	1,100	1,127
Hopkins 34-1X	(A-18-05)34bca2	11-00-68	1,138	4,450	---	---	4.75	905	918
Do.	Do.	---	---	---	---	---	4.75	1,070	1,088
Do.	Do.	---	---	---	---	---	4.75	1,098	1,132
Christensen	(A-18-07)08ddc	11-17-73	1,480	6,490	733	01-30-78	7.00	771	814
Do.	Do.	---	---	---	---	---	7.00	1,014	1,054
Do.	Do.	---	---	---	---	---	7.00	1,223	1,266
Do.	Do.	---	---	---	---	---	7.00	1,299	1,480
AZWC-5	(A-18-07)15ccc2	07-02-77	1,252	6,435	711	09-01-77	6.62	1,189	1,252
AZWC-10	(A-18-07)22baa2	10-31-77	1,330	6,455	713	10-31-77	12.00	904	1,304
Ltl Antelope	(A-18-07)27cbb	09-00-65	1,500	6,470	1,279	09-07-65	8.00	540	620
Do.	Do.	---	---	---	---	---	6.00	1,190	1,500
Oil Discovery1	(A-19-06)17dac	12-01-67	3,253	7,045	---	---	7.75	---	---
ADOT-89A	(A-19-06)W14bab	10-09-78	1,105	6,490	830	11-27-78	8.62	905	1,105
Pine Flats	(A-19-06)W27aaa	07-07-75	342	5,540	9	07-15-75	6.63	216	342
Federal 1	(A-19-07)01ddd1	08-23-76	730	7,175	420	08-23-76	8.12	405	730

See footnote at end of table.

Well name or owner	Site identifier	Date well constructed	Depth of well (feet)	Altitude of land surface (feet)	Water level (feet)	Date water level measured	Diameter of casing (inches)	Top of open interval (feet)	Bottom of open interval (feet)
Henson	(A-19-08)04bbb	07-01-79	201	6,980	25	07-30-79	6.00	156	166
Do.	Do.	---	---	---	---	---	---	---	---
Do.	Do.	---	---	---	---	---	6.00	186	196
Tilley	(A-19-08)04bbd	10-21-78	152	6,940	20	10-27-78	6.00	22	152
Walter	(A-19-08)05add	08-14-79	220	6,960	31	09-15-79	6.00	152	162
Do.	Do.	---	---	---	---	---	6.00	190	200
LMEX-1	(A-19-08)05ddd1	12-18-91	1,203	6,960	153	05-17-92	8.62	272	1,161
Do.	Do.	---	---	---	---	---	---	---	---
Pine Grove	(A-19-09)17dcd	07-01-67	1,700	6,958	1,309	08-31-67	8.00	1,439	1,700
Do.	Do.	---	---	---	---	---	---	---	---
Do.	Do.	---	---	---	---	---	---	---	---
Soshone OW	(A-19-10)05dba	08-01-63	1,125	6,491	---	---	10.75	180	1,125
Anderson 1	(A-19-10)23ddb	06-01-44	1,297	6,390	---	07-11-78	7.00	---	---
EPNG 1	(A-19-10)24bdd	08-01-61	1,730	6,393	1,296	05-16-66	8.62	---	---
Flowalt 1	(A-19-10)24cdb	02-01-67	6,500	6,406	1,277	03-31-67	7.00	---	---
Potter-1	(A-20-05)24bbd	06-00-65	3,781	7,240	1,096	09-09-66	14.00	---	---
WM-5	(A-20-06)02bbb	06-23-62	1,600	7,186	1,119	06-22-63	20.00	1,288	1,600
WM-10	(A-20-06)02bcb	07-00-95	1,790	7,230	1,139	04-02-96	16.00	1,300	1,760
Do.	Do.	---	---	---	---	---	---	---	---
WM-6	(A-20-06)02bdb	12-28-63	1,700	7,201	809	11-24-67	20.00	1,100	1,700
WM-11	(A-20-06)11baa	10-15-96	[1]1,952	7,170	[1]1,106	08-18-97	24.00	800	1,106
WM-7	(A-20-06)11bab	10-21-74	1,816	7,171	1,099	04-21-78	22.00	1,105	1,201
Do.	Do.	---	---	---	---	---	14.00	1,122	1,762
WM-9	(A-20-06)11bdc	10-10-84	1,840	7,090	982	11-07-85	14.00	1,220	1,830
WM-8	(A-20-06)11bdd	07-14-82	1,910	7,965	910	07-14-82	20.00	1,300	1,900
Morrison	(A-20-06)19bbb	07-12-81	152	7,163	83	07-14-81	6.00	90	152
FH-5	(A-20-06)24abb	08-29-87	1,350	6,770	703	09-23-87	12.00	700	1,109
Do.	Do.	---	---	---	---	---	12.00	1,125	1,345
FH-4	(A-20-06)24adb	05-08-87	1,255	6,760	679	06-13-87	12.00	682	1,030
Do.	Do.	---	---	---	---	---	12.00	1,050	1,250
North Ranch	(A-20-07)02cca	08-17-87	1,160	6,855	920	09-11-87	8.00	1,060	1,160
Skunk Canyon	(A-20-07)03aca	09-06-96	1,800	6,915	927	11-11-96	13.40	988	1,788
Do.	Do.	---	---	---	---	---	---	---	---
Airport Well	(A-20-07)04dac	10-27-95	1,590	6,960	829	10-27-95	6.00	40	1,590
Do.	Do.	---	---	---	---	---	---	---	---
Kimmerly	(A-20-07)07aaa1	04-20-85	1,005	6,980	941	05-21-85	8.00	50	95
Do.	Do.	---	---	---	---	---	6.00	95	1,005
Tyrrell	(A-20-07)07aaa2	08-25-92	1,275	6,970	1,063	10-19-92	8.00	52	1,275
Roaldstad	(A-20-07)07adb	00-00-59	995	6,895	949	06-07-60	8.00	745	995
Heckathorne	(A-20-07)12bba	00-00-60	987	6,840	900	06-29-65	12.00	10	987
LM-3	(A-20-07)12ddb	06-00-65	1,050	6,830	760	11-18-65	20.00	715	1,032
Do.	Do.	---	---	---	---	---	---	---	---
FH-3	(A-20-07)19aba	11-13-86	1,412	6,900	865	08-02-87	12.00	885	1,245
Do.	Do.	---	---	---	---	---	12.00	1,265	1,405
FH Test Well	(A-20-07)19cbb1	07-00-85	1,200	6,690	635	08-12-85	8.00	730	1,179

See footnote at end of table.

Well name or owner	Site identifier	Date well constructed	Depth of well (feet)	Altitude of land surface (feet)	Water level (feet)	Date water level measured	Diameter of casing (inches)	Top of open interval (feet)	Bottom of open interval (feet)
FH-1	(A-20-07)19cbb2	07-09-86	1,200	6,690	640	08-30-86	12.00	650	1,000
Do.	Do.	---	---	---	---	---	12.00	1,020	1,195
Kachina-3	(A-20-07)20cca	10-00-72	1,210	6,715	662	12-10-74	10.00	968	1,210
LMEX-6	(A-20-07)23dca	05-05-92	1,200	6,875	619	05-21-92	8.00	258	1,150
LMEX-4	(A-20-07)25dcb1	01-19-92	1,200	6,840	170	01-21-92	8.00	340	1,060
Mountainaire	(A-20-07)28bcc	10-10-60	845	6,785	791	03-30-78	8.00	---	---
Kachina-1	(A-20-07)30bbc	08-00-65	1,075	6,675	630	04-14-78	12.00	626	726
Do.	Do.	---	---	---	---	---	10.00	965	1,065
Do.	Do.	---	---	---	---	---	10.00	1,065	1,075
Kachina-2	(A-20-07)30bdb	09-00-69	1,004	6,685	632	10-08-69	12.00	---	---
TH 4	(A-20-07)35bac	10-16-90	1,200	6,875	605	10-29-90	2.00	---	---
LM-1	(A-20-08)18bbb	10-00-62	1,206	6,840	587	10-10-62	13.40	700	858
Do.	Do.	---	---	---	---	---	10.00	858	1,140
LM-2	(A-20-08)18bcc	11-13-64	1,091	6,832	432	04-14-65	20.00	569	1,081
Whitley-1	(A-20-08)18cac1	06-20-76	675	6,825	527	04-14-78	6.62	555	675
Whitley-2	(A-20-08)18cac2	04-22-92	1,200	6,820	620	04-28-92	8.00	560	1,200
LM-4	(A-20-08)19aba	01-10-72	1,345	6,808	335	02-20-73	20.62	800	1,280
Do.	Do.	---	---	---	---	---	---	---	---
Schnieder	(A-20-08)19dac	07-26-76	365	6,795	273	04-14-78	8.00	10	365
Suiter	(A-20-08)19dda	06-03-90	475	6,820	462	06-03-90	5.00	---	---
LMO-3	(A-20-08)20acd	11-06-85	800	6,795	562	12-10-85	---	0	800
LM-8	(A-20-08)20cca	12-28-81	1,310	6,819	257	12-28-81	20.00	600	1,300
Do.	Do.	---	---	---	---	---	---	---	---
Do.	Do.	---	---	---	---	---	---	---	---
LMO-1	(A-20-08)20cca2	01-22-85	1,020	6,820	235	04-11-85	1.50	700	1,000
LM-5	(A-20-08)20dbc	05-11-75	1,336	6,817	279	05-03-76	20.00	662	1,336
Do.	Do.	---	---	---	---	---	---	---	---
LM-6	(A-20-08)27bbb	07-24-78	1,298	6,810	1,187	12-15-78	21.00	421	1,252
Do.	Do.	---	---	---	---	---	16.00	1,252	1,298
LM-7	(A-20-08)27caa	12-07-77	1,630	6,795	925	09-02-81	14.00	1,107	1,607
Old LM-9	(A-20-08)28cba	11-29-89	1,396	6,860	640	12-05-89	2.00	1,200	1,396
Do.	Do.	---	---	---	---	---	---	---	---
LMO-2	(A-20-08)29bbb	01-22-85	1,000	6,865	260	04-11-85	1.50	700	1,000
Garrison	(A-20-08)30abb	10-11-72	410	6,800	260	11-11-72	6.00	20	410
Bathen	(A-20-08)30abc	09-03-82	500	6,820	320	01-21-94	6.00	350	500
Wahlers	(A-20-08)30bdb	06-11-85	345	6,820	120	06-12-85	5.00	265	345
Cook-1	(A-20-08)30bdc	08-21-78	174	6,840	---	---	6.00	32	174
Cook-2	(A-20-08)30cba2	08-14-90	190	6,810	172	08-21-90	6.00	30	190
LM-9	(A-20-08)30cda	09-15-91	1,398	6,875	91	08-30-91	18.00	357	1,318
Do.	Do.	---	---	---	---	---	18.00	1,358	1,378
TH-3	(A-20-08)30cdd1	11-05-90	1,200	6,870	180	11-12-90	2.00	---	---
LMEX-3	(A-20-08)32cab1	01-13-92	1,207	6,880	51	01-18-92	8.00	229	1,163
Do.	Do.	---	---	---	---	---	---	---	---
LMEX-2	(A-20-08)33cdb	12-04-91	1,203	6,940	411	01-15-92	8.00	442	1,161
Slayton	(A-20-09)22acb	00-00-57	1,465	6,655	DRY	---	---	---	---

See footnote at end of table.

Well name or owner	Site identifier	Date well constructed	Depth of well (feet)	Altitude of land surface (feet)	Water level (feet)	Date water level measured	Diameter of casing (inches)	Top of open interval (feet)	Bottom of open interval (feet)
Pickett OT	(A-20-10)26dbc	11-18-63	3,596	6,255	1,164	01-26-79	6.75	2,747	3,596
Do.	Do.	---	---	---	---	---	---	---	---
Drye	(A-20-10)S01aaa	01-01-46	935	5,910	918	02-15-67	6.00	6	935
Babbitt	(A-20-11)07add	07-01-40	950	5,915	910	02-18-67	8.00	---	---
R Owens OT	(A-20-11)12baa	06-08-62	3,628	5,725	821	07-11-78	9.62	128	3,628
Do.	Do.	---	---	---	---	---	---	---	---
Crockett	(A-21-05)01acc3	03-28-86	100	7,135	42	04-04-86	6.00	50	100
NAD-1	(A-21-05)11cbc	04-11-50	1,647	7,040	1,273	08-28-50	12.00	1,500	1,647
Do.	Do.	---	---	---	---	---	---	---	---
Burns	(A-21-06)10daa	05-13-87	1,700	7,370	1,275	05-26-87	6.00	1,475	1,700
Fried	(A-21-06)22bab	11-10-92	1,140	7,430	DRY	11-14-92	8.62	20	1,140
Henden	(A-21-06)23aad	01-27-94	1,600	7,220	1,490	06-05-94	6.62	1,480	1,600
Saskan Ranch	(A-21-06)24bcb	01-25-96	1,640	7,210	1,390	06-12-96	6.00	1,470	1,610
Do.	Do.	---	---	---	---	---	---	---	---
Flag Ranch	(A-21-06)25bcd	05-31-85	1,800	7,050	1,122	10-20-85	12.00	1,150	1,490
Do.	Do.	---	---	---	---	---	12.00	1,510	1,650
Do.	Do.	---	---	---	---	---	12.00	1,670	1,790
Flag Ranch Test	(A-21-06)25bcd2	11-01-84	1,610	7,050	1,210	03-15-85	9.88	0	1,610
WM-Test	(A-21-06)34cca	11-10-81	1,008	7,330	DRY	11-14-81	---	0	1,008
WM-3	(A-21-06)35bcc	10-00-57	1,602	7,130	1,213	11-19-58	20.00	1,300	1,600
WM-1	(A-21-06)35cba	06-23-54	1,600	7,140	1,227	03-01-55	12.00	1,329	1,580
WM-2	(A-21-06)35ccb	03-28-55	1,746	7,167	1,246	07-02-56	16.00	1,200	1,397
Do.	Do.	---	---	---	---	---	12.00	1,380	1,600
WM-4	(A-21-06)35ccc	09-14-56	1,540	7,166	1,065	11-02-57	20.00	1,213	1,518
Ritland	(A-21-07)09acc	11-01-90	1,824	7,010	1,516	02-09-91	6.62	1,554	1,804
Pugh	(A-21-07)09bac	02-01-89	1,600	7,100	1,530	06-30-89	8.00	240	1,600
Hidden Hollow	(A-21-07)19aca	01-14-77	1,551	7,070	1,320	01-14-77	6.62	1,320	1,551
Riordan	(A-21-07)20bdb	06-15-57	1,620	6,970	1,220	09-19-62	8.00	1,225	1,620
Ponderosa Paper-1	(A-21-07)22aad	11-00-57	1,433	6,855	1,273	06-25-66	12.00	450	1,410
Do.	Do.	---	---	---	---	---	8.00	1,410	1,433
Ponderosa Paper-2	(A-21-07)22ada	10-10-67	1,450	6,865	1,233	10-10-67	10.38	1,230	1,288
Do.	Do.	---	---	---	---	---	10.38	1,413	1,433
Rio de Flag MW-1	(A-21-07)23cac	04-29-93	185	6,800	44	04-29-93	6.00	120	185
LA-3	(A-21-07)23dcc	07-23-95	1,520	6,845	1,225	08-16-95	6.75	21	1,520
Foxglenn-1	(A-21-07)24aad	10-29-96	2,004	6,775	1,313	12-12-96	8.00	1,145	2,004
Do.	Do.	---	---	---	---	---	---	---	---
Potter	(A-21-07)24ccd	00-00-17	65	6,780	32	08-09-79	---	---	---
Rio de Flag MW-3	(A-21-07)25bba2	---	---	6,800	---	---	---	---	---
Purl	(A-21-07)25bbd	04-00-90	1,400	6,790	1,245	04-00-90	6.62	1,205	1,365
LA-2	(A-21-07)26abb	06-14-95	1,631	6,800	1,168	07-28-95	15.00	1,225	1,543
Do.	Do.	---	---	---	---	---	14.75	1,543	1,631
LA- 1	(A-21-07)26abd	06-06-76	1,502	6,795	1,165	09-02-76	12.75	1,205	1,275
Do.	Do.	---	---	---	---	---	10.75	1,288	1,492
Mtn Dell-1	(A-21-07)32bbc1	09-00-56	1,200	6,910	985	10-02-56	10.00	150	1,200
Mtn Dell-2	(A-21-07)32bbc2	05-22-75	1,350	6,900	975	05-22-75	8.00	100	1,350

See footnote at end of table.

Well name or owner	Site identifier	Date well constructed	Depth of well (feet)	Altitude of land surface (feet)	Water level (feet)	Date water level measured	Diameter of casing (inches)	Top of open interval (feet)	Bottom of open interval (feet)
Kohner	(A-21-07)34baa	11-16-87	1,550	6,935	1,138	04-12-88	8.62	1,149	1,550
Continental-1	(A-21-08)17bca1	09-09-96	1,650	6,750	1,550	10-21-96	12.00	0	1,650
Continental-2	(A-21-08)17bca2	01-15-97	2,001	6,750	1,304	02-22-97	8.00	1,251	2,001
Do.	Do.	---	---	---	---	---	---	---	---
NPS Walnut Canyon	(A-21-08)26dab	07-24-70	2,007	6,710	1,536	08-18-70	8.00	1,493	2,007
BBDP-Flowers	(A-21-09)05ddd	12-01-67	1,750	6,365	1,270	07-21-75	6.00	1,300	1,750
Do.	Do.	---	---	---	---	---	8.00	25	1,258
BBDP-MVR-1	(A-21-09)06baa	04-00-67	1,700	6,410	1,302	05-01-67	8.00	1,380	1,680
BBDP-Cosnino	(A-21-09)08bcc	01-01-72	1,715	6,450	1,349	01-01-72	6.38	1,396	1,604
Wilbur	(A-21-09)10bbd	07-01-66	1,338	6,290	1,227	07-30-66	10.00	300	1,338
Foster	(A-21-09)11bbb	12-16-89	1,400	6,205	1,137	04-09-90	4.00	1,120	1,320
Do.	Do.	---	---	---	---	---	6.26	1,360	1,400
Pill	(A-21-09)14acc	---	1,320	6,270	1,205	06-24-66	6.62	1,200	1,320
Porter	(A-21-09)15dda	00-00-65	1,315	6,265	1,215	00-00-65	5.00	1,275	1,315
ADOT-Winona	(A-21-09)17acc	06-00-72	1,800	6,440	1,327	06-00-72	8.00	1,352	1,800
CVWC	(A-21-09)23cba	05-20-82	1,275	6,270	1,206	01-03-83	5.00	1,200	1,270
Moody	(A-21-10)16bdc	---	1,050	6,005	990	11-30-78	8.00	---	---
Drye	(A-21-11)19bcb	---	935	5,770	785	09-18-67	8.00	719	935
Poore	(A-21-11)31cdd	---	1,000	5,865	844	11-30-78	10.00	---	---
EPNG-3	(A-22-04)08dac1	---	137	7,240	DRY	---	---	---	---
EPNG-5	(A-22-05)26acd	07-01-53	2,350	7,230	2,120	07-01-53	---	---	---
Parks Sch.	(A-22-04)27aad	---	---	7,090	---	---	---	---	---
EPNG-6	(A-22-05)26adc2	08-03-53	2,151	7,230	2,010	08-03-53	---	---	---
Fort Valley	(A-22-06)26aaa	11-20-38	1,540	7,335	DRY	07-11-77	---	---	---
Garrett-Bacon	(A-22-07)34dda	10-19-96	2,470	7,210	1,920	09-25-97	8.50	1,650	2,470
AT&T	(A-22-08)16dad	06-12-63	1,755	6,750	1,635	06-12-63	6.00	1,665	1,755
BBDP-Sunset	(A-22-08)23aab	01-01-71	1,800	6,570	1,550	01-01-71	7.00	1,590	1,660
BBDP-Marijka	(A-22-08)23abb	03-15-88	1,802	6,575	1,500	06-25-88	8.00	1,520	1,800
Do.	Do.	---	---	---	---	---	---	---	---
Do.	Do.	---	---	---	---	---	---	---	---
Cromer School	(A-22-08)26bbb	07-17-85	1,810	6,585	1,463	01-22-86	8.62	1,480	1,771
Koch Field	(A-22-08)27caa	---	1,772	6,625	1,496	---	8.00	1,406	1,654
Do.	Do.	---	---	---	---	---	6.00	1,700	1,732
Mitchell	(A-22-08)35aac	11-01-57	1,550	6,560	1,457	06-20-66	8.00	93	1,550
US Grisp	(A-22-09)29baa	11-00-59	1,447	6,390	1,383	12-17-73	6.00	---	---
Oil Test	(A-22-10)03acd	00-00-50	2,400	5,590	1,137	10-00-54	10.00	---	---
Kuttkuhn	(A-22-10)15bdc	05-00-73	1,240	5,705	1,112	00-00-75	8.00	71	1,240
Salt Well	(A-22-11)19ccc	00-00-48	1,060	5,590	1,000	10-20-54	6.00	750	1,060
IB-9	(A-23-07)33aab2	08-30-68	352	9,780	143	09-15-73	16.00	150	352
NPS Sunset Ctr-2	(A-23-08)21aad	03-30-65	2,200	6,970	1,944	03-30-65	8.00	---	---
Do.	Do.	---	---	---	---	---	---	---	---
Rhoten Spr	(A-23-10)01bbb	---	---	5,025	742	10-19-54	8.00	---	---
Ranch Well	(A-23-10)24abb	---	---	5,190	859	10-19-54	8.00	---	---
NPS-Citadel	(A-25-09)06ccd	12-00-66	1,788	5,381	1,583	01-23-67	8.00	1,780	1,788
NPS Wupatki HQ	(A-25-10)30bdb	10-00-58	904	4,930	781	10-27-58	10.00	800	904

See footnote at end of table.

Well name or owner	Site identifier	Discharge (gallons per minute)	Date discharge measured	Drawdown (feet)	Method constructed	Type of log available	Aquifer code	Other available data
Riddle 3-A	(A-17-04)03aac2	---	---	---	H	D	330RDLL	---
Harless 27A	(A-17-04)04bbd1	---	---	---	C	---	330RDLL	---
Harless 27B	(A-17-04)04bbd2	---	---	---	C	J, I	---	---
Yucc (A-Crary 1)	(A-17-04)05caa	---	---	---	---	D	341MRTN	---
Tupper Farm	(A-17-05)05bdc	---	---	---	C	G	341MRTN	---
Hopkins #1	(A-17-05)08bcb	---	---	---	H	D, T	341MRTN	---
Cathedral 1	(A-17-05)16cad	---	---	---	C	D	341MRTN	---
Hancock	(A-18-04)15dbc	6	03-05-74	---	C	G	310SUPI	---
Red Cyn Ranch	(A-18-04)25bcb	10	06-02-67	---	C	---	330RDLL	---
Bradshaw Fee-1	(A-18-04)34abb	---	---	---	H	J, N, Z	310SUPI	HP
Do.	Do.	---	---	---	---	E, L, M	---	---
Rudy Buuch 1	(A-18-05)27abb	9	06-02-67	---	C	---	330RDLL	---
Rudy Buuch 2	(A-18-05)27abc	92	---	---	C	---	330RDLL	---
Hopkins 28-1	(A-18-05)28ada	---	---	---	C	D, T, C	341MRTN	---
Do.	Do.	---	---	---	---	J, N	---	---
Do.	Do.	---	---	---	---	---	---	---
Marsland 1	(A-18-05)29adc	9	05-31-67	0	C	D	330RDLL	---
Gillett 1	(A-18-05)31bcd	---	---	---	C	D	330RDLL	---
Hallermund 1	(A-18-05)31ddb	---	---	---	P	D, G	341MRTN	---
Hopkins 34-2	(A-18-05)34bac	0	05-13-69	---	H	I, J	---	---
Hopkins 34-1Y	(A-18-05)34bca1	6	06-07-69	---	H	D	341MRTN	---
Do.	Do.	---	---	---	---	-	-	---
Hopkins 34-1X	(A-18-05)34bca2	0	12-09-68	---	H	D, I, J, C	---	---
Do.	Do.	---	---	---	---	---	---	---
Do.	Do.	---	---	---	---	---	---	---
Christensen	(A-18-07)08ddc	21	11-14-73	0	C	D	310CCNN	---
Do.	Do.	---	---	---	---	---	---	---
Do.	Do.	---	---	---	---	---	---	---
Do.	Do.	---	---	---	---	---	-	---
AZWC-5	(A-18-07)15ccc2	95	10-31-77	8	H	D	310CCNN	HP
AZWC-10	(A-18-07)22baa2	188	08-00-78	11	B	D	120VLCC	---
Ltl Antelope	(A-18-07)27cbb	26	09-00-65	58	C	D	310SUPI	---
Do.	Do.	---	---	---	---	---	---	---
Oil Discovery1	(A-19-06)17dac	---	---	---	---	D	---	---
ADOT-89A	(A-19-06)W14bab	51	10-27-78	0	A	D	310CCNN	HP
Pine Flats	(A-19-06)W27aaa	100	07-15-75	---	P	D	310SUPI	---
Federal 1	(A-19-07)01ddd1	---	---	---	A	I, U, N	310SUPI	HP
Do.	Do.	---	---	---	---	J, G, D	---	---
Henson	(A-19-08)04bbb	---	---	---	C	D	310KIBB	---
Do.	Do.	---	---	---	---	---	---	---
Tilley	(A-19-08)04bbd	---	---	---	---	D	310KIBB	
Walter	(A-19-08)05add	---	---	---	C	D	310KIBB	---
LMEX-1	(A-19-08)05ddd1	330	05-17-92	83	A	C, J, E	310CCNN	HP
Do.	Do.	---	---	---	-	F, T, Z	---	---
Pine Grove	(A-19-09)17dcd	48	07-19-67	25	C	S, G	310SUPI	HP, QW

See footnote at end of table.

Well name or owner	Site identifier	Discharge (gallons per minute)	Date discharge measured	Drawdown (feet)	Method constructed	Type of log available	Aquifer code	Other available data
Do.	Do.	15	08-31-67	25	---	---	---	---
Do.	Do.	50	09-18-67	---	---	---	---	---
Soshone OW	(A-19-10)05dba	---	---	---	---	D	310CCNN	---
Anderson 1	(A-19-10)23ddb	---	---	---	---	---	---	---
EPNG 1	(A-19-10)24bdd	---	---	---	H	D	310SUPI	---
Flowalt 1	(A-19-10)24cdb	---	---	---	A	D	310SUPI	---
Potter-1	(A-20-05)24bbd	---	---	---	C	G	310SUPI	---
WM-5	(A-20-06)02bbb	600	06-22-63	66	C	D, G	310CCNN	HP
WM-10	(A-20-06)02bcb	295	04-05-96	223	R	C, E, J	310CCNN	HP
Do.	Do.	---	---	---	---	S, T, Z	---	---
WM-6	(A-20-06)02bdb	500	03-27-68	336	C	D	310CCNN	HP, QW
WM-11	(A-20-06)11baa	---	---	---	C	G, P	310CCNN	HP
WM-7	(A-20-06)11bab	942	04-21-78	308	C	D	310CCNN	---
Do.	Do.	---	---	---	---	---	---	---
WM-9	(A-20-06)11bdc	677	09-01-86	471	---	D	310CCNN	HP, QW
WM-8	(A-20-06)11bdd	---	---	---	H	D	310CCNN	---
Morrison	(A-20-06)19bbb	---	---	---	A	D	310KIBB	---
FH-5	(A-20-06)24abb	200	10-12-87	273	R	D	310SUPI	HP, QW
Do.	Do.	---	---	---	---	-	---	---
FH-4	(A-20-06)24adb	152	06-20-87	234	R	D	310CCNN	HP
Do.	Do.	---	---	---	---	---	---	---
North Ranch	(A-20-07)02cca	40	09-00-87	20	---	D	310SUPI	HP
Skunk Canyon	(A-20-07)03aca	150	11-18-96	669	---	J, C, S	310SUPI	HP
Do.	Do.	---	---	---	---	E, T, G, V	---	---
Airport Well	(A-20-07)04dac	---	---	---	P	J, G, T	310SUPI	---
Do.	Do.	---	---	---	---	C, E	---	---
Kimmerly	(A-20-07)07aaa1	5	10-05-85	---	---	D	310CCNN	---
Do.	Do.	---	---	---	---	---	---	---
Tyrrell	(A-20-07)07aaa2	10	05-25-93	12	---	D	310CCNN	HP
Roaldstad	(A-20-07)07adb	---	---	---	C	D	310SUPI	---
Heckathorne	(A-20-07)12bba	40	09-29-65	---	C	---	310CCNN	---
LM-3	(A-20-07)12ddb	175	03-10-66	144	H	---	310CCNN	HP
Do.	Do.	167	11-18-65	211	---	---	---	---
FH-3	(A-20-07)19aba	90	08-30-87	245	---	D	310SUPI	HP
Do.	Do.	---	---	---	---	---	---	---
FH Test Well	(A-20-07)19cbb1	---	---	---	---	D	310CCNN	---
FH-1	(A-20-07)19cbb2	122	09-11-86	261	---	D, P	310CCNN	HP
Do.	Do.	---	---	---	---	---	---	---
Kachina-3	(A-20-07)20cca	130	04-12-78	---	C	D	310CCNN	---
LMEX-6	(A-20-07)23dca	---	---	---	A	D	310CCNN	HP
LMEX-4	(A-20-07)25dcb1	---	---	---	A	D	310CCNN	HP
Mountainaire	(A-20-07)28bcc	150	03-30-78	---	---	---	310CCNN	QW
Kachina-1	(A-20-07)30bbc	34	08-00-65	20	C	D	310CCNN	HP
Do.	Do. .	---	---	---	---	---	---	---
Do.	Do.	---	---	---	---	---	---	---
Kachina-2	(A-20-07)30bdb	55	10-09-69	35	C	---	310CCNN	HP

See footnote at end of table.

Well name or owner	Site identifier	Discharge (gallons per minute)	Date discharge measured	Drawdown (feet)	Method constructed	Type of log available	Aquifer code	Other available data
TH 4	(A-20-07)35bac	---	---	---	---	D, G	310CCNN	---
LM-1	(A-20-08)18bbb	300	09-08-64	76	C	D	310CCNN	HP
Do.	Do.	---	---	---	---	---	---	---
LM-2	(A-20-08)18bcc	600	03-07-75	430	H	D	310CCNN	HP
Whitley-1	(A-20-08)18cac1	33	04-14-78	---	C	D	310CCNN	---
Whitley-2	(A-20-08)18cac2	35	06-02-92	20	A	D	310CCNN	HP
LM-4	(A-20-08)19aba	701	04-03-75	342	H	C, V, Z	310CCNN	HP, QW
Do.	Do.	---	---	---	---	I, T	---	---
Schnieder	(A-20-08)19dac	---	---	---	C	D	310CCNN	---
Suiter	(A-20-08)19dda	10	06-04-90	40	---	D	310CCNN	HP
LMO-3	(A-20-08)20acd	---	---	---	---	D	310CCNN	---
LM-8	(A-20-08)20cca	750	12-00-86	146	H	V, E, T	310CCNN	HP, QW
Do.	Do.	---	---	---	---	G, N, I	---	---
Do.	Do.	---	---	---	---	J, C	---	---
LMO-1	(A-20-08)20cca2	---	---	---	---	D	310CCNN	HP
LM-5	(A-20-08)20dbc	1,000	12-02-75	182	C	D, C, E	310CCNN	HP
Do.	Do.	---	---	---	---	J, T	---	---
LM-6	(A-20-08)27bbb	---	---	---	---	Z	310CCNN	---
Do.	Do.	---	---	---	---	---	---	---
LM-7	(A-20-08)27caa	---	---	---	---	Z	310CCNN	---
Old LM-9	(A-20-08)28cba	---	---	---	---	D, E, J	310SUPI	---
Do.	Do.	---	---	---	---	S, C	---	---
LMO-2	(A-20-08)29bbb	---	---	---	---	D	310CCNN	---
Garrison	(A-20-08)30abb	---	---	---	C	D	310KIBB	---
Bathen	(A-20-08)30abc	12	09-15-82	50	---	D	310CCNN	---
Wahlers	(A-20-08)30bdb	15	06-15-85	60	---	D	310CCNN	HP
Cook 1	(A-20-08)30bdc	---	---	---	---	D	310KIBB	---
Cook 2	(A-20-08)30cba2	---	---	---	---	D	310CCNN	---
LM-9	(A-20-08)30cda	---	---	---	R	G	310CCNN	HP, QW
Do.	Do.	---	---	---	---	---	---	---
TH-3	(A-20-08)30cdd1	---	---	---	---	D	310CCNN	HP
LMEX-3	(A-20-08)32cab1	320	---	270	A	D, C, G	310CCNN	HP
Do.	Do.	---	---	---	---	E	---	---
LMEX-2	(A-20-08)33cdb	69	---	63	A	D	310CCNN	HP
Slayton	(A-20-09)22acb	---	---	---	---	D	---	---
Pickett OT	(A-20-10)26dbc	---	---	---	A	D, J, S	310SUPI	---
Do.	Do.	---	---	---	---	E	---	---
Drye	(A-20-10)S01aaa	---	---	---	C	---	310CCNN	---
Babbitt	(A-20-11)07add	---	---	---	C	D	310CCNN	---
R Owens OT	(A-20-11)12baa	---	---	---	A	D, I, M	310CCNN	---
Do.	Do.	---	---	---	---	E, S	---	---
Crockett	(A-21-05)01acc3	---	---	---	---	D	310KIBB	---
NAD-1	(A-21-05)11cbc	35	07-20-50	100	---	G	310SUPI	HP
Do.	Do.	60	05-15-51	---	---	---	---	---
Burns	(A-21-06)10daa	5	08-17-88	347	---	D	310CCNN	HP
Fried	(A-21-06)22bab	---	---	---	---	D	---	---

See footnote at end of table.

Well name or owner	Site identifier	Discharge (gallons per minute)	Date discharge measured	Drawdown (feet)	Method constructed	Type of log available	Aquifer code	Other available data
Henden	(A-21-06)23aad	15	02-00-95	0	---	D	310SUPI	HP, QW
Saskan Ranch	(A-21-06)24bcb	18	06-17-96	15	A	J, T, D	310SUPI	HP
Do.	Do.	17	01-31-97	53	---	F, G	---	---
Flag Ranch	(A-21-06)25bcd	67	00-00-85	---	---	D	310SUPI	HP, QW
Do.	Do.	86	11-00-90	287	---	---	---	---
Do.	Do.	---	---	---	---	---	---	---
Flag Ranch Test	(A-21-06)25bcd2	---	---	---	---	---	---	---
WM-Test	(A-21-06)34cca	---	---	---	---	---	---	---
WM-3	(A-21-06)35bcc	500	---	92	C	D, G	310SUPI	HP
WM-1	(A-21-06)35cba	207	12-07-54	68	D	D	310CCNN	HP, QW
WM-2	(A-21-06)35ccb	362	07-03-56	33	---	D, G	310CCNN	HP
WM-4	(A-21-06)35ccc	490	03-31-58	211	C	D, G	310CCNN	HP
Ritland	(A-21-07)09acc	---	---	---	A	D	310SUPI	---
Pugh	(A-21-07)09bac	18	06-30-93	30	---	D	310SUPI	HP
Hidden Hollow	(A-21-07)19aca	10	01-14-77	---	---	D	310SUPI	HP, QW
Riordan	(A-21-07)20bdb	30	09-19-62	---	C	G	310SUPI	HP
Ponderosa Paper-1	(A-21-07)22aad	---	---	---	---	D	310SUPI	---
Do.	Do.	---	---	---	---	---	---	---
Ponderosa Paper-2	(A-21-07)22ada	---	---	---	C	D	310SUPI	---
Do.	Do.	---	---	---	---	---	---	---
Rio de Flag MW-1	(A-21-07)23cac	---	---	---	A	---	---	QW
LA-3	(A-21-07)23dcc	---	---	---	A	D	310SUPI	---
Foxglenn-1	(A-21-07)24aad	450	05-30-97	167	H	P, Z, G	310SUPI	HP,QW
Do.	Do.	---	---	---	---	C	---	---
Potter	(A-21-07)24ccd	---	---	---	D	---	310KIBB	---
Rio de Flag MW-3	(A-21-07)25bba2	---	---	---	---	---	---	QW
Purl	(A-21-07)25bbd	8	04-00-90	0	---	D	310CCNN	HP, QW
LA-2	(A-21-07)26abb	---	---	---	A	D, P	310SUPI	---
Do.	Do.	---	---	---	---	---	---	---
LA-1	(A-21-07)26abd	101	08-25-76	30	C	D	310SUPI	HP
Do.	Do.	---	---	---	---	---	---	---
Mtn Dell-1	(A-21-07)32bbc1	206	10-02-56	100	---	G	310SUPI	HP, QW
Mtn Dell-2	(A-21-07)32bbc2	37	05-22-75	---	C	D	310SUPI	QW
Kohner	(A-21-07)34baa	23	04-12-88	---	A	D	310CCNN	---
Continental-1	(A-21-08)17bca1	---	---	---	---	G, P	310SUPI	---
Continental-2	(A-21-08)17bca2	490	04-17-97	281	---	P, J, C	310SUPI	HP, QW
Do.	Do.	---	---	---	---	G	---	---
NPS Walnut Canyon	(A-21-08)26dab	44	08-20-70	271	A	---	310SUPI	HP, QW
BBDP-Flowers	(A-21-09)05ddd	15	12-01-61	15	C	D, V	310SUPI	HP
Do.	Do.	30	07-21-75	---	C	---	---	---
BBDP-MVR-1	(A-21-09)06baa	30	05-01-67	151	C	D, V	310SUPI	HP, QW
BBDP-Cosnino	(A-21-09)08bcc	30	01-01-73	130	---	D, V	310SUPI	HP
Wilbur	(A-21-09)10bbd	7	07-30-66	---	C	D, G	310SUPI	HP
Foster	(A-21-09)11bbb	18	04-09-90	---	---	D	310CCNN	HP
Do.	Do.	---	---	---	---	---	---	---
Pill	(A-21-09)14acc	7	06-24-66	12	C	D	310CCNN	HP

See footnote at end of table.

Well name or owner	Site identifier	Discharge (gallons per minute)	Date discharge measured	Drawdown (feet)	Method constructed	Type of log available	Aquifer code	Other available data
Porter	(A-21-09)15dda	---	---	---	C	D	310SUPI	---
ADOT-Winona	(A-21-09)17acc	17	06-20-72	150	---	---	310SUPI	HP
CVWC	(A-21-09)23cba	---	---	---	---	D	310SUPI	HP
Moody	(A-21-10)16bdc	22	03-07-79	30	---	D	310CCNN	HP
Drye	(A-21-11)19bcb	14	01-00-57	0	C	D	310CCNN	HP
Poore	(A-21-11)31cdd	---	---	---	---	---	310CCNN	---
EPNG-3	(A-22-04)08dac1	---	---	---	---	---	120VLCC	---
EPNG-5	(A-22-05)26acd	---	---	---	---	D	310SUPI	---
Parks Sch.	(A-22-04)27aad	---	---	---	C	---	120VLCC	QW
EPNG-6	(A-22-05)26adc2	---	---	---	---	---	---	---
Fort Valley	(A-22-06)26aaa	---	---	---	---	D	---	---
Garrett-Bacon	(A-22-07) 34dda	---	---	---	A	G, J, C	310SUPI	---
AT&T	(A-22-08)16dad	12	06-12-63	15	C	D	310SUPI	HP
BBDP-Sunset	(A-22-08)23aab	40	04-25-71	---	C	D, V	310SUPI	HP, QW
BBDP-Marijka	(A-22-08)23abb	233	07-16-88	7	---	D, G	310SUPI	HP
Do.	Do.	82	06-25-88	---	---	---	---	---
Do.	Do.	177	07-15-88	44	---	---	---	---
Cromer School	(A-22-08)26bbb	79	01-22-86	6	---	D	310SUPI	HP
Koch Field	(A-22-08)27caa	---	---	---	---	D, V	310SUPI	---
Do.	Do.	---	---	---	---	---	---	---
Mitchell	(A-22-08)35aac	25	06-20-66	---	C	D	310SUPI	HP
US Grisp	(A-22-09)29baa	4	00-00-59	---	C	D	310SUPI	HP
Oil Test	(A-22-10)03acd	---	---	---	C	D	330RDLL	---
Kuttkuhn	(A-22-10)15bdc	6	05-00-73	---	C	D	310SUPI	HP
Salt Well	(A-22-11)19ccc	10	09-20-67	---	C	-	310CCNN	HP
IB-9	(A-23-07)33aab2	859	09-15-73	102	C	D	110ALVM	QW
NPS Sunset Ctr-2	(A-23-08)21aad	21	05-03-65	58	C	D, J, C	310SUPI	HP
Do.	Do.	---	---	---	---	E, I, Z	---	---
Rhoten Spr	(A-23-10)01bbb	6	10-19-54	---	C	---	310CCNN	---
Ranch Well	(A-23-10)24abb	6	10-19-54	---	---	---	310CCNN	---
NPS-Citadel	(A-25-09)06ccd	18	01-23-67	5	C	D	310SUPI	HP
NPS Wupatki HQ	(A-25-10)30bdb	50	10-27-58	45	C	---	310CCNN	HP, QW
Grassy Meadow	(A-19-06)E27bcc	35°00'14"	111°44'02"	5,465	SEEP	08-17-49	310SUPI	---
Lolami	(A-19-06)34wa	34°59'37"	111°44'37"	5,400	25.0	08-17-49	310SUPI	---
Hummingbird	(A-19-06)34wc2	34°59'03"	111°44'50"	5,300	25.0	08-18-49	SCBH	---
Sherwood	(A-19-06)34wc1	34°59'08"	111°44'50"	5,300	50.0	08-18-49	SCBH	---
Cave	(A-19-06)dbc	34°59'10"	111°43'20"	5,440	---	---	SCBH	---
Sterling	(A-19-06)15ddd1	35°01'30"	111°44'22"	5,760	291.0	08-13-49	310CCNN	QW
Hoxworth	(A-19-08)08cab	35°02'25"	111°34'27"	7,015	25.0	12-01-89	310KIBB	---
Do.	Do.	Do.	Do.	Do.	10.0	05-02-96	Do.	---
Newman Canyon	(A-19-08)10cdd	35°02'10"	111°32'10"	6,940	.5	06-04-96	310KIBB	---
Clark	(A-20-08)32cca	35°04'02"	111°34'44"	7,005	3.1	05-02-96	310KIBB	QW
Babbitt	(A-20-08)34cdb	35°04'01"	111°32'16"	6,895	4.0	07-16-59	310KIBB	---
Do.	Do.	Do.	Do.	Do.	3.0	12-01-89	Do.	---
Do.	Do.	Do.	Do.	Do.	5.1	05-02-96	Do.	QW
NAD-1	(A-21-05)11abc	35°13'15"	111°50'00"	7,080	64.0	08-02-78	120VLCC	QW
Old Town	(A-21-07)16cdb	35°11'53"	111°39'38"	7,020	---	---	120VLCC	QW

[1]Well not completed.

[QW, quality of water; SW, surface water; SN, snowmelt; IB, Inner Basin]

Miscellaneous sites	Latitude	Longitude	Altitude of land surface (feet)	Other available data
Lake Mary	35°04'16"	111°31'02"	6,825	QW, SW
Quarry	35°12'01"	111°49'31"	7,080	QW, SW
IB snowmelt	35°20'27"	111°39'00"	9,840	QW, SN
Center snowmelt	34°12'27"	111°37'57"	7,115	QW, SN

SUPPLEMENTAL DATA—CONTINUED
C. X-Ray Diffraction Mineralogy for Selected Wells that Discharge Water from the Regional Aquifer, Flagstaff, Arizona

X-ray diffraction mineralogy for selected wells that discharge water from the regional aquifer, Flagstaff, Arizona

[N/A, not applicable. Numbers in parentheses are in percent and are rounded to nearest whole number. Queries indicate uncertainty. <, less than]

Depth interval below land surface, in feet	Bulk mineralogy	Formation
	Airport well	
100–110	Quartz (80), dolomite (19), calcite (1), kaolinite, plagioclase, K-feldspar	Kaibab Formation
190–200	N/A	Toroweap Formation
230–240	Quartz (96), illite, kaolinite, dolomite, calcite, plagioclase, K-feldspar	Coconino Sandstone
300–310	N/A	Do.
400–410	Quartz (85), dolomite (9), calcite (6), illite, kaolinite, plagioclase	Do.
500–510	N/A	Do.
600–610	Quartz[1], illite, kaolinite, plagioclase, dolomite, calcite	Do.
700–710	N/A	Do.
800–810	Quartz[1], illite, kaolinite, plagioclase, dolomite, calcite	Do.
890–900	N/A	Do.
950–960	Quartz[1], kaolinite, dolomite, calcite, feldspar	Do.
1,000–1,010	Quartz[1], illite, kaolinite, dolomite, calcite, plagioclase	Schnebly Hill Formation
1,050–1,060	N/A	Do.
1,100–1,110	Quartz[1], illite, kaolinite, plagioclase, K-feldspar, dolomite, calcite	Do.
1,200–1,210	Quartz[1], illite, kaolinite, dolomite, feldspar, calcite, mica	Supai Formation (Upper)
1,300–1,310	N/A	Do.
1,400–1,410	Quartz[1], illite, kaolinite, plagioclase, calcite, dolomite, K-feldspar	Do.
1,500–1,510	Quartz[1], illite, kaolinite, plagioclase, dolomite, calcite	Supai Formation (Middle?)
1,580–1,590	Quartz[1], illite, kaolinite, K-feldspar, calcite, dolomite	Do.
	Foxglenn-1	
50–60	Dolomite (70), quartz (24), calcite (6), kaolinite/illite (<1)	Kaibab Formation
110–120	Quartz (49), dolomite (49), calcite (1), kaolinite/illite (1)	Do.
220–230	Quartz (72), dolomite (26), calcite (2), kaolinite/illite (<1)	Toroweap Formation
370–380	Quartz (99), dolomite (1)	Coconino Sandstone
670–680	Quartz (99), dolomite/kaolinite/K-feldspar/kaolinite/illite (1)	Do.
1,020–1,030	Quartz (99), dolomite (1), K-feldspar/kaolinite/illite (<1)	Do.
1,070–1,080	Quartz (99), dolomite/K-feldspar (1), kaolinite (<1)	Schnebly Hill Formation
1,170–1,180	Quartz (97), K-feldspar (2), dolomite (1)	Do.
1,220–1,230	Quartz (97), dolomite (2), K-feldspar (1), kaolinite (<1)	Supai Formation (Upper)
1,320–1,330	Quartz (99), K-feldspar (1), dolomite/calcite/kaolinite (<1)	Do.
1,570–1,580	Quartz (98), dolomite (1), K-feldspar (1), kaolinite (<1)	Do.
1,670–1,680	Quartz (95), K-feldspar (4), dolomite (1), kaolinite (<1)	Supai Formation (Middle?)
1,820–1,830	Quartz (93), K-feldspar (4), dolomite (2), kaolinite/illite (1)	Do.
1,920–1,930	Quartz (95), K-feldspar (3), dolomite (1), kaolinite/illite (1)	Do.
2,070–2,080	Quartz (96), dolomite (2), K-feldspar (1), kaolinite/illite (1)	Do.
2,220–2,230	Quartz (96), dolomite (3), K-feldspar (1)	Do.
2,270–2,280	Quartz (95), dolomite (3), K-feldspar (2), kaolinite (<1)	Supai Formation (Lower?)

See footnote at end of table.

X-ray diffraction mineralogy for selected wells that discharge water from the regional aquifer, Flagstaff, Arizona—Continued

Depth interval below land surface, in feet	Bulk mineralogy	Formation
	Continental-1	
240–250	Quartz (73), K-feldspar (26), dolomite (1), kaolinite (<1)	Kaibab Formation (Fossil Mountain Member)
350–360	Quartz (71), dolomite (19), K-feldspar (9), kaolinite/calcite (1)	Do.
400–410	Quartz (about 100), dolomite/kaolinite (<1)	Coconino Sandstone
470–480	Quartz (95), dolomite (4), K-feldspar (1), kaolinite (<1)	Do.
870–880	Quartz (92), K-feldspar (6), dolomite (1), kaolinite (<1)	Do.
1,210–1,220	Quartz (about 100), kaolinite (<1)	Schnebly Hill Formation
1,300–1,310	Quartz (95), K-feldspar (3), dolomite (2), calcite/kaolinite (<1)	Do.
1,370–1,380	Quartz (91), calcite (6), dolomite (2), K-feldspar (1), kaolinite (<1)	Supai Formation (Upper)
1,430–1,440	Quartz (97), calcite (1.5), dolomite (1.5)	Do.
1,510–1,520	Quartz (92), calcite (5), dolomite (2), K-feldspar (1), kaolinite (<1)	Do.
1,590–1,600	Quartz (97), calcite (2), dolomite/K-feldspar/kaolinite (<1)	Do.
1,620–1,630	Quartz (94), calcite (3), K-feldspar (1), dolomite (1), kaolinite (<1)	Supai Formation (Middle?)
	Continental-2	
80–90	Quartz (77), dolomite (8), plagioclase 7), calcite (4), K-feldspar (3), kaolinite/illite (<1)	Alluvium
200–210	Quartz (84), dolomite (16)	Kaibab Formation (Harrisburg Member)
360–370	Quartz (73), dolomite (26), K-feldspar (1), kaolinite (<1)	Kaibab Formation (Fossil Mountain Member)
500–510	Quartz (94), dolomite (6), kaolinite (<1)	Toroweap Formation
610–620	Quartz (100)	Coconino Sandstone
860–870	Quartz (99), calcite (1), kaolinite (<1)	Do.
1,060–1,070	Quartz (94), calcite (5), kaolinite (<1)	Schnebly Hill Formation
1,130–1,140	Quartz (97), K-feldspar (2), dolomite (1), calcite (<1)	Do.
1,410–1,420	Quartz (92), K-feldspar (5), calcite (2), dolomite (1), kaolinite (<1)	Do.
1,490–1,500	Quartz (93), calcite (3), K-feldspar (2), dolomite (1), kaolinite (<1)	Supai Formation (Upper)
1,560–1,570	Quartz (98), calcite (2), kaolinite (<1)	Do.
1,770–1,780	Quartz (91), K-feldspar (6), calcite (2), dolomite (1), kaolinite (<1)	Supai Formation (Middle?)
1,940–1,950	Quartz (98), calcite (2), dolomite (<1)	Do.
2,060–2,070	Quartz (95), calcite (4), K-feldspar (1)	Do.
2,130–2,140	Quartz (78), K-feldspar (13), calcite (9), dolomite/kaolinite (<1)	Supai Formation (Lower?)

[1]Predominantly quartz.

U.S. DEPARTMENT OF THE INTERIOR
U.S. GEOLOGICAL SURVEY

PREPARED IN COOPERATION WITH THE
CITY OF FLAGSTAFF

WATER-RESOURCES INVESTIGATIONS REPORT 00—4122

Hydrogeology of the regional aquifer near Flagstaff, Arizona, 1994–97—Plate 1

Donald J. Bills, Margot Truini, Marilyn E. Flynn, Herbert A. Pierce, Rufus D. Catchings, and Michael J. Rymer

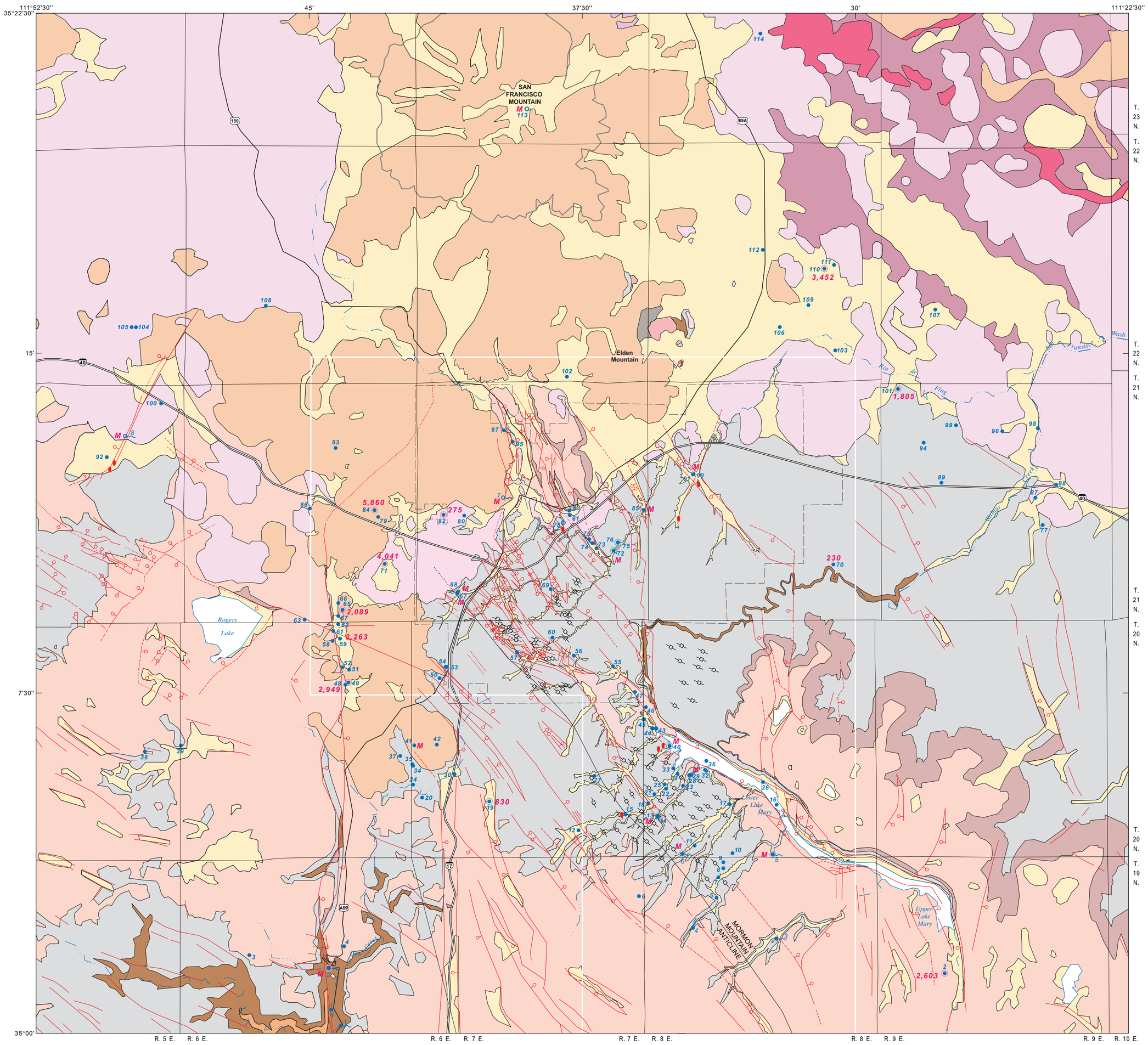

Base from U.S. Geological Survey digital data, 1:100,000, 1982 Universal Transverse Mercator projection, Zone 12

NATIONAL GEODETIC VERTICAL DATUM OF 1929

Geology, geologic descriptions, and geologic structure modified from:

1. G.M. Mann and Dr. A.E. Springer (geologists, Northern Arizona University, written commun., 1997)
2. Ulrich and others (1984)
3. Thorstenson and Beard (1998)
4. Blakey and Knepp (1989)
5. Wolfe and others (1987)
6. Additional geologic structure interpretations by D.J. Bills and G.H. Billingsley (hydrologists, geologists, USGS, written commun.,1997)

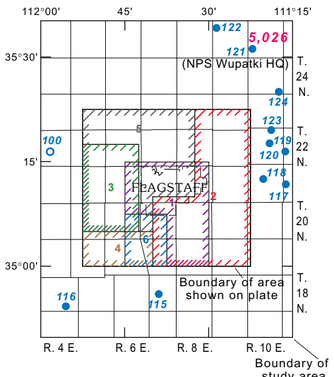

NOTE: The area mapped by Mann and Springer (**1**) was mapped at greater detail and is highlighted on the geologic map with a white outline.

EXPLANATION

SURFICIAL DEPOSITS

- UNCONSOLIDATED SEDIMENTS—Includes alluvium, colluvium, eolian, glacial, glaciofluvial (on San Francisco Mountain), and landslide deposits. Postdates bounding faults — HOLOCENE AND PLEISTOCENE

ROCKS OF THE SAN FRANCISCO VOLCANIC FIELD

- BASALT OF SUNSET CRATER ERUPTIVE SEQUENCE—Approximately A.D. 1065 to 1250 (Smiley, 1958)
- BASALTIC CINDER AND ASH BLANKET FROM ERUPTION OF SUNSET CRATER — HOLOCENE
- BASALT OF PRE-MERRIAM AGE, OR PRE-BRUNHES AGE, OR POSSIBLY PLIOCENE—Basalts are aphanitic to very fine-grained and highly vesicular with moderate to abundant plagioclase, clinopyroxene, and olivine, or varying plagioclase and olivine. Flows of pre-Merriam age are undissected and lie close to level of present drainage, are of normal polarity, and less than approximately 0.7 million years old. Includes flows of Tappan age (0.2–0.7 million years; Moore and others, 1976). Basalts of pre-Brunhes age have normal or reversed polarity and are between approximately 0.7 and 1.8 million years old. Includes most flows of Woodhouse area (0.8–3.0 million years old; Moore and others, 1976). Basalts of Pliocene age are flow or cone deposits with uncertain stratigraphic relation to rocks of known age generally west of San Francisco Mountain
- BENMOREITE; ANDESITE FLOWS, FLOW BRECCIA, AND TUFF BRECCIA; DACITE FLOWS AND DOMES; AND DACITE PYROCLASTIC-FLOW BRECCIA—Benmoreite is a high sodium, commonly aphanitic andesite with abundant plagioclase and apatite, abundant plagioclase, biotite, and feldspar, or abundant olivine and plagioclase; forms flows, cinder cones, and domes west or southwest of San Francisco Mountain. Andesite flows, flow breccia, or tuff breccia are silica-rich (60.5 percent SiO_2) pyroxene or hornblende-pyroxene with abundant plagioclase and augite. Dacite flows and domes are massive and porphyritic with abundant plagioclase, biotite, and feldspar, or abundant plagioclase, hornblende, hypersthene, and magnetite. Dacite pyroclastic-flow breccia is mostly pumiceous dacite, dacite ash, lapilli, and dacite blocks in dacite lapilli ash, pumice, and glass shards. Andesite flows, flow breccia, and tuff breccia, and dacite flows and domes are associated principally with San Francisco Mountain stratovolcano, O'Leary Peak, and Elden Mountain. Vents in San Francisco Mountain and Elden Mountain exhibit dacite pyroclastic-flow breccia — PLEISTOCENE
- BASALTIC FLOWS AND OLD BASALTS—Basalt flows or cones with uncertain stratigraphic relation that are aphanitic to fine grained and moderately vesicular with abundant plagioclase and moderate olivine and clinopyroxene that commonly cap mesas south of San Francisco Mountain, Rogers Lake, and near the Lake Mary area. Old basalts, informally called rim basalts, are aphanitic to coarse grained with abundant plagioclase and moderate olivine and clinopyroxene, quartz, xenocrysts, and mafic to ultra-mafic xenoliths. These units include four flows with K-Ar ages of 3.9–9.0 million years (Damon and others, 1974) and occur south of the Lake Mary area to west of Rogers Lake — PLIOCENE AND MIOCENE

SEDIMENTARY ROCKS OF THE COLORADO PLATEAU

- MOENKOPI FORMATION—Red to dark-red to reddish-brown mudstone, siltstone, silty sandstone, and sandstone, typically thin bedded. Discontinuous erosional remnant occurring in small localized areas now buried by volcanic rocks. Thickness of unit is 0–150 feet — MIDDLE? AND LOWER TRIASSIC
- KAIBAB FORMATION—Innerbedded sequence of light-red to gray limestone, dolomite, siltstone, sandstone, and gypsum (Harrisburg Member). Thick-bedded light-gray cherty limestone to sandy limestone (Fossil Mountain Member). Dolomitic limestone and sandy limestone are commonly cherty. The whole formation is thickest to the southwest, pinches out eastward. The eroded top of the formation forms most of the surface now buried by the volcanic rocks to the west, north, and south. Thickness of unit is 100–650 feet — UPPER PERMIAN
- TOROWEAP FORMATION AND COCONINO SANDSTONE—Light-colored (white to tan to buff to orange to light red) cross-stratified well-sorted, fine- to medium-grained sandstones. Siltstones, silty sandstones, carbonate sandstone, and limestone occur in the Toroweap Formation. The Coconino Sandstone is almost exclusively fine-grained quartz sandstone and exhibits the most prominent crossbedding. The Coconino Sandstone is exposed along the Anderson Mesa Fault in the Lake Mary area, in Oak Creek and Walnut Canyons, and east of Elden Mountain where the formation is brought to the surface by intruding volcanic rocks. Thickness of units is 300–1,100 feet — UPPER TO MIDDLE PERMIAN
- SCHNEBLY HILL FORMATION—Orange to light-red, fine sandstone and siltstone crossbedded to planar, with gray limestone and dolomite. The upper units of the Schnebly Hill Formation alternate and intertongue with the lower part of the Coconino Sandstone. The only exposure of the Schnebly Hill Formation in the area is in Oak Creek Canyon. Thickness of unit is 0–800 feet — MIDDLE PERMIAN
- SUPAI GROUP—Composed of upper, middle, and lower formations. The Upper Supai Formation is a reddish-brown, fine-grained sandstone with subordinate siltstone, mudstone, and limestone. The Middle Supai Formation is orange, very fine-grained calcareous sandstone. The Lower Supai Formation is red and purple sandstone, siltstone, and gray limestone and dolomite with an occasional basal conglomerate or breccia of chert clasts, cherty limestone, and reworked material from the underlying Redwall Limestone. The only exposure of the Supai Group in the area is east of Elden Mountain where the formation is brought to the surface by intruding volcanic rocks. Thickness of unit is 600–2,000 feet — LOWER PERMIAN TO PENNSYLVANIAN
- REDWALL LIMESTONE—Massive light-gray limestone and dolomite. The only exposure of the Redwall Limestone in the area is east of Elden Mountain where the formation is brought to the surface by intruding volcanic rocks. Thickness of unit is 50–300 feet — MISSISSIPPIAN

- FAULT—Inferred photogrammatically and utilizing remotely sensed data, partly field verified where accesssible. Dashed where uncertain, dotted where concealed. Bar and ball on the downthrown side
- ANTICLINE SHOWING TRACE OF AXIAL SURFACE—Dotted where concealed
- FRACTURE ALIGNMENT—Inferred photogrammatically and utilizing remotely sensed data
- MULTIPLE VERTICAL TO NEAR-VERTICAL JOINTS—Inferred photogrammatically and utilizing remotely sensed data
- 85 REGIONAL-AQUIFER WELL—Number corresponds to well number in data table (plate 4)
- 116 PERCHED-AQUIFER WELL—Number corresponds to well number in data table (plate 4)
- 1 REGIONAL-AQUIFER SPRING—Number corresponds to spring number in data table (Supplimental Data, Part B)
- 7 PERCHED-AQUIFER SPRING—Number corresponds to spring number in data table (Supplimental Data, Part B)
- SINKHOLE
- WELLS AND SPRINGS SAMPLED FOR STRONTIUM–87
  - Ground water receives recharge through volcanic rocks and limestone
  - Ground water receives recharge through volcanic rocks
  - Ground water receives recharge through limestone
- CARBON–14 AGES, ESTIMATED-
  - 2,089 Number, *2,089*, indicates carbon–14 age of water
  - M Letter, *M*, indicates water of modern age (less than 200 years)

GEOLOGY, GEOLOGIC STRUCTURE, LOCATIONS OF WELLS AND SPRINGS, AND CARBON–14 AGES OF GROUND WATER NEAR FLAGSTAFF, ARIZONA

HYDROGEOLOGY OF THE REGIONAL AQUIFER NEAR FLAGSTAFF, ARIZONA

By

Donald J. Bills, Margot Truini, Marilyn E. Flynn, Herbert A. Pierce, Rufus D. Catchings, and Michael J. Rymer

2000

U.S. DEPARTMENT OF THE INTERIOR
U.S. GEOLOGICAL SURVEY

PREPARED IN COOPERATION WITH THE
CITY OF FLAGSTAFF

WATER-RESOURCES INVESTIGATIONS REPORT 00—4122
Hydrogeology of the regional aquifer near
Flagstaff, Arizona, 1994–97—Plate 2

Donald J. Bills, Margot Truini, Marilyn E. Flynn, Herbert A. Pierce, Rufus D. Catchings, and Michael J. Rymer

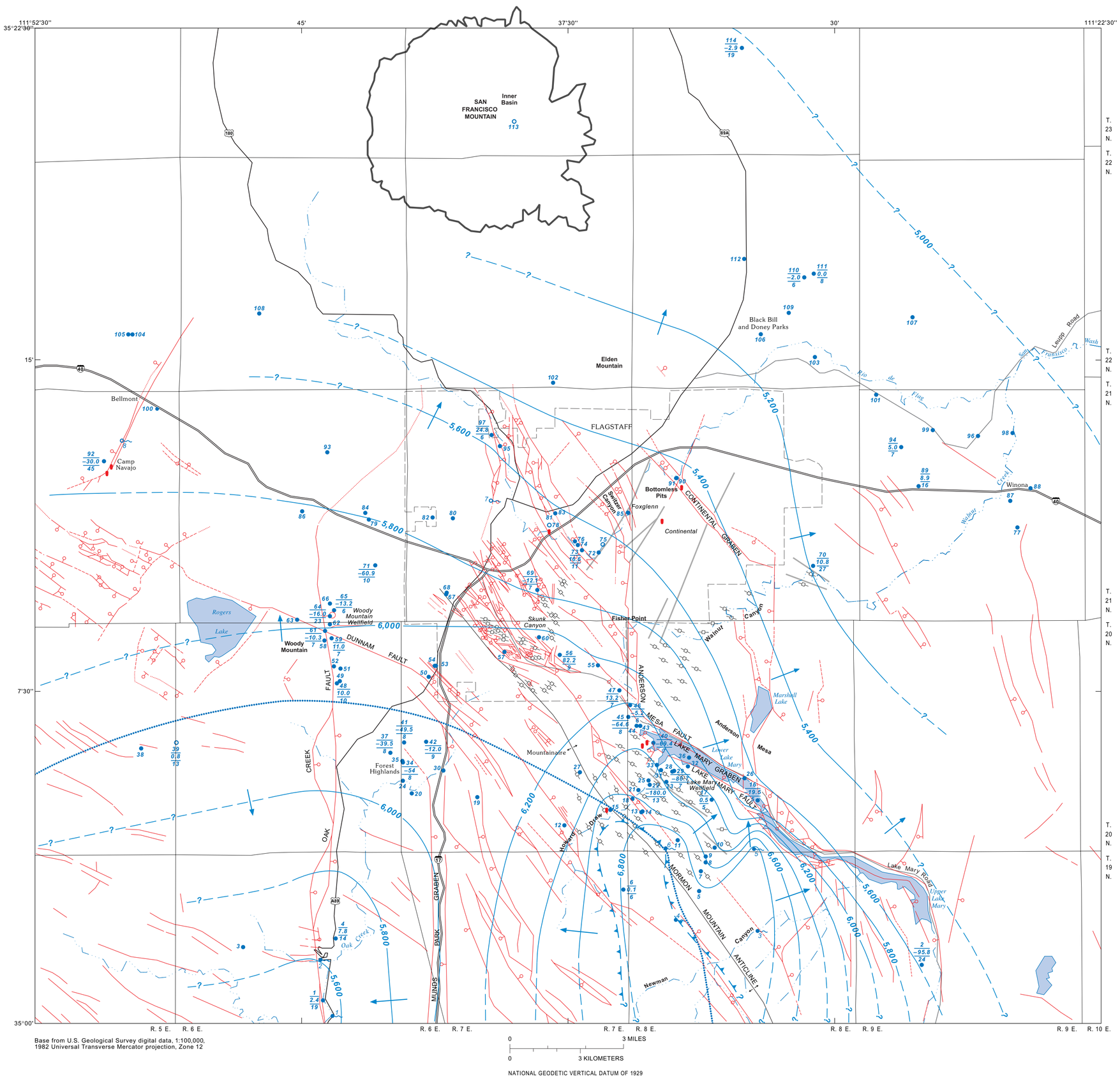

Base from U.S. Geological Survey digital data, 1:100,000,
1982 Universal Transverse Mercator projection, Zone 12

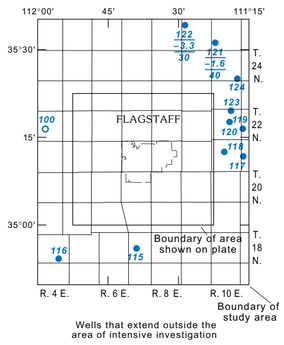

EXPLANATION

- 6,400 — POTENTIOMETRIC CONTOUR—Shows the altitude at which the water level would have stood in a tightly cased well, 1994–97, in feet above mean sea level. Dashed where approximately located, queried where uncertain. Contour interval 200 feet
- EXTENT OF CONFINED PART OF THE REGIONAL AQUIFER, 1994–97
- DIRECTION OF GROUND-WATER FLOW
- GROUND-WATER DIVIDE
- FAULT—Inferred photogrammatically and utilizing remotely sensed data, partly field verified where accesssible. Dashed where uncertain, dotted where concealed. Bar and ball on the downthrown side
- ANTICLINE SHOWING TRACE OF AXIAL SURFACE—Dotted where concealed
- FRACTURE ALIGNMENT—Inferred photogrammatically and utilizing remotely sensed data
- MULTIPLE VERTICAL TO NEAR-VERTICAL JOINT FRACTURES—Inferred photogrammatically and utilizing remotely sensed data
- 97 / 24.8 / 6 — REGIONAL-AQUIFER WELL—First number, 97, corresponds to well number in data table on plate 4. Second number, 24.8, is the water-level change, in feet, since previous measurement. Third number, 6, is the time since previous measurement, in years. Wells with well number only have no historic data
- 78 — PERCHED-AQUIFER WELL—Number corresponds to well number in data table (Supplemental Data, Part B)
- 1 — REGIONAL-AQUIFER SPRING—Number corresponds to spring number in data table (Supplemental Data, Part B)
- 7 — PERCHED-AQUIFER SPRING—Number corresponds to spring number in data table on plate 4
- SINKHOLE

POTENTIOMETRIC SURFACE OF THE REGIONAL AQUIFER (1994–97), GEOLOGIC STRUCTURE, AND SELECTED WELL AND SPRING DATA NEAR FLAGSTAFF, ARIZONA

HYDROGEOLOGY OF THE REGIONAL AQUIFER NEAR FLAGSTAFF, ARIZONA

By

Donald J. Bills, Margot Truini, Marilyn E. Flynn, Herbert A. Pierce, Rufus D. Catchings, and Michael J. Rymer

2000

U.S. DEPARTMENT OF THE INTERIOR
U.S. GEOLOGICAL SURVEY

PREPARED IN COOPERATION WITH THE
CITY OF FLAGSTAFF

WATER-RESOURCES INVESTIGATIONS REPORT 00—4122
Hydrogeology of the regional aquifer near
Flagstaff, Arizona, 1994–97—Plate 3

Donald J. Bills, Margot Truini, Marilyn E. Flynn, Herbert A. Pierce, Rufus D. Catchings, and Michael J. Rymer

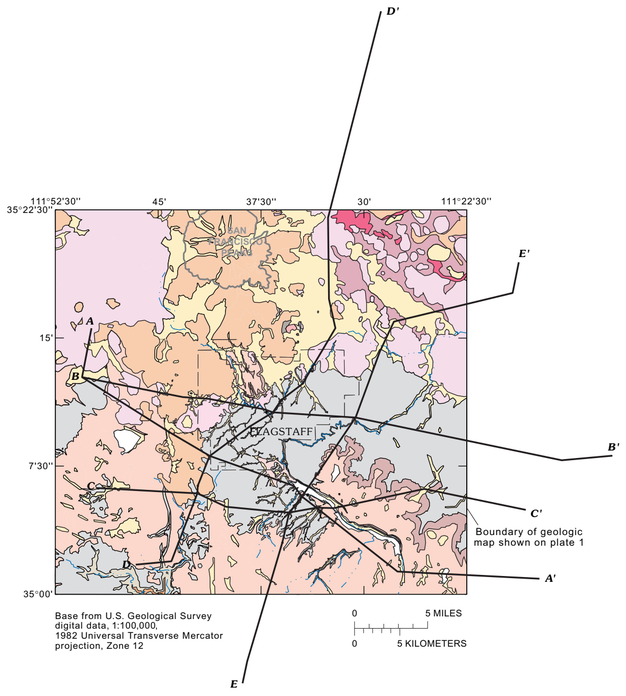

EXPLANATION

	GEOLOGIC AGE OR EPOCH
SURFICIAL DEPOSITS	
UNCONSOLIDATED SEDIMENTS—Includes alluvium, colluvium, eolian, glacial, glaciofluvial (on San Francisco Mountain), and landslide deposits. Postdates bounding faults	HOLOCENE AND PLEISTOCENE
ROCKS OF THE SAN FRANCISCO VOLCANIC FIELD	
BASALT OF SUNSET CRATER ERUPTIVE SEQUENCE—Approximately A.D. 1065 to 1250 (Smiley, 1958)	HOLOCENE
BASALTIC CINDER AND ASH BLANKET FROM ERUPTION OF SUNSET CRATER	HOLOCENE
BASALT OF PRE-MERRIAM AGE, OR PRE-BRUNHES AGE, OR POSSIBLY PLIOCENE—Basalts are aphanitic to very fine-grained and highly vesicular with moderate to abundant plagioclase, clino-pyroxene, and olivine, or varying plagioclase and olivine. Flows of pre-Merriam age are undissected and lie close to level of present drainage, are of normal polarity, and less than approximately 0.7 million years old. Includes flows of Tappan age (0.2–0.7 million years; Moore and others, 1976). Basalts of pre-Brunhes age have normal or reversed polarity and are between approximately 0.7 and 1.8 million years old. Includes most flows of Woodhouse area (0.8–3.0 million years old; Moore and others, 1976). Basalts of Pliocene age are flow or cone deposits with uncertain stratigraphic relation to rocks of known age generally west of San Francisco Mountain	PLEISTOCENE
BENMOREITE; ANDESITE FLOWS, FLOW BRECCIA, AND TUFF BRECCIA; DACITE FLOWS AND DOMES; AND DACITE PYROCLASTIC-FLOW BRECCIA—Benmoreite is a high sodium, commonly aphanitic andesite with abundant plagioclase and apatite, abundant plagioclase, biotite, and feldspar, or abundant olivine and plagioclase; forms flows, cinder cones, and domes west or southwest of San Francisco Mountain. Andesite flows, flow breccia, or tuff breccia are silica-rich (60.5 percent SiO_2) pyroxene or hornblende-pyroxene with abundant plagioclase and augite. Dacite flows and domes are massive and porphyritic with abundant plagioclase, biotite, and feldspar, or abundant plagioclase, hornblende, hypersthene, and magnetite. Dacite pyroclastic-flow breccia is mostly pumiceous dacite, dacite ash, lapilli, and dacite blocks in dacite lapilli ash, pumice, and glass shards. Andesite flows, flow breccia and tuff breccia and dacite flows and domes are associated principally with San Francisco Mountain stratovolcano, O'Leary Peak, and Elden Mountain. Vents in San Francisco Mountain and Elden Mountain exhibit dacite pyroclastic-flow breccia	PLEISTOCENE
BASALTIC FLOWS AND OLD BASALTS—Basalt flows or cones with uncertain stratigraphic relation that are aphanitic to fine grained and moderately vesicular with abundant plagioclase and moderate olivine and clino-pyroxene that commonly cap mesas south of San Francisco Mountain, Rogers Lake, and near the Lake Mary area. Old basalts, informally called rim basalts, are aphanitic to coarse grained with abundant plagioclase and moderate olivine and clino-pyroxene, quartz, xenocrysts, and mafic to ultra-mafic xenoliths. These units include four flows with K-Ar ages of 3.9–9.0 million years (Damon and others, 1974) and occur south of the Lake Mary area to west of Rogers Lake	PLIOCENE AND MIOCENE
SEDIMENTARY ROCKS OF THE COLORADO PLATEAU	
MOENKOPI FORMATION—Red to dark-red to reddish-brown mudstone, siltstone, silty sandstone, and sandstone, typically thin bedded. Discontinuous erosional remnant occurring in small localized areas now buried by volcanic rocks. Thickness of unit is 0–150 feet	MIDDLE? AND LOWER TRIASSIC
KAIBAB FORMATION—Inner-bedded sequence of light-red to gray limestone, dolomite, siltstone, sandstone, and gypsum (Harrisburg Member). Thick-bedded light-gray cherty limestone to sandy limestone (Fossil Mountain Member). Dolomitic limestone and sandy limestone are commonly cherty. The whole formation is thickest to the southwest, pinching out eastward. The eroded top of the formation forms most of the surface now buried by the volcanic rocks to the west, north, and south. Thickness of unit is 100–650 feet	UPPER PERMIAN
TOROWEAP FORMATION—Light-colored (white to tan to buff to orange to light red) cross-stratified well-sorted, fine- to medium-grained sandstones. Siltstones, silty sandstones, carbonate sandstone, and limestone occur in the Toroweap Formation. Thickness of unit varies from 0–250 feet	UPPER TO MIDDLE PERMIAN
COCONINO SANDSTONE—Almost exclusively fine-grained quartz sandstone and exhibits the most prominent crossbedding. The Coconino Sandstone is exposed along the Anderson Mesa Fault in the Lake Mary area, in Oak Creek and Walnut Canyons, and east of Elden Mountain where the formation is brought to the surface by intruding volcanic rocks. Thickness of unit is 300–1,100 feet	UPPER TO MIDDLE PERMIAN
SCHNEBLY HILL FORMATION—Orange to light-red, fine sandstone and siltstone crossbedded to planar, with gray limestone and dolomite. The upper units of the Schnebly Hill Formation alternate and intertongue with the lower Coconino Sandstone. The only exposure of the Schnebly Hill Formation in the area is in Oak Creek Canyon. Thickness of the unit is 0–800 feet	MIDDLE PERMIAN
SUPAI GROUP—Composed of upper, middle, and lower formations. The Upper Supai Formation is a reddish-brown, fine-grained sandstone with subordinate siltstone, mudstone, and limestone. The Middle Supai Formation is orange very fine-grained calcareous sandstone. The Lower Supai Formation is red and purple sandstone, siltstone, and gray limestone and dolomite with an occasional basal conglomerate or breccia of chert clasts, cherty limestone, and reworked material from the underlying Redwall Limestone. The only exposure of the Supai Group in the area is east of Elden Mountain where the formation is brought to the surface by intruding volcanic rocks. The combined thickness of the unit is 600–2,000 feet	LOWER PERMIAN TO PENNSYLVANIAN
REDWALL LIMESTONE—Massive light-gray limestone and dolomite. The only exposure of the Redwall Limestone in the area is east of Elden Mountain where the formation is brought to the surface by intruding volcanic rocks. The thickness of the formation is 50–300 feet	MISSISSIPPIAN
TEMPLE BUTTE (MARTIN) LIMESTONE—Grayish-brown to grayish-red to grayish-purple dolomite and dolomitic limestone. Thickest in the southeast and southwest and thinning to the north. The thickness of this formation is about 0–400 feet	DEVONIAN
MUAV LIMESTONE—Mottled gray and purple dolomitic limestone. Not present in the southeastern part of the area, thickening to the northwest. The thickness of this formation is 0–200 feet	MIDDLE TO LOWER CAMBRIAN
GRANITE AND SCHIST—Granite, granodiorite, and granite rubble, in some well logs described as pink granite	PRECAMBRIAN

D U FAULT—U, indicates the upthrown side and D, indicates the downthrown side

POTENTIOMETRIC SURFACE (1994–97)

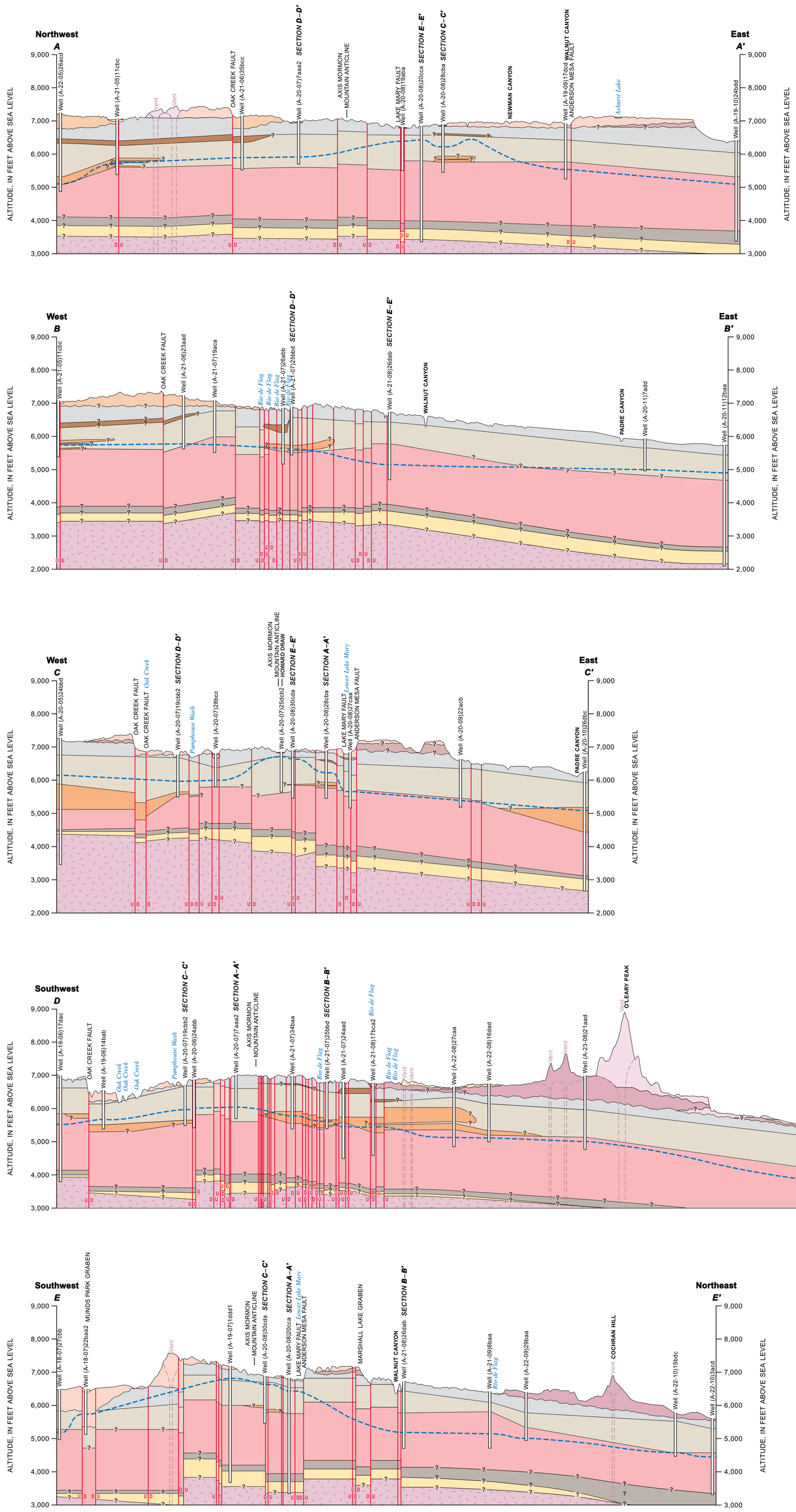

GEOLOGIC SECTIONS NEAR FLAGSTAFF, ARIZONA

HYDROGEOLOGY OF THE REGIONAL AQUIFER NEAR FLAGSTAFF, ARIZONA

By

Donald J. Bills, Margot Truini, Marilyn E. Flynn, Herbert A. Pierce, Rufus D. Catchings, and Michael J. Rymer

2000

Donald J. Bills, Margot Truini, Marilyn E. Flynn, Herbert A. Pierce, Rufus D. Catchings, and Michael J. Rymer

Water-level data for wells near Flagstaff, Arizona

[Wells are in order by well-reference number. Dashes indicate no data]

Well-reference number	Well name or owner	Site identifier	Latitude	Longitude	Water level: Date of measurement	Water level: Depth below land surface, in feet	Water level: Altitude, in feet
1	Pine Flats	(A-19-06)W27aaa	35°00'35"	111°44'18"	07-15-75	9.0	5,531
Do.	Do.	do	do		04-11-94	6.6	5,533
2	Pine Grove	(A-19-09)17dcd	35°01'24"	111°27'35"	12-11-67	1,320.2	5,637
Do.	Do.	do	do		06-05-95	1,416.0	5,541
3	Oil Discovery 1	(A-19-06)17dac	35°01'47"	111°46'32"	11-05-74	Dry	---
4	ADOT-89A	(A-19-06)W14bab	35°02'00"	111°43'55"	05-20-80	826.8	5,663
Do.	Do.	do	do		04-07-94	819.0	5,671
5	LMEX-1	(A-19-08)05ddd1	35°03'05"	111°33'50"	04-05-94	141.8	6,818
6	Federal 1	(A-19-07)01ddd1	35°03'06"	111°35'55"	06-02-89	365.7	6,809
Do.	Do.	do	do		08-17-95	365.6	6,809
7	Walter	(A-19-08)05add	35°03'30"	111°33'50"	09-15-79	31.0	6,929
8	Tilley	(A-19-08)04bbd	35°03'43"	111°33'37"	10-27-78	19.5	6,920
9	Henson	(A-19-08)04bbb	35°03'50"	111°33'35"	07-30-79	25.0	6,955
10	LMEX-2	(A-20-08)33cdb	35°04'05"	111°33'20"	04-05-94	407.6	6,532
11	LMEX-3	(A-20-08)32cab1	35°04'15"	111°34'25"	11-01-94	13.0	6,867
12	TH-4	(A-20-07)35bac	35°04'33"	111°37'34"	08-17-95	545.3	6,330
13	LM-9	(A-20-08)30cda	35°04'51"	111°35'25"	08-01-94	243.0	6,632
14	TH-3	(A-20-08)30cdd1	35°04'50"	111°35'25"	04-05-94	219.6	6,650
15	LMEX-4	(A-20-07)25dcb1	35°04'55'	111°36'15"	08-17-95	125.4	6,715
16	LM-7	(A-20-08)27caa	35°05'07"	111°32'10"	03-01-89	1,119.0	5,676
Do.	Do.	do	do		08-01-94	1,138.5	5,656
17	Old LM-9	(A-20-08)28cba	35°05'10"	111°33'25"	12-05-89	640.0	6,220
Do.	Do	do	do		04-05-94	639.5	6,220
18	Cook-2	(A-20-08)30cba2	35°05'10"	111°35'40"	04-13-95	127.1	6,683
19	Mountainaire	(A-20-07)28bcc	35°05'11"	111°40'00"	03-30-78	791.0	5,994
20	Kachina-2	(A-20-07)30bdb	35°05'16"	111°41'50"	04-14-94	655.3	6,030
21	Wahlers	(A-20-08)30bdb	35°05'20"	111°35'30"	06-12-85	120.0	6,700
22	Bathen	(A-20-08)30abc	35°05'30"	111°35'10"	09-06-82	150.0	6,670
Do.	Do.	do	do		06-07-95	330.0	6,490
23	LMO-2	(A-20-08)29bbb	35°05'32"	111°34'43"	04-11-85	260.0	6,605
24	Kachina-1	(A-20-07)30bbc	35°05'33"	111°42'05"	04-14-94	628.5	6,046
25	Garrison	(A-20-08)30abb	35°05'35"	111°35'15"	11-11-72	260.0	6,540
26	LM-6	(A-20-08)27bbb	35°05'37"	111°32'32"	09-01-81	990.0	5,820
27	LMEX-6	(A-20-07)23dca	35°05'45"	111°37'10"	08-17-95	617.8	6,257
28	LMO-1	(A-20-08)20cca2	35°05'50"	111°34'30"	04-11-85	235.0	6,585
29	LM-8	(A-20-08)20cca	35°05'47"	111°34'30"	02-01-88	313.3	6,506
Do.	Do.	do	do		02-01-95	394.0	6,425
30	Kachina-3	(A-20-07)20cca	35°05'47"	111°40'57"	05-12-95	694.3	6,021
31	Suiter	(A-20-08)19dda	35°05'50"	111°34'50"	08-09-95	379.2	6,441
32	LM-5	(A-20-08)20dbc	35°05'53"	111°34'07"	10-01-88	301.9	6,515
33	Schnieder	(A-20-08)19dac	35°05'55"	111°34'59"	04-14-78	273.0	6,522
34	FH-1	(A-20-07)19cbb2	35°05'58"	111°42'05"	09-01-87	697.0	5,993
Do.	Do.	do	do		04-11-95	720.4	5,970
35	FH Test Well	(A-20-07)19cbb1	35°06'00"	111°42'05"	08-12-85	635.0	6,055
36	LMO-3	(A-20-08)20acd	35°06'10"	111°34'10"	12-10-85	562.0	6,233
37	FH-4	(A-20-06)24adb	35°06'10"	111°42'25"	06-30-87	678.0	6,082
Do.	Do.	do	do		04-11-95	717.5	6,042
38	Potter-1	(A-20-05)24bbd	35°06'16"	111°49'24"	09-09-66	1,096.5	6,144
39	Morrison	(A-20-06)19bbb	35°06'25"	111°48'25"	07-14-81	83.0	7,080
Do.	Do.	do	do		04-07-94	82.2	7,081
40	LM-4	(A-20-08)19aba	35°06'25"	111°35'05"	02-01-88	347.6	6,461
Do.	Do.	do	do		02-01-95	417.0	6,392
41	FH-5	(A-20-06)24abb	35°06'25"	111°42'03"	09-23-87	703.0	6,067
Do.	Do.	do	do		04-11-95	752.5	6,017
42	FH-3	(A-20-07)19aba	35°06'26"	111°41'26"	08-30-87	863.0	6,037
Do.	Do.	do	do		11-01-96	875.0	6,025
43	Whitley-1	(A-20-08)18cac1	35°06'48"	111°35'27"	07-23-97	516.0	6,209
44	Whitley-2	(A-20-08)18cac2	35°06'50"	111°35'35"	04-28-92	620.0	6,200
45	LM-2	(A-20-08)18bcc	35°07'00"	111°35'47"	12-01-86	477.4	6,355
Do.	Do.	do	do		11-01-94	542.0	6,290
46	LM-1	(A-20-08)18bbb	35°07'16"	111°35'44"	03-01-89	591.8	6,248
Do.	Do.	do	do		11-01-95	597.0	6,243
47	LM-3	(A-20-07)12ddb	35°07'36"	111°36'02"	07-01-87	761.2	6,069
Do.	Do.	do	do		10-01-94	748.5	6,082
48	WM-9	(A-20-06)11bdc	35°07'45"	111°43'56"	11-07-85	982.0	6,108
Do.	Do.	do	do		06-01-95	972.0	6,118
49	WM-8	(A-20-06)11bdd	35°07'50"	111°43'50"	07-14-82	910.0	6,155
50	Roaldstad	(A-20-07)07adb	35°07'55"	111°41'20"	06-07-60	949.0	---
51	WM-11	(A-20-06)11baa	35°08'05"	111°43'50"	08-18-97	1,103.0	6,067
52	WM-7	(A-20-06)11bab	35°08'08"	111°44'01"	02-01-95	1,110.0	6,061
53	Tyrrell	(A-20-07)07aaa2	35°08'10"	111°41'10"	10-19-92	1,063.0	5,907
54	Kimmerly	(A-20-07)07aaa1	35°08'10"	111°41'10"	05-21-85	941.0	6,039
55	Heckathorne	(A-20-07)12bba	35°08'10"	111°36'40"	06-29-65	900.0	5,940
56	North Ranch	(A-20-07)02cca	35°08'25"	111°37'40"	09-11-87	900.0	5,955
Do.	Do.	do	do		10-23-96	817.8	6,037
57	Airport Well	(A-20-07)04dac	35°08'28"	111°39'15'	11-08-95	830.3	6,130
58	WM-10	(A-20-06)02bcb	35°08'43"	111°44'17"	04-02-96	1,139.0	6,091
59	WM-6	(A-20-06)02bdb	35°08'49"	111°44'04"	05-01-87	1,132.0	6,069
Do.	Do.	do	do		04-19-94	1,121.0	6,080
60	Skunk Canyon	(A-20-07)03aca	35°08'48"	111°38'17"	10-31-96	897.6	6,017
61	WM-5	(A-20-06)02bbb	35°08'55"	111°44'15"	12-08-88	1,108.7	6,077
Do.	Do.	do	do		11-01-95	1,119.0	6,067
62	WM-4	(A-21-06)35ccc	35°09'05"	111°44'08"	02-01-96	1,228.0	5,938
63	WM-Test	(A-21-06)34cca	35°09'10"	111°45'05"	11-14-81	Dry	---
64	WM-2	(A-21-06)35ccb	35°09'16"	111°44'08"	02-01-72	1,246.0	5,921
Do.	Do.	do	do		02-01-95	1,262.0	5,905
65	WM-1	(A-21-06)35cba	35°09'24"	111°44'01"	12-08-88	1,246.8	5,893
Do.	Do.	do	do		04-19-94	1,260.0	5,880
66	WM-3	(A-21-06)35bcc	35°09'35"	111°44'10"	11-01-95	1,234.0	5,896
67	Mtn Dell-1	(A-21-07)32bbc1	35°09'46"	111°40'53"	08-09-95	1,023.5	5,886
68	Mtn Dell-2	(A-21-07)32bbc2	35°09'48"	111°40'52"	05-22-75	975.0	5,925
69	Kohner	(A-21-07)34baa	35°09'50"	111°38'20"	04-12-88	1,138.0	5,797
Do.	Do.	do	do		08-16-95	1,150.1	5,784
70	NPS Walnut Canyon	(A-21-08)26dab	35°10'25"	111°30'37"	08-18-70	1,536.0	5,174
Do.	Do.	do	do		08-13-97	1,525.2	5,185
71	Flag Ranch	(A-21-06)25bcd	35°10'25"	111°42'52"	10-20-85	1,122.0	5,928
Do.	Do.	do	do		08-11-95	1,182.9	5,867
72	Purl	(A-21-07)25bbd	35°10'43"	111°36'37"	11-17-96	1,173.0	5,617
73	LA-1	(A-21-07)26abd	35°10'45"	111°37'05"	10-05-84	1,168.0	5,627
Do.	Do.	do	do		11-13-95	1,151.4	5,644
74	LA-2	(A-21-07)26abb	35°10'53"	111°37'12"	07-20-95	1,150.0	5,650
75	Potter	(A-21-07)24ccd	35°10'55"	111°36'30"	08-09-79	32.4	6,748
76	LA-3	(A-21-07)23dcc	35°10'58"	111°37'17"	11-13-95	1,218.2	5,627
77	CVWC	(A-21-09)23cba	35°11'15"	111°24'55"	01-03-83	1,206.0	5,064
78	Rio de Flag MW-1	(A-21-07)23cac	35°11'20"	111°38'00"	04-29-96	44.0	6,751
79	Saskan Ranch	(A-21-06)24bcb	35°11'27"	111°43'03"	06-12-96	1,390.0	5,820
80	Roirdan	(A-21-07)20bdb	35°11'30"	111°40'40"	09-19-62	1,220.0	5,750
81	Ponderosa Paper-2	(A-21-07)22ada	35°11'30"	111°37'50"	10-10-67	1,233.0	5,632
82	Hidden Hollow	(A-21-07)19aca	35°11'30"	111°41'16"	01-14-77	1,320.0	5,750
83	Ponderosa Paper-1	(A-21-07)22aad	35°11'35"	111°37'50"	06-25-66	1,273.0	5,582
84	Henden	(A-21-06)23aad	35°11'35"	111°43'10"	09-06-95	1,440.0	5,780
85	Foxglenn-1	(A-21-07)24aad	35°11'37"	111°35'48"	12-21-96	1,319.0	5,456
86	Fried	(A-21-06)22bab	35°11'40"	111°44'55"	11-14-92	Dry	---
87	Porter	(A-21-09)15dda	35°11'55"	111°25'05"	01-01-65	1,215.0	5,050
88	Pill	(A-21-09)14acc	35°12'10"	111°24'30"	06-24-66	1,205.0	5,065
89	ADOT-Winona	(A-21-09)17acc	35°12'15"	111°27'40"	08-08-79	1,323.0	5,117
Do.	Do.	do	do		08-08-95	1,314.1	5,126
90	Continental-2	(A-21-08)17bca2	35°12'23"	111°34'28"	02-22-97	1,303.5	5,446
91	Continental-1	(A-21-08)17bca1	35°12'24"	111°34'27"	10-21-96	[1]1,550.0	5,200
92	NAD-1	(A-21-05)11cbc	35°12'45"	111°50'30"	08-28-50	1,273.0	5,767
Do.	Do.	do	do		09-10-95	1,303.1	5,737
93	Burns	(A-21-06)10daa	35°13'00"	111°44'15"	05-26-87	[2]1,275.0	---
94	BBDP-Cosnino	(A-21-09)08bcc	35°13'05"	111°28'10"	07-18-90	1,338.0	5,112
Do.	Do.	do	do		03-12-97	1,333.0	5,117
95	Ritland	(A-21-07)09acc	35°13'05"	111°39'25"	02-09-91	1,516.0	5,494
96	Wilbur	(A-21-09)10bbd	35°13'20"	111°26'00"	07-30-66	1,227.0	5,063
97	Pugh	(A-21-07)09bac	35°13'22"	111°39'37"	06-30-89	1,530.0	5,570
Do.	Do.	do	do		08-09-95	1,505.2	5,595
98	Foster	(A-21-09)11bbb	35°13'25"	111°25'00"	04-09-90	1,137.0	5,068
99	BBDP-Flowers	(A-21-09)05ddd	35°13'30"	111°27'15"	07-21-75	1,270.0	5,095
Do.	Do.	do	do		05-01-95	1,269.0	5,096
100	Crockett	(A-21-05)01acc3	35°13'55"	111°48'50"	04-20-94	97.2	7,037
101	BBDP-MVR-1	(A-21-09)06baa	35°14'16"	111°28'50"	08-08-95	1,264.2	5,146
102	Garrett-Bacon	(A-22-07)34dda	35°14'33"	111°37'54"	09-25-97	1,920.0	5,290
103	Mitchell	(A-22-08)35aac	35°15'10"	111°30'35"	06-20-66	1,456.7	5,103
104	EPNG-6	(A-22-05)26adc2	35°15'35"	111°49'40"	08-03-53	2,010.0	5,220
105	EPNG-5	(A-22-05)26acd	35°15'35"	111°49'50"	07-01-53	2,120.0	5,110
106	Koch Field	(A-22-08)27caa	35°15'40"	111°32'05'	05-01-94	1,496.0	5,129
107	US Grisp	(A-22-09)29baa	35°16'00"	111°27'50"	12-17-73	1,383.0	5,007
108	Fort Valley	(A-22-06)26aaa	35°16'06"	111°46'08'	02-23-88	Dry	---
109	Cromer School	(A-22-08)26bbb	35°16'08"	111°31'18"	01-22-86	1,463.0	5,122
110	BBDP-Marijka	(A-22-08)23abb	35°16'56"	111°30'52"	06-25-88	1,500.0	5,075
Do.	Do.	do	do		05-01-94	1,502.0	5,073
111	BBDP-Sunset	(A-22-08)23aab	35°17'00"	111°30'35"	12-05-86	1,507.0	5,063
Do.	Do.	do	do		05-01-94	1,507.0	5,063
112	AT&T	(A-22-08)16dad	35°17'20"	111°32'35"	06-12-63	1,635.0	5,115
113	IB-9	(A-23-07)33aab2	35°20'27"	111°39'00"	09-15-73	143.2	9,637
114	NPS Sunset Ctr-2	(A-23-08)21aad	35°22'05"	111°32'35"	01-31-79	1,960.3	5,010
Do.	Do.	do	do		10-02-98	1,962.6	5,007
115	AZWC-5	(A-18-07)15ccc2	34°56'16"	111°38'54"	01-09-81	706.9	5,728
116	Bradshaw Fee-1	(A-18-04)34abb	34°54'14"	111°55'32"	08-22-74	329.2	4,151
117	Drye	(A-21-11)19bcb	35°11'45"	111°16'10"	04-04-78	796.0	4,974
118	Moody	(A-21-10)16bdc	35°12'30"	111°20'15"	11-30-78	990.0	5,015
119	Kuttkuhn	(A-22-10)15bdc	35°17'40"	111°19'10"	01-01-75	1,112.0	4,593
120	Salt Well	(A-22-11)19ccc	35°16'25"	111°16'20"	10-20-54	1,000.0	4,590
121	NPS Wupatki HQ	(A-25-10)30bdb	35°31'10"	111°22'20"	10-27-58	781.0	4,149
Do.	Do.	do	do		05-26-98	782.6	4,152
122	NPS-Citadel	(A-25-09)06ccd	35°34'10"	111°28'45"	01-23-67	1,582.9	3,798
Do.	Do.	do	do		02-21-97	1,587.2	3,794
123	Oil test	(A-22-10)03acd	35°19'30"	111°18'45"	10-05-66	1,138.0	4,452
124	Rhoten Spr.	(A-23-10)01bbb	35°25'05"	111°17'20"	10-19-54	740.0	4,283

[1] Well caved in and collapsed before water level stabilized.
[2] Well obstructed.

gallons per day

Hydrogeologic data for wells that discharge water from the regional aquifer, Flagstaff, Arizona

[Wells are in order by well-reference number. Dashes indicate no data. >, greater than. CS, Coconino Sandstone; SG, Supai Group; KF, Kaibab Formation; SH, Schnebly Hill Formation]

Well-reference number	Local well name	Site identifier	Latitude	Longitude	Year of test	Well yield, in gallons per minute	Draw-down, in feet	Saturated thickness, in feet	Screened interval, in feet	Pumping period, in days	Recovery period, in days	Transmissivity, in gallons per day per foot: Drawdown	Transmissivity: Recovery	Hydrologic conductivity, in gallons per day per foot squared: Drawdown	Hydrologic conductivity: Recovery	Storativity, dimensionless	Specific yield	Porosity	Specific capacity, in gallons per minute per foot	Lithology of saturated zone	Surface strike of principal structure
2	Pine Grove	(A-19-09)17dcd	35°01'24 "	111°27'35"	1967	50.0	---	391	261	---	---	---	---	---	---	---	---	---	0.6	SG	---
Do.	Do.	do	do		1967	15	25	---	---	0.66	---	---	---	---	---	---	---	---	---	---	---
4	ADOT-89A	(A-19-06)W14bab	35°02'00"	111°43'55"	1978	51.0	0	275	200	2.00	---	---	---	---	---	---	---	---	---	SG	---
5	LMEX-1[2]	(A-19-08)05ddd1	35°03'05"	111°33'50"	1992	330	83.0	1,008	889	.50	.50	2,500	2,600	2.81	2.92	---	---	---	3.98	CS, SG	---
6	Federal 1[2]	(A-19-07)01ddd1	35°03'06"	111°35'55"	1992	270	74.0	360	825	.50	.50	1,500	1,800	4.62	5.54	---	---	---	3.65	KF, CS, SG	---
10	LMEX-2[2]	(A-20-08)33cdb	35°04'05"	111°33'20"	1992	69.0	63.0	749	719	.50	.50	800	700	1.11	.97	---	---	---	1.10	CS, SG	---
11	LMEX-3[2]	(A-20-08)32cab1	35°04'15"	111°34'25"	1992	320	270.0	1,141	934	.50	.50	600	300	.64	.32	---	---	---	1.18	CS, SG	N.60°W.
13	LM-9[2]	(A-20-08)30cda	35°04'51"	111°35'25"	1991	420	513.0	1,284	982	10.0	10.0	940	1,200	.73	.93	---	---	---	.82	CS, SG	N.54°W.
14	TH-3[2]	(A-20-08)30cdd1	35°04'50"	111°35'25"	1992	---	56.0	1,079	45	10.0	10.0	3,350	3,974	3.10	3.68	0.01 to 0.03	---	---	---	KF, CS, SG	---
15	LMEX-4[2]	(A-20-07)25dcb1	35°04'55"	111°36'15"	1992	100	251.0	900	720	.10	.10	100	100	.14	.14	---	---	---	.40	CS, SG	---
20	Kachina-2	(A-20-07)30bdb	35°05'16"	111°41'50"	1969	55.0	35.0	372	----	.20	---	---	---	---	---	---	---	---	1.60	CS	---
21	Whalers	(A-20-08)30bdb	35°05'20"	111°35'30"	1985	15.0	60.0	85	100	---	---	---	---	---	---	---	---	---	.25	KF, CS	---
24	Kachina-1	(A-20-07)30bbc	35°05'33"	111°42'05"	1978	34.0	20.0	452	210	.08	---	---	---	---	---	---	---	---	1.70	CS,SG	---
27	LMEX-6[2]	(A-20-07)23dca	35°05'45"	111°37'10"	1992	57.0	60.0	531	892	.50	.50	400	500	.75	.94	---	---	---	.95	CS, SG	---
28	LMO-1	(A-20-08)20cca2	35°05'50"	111°34'30"	1992	---	38.0	659	300	---	84.0	17,000	16,000	28.8	24.3	.05	---	---	---	KF, CS	---
29	LM-8[3]	(A-20-08)20cca	35°05'47"	111°34'30"	1992	1,700	285.0	914	700	90.0	90.0	26,000	24,000	---	28.0	---	---	0.095 to 0.14	6.00	CS, SG	N.13°W.
31	Suiter	(A-20-08)19dda	35°05'50"	111°34'50"	1990	10.0	40.0	113	----	---	---	---	---	---	---	---	---	---	.25	CS	---
32	LM-5[3]	(A-20-08)20dbc	35°05'53"	111°34'07"	1992	485	178.0	929	675	90.0	90.0	3,000	3,000	---	4.00	---	---	---	2.70	CS, SG	N.76°W.
34	FH-1[4]	(A-20-07)19cbb2	35°05'58"	111°42'05"	1986	110	205.0	555	525	9.70	9.70	[5]2,904	[6]3,630	5.23	6.54	.00023	0.0002	---	.54	SH, SG	N.53°W.
37	FH-4	(A-20-06)24adb	35°06'10"	111°42'25"	1987	152	234.0	577	545	1.50	---	[7]747	---	1.29	---	---	---	---	.65	CS, SH, SG	N.53°W.
40	LM-4[3]	(A-20-08)19aba	35°06'25"	111°35'05"	1992	620	288.0	937	480	90.0	90.0	20,000	11,690	21.3	8.50	---	---	---	2.20	CS, SG	N.68°W.; N.42°W.
41	FH-5	(A-20-06)24abb	35°06'25"	111°42'03"	1987	220	274.0	647	625	4.00	.05	2,159	1,930	3.30	3.04	---	---	---	.80	CS, SG	N.53°W.
42	FH-3	(A-20-07)19aba	35°06'26"	111°41'26"	1987	90.0	245.0	547	520	3.10	---	[7]456	---	.83	---	---	---	---	.37	CS, SH, SG	---
44	Whitley-2	(A-20-08)18cac2	35°06'50"	111°35'35"	1992	35.0	20.0	590	640	---	---	---	---	---	---	---	---	---	1.80	CS	---
45	LM-2[3]	(A-20-08)18bcc	35°07'00"	111°35'47"	1992	430	346.0	523	512	90.0	90.0	---	4,000	---	6.00	---	---	---	1.24	CS	N.68°W.
46	LM-1	(A-20-08)18bbb	35°07'16"	111°35'44"	1963	500	276	700	108	7.63	15.4	[7]1,386	---	1.98	2.77	---	---	---	1.81	CS	N.67°W.
Do.	LM-1 redevelopment	do	do		1996	300	267	540	439	.5	1.04	---	444.9	---	.82	---	---	---	---	---	---
47	LM-3	(A-20-07)12ddb	35°07'36"	111°36'02"	1966	167	211.0	281	317	1.50	.90	1,000	1,000	3.60	3.60	---	---	---	.79	CS	N.64°W.
48	WM-9	(A-20-06)11bdc	35°07'45"	111°43'56"	1986	677	471.0	858	610	4.67	.16	2,201	---	2.56	---	---	---	---	1.43	KF, CS, SG	N.24°W.
51	WM-11	(A-20-06)11baa	35°08'05"	111°43'50"	1998	491	249	844	702	3.25	.19	3,700	7,200	5.48	4.87	---	.13	---	1.97	CS, SH, SG	N.24°W.
52	WM-7[1]	(A-20-06)11bab	35°08'08"	111°44'01"	1978	727	308.5	680	640	18.2	1.80	18,300	35,000	28.6	54.7	---	.14	.20 to .50	4.60	CS, SG	N.24°W.
53	Tyrrell	(A-20-07)07aaa2	35°08'10"	111°41'10"	1993	10.0	12.0	212	----	---	---	---	---	---	---	---	---	---	.83	CS	N.50°W.
56	North Ranch	(A-20-07)02cca	35°08'25"	111°37'40"	1987	40.0	20.0	240	----	---	---	---	---	---	---	---	---	---	2.00	SG	N.60°W.
58	WM-10[9]	(A-20-06)02bcb	35°08'43"	111°44'17"	1996	321	250.0	640	460	3.00	.30	4,460	4,013	6.97	6.27	---	.08	---	1.28	CS, SG	N.24°W.
59	WM-6[1]	(A-20-06)02bdb	35°08'47"	111°44'04"	1972	560	365.5	584	600	208	150	8,400	15,100	14.4	25.8	---	---	---	1.53	CS	N.24°W.; N.83°W.
60	Skunk Canyon	(A-20-07)03aca	35°08'48"	111°38'17"	1996	150	669.0	884	800	1.00	1.00	[7]237	373	.27	.42	---	---	---	.22	CS, SH, SG	N.56°W.; N.30°W.
61	WM-5[1]	(A-20-06)02bbb	35°08'55"	111°44'15"	1972	400	82.2	500	550	24.0	114	31,200	30,750	62.4	61.4	---	.08	---	4.87	CS	N.83°W.; N.24°W.
62	WM-4[1]	(A-21-06)35ccc	35°09'05"	111°44'08"	1972	436	283.0	410	304	193	150	5,700	8,600	13.9	20.9	---	---	---	1.54	CS	N.24°W.
64	WM-2[1]	(A-21-06)35ccb	35°09'16"	111°44'08"	1972	295	64.8	375	300	185	150	18,150	21,850	48.4	58.3	---	---	---	4.56	CS	N.24°W.
65	WM-1[1]	(A-21-06)35cba	35°09'24"	111°44'01"	1972	---	13.1	363	360	208	127	29,600	28,700	81.5	79.1	---	.08	---	---	CS	N.24°W.
66	WM-3[1]	(A-21-06)35bcc	35°09'35"	111°44'10"	1979	403	81.4	385	300	168	150	14,500	20,000	37.7	51.9	---	---	---	4.95	CS	N.24°W.
67	Mtn Dell-1	(A-21-07)32bbc1	35°09'46"	111°40'53"	1976	206	200.0	215	1,050	.004	.03	---	---	---	---	---	---	---	1.03	CS, SG	N.73°W.
70	NPS Walnut Canyon	(A-21-08)26dab	35°10'25"	111°30'37"	1970	36.0	252.5	444	514	.70	.91	[7]204	---	.46	---	---	---	---	.14	SG	---
71	Flag Ranch	(A-21-06)25bcd	35°10'25"	111°42'52"	1990	86.0	287.0	626	590	1.00	---	---	---	---	---	---	---	---	.30	SG	N.70°W.; N.63°W.
72	Purl	(A-21-07)25bbd	35°10'43"	111°36'37"	1990	8.00	0	155	160	---	---	---	---	---	---	---	---	---	---	CS, SH, SG	---
73	LA-1	(A-21-07)26abd	35°10'45"	111°37'05"	1975	101	30.1	322	274	4.84	.98	[7]4,504	---	13.99	---	---	.098	---	3.36	SG	N.59°W.
77	CVWC	(A-21-09)23cba	35°11'15"	111°24'55"	1983	7.00	---	69	70	---	---	---	---	---	---	---	---	---	---	SG	---
79	Saskan Ranch	(A-21-06)24bcb	35°11'27"	111°43'03"	1997	17.0	53.0	287	140	1.10	.10	[7]444	---	1.55	---	---	---	---	.32	SH, SG	---
80	Roirdan	(A-21-07)20bdb	35°11'30"	111°40'40"	1962	30.0	---	400	395	---	---	---	---	---	---	---	---	---	---	SG	---
82	Hidden Hollow	(A-21-07)19aca	35°11'30"	111°41'16"	1977	10.0	---	231	231	---	---	---	---	---	---	---	---	---	---	SG	---
84	Henden	(A-21-06)23aad	35°11'35"	111°43'10"	1994	15.0	0	110	120	1.50	---	---	---	---	---	---	---	---	---	CS, SG	---
85	Foxglenn-1	(A-21-07)24aad	35°11'37"	111°35'48"	1997	450	168.0	691	1,135	3.05	3.45	2,536	2,343	3.67	3.99	---	---	---	2.68	SG	N.8°W.; N.42°W.
88	Pill	(A-21-09)14acc	35°12'10"	111°24'30"	1966	7.50	8.80	112	120	.09	.02	[7]818	---	1.30	---	---	---	---	.85	CS	---
89	ADOT-Winona	(A-21-09)17acc	35°12'15"	111°27'40"	1972	18.0	150.0	512	448	.99	---	[7]143	---	.28	---	---	---	---	.12	SG	---
90	Continental-2	(A-21-08)17bca2	35°12'23"	111°34'28"	1997	490	280.0	692	---	.75	20.0	[7]2,231	2,246	3.22	3.25	---	---	---	1.75	SG	N.6°W.; N.56°W.
92	NAD-1	(A-21-05)11cbc	35°12'45"	111°50'30"	1950	35.0	100.0	374	147	1.20	---	---	---	---	---	---	---	---	.35	SG	N.35°W.
93	Burns	(A-21-06)10daa	35°13'00"	111°44'15"	1988	5.00	347.0	425	155	1.00	---	---	---	---	---	---	---	---	.014	CS, SG	---
94	BBDP-Cosnino	(A-21-09)08bcc	35°13'05"	111°28'10"	1973	28.5	184.0	367	208	.53	---	[7]162	---	.44	---	---	---	---	.15	SG	---
96	Wilbur	(A-21-09)10bbd	35°13'20"	111°26'00"	1966	7.00	---	111	1,038	---	---	---	---	---	---	---	---	---	---	SG	---
97	Pugh	(A-21-07)09bac	35°13'22"	111°39'37"	1993	18.0	30.0	70	1,360	2.00	---	---	---	---	---	---	---	---	.60	SG	N.27°W.
98	Foster	(A-21-09)11bbb	35°13'25"	111°25'00"	1990	8.00	---	263	200	---	---	---	---	---	---	---	---	---	---	CS, SG	---
99	BBDP-Flowers	(A-21-09)05ddd	35°13'30"	111°27'15"	1975	30.0	---	455	---	2.00	---	---	---	---	---	---	---	---	---	SG	---
101	BBDP-MVR-1	(A-21-09)06baa	35°14'16"	111°28'50"	1967	30.0	151.0	398	400	.21	.03	[7]202	---	.51	---	---	---	---	.20	SG	---
103	Mitchell	(A-22-08)35aac	35°15'10"	111°30'35"	1966	25.0	---	[2]93	1,457	---	---	---	---	---	---	---	---	---	---	CS, SG	---
107	US Grisp	(A-22-09)29baa	35°16'00"	111°27'50"	1959	4.00	---	64	---	---	---	---	---	---	---	---	---	---	---	SG	---
109	Cromer School	(A-22-08)26bbb	35°16'08"	111°31'18"	1986	79.0	6.0	347	291	.08	---	---	---	---	---	---	---	---	13.0	CS, SG	---
110	BBDP-Marijka	(A-22-08)23abb	35°16'56"	111°30'52"	1988	178	44.0	302	280	1.00	---	[7]5,897	---	19.5	---	---	---	---	4.05	SG	---
111	BBDP-Sunset	(A-22-08)23aab	35°17'00"	111°30'35"	1991	40.0	---	215	70	.75	---	---	---	---	---	---	---	---	---	SG	---
112	AT&T	(A-22-08)16dad	35°17'20"	111°32'35"	1963	12.0	15.0	120	90	.12	---	---	---	---	---	---	---	---	.80	SG	---
114	NPS Sunset Ctr-2[10]	(A-23-08)21aad	35°22'05"	111°32'35"	1979	21.0	2.02	256	---	3.04	3.16	4,710	4,635	18.4	18.1	---	.008	---	10.4	SG	---
115	AZWC-5	(A-18-07)15ccc2	34°56'16"	111°38'54"	1977	96.0	7.9	541	63	2.10	.08	[7]19,377	---	35.8	---	---	---	---	12.2	CS	---
116	Bradshaw Fee-1	(A-18-04)34abb	34°54'14"	111°55'32"	1971	---	---	77	3,113	---	---	---	---	---	---	---	---	.04	---	SG	---
117	Drye	(A-21-11)19bcb	35°11'45"	111°16'10"	1957	14.0	0	150	216	---	---	---	---	---	---	---	---	---	---	CS	---
118	Moody	(A-21-10)16bdc	35°12'30"	111°20'15"	1979	22.0	30.0	60	---	---	---	---	---	---	---	---	---	---	.73	CS	---
119	Kuttkuhn	(A-22-10)15bdc	35°17'40"	111°19'10"	1973	6.00	---	128	1,170	---	---	---	---	---	---	---	---	---	---	CS, SG	---
120	Salt Well	(A-22-11)19ccc	35°16'25"	111°16'20"	1967	10.0	---	60	310	.33	---	---	---	---	---	---	---	---	---	CS	---
121	NPS Wupatki HQ[10]	(A-25-10)30bdb	35°31'10"	111°22'20"	1972	50.0	45.0	123	96	1.0	---	1,269	---	10.3	---	---	---	---	1.10	SG	---
122	NPS-Citadel[10]	(A-25-09)06ccd	35°34'10"	111°28'45"	1967	17.6	5.05	205	8.0	3.02	.07	841	---	28.5	6.2	---	---	---	3.48	SG	---

[1] Harshbarger and Associates and John Carollo Engineers (1972).
[2] Montgomery and Associates (1992).
[3] Montgomery and Associates (1993).
[4] Manera Incorporated (1987).
[5] Estimated.
[6] Observation well.
[7] Estimated from specific capacity.
[8] No stable discharge.
[9] Montgomery Watson (1996).
[10] P.K. Christensen (1982).

WATER-LEVEL AND HYDROGEOLOGIC DATA FOR WELLS NEAR FLAGSTAFF, ARIZONA

HYDROGEOLOGY OF THE REGIONAL AQUIFER NEAR FLAGSTAFF, ARIZONA

By
Donald J. Bills, Margot Truini, Marilyn E. Flynn, Herbert A. Pierce, Rufus D. Catchings, and Michael J. Rymer
2000